

2021

Experimental and CFD–PBM investigation of an agitated bioreactor using a dual helical ribbon impeller

Maryamsadat Amiraftabi
Edith Cowan University

Follow this and additional works at: <https://ro.ecu.edu.au/theses>



Part of the [Engineering Commons](#)

Recommended Citation

Amiraftabi, M. (2021). *Experimental and CFD–PBM investigation of an agitated bioreactor using a dual helical ribbon impeller*. Edith Cowan University. Retrieved from <https://ro.ecu.edu.au/theses/2424>

This Thesis is posted at Research Online.
<https://ro.ecu.edu.au/theses/2424>

Edith Cowan University

Copyright Warning

You may print or download ONE copy of this document for the purpose of your own research or study.

The University does not authorize you to copy, communicate or otherwise make available electronically to any other person any copyright material contained on this site.

You are reminded of the following:

- Copyright owners are entitled to take legal action against persons who infringe their copyright.
- A reproduction of material that is protected by copyright may be a copyright infringement. Where the reproduction of such material is done without attribution of authorship, with false attribution of authorship or the authorship is treated in a derogatory manner, this may be a breach of the author's moral rights contained in Part IX of the Copyright Act 1968 (Cth).
- Courts have the power to impose a wide range of civil and criminal sanctions for infringement of copyright, infringement of moral rights and other offences under the Copyright Act 1968 (Cth). Higher penalties may apply, and higher damages may be awarded, for offences and infringements involving the conversion of material into digital or electronic form.



**Experimental and CFD–PBM investigation of an agitated
bioreactor using a dual helical ribbon impeller**

A thesis submitted in fulfilment of the requirements for the degree of
Doctor of Philosophy

Maryamsadat Amiraftabi

M.Sc. (University of Tehran)

B.Sc. (University of Tehran)

School of Engineering

Edith Cowan University

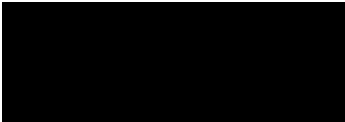
2021

DECLARATION

I *Maryam Amirafabi* declare that all information in this document has been obtained and presented in accordance with academic rules and ethical conduct. I also declare that have fully cited and referenced all materials and results that are not original to this work, as defined by the university's policy on plagiarism.

Maryam Amirafabi

30/11/2020



ACKNOWLEDGEMENT

I am so grateful to have Professor Mehdi Khiadani and Dr Hussein A Mohammed as my supervisors. I appreciate for all the time, patience, and support that Mehdi has extended to me during my time here at ECU. I would like to thank Michael Stein– who provided professional editing and proofreading services for Student at ECU. Additionally, I would like to extend my special thanks to my friend – Firouzeh Bavand – for assistance with proofreading.

I wish to thank my family for all their love and encouragement, and I would like to thank my parents, who raised me with a love of science and supported me in all my pursuits. And most of all I would like to thank my supportive, encouraging, and patient husband, Bardia, whose faithful support during all stages of my life is so appreciated.

Thank you.

PUBLICATIONS DURING CANDIDATURE

- M.Amiraftabi, M. Khiadani, H. A. Mashhadani, A. Arshad; CFD-PBM and experimental investigation of a shear thinning fluid in a gas-liquid tank agitated by a helical ribbon impeller. *Chemical Engineering and Processing: Separation and Purification Technology*, <https://doi.org/10.1016/j.seppur.2021.118855>.
- M. Amiraftabi, Khiadani Mehdi; Transparent polymers to emulate the rheological properties of primary, activated, and digested sludge. *Chem. Eng. Res. Des.* (2019). <https://doi.org/10.1016/j.chemd.2019.03.040>.
- M.Amiraftabi, M. Khiadani, H. A. Mashhadani; Performance of a Dual Helical Ribbon Impeller in a Two-Phase (Gas-Liquid) Stirred Tank Reactor. *Chemical Engineering and Processing: Process Intensification*, <https://doi.org/10.1016/j.cep.2020.107811>.

NOMENCLATURE

A	Cross sectional area (m ²)
Alg	Alginate
AS	Activated sludge
AR	Aspect Ratio
C	Equation Constant
CFD	Computational fluid dynamics
C _D	Crag coefficient
D	Vessel inner diameter (cm)
d	Impeller Diameter (cm)
d _i	Impeller blade diameter (cm)
d _s	Shaft diameter (mm)
DS	Digested sludge
E-E	Eulerian-Eulerian
\vec{F}_i	Momentum transferred from bubbles to the liquid phase
Flg	Gas flow number
g	Gravitational acceleration (m/s ²)
G	Generation of turbulent kinetic energy
G _f	Gas flow rate (Lpm)
H _L	Depth of Fluid (cm)
h	Impeller Height (cm)
IC	Impeller Clearance
IS	Impeller Speed
K	Consistency Index (Pa.s ⁿ)
k	Turbulent kinetic energy
K _s	Metzner and Otto's constant
K _{ji}	Exchange coefficient for bubbly phase
M _{Adjusted}	Actual torque required to rotate the shaft (N.m)
M _{display}	Torque displayed by torquemeter (N.m)

M_{friction}	Friction torque (N.m)
MRF	Multiple Reference Frame
mv	Milli volt
N	Impeller Rotational Speed (rpm)
NaCMC	Sodium Carboxymethyl Cellulose
NaOH	Sodium hydroxide
N_p	Power number (Dimensionless)
n	Flow index behaviour
$n(\vec{x}, V_b, t)$	Bubble density distribution function at the time of t and position of \vec{x} . V_b
P_0	Input power (W)
P_g	Power consumption after injection of gas (W)
Pa.s	Pascal second
PS	Primary sludge
PBM	Population balanced model
PEG	Polyethylene Glycol
PIV	Particle Image Velocimetry
Q_p	Upward pumping rate by fluid (Lpm)
Q_{AX}	Pumping rate by rising bubbles (Lpm)
\vec{R}_{ji}	interphase force
Re	Reynold number (Dimensionless)
RSM	Response surface methodology
STR	Stirred Tank Reactor
$S(\vec{x}, V_b, t)$	Source term of breakage / coalescence
t	Time (s)
TS%	Percentage of total solid content
u_g	Superficial gas velocity (m/s)
u_b	Local velocity of bubbles (m/s)
wt%	Weight percentage (%)
X	Variables

XG	Xanthan gum
Y	RSM Response
α_i	Volume fraction of the continuous phase
β_0	RSM regression coefficients
β_i	RSM regression coefficients
β_{ii}	RSM interaction coefficient
β_{ij}	RSM interaction coefficient
ε	Dissipation rate
γ_g	Gas shear rates (1/s)
γ_l	Liquid shear rates (1/s)
$\dot{\gamma}_T$	Average shear rates (1/s)
μ_{eff}	Effective viscosity (Pa.s)
μ_i	Molecular viscosity (Pa.s)
$\mu_{t,i}$	Shear induced viscosity (Pa.s)
$\mu_{b,i}$	Turbulence viscosity (Pa.s)
v_i	Liquid mean velocity (m/s)
ρ	Density (kg/m ³)
τ	Average shear stress (N/m ²)
ζ -potential	Zeta Potential

EXECUTIVE SUMMARY

Throughout past decades, the management of solid waste by producing methane gas, as a renewable source of energy, has featured as an important research objective. Anaerobic digesters are widely used in countries with environmental initiatives and green approaches, where biogas produced from a bioreactor is a carbon neutral source of energy. Biogas contains 70% methane, 30% CO₂ and some other gases. The by-product of an anaerobic digester is solid sludge that can be used as either fertilizer or compost.

Anaerobic digestion biogas plants can benefit industries by adding value to solid organic waste, reducing fossil fuel usage, eliminating solid waste disposal costs, in addition to generating power. Setting up an anaerobic digestion biogas plant is a green investment for industries interested in environmentally friendly biological processes. A variety of organic solid waste including municipal, industrial, livestock, poultry, meat, and food waste can be digested in an anaerobic system.

To treat the large volume of waste generated by industries and urban sewerage systems, more efficient digesters and a continuous improvement of digestion processes are required. To accomplish these objectives, crucial factors including the size, design, and shape of a bioreactor, its working temperature, pH and the hydrodynamics of a system need to be studied. A considerable amount of literature has been published regarding the hydrodynamics of anaerobic digesters. Further, several studies have explored the factors thought to influence the hydrodynamics of anaerobic digesters. These studies have identified that the hydrodynamics of a system could be influenced by the rheological characteristics of sludge, as well as mixer type and shape. Inadequate and poor mixing in a digester can cause the failure of a reactor, non-uniform distribution of mass and heat, imbalanced microbial activity, as well as formation of sediment and scum. Although studies have successfully demonstrated that close-clearance

mixers (screw, helical, anchor impellers) increase biogas production, the information about hydrodynamic characteristics and flow field generated by these types of agitators is inadequate.

Although hydrodynamics and the rheology of sludge have been studied in the past, more research is required to address these gaps. The application of visual and measuring instruments could facilitate further research on sludge behaviour in an agitated anaerobic digester, but this type of study is not possible due to the opaque nature of real sludge.

The main objectives of this project are (i) to find a safe, cheap, clear and stable material that can emulate digested sludge rheological characteristics in a laboratory; (ii) to study and optimize the mixing performance of a dual helical ribbon as an efficient impeller to create an ideal mixing pattern (iii) to investigate the flow pattern and hydrodynamics of a shear thinning fluid in a batch gas-liquid reactor using a combination of a computational fluid dynamics (CFD) simulation and a population balance model (PBM).

Study 1 has analysed and compared the Zeta potential, pH resistance, flow curve, viscoelasticity, and thixotropy of four popular model fluids reported previously as ideal simulant of primary, activated, and digested sludge. The results of the correlational analysis indicate that xanthan gum is the best simulant to mimic the rheological characteristics of activated sludge that is sheared less than 100 S^{-1} . There are similarities between the viscosity and flow curve of activated sludge and xanthan gum which can be described by its internal network and molecular structure. This study also compares rheological properties of 2% NaCMC solution and digested sludge containing 3.23% solid sheared between $10\text{-}300 \text{ S}^{-1}$, concluding that they behave in an essentially identical manner. The findings from this study provide several contributions towards selecting and applying a clear and safe polymer that emulates the rheological behaviour of sludge.

Study 2 has evaluated the performance of a dual helical ribbon impeller in agitating shear thinning fluid. The effects of impeller rotational speed, gas flow rate, clearance to the bottom, and viscosity on power uptake and mixing time have been studied. This study suggests that determining optimum operating conditions can minimize power consumption and time required to achieve the maximum volume of uniformity in reactor. Although the study successfully reports a significant positive correlation between the rotational speed of the impeller and the performance of mixing, there is still a threshold limit for rotational speed. Experimental data shows that power consumption would increase with rotational speed however increasing the rotational speed beyond the certain level does not affect the mixing time significantly. This study suggests two practical equations to estimate power consumption and mixing time under specific operating conditions by applying an ANOVA method.

To cover some of the limitations related to the experimental study of hydrodynamics of gas-liquid systems, a combination of computational fluid dynamics (CFD) simulation and population balance model (PBM) has been used in the third study. The main purpose of this work is to evaluate the impacts of using a dual helical ribbon on the hydrodynamics of a multiphase reactor. The governing equations and turbulent model of agitated bubbly flow have been solved through a standard $k - \varepsilon$ model and Eulerian-Eulerian (E-E) multiphase approach. Following grid sensitivity analyses, findings through simulation have been verified by PIV measuring tests. Further, the PBM model has been discretized into five bubble size groups. The results show a positive relationship between rotational speed and bubble breakage. The comparative study indicates an increase in the likelihood of bubble channeling when the rotational speed is insufficient to break the gel-like structure of the liquid. By increasing rotational speed, the bubble hits the blades, breaks, and disperses, leading to improved interfacial area between phases. Further, rotating mechanical blades induce shear stress to bulk of liquid, resulting in a significant drop in viscosity and diminishing the stagnant regions.

Keywords *Anaerobic digesters, Clear model fluid, Rheological characteristics of sludge, Multiphase hydrodynamics, Dual helical ribbon impeller, Bubble breakage and coalescence rate, CFD-PBM simulation*

TABLE OF CONTENTS

DECLARATION	2
ACKNOWLEDGEMENT	3
PUBLICATIONS DURING CANDIDATURE	4
NOMENCLATURE	5
EXECUTIVE SUMMARY	8
TABLE OF CONTENTS	12
LIST OF FIGURES	16
LIST OF TABLES	18
Chapter 1: Introduction	1
1.1 Project rationale	1
1.2 Scope, significance, and objectives	7
1.3 Thesis outline	8
1.4 References.....	9
Chapter 2: Literature review	14
2.1 Background	14
2.2 Sludge	17
2.2.1 Working fluid.....	18
2.3 Importance of mixing in digesters	18
2.3.1 Mechanical mixing.....	19
2.3.2 Gas-lift loop mixing.....	21
2.3.3 Mixing time.....	22
2.4 Two distinctive regions	23
2.5 Shear rate	24
2.6 Dimensionless numbers	25
2.6.1 Reynolds number (Re).....	26
2.6.2 Power number (Np).....	27
2.6.3 Froude number (Fr).....	27
2.6.4 Gas flow number (Fl _g)	28
2.6.5 Mixing time number (N _θ).....	28
2.7 Power consumption.....	29
2.8 Gas holdup	30
2.8.1 Influential factors on bubble deformation.....	31
2.9 Computational fluid dynamics (CFD)	32
2.9.1 Governing equations	33
2.9.2 Population balance model (PBM).....	35

2.10	References.....	35
Chapter 3: Material and methods.....		45
3.1	Reactor setup.....	45
3.2	Sample preparation	47
3.3	Measurement of pH and zeta potential	47
3.4	Rheological measurement and test procedures	48
3.5	Mixing pattern.....	49
3.5.1	Mixing time.....	49
3.6	Experimental design.....	50
3.6.1	Installing impeller	51
3.6.2	Data analysis	51
3.7	CFD simulation.....	52
3.8	PIV measurements	53
3.8.1	PIV setup.....	53
3.9	References.....	54
Chapter 4: Transparent polymers to emulate the rheological properties of primary, activated, and digested sludge.....		57
4.1	Abstract.....	58
4.2	Introduction.....	59
4.3	Materials and Methods.....	63
4.3.1	Sample preparation	63
4.3.2	Measurement of pH.....	64
4.3.3	Zeta potential	64
4.3.4	Rheological measurement and test procedures	65
4.3.5	Non-Newtonian flow models.....	66
4.4	Results and Discussion	67
4.4.1	Resistance to pH changes.....	67
4.4.2	Zeta-potential analysis	69
4.4.3	Shear-thinning behaviour of selected polymers.....	70
4.4.4	Comparison between the flow behaviour of sludge and polymers.....	72
4.4.5	Comparison between Herschel- Bulkely parameters of sludge and polymers ...	78
4.4.6	Comparison between the viscoelastic behaviour of digested sludge and XG	81
4.4.7	Comparison between the thixotropic behaviour of activated sludge and XG	83
4.5	Conclusions.....	84
4.6	References.....	85
Chapter 5: Performance of a dual helical ribbon impeller in a two-phase (gas-liquid) stirred tank reactor.....		91

5.1	Abstract	92
5.2	Introduction.....	93
5.3	Materials and methods	98
5.3.1	Experimental Setup.....	98
5.3.2	Acid-Base reaction.....	100
5.3.3	Torquemeters	101
5.3.4	Rheometer	102
5.3.5	Theoretical considerations	102
5.3.6	Response Surface Method.....	106
5.4	Results and discussion	107
5.4.1	Mixing pattern.....	107
5.4.2	Impact of impeller speed.....	110
5.4.3	Influence of bubble motion.....	113
5.4.4	Power consumption.....	115
5.4.5	Statistical analysis	120
5.5	Conclusions.....	124
5.6	References.....	124
Chapter 6: CFD-PBM and experimental investigation of a shear thinning fluid in a gas-liquid tank agitated by a helical ribbon impeller		133
6.1	Abstract	134
6.2	Introduction.....	135
6.3	Experimental methodology	138
6.3.1	Two-phase stirred tank reactor configuration	138
6.3.2	Rheological properties of working fluid (NaCMC).....	141
6.3.3	PIV measurements	141
6.4	Numerical simulation.....	143
6.4.1	Governing equations	143
6.4.2	Turbulence model	145
6.4.3	Population balance model (PBM).....	145
6.5	Solution domain, mesh generation and boundary conditions.....	147
6.5.1	Mesh Processing	147
6.5.2	Solver setup and boundary conditions	149
6.5.3	Model validation	150
6.6	Gas velocity	150
6.7	Hydrodynamics	151
6.8	Results and discussion	153
6.8.1	Effect of impeller speed on bubble size distribution and gas holdup	153

6.8.2	Liquid velocity contour.....	156
6.8.3	Effective viscosity contour	159
6.9	Conclusions.....	162
6.10	References.....	163
Chapter 7: General discussion and conclusions		169
7.1	General discussion	169
7.1.1	Rheological study.....	170
7.1.2	Performance of a dual helical ribbon impeller.....	171
7.1.3	CFD Simulation	172
7.2	Conclusions.....	173
7.3	Future recommendation	175

LIST OF FIGURES

<i>Figure 1-1 Different stages of the anaerobic digestion process</i>	2
<i>Figure 1-2 Different types of anaerobic digester (Hamilton and Gould 2012)</i>	3
<i>Figure 1-3 Different types of close-clearance impellers</i>	5
<i>Figure 2-1 Different types of impeller</i>	20
<i>Figure 2-2 Gas-Liquid flow pattern in an agitated vessel; a) Flooding; b) Complete Dispersion; c) Loading (Paglianti, Pintus, and Giona 2000).</i>	22
<i>Figure 3-1: The Schematic of experimental setup</i>	46
<i>Figure 3-2 a) Schematic diagram of PIV system; and b) Real experimental setup.</i>	54
<i>Figure 4-1 (a) Neutralized pH for different polymers with concentration of 1 wt%, (b) the sensitivity of polymers viscosity to pH changes</i>	68
<i>Figure 4-2 Effect of pH changes on viscosity of XG with concentration of 0.5% wt%.</i>	69
<i>Figure 4-3 Zeta potential of different simulant materials as a function of pH.</i>	70
<i>Figure 4-4 Viscosity versus shear rate for NaCMC, PEG, Alg, and XG for different concentrations where γ_c in (a) is the critical shear stress.</i>	71
<i>Figure 4-5 Comparison of NaCMC flow behaviour with: (a) primary, (b) activated, and (c) digested sludge.</i>	73
<i>Figure 4-6 Comparison of PEG flow behaviour with: (a) primary, (b) activated, and (c) digested sludge.</i>	74
<i>Figure 4-7 Comparison of Alg flow behaviour with: (a) primary, (b) activated, and (c) digested sludge</i>	75
<i>Figure 4-8 Comparison of XG flow behaviour with: (a) primary, (b) activated, and (c) digested sludge</i>	77
<i>Figure 4-9 Storage modulus (G') and loss modulus (G'') as a function of strain for different concentration of xanthan gum and digested sludge (3.23 wt%)</i>	82
<i>Figure 4-10 Dependency of cross-over points ($G'=G''$) to xanthan gum concentration at 25°C and one Hz</i>	83
<i>Figure 4-11 Comparison of hysteresis loop of xanthan gum 0.3 wt% with activated sludge (AS) 2.8 wt%</i>	84
<i>Figure 5-1 Schematic of experimental setup</i>	99
<i>Figure 5-2 The evolution of mixed area inside the reactor when the impeller speed is 75 rpm and concentration of NaCMC solution is 1%.</i>	108
<i>Figure 5-3 The evolution of mixed area inside the aerated reactor when the impeller speed is 75 rpm and concentration of NaCMC solution is 1%.</i>	109
<i>Figure 5-4 a) Mean mixing time and b) mean power consumption with error bars over impeller speed in different concentration of NaCMC solutions.</i>	112
<i>Figure 5-5 Comparison between the percentage of power consumption and percentage of enhancing mixing time.</i>	113

<i>Figure 5-6 Comparison between the mean gassed mixing time with error bars in both stirred and non-stirred conditions</i>	<i>114</i>
<i>Figure 5-7 a) Mean power curve and b) Power number (Np) vs. Reynolds number (Re) for a dual helical ribbon in five different rotational speeds for various concentrations of NaCMC.</i>	<i>116</i>
<i>Figure 5-8 Influence of gas injection on mean mixing time with error bars over power number (Np)</i>	<i>118</i>
<i>Figure 5-9 The role of bubble motion around the impeller on mean power consumption....</i>	<i>119</i>
<i>Figure 5-10 Influential interaction model parameters analysed by ANOVA test.....</i>	<i>123</i>
<i>Figure 6-1 Schematic of experimental setup</i>	<i>139</i>
<i>Figure 6-2 a) Schematic diagram of PIV system; and b) Real experimental setup.....</i>	<i>143</i>
<i>Figure 6-3 Schematic view of the reactor with dual helical ribbon impeller; a) MRF zones, b) mesh topology.</i>	<i>148</i>
<i>Figure 6-4 The model grid sensitivity analysis.....</i>	<i>149</i>
<i>Figure 6-5 Comparison of average velocities obtained from experiment and CFD simulation for the initial gas flowrates: a) 0.5 LPM and b) 2 LPM.</i>	<i>151</i>
<i>Figure 6-6 Comparison of the flow field and velocity magnitude between CFD simulation (left Image) and PIV measurements (right image); at a) 75 rpm, and b) 150 rpm.....</i>	<i>152</i>
<i>Figure 6-7 Bubble size distribution at rotational speed 25 rpm, column 2; 75 rpm, column 3; and 150 rpm, column 4.</i>	<i>155</i>
<i>Figure 6-8 Gas volume fraction profile at rotational speed 25, 75, and 150 rpm.</i>	<i>156</i>
<i>Figure 6-9 Flow field and velocity magnitude at rotational speeds 25, 75, and 150 rpm at two perpendicular positions of blades.....</i>	<i>158</i>
<i>Figure 6-10 Changes in effective viscosity based at rotational speeds 25, 75, and 150 rpm and two perpendicular blade positions.....</i>	<i>160</i>

LIST OF TABLES

<i>Table 1-1 Pros and cons of anaerobic digester</i>	1
<i>Table 1-2 Different types of industrial anaerobic digesters</i>	4
<i>Table 2-1 Commercial Non-Newtonian fluids applied as simulant in different papers (Wiedemann et al. 2017; Eshtiaghi et al. 2012)</i>	18
<i>Table 2-1 The correlation between ungasged and gassed systems reported in literature (Luong and Volesky 1979) (Michel and Miller 1962) (Shewale and Pandit 2006)</i>	30
<i>Table 3-1 The geometric configuration of the stirred system</i>	45
<i>Table 3-2 Variables applied in the optimization procedure of the impeller performance using RSM method</i>	50
<i>Table 4-1 Summary of previous studies that have used simulant fluids to mimic primary sludge (PS), activated sludge (AS), and digested sludge (DS).</i>	61
<i>Table 4-2 Popular non-Newtonian equations for rheological behaviour of sludge.</i>	66
<i>Table 4-3 Recommended xanthan gum concentrations for primary, activated and digested sludge of different TS%.</i>	78
<i>Table 4-4 Herschel-Bulkley parameters for primary, activated, and digested sludge.</i>	79
<i>Table 4-5 Model parameters for polymers of different concentrations.</i>	80
<i>Table 5-1 The geometric configuration of the stirred system</i>	100
<i>Table 5-2. The rheological parameters of NaCMC (M. Amirafatabi and Khiadani Mehdi 2019a).</i>	104
<i>Table 5-3 Variables used in RSM method to optimize the mixer performance and uncertainty analysis for different variables.</i>	106
<i>Table 5-4 Plan for ANOVA analysis</i>	120
<i>Table 5-5 Results of ANOVA test for Quadratic model</i>	121
<i>Table 6-1 The geometric configuration of the stirred system</i>	140
<i>Table 6-2. The rheological parameters of NaCMC (M. Amirafatabi and Khiadani Mehdi 2019a).</i>	141

Chapter 1: Introduction

1.1 Project rationale

A continuous increase in the generation and accumulation of solid waste is a crisis that threatens the future of the planet. Waste-to-energy processes can be used to manage and control solid waste, and to reuse, recover, and recycle natural resources. In recent years, biological treatment systems have become more popular as a means of degrading: wastewater; agricultural, municipal and food industry wastes; and plant residue, into organic and environmentally friendly products. Anaerobic digestion is an efficient process that degrades different types of organic solid waste into biosolids and biogas under oxygen free and warm conditions, which is an ideal environment for microorganism activities. Produced biogas typically contains around 50-75% methane, whereby it can be considered a carbon neutral and valuable source of renewable energy (Rasi, Läntelä, and Rintala 2011; Rasi, Veijanen, and Rintala 2007; Axelsson et al. 2012). The by-product of anaerobic process could be applied as a rich source of nutrients for agricultural and fertilizing purposes. Table 1-1 lists some benefits of anaerobic digesters from the environmental and economic standpoints.

Table 1-1 Pros and cons of anaerobic digester

Environmental Advantages	Economic Benefits
Elimination of landfill	Production of biogas as a renewable and carbon-neutral source of energy
Control and management of solid wastes	Reduction of the time needed for handling and moving manure
Elimination of odours	Creation of a source of income including biogas, electricity, and bio solids
Removal of pathogens	Reduction of water consumption
Protection of surface water and groundwater	

Chapter 1: Introduction

Production of compost

In initial stages of the digestion process, enzymes produced by hydrolytic microorganisms hydrolyse and decompose complex organic polymers into simple and soluble monomers. For instance, starch molecules are broken into glucose, carbohydrates into sugars, proteins into amino acids, and lipids into fatty acids. In the next stage of acidogenesis, fermentative bacteria convert products from hydrolysis stages into various types of volatile fatty acids (VFAs) such as butyric and propionic acids. Then, all volatile fatty acids are converted to hydrogen, acetate, and carbon dioxide by acetogenic bacteria. Finally, all products are converted into methane and bio solids. The digestion processes have been summarized in Fig. 1-1.

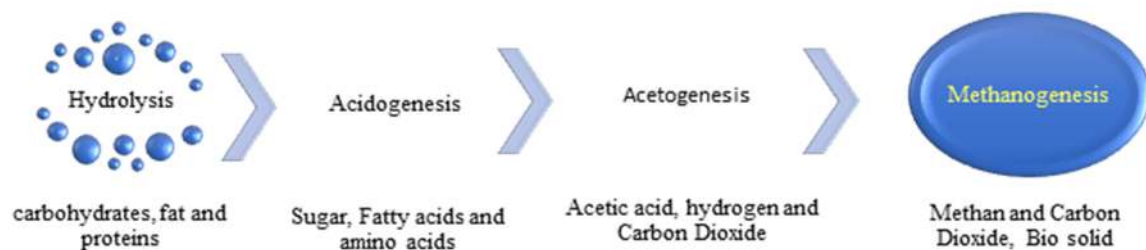


Figure 1-1 Different stages of the anaerobic digestion process

Since all these stages occur under microbial dependent reactions, some factors including pH level, temperature, and nutrient concentration have the maximum impact on the yield of bioreactor and quality and composition of the end products (Tira, Padang, and Supriadi 2019; Cioabla et al. 2012). Some of bio digestion steps contain the rate-limiting reactions. The first two stages (hydrolysis and acidogenesis) shown in Fig. 1-1 are the fastest, however, they are the most sensitive ones to pH level, initial substrate concentration and temperature changes. Several novel multi-stage bioreactors have been recently designed and built. In some of them, hydrolysis and acidogenesis reactions occur in the first bioreactor, while acetogenesis and methanogenesis processes take place in the second digester. Most industrial full-scale reactors (around 95% of the plants in Europe) are still single stage, which means that all of the reactions (ranging from hydrolysis to methanogenesis) take place in one stage at the same time (Nagao et al. 2012; Zhang et al. 2014).

The design and configuration of anaerobic digesters determines efficiency, conversion rate, and capital costs of the plant (Vilms Pedersen et al. 2020; Kumar and Ramanathan 2020; Irizar 2020). Bioprocess inside anaerobic digesters is severely affected by the hydrodynamics of a

Chapter 1: Introduction

system, which is governed by size, type, and design of the impeller. An ideal anaerobic digester should be able to produce a maximum volume of methane in a minimum size reactor. Reactor shape should comply with construction practices related to both heat loss and mixing pattern.

Typically, the configuration of engineered digesters is classified into three categories: completely mixed digesters, plug flow digesters and fixed film digesters. The characteristics of these digesters are illustrated in Figure 1-2 and summarized in Table 1-2.

This research focuses on the completely mixed digester, which is the conventional and most commonly used system and is suitable for all climate conditions and most types of wastewater (Roos, Martin Jr., and Moser 2004).

Figure 1-2 Different types of anaerobic digester <https://farm-energy.extension.org/types-of-anaerobic-digesters/>

Having a proper mixing pattern is essential in an anaerobic digester to (i) achieve adequate contact between substrate and microorganism (ii) release trapped bubbles, (iii) prevent solid sedimentation and scum formation, and (iv) to create a homogenous environment for bacterial growth (Ward et al. 2008). Poor mixing leads to sludge thickening, non-uniformity of pH and

Chapter 1: Introduction

temperature, short circuiting levels, aggregation, high energy consumption and finally, failure of the system. To overcome poor mixing efficiency, oversizing the digester would be necessary for industries which increases unnecessary capital cost of plant (Bhattacharjee et al. 2015).

Table 1-2 Different types of industrial anaerobic digesters

Reactor Types	Characteristics
Completely Mixed	<ul style="list-style-type: none">- Equal inflow and outflow rate- Retention time is more than 20 days- Requires mixing- Manure percentage is about 3-13% by solid mass
Plug Digester	<ul style="list-style-type: none">- Equal inflow and outflow rate- Retention time is less than 15 days- Mixing not necessary- Manure percentage is about 10-20% by solid mass
Fixed Film Digester	<ul style="list-style-type: none">- It is a column packed reactor containing small wood chips or plastic rings- Retention time is less than 5 days- Mixing not necessary- Manure percentage is about 1-5% by solid mass

Operating a digester at maximum efficiency is the ideal goal, which may be achieved by combining various mixing methods and evaluating the hydraulics of a system. In practice, mixing can progress through three different methods, including installing internal multiple impellers (Stroot et al. 2001; Gómez et al. 2006; Karim et al. 2005), recirculating biogas through the sparger (Bobade et al. 2017; Vesvikar and Al-Dahhan 2016; Bassani et al. 2017), and recirculating the substrate (Low et al. 2017; S. Kennedy et al. 2014; Meister et al. 2018; Ratanatamskul and Saleart 2016; Bhattacharjee et al. 2015).

Increasing impeller rotational speed appears as a good way for enhancing the mixing pattern of bioreactors; however, excessive power uptake and failure of microbial activity are the main drawbacks of high rotational speed. Some research has noted that microorganisms are

Chapter 1: Introduction

extremely shear-sensitive (Lamberto et al. 1996). Additionally, some studies indicate that excessive mixing may reduce biogas production and mass transfer due to decreasing the gas hold up (Stroot et al. 2001; Gómez et al. 2006; De Bok, Plugge, and Stams 2004). Sindall et al., (2013) has reported a significant drop in biogas production and counterproductivity as the intensity of mixing exceeds thresholds (Stroot et al. 2001; Sindall, Bridgeman, and Carliell-Marquet 2013).

Although applying the coaxial mixer in a bioreactor seems to be highly efficient, the shear-thinning characteristics of working fluid acts negatively (Kazemzadeh et al. 2016; Pakzad et al. 2012, 2013; Bonnot et al. 2007). The main drawback of using coaxial impellers is rotating two impellers with a central shaft at the same speed. Recently, multi-shaft impellers rotating in different speeds and directions have become favourable in literature, for dispersion and mixing of non-Newtonian fluids and emulsification (Kazemzadeh et al. 2016; Pakzad et al. 2012, 2013; Bonnot et al. 2007). High power consumption is the main disadvantage of using multi-impeller systems in industry (Kazemzadeh et al. 2016; Pakzad et al. 2012, 2013; Bonnot et al. 2007).

Additionally, there are some complex close-clearance single-shaft impellers, including helical ribbon, anchor, and screw, that have rarely been studied in the literature. Some close-clearance impellers are illustrated and demonstrated in Fig. 1-3. The helical ribbon is one of the most efficient impellers applied in agitated bioreactors containing non-Newtonian fluids, while the anchor is not a popular impeller in the industry because of its low efficiency (Anne-Archard, Marouche, and Boisson 2006; Doraiswamy, Grenville, and Etchells 1994). The high efficiency of using a dual helical ribbon in biogas production in an anaerobic digester has been reported in the literature (Lebranchu et al. 2017).

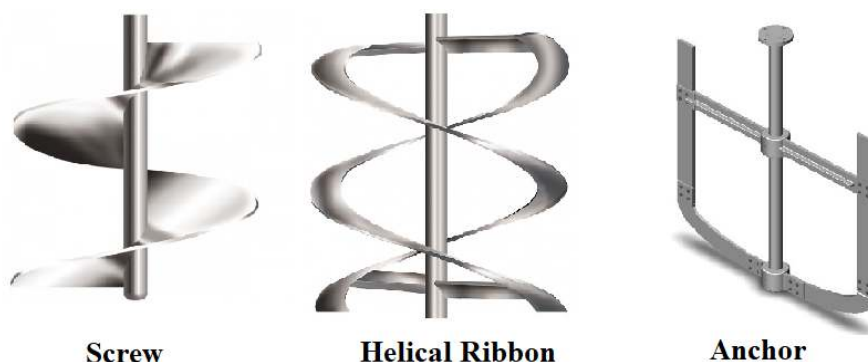


Figure 1-3 Different types of close-clearance impellers

According to the author's knowledge, the hydrodynamics of a multi-phase bioreactor equipped with a dual helical ribbon has been rarely studied. This occurs because hydrodynamic

Chapter 1: Introduction

visualization methods have been unsuccessful in an anaerobic digester due to the opaque nature of sludge. This explains why most researchers have considered hydrodynamics of a digester as a 'black box', and have focused on simulation and mathematical modelling of sludge behaviour as a non-Newtonian fluid (Meroney and Colorado 2009; Delafosse et al. 2014; Samstag et al. 2016; Craig, Nieuwoudt, and Niemand 2013; B. Wu 2010, 2011). Although extensive CFD simulations have been carried out on the performance of close-clearance impellers in single-phase shear-thinning liquids, there is yet to be a study working on bubble size and distribution in multiphase bioreactors equipped with a helical ribbon impeller.

In some studies, different approaches have been applied to visualize phases trajectory inside a multiphase bioreactor. Some of these methods are chemical tracer, Computer Automated Radioactive Particle Tracking (CARPT), Electrical Resistivity Tomography (ERT), shadow imaging, Laser Doppler Velocimeter (LDV), and Particle Image Velocimetry (PIV) (Wiedemann et al. 2017; Siverts-Wong et al. 2017; Pakzad, Ein-Mozaffari, and Chan 2008; Low et al. 2018; S. Kennedy et al. 2014; S. Kennedy, Bhattacharjee, and Eshtiaghi 2015; S. Kennedy et al. 2018; S. Kennedy 2017; Karim, Thoma, and Al-Dahhan 2007; Karim et al. 2005; Babaei, Bonakdarpour, and Ein-Mozaffari 2015; Houari Ameer, Bouzit, and Helmaoui 2011). The current study applies an optically transparent fluid to mimic the behaviour of real sludge. To investigate the bubbly flow pattern inside the reactor under agitation, high speed camera and PIV technique as well as CFD-PBM modelling approach have been applied.

To analyse the hydrodynamics of an agitated gas-liquid anaerobic digester, several critical factors should be separately studied including the rotational speed of the impeller, gas flow rate, the impeller distance from the base of the reactor, and rheological characteristics of a shear thinning fluid. The impacts of these factors on performance of bioreactor have been evaluated by measuring the mixing time and power consumption. Image processing technique will be used to assess the impacts of the aforementioned parameters on mixing performance and hydrodynamics of the fluid. In addition, optimal mixing time and power consumption, as well as the relation between these factors, have been explored by response surface methodology (RSM).

Finally, experimental results have been compared to the outcomes predicted by a combination of computational fluid dynamics (CFD) and population balance model (PBM) methods. The simulation results have been validated by data collected through particle image velocimetry (PIV) as a non-intrusive laser optical measurement technique.

Chapter 1: Introduction

1.2 Scope, significance, and objectives

The significance of this project is underpinned by the need for an appropriate understanding of multiphase non-Newtonian flow hydrodynamics inside an agitated anaerobic digester. Information from this research can be of significant value to industries and researchers in the field of design and operation of bioreactors. Project deliverables include scientific publications at various stages and detailed descriptions of the overall research in a PhD thesis.

Some objectives of this research project are classified as follows:

1. Analysis and investigation of pH sensitivity, stability, Zeta potential, and rheological characteristics of four polymers to select a clear, safe, stable, and cheap alternative for sludge.
2. Comparing the viscoelasticity, thixotropy and flow curve of simulant polymers to primary, activated, and digested sludge.
3. Evaluating the rheological characteristics of sludge and its effects on mixing.
4. Analyzing the power uptake and mixing time required by a dual helical ribbon impeller under different operating conditions including impeller speed, gas flow rate, and various concentration. Then, rotational speed can be optimized based on the power curve (a correlation between gas flow number and power number).
5. Identifying the threshold level of impeller rotational speed considering economic mixing in a shorter period of time.
6. Understanding the impacts of gas flow rate and dispersion on mixing time and power consumption.
7. Optimizing the operating conditions in a mixed two-phase reactor to maximize the mixing performance of a dual helical ribbon impeller.
8. Applying RSM techniques to understand how critical operating parameters, including, rotational speed, the viscosity of working fluid and gas flow rate, influence the reactor performance and correlate with each other.
9. Applying experimental investigation and CFD-PBM modelling to analyze the hydrodynamic characteristics including velocity field, viscosity gradient, bubble size

Chapter 1: Introduction

and distribution, and flow pattern of a multiphase mixed bioreactor filled with non-Newtonian fluid equipped with a dual helical ribbon impeller.

This study seeks to address the following research questions which will help to respond to the aforementioned research gaps:

1. Which simulant polymers emulate the rheological behaviour of sludge under a specific shear stress range? To examine the general hypothesis of whether clear model fluids can mimic the rheological behaviour of sludge.
2. How do rheological characteristics of sludge change the mixing pattern in a bioreactor?
3. Amongst liquid viscosity, rotational speed, and gas flow rate, which factor/element has the most influence on mixing time and power consumption, and how are these critical factors interlinked?
4. How do gas flow rate and dispersion reduce viscosity and enhance the mixing pattern in a mixing vessel using a dual helical ribbon impeller?
5. Can CFD modelling successfully predict hydrodynamic characteristics of simulant polymers that can be used to emulate the rheological behaviour of sludge?

1.3 Thesis outline

Chapter 1 provides an overview of the thesis and takes the form of seven chapters, including this introductory chapter.

Chapter 2 lays out the theoretical dimensions of the research and provides a comprehensive literature review. This chapter begins by examining basic concepts of complex rheological characteristics of sludge as a non-Newtonian fluid, along with several limitations in experimental studies of sludge. The chapter will then explain the theoretical concept of mechanical mixing, the definition of mixing time, power consumption, complicated interactions between agitated phases, the importance of size and distribution of bubbles, and three-dimensional CFD-PBM couple model theory.

Chapter 3 focused on the methodology and research design used in this study. The system configuration and geometric details, qualitative and quantitative methods, instruments, and modelling software applied in this study will also be explained.

Chapter 1: Introduction

Chapter 4 compares the rheological characteristics of different simulants offered within literature to primary, activated, and digested sludge. The results reveal that xanthan gum can be an ideal candidate which demonstrate the same rheological behaviour to activated sludge in terms of yield stress and viscosity due to their similar molecular and internal network structures. Further, xanthan gum follows the Herschel-Bulkley model, which is one of the most popular practical equations to represent sludge rheology. Additionally, the results indicate that NaCMC in some working conditions behaves like the digested sludge.

Chapter 5 discusses how a close-clearance impeller can increase the active region and reduce the time and energy required to achieve the completely mixed system. The findings suggest that there is a threshold for the rotational speed of an impeller, beyond which power consumption increases exponentially whilst mixing time fails to be enhanced. Within this chapter, the impacts of gas flow rate on mixing process has been investigated. Finally, the statistical analysis indicates that impeller speed and viscosity have the maximum impact on mixing performance.

Chapter 6 verifies the results predicted by CFD simulation and compares them with the experimental data. CFD method is a feasible approach to understand the flow pattern inside an anaerobic digester, which is impossible to visualize using experimental techniques.

Chapter 7 draws upon the entire thesis to highlights the potential of using a helical ribbon impeller as an ideal type of agitator in an anaerobic digester. Additionally, this chapter has summarized the key conclusion from this thesis and recommended some points for further research.

1.4 References

Ameur, Houari, Mohamed Bouzit, and Mustapha Helmaoui. 2011. "Numerical Study of Fluid Flow and Power Consumption in a Stirred Vessel with a CABA 6SRGT Impeller." *Chemical and Process Engineering* 32 (4): 351–66. <https://doi.org/10.2478/v10176-011-0028-0>.

Anne-Archard, D., M Marouche, and H C Boisson. 2006. "Hydrodynamics and Metzner – Otto Correlation in Stirred Vessels for Yield Stress Fluids." *Chemical Engineering Journal* 125: 15–24. <https://doi.org/10.1016/j.cej.2006.08.002>.

Axelsson, Lisa, Maria Franzén, Madelene Ostwald, Göran Berndes, G. Lakshmi, and N. H. Ravindranath. 2012. "Perspective: Jatropha Cultivation in Southern India: Assessing Farmers' Experiences." *Biofuels, Bioproducts and Biorefining* 6 (3): 246–56. <https://doi.org/10.1002/bbb>.

Chapter 1: Introduction

Babaei, Roghayyeh, Babak Bonakdarpour, and Farhad Ein-Mozaffari. 2015. "The Use of Electrical Resistance Tomography for the Characterization of Gas Holdup inside a Bubble Column Bioreactor Containing Activated Sludge." *Chemical Engineering Journal* 268: 260–69. <https://doi.org/10.1016/j.cej.2015.01.042>.

Bassani, Ilaria, Panagiotis G. Kougiass, Laura Treu, Hugo Porté, Stefano Campanaro, and Irini Angelidaki. 2017. "Optimization of Hydrogen Dispersion in Thermophilic Up-Flow Reactors for Ex Situ Biogas Upgrading." *Bioresource Technology* 234: 310–19. <https://doi.org/10.1016/j.biortech.2017.03.055>.

Bhattacharjee, Pradipto K., Stephen Kennedy, Nicky Eshtiaghi, and Rajarathinam Parthasarathy. 2015. "Flow Regimes in the Mixing of Municipal Sludge Simulant Using Submerged, Recirculating Jets." *Chemical Engineering Journal* 276 (3145364): 137–44. <https://doi.org/10.1016/j.cej.2015.04.068>.

Bobade, Veena, Jean Christophe Baudez, Geoffery Evans, and Nicky Eshtiaghi. 2017. "Impact of Gas Injection on the Apparent Viscosity and Viscoelastic Property of Waste Activated Sewage Sludge." *Water Research* 114: 296–307. <https://doi.org/10.1016/j.watres.2017.02.039>.

Bok, F. A M De, C. M. Plugge, and A. J M Stams. 2004. "Interspecies Electron Transfer in Methanogenic Propionate Degrading Consortia." *Water Research* 38 (6): 1368–75. <https://doi.org/10.1016/j.watres.2003.11.028>.

Bonnot, S., F. Cabaret, L. Fradette, and P. A. Tanguy. 2007. "Characterization of Granular Mixing Patterns in a Fluid." *Chemical Engineering Research and Design* 85: 1129–35. <https://doi.org/10.1205/cherd06215>.

Cioabla, Adrian Eugen, Ioana Ionel, Gabriela Alina Dumitrel, and Francisc Popescu. 2012. "Comparative Study on Factors Affecting Anaerobic Digestion of Agricultural Vegetal Residues." *Biotechnology for Biofuels* 5 (1): 1. <https://doi.org/10.1186/1754-6834-5-39>.

Craig, K. J., M. N. Nieuwoudt, and L. J. Niemand. 2013. "CFD Simulation of Anaerobic Digester with Variable Sewage Sludge Rheology." *Water Research* 47 (13): 4485–97. <https://doi.org/10.1016/j.watres.2013.05.011>.

Delafosse, Angélique, Marie Laure Collignon, Sébastien Calvo, Frank Delvigne, Michel Crine, Philippe Thonart, and Dominique Toyé. 2014. "CFD-Based Compartment Model for Description of Mixing in Bioreactors." *Chemical Engineering Science* 106: 76–85. <https://doi.org/10.1016/j.ces.2013.11.033>.

Doraiswamy, Deepak, Richard K Grenville, and Arthur W Etchells I. 1994. "Two-Score Years of the Metzner-Otto Correlation" 0323: 2253–58. <https://doi.org/10.1021/ie00034a001>.

Gómez, X., M. J. Cuetos, J. Cara, A. Morán, and A. I. García. 2006. "Anaerobic Co-Digestion of Primary Sludge and the Fruit and Vegetable Fraction of the Municipal Solid Wastes. Conditions for Mixing and Evaluation of the Organic Loading Rate." *Renewable Energy* 31 (12): 2017–24. <https://doi.org/10.1016/j.renene.2005.09.029>.

Hamilton, Douglas W, and M Charles Gould. 2012. "Types of Anaerobic Digesters (Module 3)." US EPA. <https://www.epa.gov/anaerobic-digestion/types-anaerobic-digesters%0Ahttp://fyi.uwex.edu/biotrainingcenter/>.

Chapter 1: Introduction

Irizar, Ion. 2020. "A Mathematical Framework for Optimum Design and Operation of SBR Processes." *Journal of Water Process Engineering*, no. June: 101703. <https://doi.org/10.1016/j.jwpe.2020.101703>.

Karim, Khursheed, Rebecca Hoffmann, K Thomas Klasson, and M H Al-dahhan. 2005. "Anaerobic Digestion of Animal Waste: Effect of Mode of Mixing" 39: 3597–3606. <https://doi.org/10.1016/j.watres.2005.06.019>.

Karim, Khursheed, Gregory J. Thoma, and Muthanna H. Al-Dahhan. 2007. "Gas-Lift Digester Configuration Effects on Mixing Effectiveness." *Water Research* 41 (14): 3051–60. <https://doi.org/10.1016/j.watres.2007.03.042>.

Kazemzadeh, Argang, Farhad Ein-Mozaffari, Ali Lohi, and Leila Pakzad. 2016. "A New Perspective in the Evaluation of the Mixing of Biopolymer Solutions with Different Coaxial Mixers Comprising of Two Dispersing Impellers and a Wall Scraping Anchor." *Chemical Engineering Research and Design* 114: 202–19. <https://doi.org/10.1016/j.cherd.2016.08.017>.

Kennedy, Stephen. 2017. "Improving the Mixing Performance of Anaerobic Digesters in Wastewater Treatment."

Kennedy, Stephen, Pradipto K Bhattacharjee, Sati N Bhattacharya, Nicky Eshtiaghi, and Rajarathinam Parthasarathy. 2018. "Control of the Mixing Time in Vessels Agitated by Submerged Recirculating Jets Subject Category: Subject Areas:"

Kennedy, Stephen, Pradipto K Bhattacharjee, and Nicky Eshtiaghi. 2015. "Submerged, Recirculating Jets: Nozzle Geometry and Its Effect on Active Volume Creation in the Mixing of Municipal Sludge Simulant 1 Introduction 2 Methodology" c (3145323): 2236–41.

Kennedy, Stephen, Rajarathinam Parthasarathy, Nicky Eshtiaghi, and Sati Bhattacharya. 2014. "Liquid Jet Recirculation in a Model Digester: Flow Characteristics." In, 1–7.

Kumar, Alok, and Anand Ramanathan. 2020. "Design of an Agitator in the Anaerobic Digester for Mixing of Biomass Slurry." *Materials Today: Proceedings*, no. xxxx. <https://doi.org/10.1016/j.matpr.2020.08.011>.

Lamberto, D. J., F. J. Muzzio, P. D. Swanson, and A. L. Tonkovich. 1996. "Using Time-Dependent RPM to Enhance Mixing in Stirred Vessels." *Chemical Engineering Science* 51 (5): 733–41. [https://doi.org/10.1016/0009-2509\(95\)00203-0](https://doi.org/10.1016/0009-2509(95)00203-0).

Lebranchu, Aline, Stéphane Delaunay, Philippe Marchal, Fabrice Blanchard, Stéphane Pacaud, Michel Fick, and Eric Olmos. 2017. "Impact of Shear Stress and Impeller Design on the Production of Biogas in Anaerobic Digesters." *Bioresource Technology* 245: 1139–47. <https://doi.org/10.1016/j.biortech.2017.07.113>.

Low, Siew Cheng, Douglas Allitt, Nicky Eshtiaghi, and Rajarathinam Parthasarathy. 2018. "Measuring Active Volume Using Electrical Resistance Tomography in a Gas-Sparged Model Anaerobic Digester." *Chemical Engineering Research and Design* 130: 42–51. <https://doi.org/https://doi.org/10.1016/j.cherd.2017.11.039>.

Low, Siew Cheng, Nicky Eshtiaghi, Li Shu, and Rajarathinam Parthasarathy. 2017. "Flow Patterns in the Mixing of Sludge Simulant with Jet Recirculation System." *Process Safety and Environmental Protection* 112: 209–21. <https://doi.org/10.1016/j.psep.2017.08.016>.

Chapter 1: Introduction

Meister, Michael, Massoud Rezavand, Christian Ebner, Thomas Pümpel, and Wolfgang Rauch. 2018. "Mixing Non-Newtonian Flows in Anaerobic Digesters by Impellers and Pumped Recirculation." *Advances in Engineering Software* 115 (October 2017): 194–203. <https://doi.org/10.1016/j.advengsoft.2017.09.015>.

Meroney, Robert N., and P. E. Colorado. 2009. "CFD Simulation of Mechanical Draft Tube Mixing in Anaerobic Digester Tanks." *Water Research* 43 (4): 1040–50. <https://doi.org/10.1016/j.watres.2008.11.035>.

Nagao, Norio, Nobuyuki Tajima, Minako Kawai, Chiaki Niwa, and Norio Kurosawa. 2012. "Bioresource Technology Maximum Organic Loading Rate for the Single-Stage Wet Anaerobic Digestion of Food Waste." *BIORESOURCE TECHNOLOGY* 118: 210–18. <https://doi.org/10.1016/j.biortech.2012.05.045>.

Pakzad, Leila, Farhad Ein-Mozaffari, and Philip Chan. 2008. "Measuring Mixing Time in the Agitation of Non-Newtonian Fluids through Electrical Resistance Tomography." *Chemical Engineering and Technology* 31 (12): 1838–45. <https://doi.org/10.1002/ceat.200800362>.

Pakzad, Leila, Farhad Ein-Mozaffari, Simant R. Upreti, and Ali Lohi. 2013. "Characterisation of the Mixing of Non-Newtonian Fluids with a Scaba 6SRGT Impeller through Ert and CFD." *Canadian Journal of Chemical Engineering* 91 (1): 90–100. <https://doi.org/10.1002/cjce.21616>.

Pakzad, Leila, Farhad Ein-mozaffari, Simant R Upreti, and Ali Lohi. 2012. "Chemical Engineering Research and Design Agitation of Herschel – Bulkley Fluids with the Scaba – Anchor Coaxial Mixers." *Chemical Engineering Research and Design* 91 (5): 761–77. <https://doi.org/10.1016/j.cherd.2012.09.008>.

Rasi, S., J. Lântelä, and J. Rintala. 2011. "Trace Compounds Affecting Biogas Energy Utilisation - A Review." *Energy Conversion and Management* 52 (12): 3369–75. <https://doi.org/10.1016/j.enconman.2011.07.005>.

Rasi, S., A. Veijanen, and J. Rintala. 2007. "Trace Compounds of Biogas from Different Biogas Production Plants." *Energy* 32 (8): 1375–80. <https://doi.org/10.1016/j.energy.2006.10.018>.

Ratanatamskul, Chavalit, and Tawinan Saleart. 2016. "Effects of Sludge Recirculation Rate and Mixing Time on Performance of a Prototype Single-Stage Anaerobic Digester for Conversion of Food Wastes to Biogas and Energy Recovery." *Environmental Science and Pollution Research* 23 (8): 7092–98. <https://doi.org/10.1007/s11356-015-4448-0>.

Roos, K.F., J.B. Martin Jr., and M.A. Moser. 2004. "A Manual For Developing Biogas Systems at Commercial Farms in the United States." *AgSTAR Handbook*, 70. <http://nepis.epa.gov/Exe/ZyPDF.cgi/P1008VFM.PDF?Dockey=P1008VFM.PDF>.

Samstag, R. W., J. J. Ducoste, A. Griborio, I. Nopens, D. J. Batstone, J. D. Wicks, S. Saunders, E. A. Wicklein, G. Kenny, and J. Laurent. 2016. "CFD for Wastewater Treatment: An Overview." *Water Science and Technology* 74 (3): 549–63. <https://doi.org/10.2166/wst.2016.249>.

Sindall, R., J. Bridgeman, and C. Carliell-Marquet. 2013. "Velocity Gradient as a Tool to Characterise the Link between Mixing and Biogas Production in Anaerobic Waste Digesters." *Water Science and Technology* 67 (12): 2800–2806. <https://doi.org/10.2166/wst.2013.206>.

Chapter 1: Introduction

Siverts-Wong, Elena, Taira Newman, Tom Chapman, and Chein-Chi Chang. 2017. "Mixing and Transport." *Water Environment Research* 89 (10): 1503–16. <https://doi.org/10.2175/106143017X15023776270548>.

Stroot, P G, K D McMahon, R I Mackie, and L Raskin. 2001. "Anaerobic Codigestion of Municipal Solid Waste and Biosolids under Various Mixing Conditions - II: Microbial Population Dynamics." *Water Research* 35 (7): 1804–16. [https://doi.org/10.1016/S0043-1354\(00\)00439-5](https://doi.org/10.1016/S0043-1354(00)00439-5).

Tira, Hendry Sakke, Yesung Allo Padang, and Supriadi. 2019. "Effect of Acidity Level of Substrate by Lime Water and Acetic Acid Addition on Biogas Production." *AIP Conference Proceedings* 2114 (June). <https://doi.org/10.1063/1.5112477>.

Vesvikar, Mehul S., and Muthanna Al-Dahhan. 2016. "Hydrodynamics Investigation of Laboratory-Scale Internal Gas-Lift Loop Anaerobic Digester Using Non-Invasive CAPRT Technique." *Biomass and Bioenergy* 84: 98–106. <https://doi.org/10.1016/j.biombioe.2015.11.014>.

Vilms Pedersen, S., J. Martí-Herrero, A. K. Singh, S. G. Sommer, and S. D. Hafner. 2020. "Management and Design of Biogas Digesters: A Non-Calibrated Heat Transfer Model." *Bioresource Technology* 296 (October 2019): 122264. <https://doi.org/10.1016/j.biortech.2019.122264>.

Ward, Alastair J., Phil J. Hobbs, Peter J. Holliman, and David L. Jones. 2008. "Optimisation of the Anaerobic Digestion of Agricultural Resources." *Bioresource Technology* 99 (17): 7928–40. <https://doi.org/10.1016/j.biortech.2008.02.044>.

Wiedemann, Leonhard, Fosca Conti, Tomasz Janus, Matthias Sonnleitner, Wilfried Zörner, and Markus Goldbrunner. 2017. "Mixing in Biogas Digesters and Development of an Artificial Substrate for Laboratory-Scale Mixing Optimization." *Chemical Engineering and Technology* 40 (2): 238–47. <https://doi.org/10.1002/ceat.201600194>.

Wu, Binxin. 2010. "CFD Simulation of Gas and Non-Newtonian Fluid Two-Phase Flow in Anaerobic Digesters." *Water Research* 44 (13): 3861–74. <https://doi.org/10.1016/j.watres.2010.04.043>.

Zhang, Cunsheng, Haijia Su, Jan Baeyens, and Tianwei Tan. 2014. "Reviewing the Anaerobic Digestion of Food Waste for Biogas Production." *Renewable and Sustainable Energy Reviews* 38: 383–92. <https://doi.org/10.1016/j.rser.2014.05.038>.

Chapter 2: Literature review

2.1 Background

In recent years, handling the large quantity of agricultural, municipal, and industrial organic wastes has been a challenge for waste management authorities. Since the global urban population has grown at a very rapid pace, governments are obliged by environmental regulators to establish efficient and adequate waste treatment facilities. Different conventional waste management techniques like physical, chemical, and biological methods have been widely used in wastewater treatment plants. Physical techniques including sedimentation, screening and filtration are processes where no chemical material or biological activity is involved. When a chemical material is added to the process of treatment or a chemical reaction takes place, the process is classified as a chemical method (e.g. ozonation, coagulation and ion exchange). In a biological process, contaminants are removed by microbial activities in lagoons, and in aerobic and anaerobic digesters.

Due to the better safety, less cost, and environmental sustainability, biological treatment methods have been very popular. Experimental limitation, complex physical and chemical characteristics of sludge, expensive analytical instrument, and complicated hydrodynamics of a multiphase flow lead to much uncertainty about the process and hydrodynamics of biological units.

Non-homogenous distribution of temperature, pH, nutrient and substrate is increasingly recognised as a serious concern which may lead to the bioreactors failure (Houari Ameer, Bouzit, and Ghenaïm 2013; Delafosse et al. 2014; Curry and Pillay 2012). Mechanical mixing

Chapter 2: Literature review

is used as an effective technique to make biological system homogenous and improve distribution of both nutrients and buffering agents while preventing production of metabolic by-products (Forster-Carneiro, Pérez, and Romero 2008; Singh, Szamosi, and Siménfalvi 2019, 2020). Additionally, sparging gas has been reported as an another efficient mixing technique which has significant effect on velocity fields and hydrodynamics pattern (Anne-Archard, Marouche, and Boisson 2006). Improved mixing pattern would stop the solid particles from settling and forming a thick unmixed zone. Poor mixing leads to the failure of the digester due to the formation of viscous and stagnant regions (Low et al. 2013; Curry and Pillay 2012). A proper mixing method increases stability and productivity of process, prevents sludge from floating (scum) and settling (sediments), and drives produced biogas out of the substrate (Kariyama, Zhai, and Wu 2018).

The hydraulic regime in the bioreactor is controlled by different parameters including size and shape of the vessel, type of mixer, and substrate rheology. Agitation changes the rheology and hydrodynamic of the sludge which can affect the performance of bioreactor. Several researchers have used different visualization methods like computer automated radioactive particle tracking (CARPT) (Karim, Thoma, and Al-Dahhan 2007) and electrical residence (Babaei, Bonakdarpour, and Ein-Mozaffari 2015) to evaluate the hydrodynamics of sludge. Due the experimental limitations, only average figures for hydrodynamic properties (e.g. mean liquid velocity and gas holdup) were obtained from visualization studies (Ratanatamskul and Saleart 2016; Hui, Bennington, and Dumont 2009). Further, a few research have used computer and numerical models to simulate liquid hydrodynamic behaviour (Vesvikar and Al-Dahhan 2015).

Recently some studies have applied transparent non-Newtonian liquids with the hope that they can mimic sludge rheological behaviour (Eshtiaghi et al. 2012; Wiedemann et al. 2017). This method provided an opportunity to understand the flow field and streams inside the digester.

Chapter 2: Literature review

Generally, fluid can be visualized using optical measurement techniques such as shadow imaging, Laser Doppler Velocimeter (LDV), Electrical Resistivity Tomography (ERT), and Particle Image Velocimetry (PIV) (Wiedemann et al. 2017; Siverts-Wong et al. 2017; Pakzad, Ein-Mozaffari, and Chan 2008; S. Kennedy et al. 2014; S. Kennedy, Bhattacharjee, and Eshtiaghi 2015; S. Kennedy et al. 2018; S. Kennedy 2017; Houari Ameer, Bouzit, and Helmaoui 2011).

To sum up, impeller shape, size and rotational speed, gas flow rate, and rheological properties of fluids are considered as the most influential factors which can change the hydrodynamics of bioreactors (Paul, Atiemo-obeng, and Kresta 2004; Crawford and Crawford 2006). Collectively, experimental studies outline a critical role of mixing in the performance of bioreactors (Lindmark et al. 2014). To examine the aims and objectives described in the previous chapters, a transparent simulant liquid should be selected as a working fluid, due to the complexity of pseudoplastic materials including different types of sludge as a time dependent fluid. Therefore, this study will employ different transparent non-Newtonian materials as clear simulant to visualise the hydrodynamics of system. As the rheological characteristics of pseudoplastic fluids and hydrodynamics of system are linked together, this work will investigate both characteristics at the same time.

The focus of this work is to investigate the performance and hydrodynamics of an agitated multiphase anaerobic digester equipped with a dual helical ribbon impeller. To maximize the mixing performance, it is necessary to optimize operating conditions whereas mixing process occurs in a minimum time with lowest energy input. Hydrodynamics of an agitated anaerobic digester will be examined and optimized through experimental, statistical, and modelling methods to broaden detailed knowledge of mixing process in bioreactor.

Chapter 2: Literature review

2.2 Sludge

Sludge is a form of fluid containing different types of organic wastes, microorganisms, protozoa, solids, and agglomerated particles resulting in thixotropic behaviour (Bhattacharjee et al. 2015; Baudez et al. 2013, 2011; Holliger et al. 2016). Accordingly, the rheological characteristics of sludge have been considered an influential factor in the design, sizing, and performance of bioreactors (Bhattacharjee et al. 2015; Baudez et al. 2013, 2011; Holliger et al. 2016). Increasing the shear rate affects the internal structure of a thixotropic fluid and viscosity would drop consequently. Due to lower viscosity, handling the sheared sludge is much easier than unmixed sludge (Ruiz-Hernando, Labanda, and Llorens 2015). In addition, viscosity would drop by increasing temperature levels or decreasing the solid contents (Farno, Parthasarathy, and Eshtiaghi 2015; Ratkovich et al. 2013; Tixier, Guibaud, and Baudu 2003). Sludge granulation process is divided into two different stages: nucleation and maturation (Jing Wu et al. 2009). Nucleation is the initial and core phase of sludge flocculation, and it is closely related to the hydrodynamics of system. Nucleation process under optimum shear rates is faster than nucleation process under weak shear rates since heat and nutrient would be distributed uniformly under optimum operating conditions. When shear rate goes beyond the threshold level of mixing, poor nucleation would occur, and extracellular protein segregation would happen in sludge (Kaparaju et al. 2008). Additionally, mixing can prevent the short-circuiting and settlement of solid materials and particles inside a digester (Jing Wu et al. 2009). Most of the granules formed are particles with a diameter between 0.1-0.6 mm. Average diameter (ASD) and nucleus ratio (NR) of particles are two important factors for characterising sludge rheological behaviour (Jing Wu et al. 2009).

Chapter 2: Literature review

2.2.1 Working fluid

Optimizing the design and operation of a bio-digester is important to reduce the running cost and increase the biogas production rate. Further, the sludge mixing pattern can affect the total energy consumption in biodigester (Wiedemann et al. 2017). Studying the mixing pattern inside the bioreactor can be challenging and impractical, since the opaque nature of sludge limits the visualising the flow behaviour inside the digester. Therefore, transparent substances with similar rheological behaviour to real sludge may provide reliable information about the digester. Some of these clear model fluids and their main applications are summarized in Table 2-1.

It should be noted that there is a significant knowledge gap regarding the efficiency and the productivity of the mixing pattern inside bioreactor. Fluid rheological behaviour in an agitated digester is vitally important as it can affect energy consumption and biogas production. Having a good understanding about behaviour of sludge during digestion process is essential to optimize the design factors, to maximize the productivity and to minimize the operational cost.

Table 2-1 Commercial Non-Newtonian fluids applied as simulant in different papers (Wiedemann et al. 2017; Eshtiaghi et al. 2012)

No.	Working Fluid	Application
1	Xanthan gum	Thickening agent
2	Ply Ethylene Glycol	Gel-forming
3	Sodium alginate	Gel-forming
4	Walocel 30000	Gel-forming
5	NaCMC	Gel-forming

2.3 Importance of mixing in digesters

Understanding the mixing process is important to design and operate of an anaerobic digester. An optimum mixing pattern is necessary to achieve uniform heat and nutrient transfer, to prevent settled and scum layers, to maximise the suspension of solids, and to enhance microbial

Chapter 2: Literature review

activity (Forster-Carneiro, Pérez, and Romero 2008; Singh, Szamosi, and Siménfalvi 2019, 2020). Although the mechanical mixer enhances biogas production in a digester, auxiliary methods of mixing including gas injection and recirculation of a part of substrate are suggested to obtain optimum performance (Turovskiy 2006). The effectiveness of mixing process can be evaluated through measuring the mixing time, energy consumed, volume of dead zone, forming the scum and settlement layers, and biogas production (Forster-Carneiro, Pérez, and Romero 2008; Singh, Szamosi, and Siménfalvi 2019, 2020).

2.3.1 Mechanical mixing

The mechanical mixer is an internal system that employs a rotating impeller, usually mounted at the centre or corner of a bioreactor. The performance of mechanical mixing depends on several factors such as power consumption, stirring speed, type and design of impeller, rheological characteristics of the fluid, and other operating conditions. Mechanical agitators, as the best method of mixing, can ensure high mixing efficiency and can disperse solid particles (Kariyama, Zhai, and Wu 2018). However, the most serious disadvantage of this method is high-power consumption. Ideally mixing power consumption is estimated at around 0.007 kW/m³, as based on the digester's volume (Metcalf & Eddy, George Tchobanoglous, H. David Stensel, Ryujiro Tsuchihashi 2003). To optimize the mixing process, it is essential to maintain a balance between short mixing time and power consumed by the impeller. However, there is a threshold level where beyond that the mixing process can negatively affects the biological activity and subsequently biogas production (Wiedemann et al. 2017; Kariyama, Zhai, and Wu 2018).

Impellers are the main mechanical devices responsible for mixing fluid in a bioreactor. Impeller blades transmit shear forces to nearby fluid, and gradually transfer shear alongside the stagnant parts of the fluid. Therefore, it can be concluded that impellers with different shapes will

Chapter 2: Literature review

generate different flow patterns inside stirring vessels. Various types of agitators, including turbine stirrers, propellers, crossbeams, frames, blade stirrers, pitched blades, anchors, intermigs, anchors, and helical ribbon impellers have been examined within the literature to determine an optimum shape, design and size (Kariyama, Zhai, and Wu 2018; Singh, Szamosi, and Siménfalvi 2019). These impellers differ from each other in terms of geometry, angle and number of blades, rotational speed, and the clearance from the wall and bottom of the tank. Some popular types of impellers previously studied have been demonstrated in Fig. 2-1.



Figure 2-1 Different types of impeller

Lebranchu et al. (2017) have studied the impact of impeller design on biogas production measuring by biogas production level. Both experimental and computational dynamic simulations were used to compare the impact of using a classical Rushton turbine with a dual helical ribbon on biogas production. The authors concluded that a dual helical ribbon increases the dispersion and uniformity of substrate that will lead to greater biogas production (Lebranchu et al. 2017). Subsequently, it is important to know that low speed scraping wall impellers, including anchor and helical ribbon forms, are the most effective types of mixers

Chapter 2: Literature review

inside bioreactors (Lebranchu et al. 2017). Dual helical ribbon impellers rotate with a low speed and can clean the vessel wall and return accumulated fluid to the centre of the reactor.

2.3.2 Gas-lift loop mixing

Hydrodynamics of multiphase gas-liquid system including aerated reactors, gas-liquid bioreactors, and biogas recirculation in agitated anaerobic digesters have not been studied and discuss much in available literature. The injection of produced biogas, air, nitrogen, and other gases back into the reactor is a popular method for improving the efficiency of agitation and accelerating the reaction. Recycling the gas proportion offers advantages including higher reactor yield, lower power consumption and less shear stress and tension (Vesvikar and Al-Dahhan 2015). Some research has shown that injecting gas decreases the viscosity by inducing shear stress in working fluid (Meng et al. 2008; Bobade et al. 2018). A gas injection method applies a theory first suggested by Verhoff et. al (Verhoff, Tenney, and Echelberger 1974). Overall, there are two different types of biogas injections: confined and unconfined methods. In the confined method, a small part of a produced biogas is injected through the cylindrical tube at the top of the reactor. While in unconfined method the small amount of produced biogas is injected through diffuser pipes located at the bottom of reactor. In this proposed study, the unconfined method will be applied. According to this technique, the gas will be injected using a sparger located at the bottom of the tank.

Generally, the flow regime inside a stirred multiphase reactor can vary based on the impeller rotational speed and gas flow rate. Three different flow regimes can form, including flooding (F), loading (L), and complete dispersion (CD) (Paglianti, Pintus, and Giona 2000). Figure 2-2 (a) shows the flooding regime, where high gas flow rate or low impeller speed leads to inefficient mixing.

In this situation, the quickly rising gas bubbles are not affected by impeller speed. Loading regime can also be observed in Figure 2-2 (c), whereby decreasing gas flow rate or increasing

Chapter 2: Literature review

impeller velocity, the loading occurs. In this case, bubbles are trapped behind the blade and consequently accumulate. The most desired scenario is complete dispersion, where bubbles are evenly distributed. Figure 2-2 (b) represents the optimum impeller speed and gas flow rate leading to complete dispersion.

Figure 2-2 Gas-Liquid flow pattern in an agitated vessel; a) Flooding; b) Complete Dispersion; c) Loading (Paglianti, Pintus, and Giona 2000).
[https://doi.org/10.1016/S0009-2509\(00\)00125-1](https://doi.org/10.1016/S0009-2509(00)00125-1)

2.3.3 Mixing time

Uniformity of temperature, pH, nutrient, and substrate is the main targets of agitation within the industrial processes. Mixing time is a quantitative term that commonly defines the required time to achieve the maximum level of uniformity in agitated systems (Houari Ameer, Bouzit, and Ghenaim 2013). As mentioned above, inadequate, and poor mixing or over-mixing can lead to the failure of system and the death of microorganisms in bioreactors. Some literature

Chapter 2: Literature review

has defined mixing time as the recorded time to reach 95% of full homogeneity degree (Delafosse et al. 2014; Curry and Pillay 2012). Studies have indicated that impeller geometries have significant impact on mixing time. Dieulot et al. (2002) have investigated the impact of mixing time on improving the performance of agitation using a special type of helical ribbon impeller when a vessel is filled with a highly viscous fluid (Dieulot et al. 2002). Additionally, the authors determined that variable time-dependent rotational speed is more energy efficient than mixing at a constant speed.

To date, various methods have been developed and employed to measure mixing time including conductivity (Bouaifi and Roustan 2001), pH meter (Guillard, Trägårdh, and Fuchs 2000), coloured dye addition method and colorimetry (F. Cabaret, Fradette, and Tanguy 2008; Bobade et al. 2018), radioactive thermal tracing (Pant et al. 2015), and electrical resistance tomography (ERT)(Pakzad, Ein-Mozaffari, and Chan 2008).

This study follows available practical guidelines for titration techniques as a most popular method for measuring mixing time (Paul, Atiemo-obeng, and Kresta 2004). This method is non-intrusive and suitable for clear and pH resistant liquids.

2.4 Two distinctive regions

Based on the specific rheological characteristics of non-Newtonian fluids such as sludge, two distinctive volumes will form during agitation process: inactive and active volume. An ‘inactive volume’ is a region where fluid is stagnant and there is no specific contribution to chemical or biological activities (Bhattacharjee et al. 2015). In this region, settling of solids and particles may be observed. However, the region of ‘active volume’ is mobile, where maximum microbial and chemical activities can occur. To reach an optimum point with minimum costs and maximum efficiency, entire inactive regions should be converted into

Chapter 2: Literature review

active regions. This target may be achieved by improving agitation patterns through three different methods of mixing: recirculation, mechanical mixing, and gas sparging.

2.5 Shear rate

In this study, the maximum shear rate will be imposed on the fluid by the rotational part. However, rising gas bubbles can also cause deformation of the gel network structure. Therefore, it is essential to consider a combination of both gas shear rate (γ_g) and impeller shear

rate (γ_i) expressed as: $\dot{\gamma}_T = \sqrt{\gamma_g^2 + \gamma_i^2}$

Equation 2-1

$$\gamma_i = K_s N$$

Equation 2-2

In this equation, N is the rotational speed, γ_i refers to the effective shear rate, and K_s is the Metzner–Otto coefficient differing for each type of impeller (A. Metzner and Otto 1957).

Several studies have explored the factors to influence K_s . The literature offers contradictory findings regarding the relationship between these factors. Some research has indicated a significant positive correlation between flow index behaviour (n) which shows the degree of non-Newtonian characteristics of the fluid and K_s (Carreau, Chhabra, and Cheng 1993; Brito-De La Fuente, Choplin, and Tanguy 1997; Tanguy, Polytechnique, and Centre-ville 1996), whilst others have reported an inverse correlation between n and K_s (S. Nagata et al. 1970; Houska 1986).

There are many correlation in literature addressing a significant positive correlation between shear rates (γ_g) and superficial gas velocity (u_g) (Cheng and Carreau 1994; Al-Masry and Chetty 1998). The most common used equation for expressing the correlation between shear rates (γ_g) and superficial gas velocity (u_g) for non-Newtonian fluids and air interactions has been considered in this study.

Chapter 2: Literature review

$$\gamma_g = 1500u_g \quad \text{Equation 2-3}$$

2.6 Dimensionless numbers

Mixing patterns inside a tank may be evaluated by considering different dimensionless numbers including Froude number (Fr), power number (N_p), and Reynolds number (Re). These dimensionless numbers scale up the mixing process and correlate flow structures to impeller and vessel geometry. If we assume that gravity force is negligible, then only the Reynolds number and the Power number can be applied. Many researchers have calculated power consumption and heat transfer coefficient in a vessel equipped with a helical ribbon impeller operating in a laminar regime (Niedzielska and Kuncewicz 2005). A correlation between a Power number and Reynolds number for a Newtonian fluid inside a mixer has been suggested by Metzner and Otto, based on the flow regime (A. Metzner and Otto 1957). Accordingly, they considered Power number as a constant term in turbulent fluids (high Reynolds number), while for a laminar regime they demonstrated the power number to be reversely proportional to the Reynolds number.

$$N_p Re = K_p \quad \text{Equation 2-4}$$

whereas K_p refers the geometric factor related to geometry of the system. This equation has been widely applied within the literature.

The value of K_p has been widely reported in the literature for helical ribbon and other types of impellers. Novak and Rieger have reported $K_p=296$ for a dual helical ribbon installed in a cylindrical flat bottom vessel ($Re<60$, $d/D=0.95$, $H/D=1.1$)(Novak and Rieger 1975). $K_p=351.1$ has been calculated for a flat bottom cylindrical vessel equipped with a helical ribbon impeller ($d/D=0.937$, $H/D=1$)(Takahashi, Arai, and Saito 1980). Rieger et al. have reported $K_p=276.6$ for a dual helical ribbon installed in a cylindrical flat bottom vessel ($Re<20$, $d/D=0.89$, $H/D=1$)(Rieger, Novak, and Dagmar 1986).

Chapter 2: Literature review

Further, Metzner and Otto (1957) have defined two concepts including effective viscosity and shear stress in order to generalize this equation for shear-thinning fluids (A. Metzner and Otto 1957). The correlation between effective shear stress and viscosity can be obtained for a vessel filled with non-Newtonian fluid equipped with a dual helical ribbon impeller in a laminar flow regime $\eta(\dot{\gamma}_i)$. Effective viscosity is the viscosity of a Newtonian fluid which consume the same power as a non-Newtonian system. Therefore, in the case of using a non-Newtonian fluid, the Reynolds number should be calculated based on the effective viscosity, after which Equation 2-5 should be substituted in.

2.6.1 Reynolds number (Re)

While a turbulent mixing mechanism is defined based on highly energetic eddies imposed on the fluid body, a laminar mixing regime is related to a folding, breaking, and stretching system. Hence, laminar flow is a favourable flow pattern in most biological systems. Reynolds number, as the ratio of internal to viscous forces, is the best method to distinguish between different flow regimes including turbulent, transitional, and laminar. The Reynolds number in this proposed study should be calculated based on the effective viscosity measured by a rheometer. In this system, effective viscosity and shear rate should be altered to normal viscosity and impeller shear rate.

$$\text{Re} = \frac{\rho N D^2}{\eta_{\text{eff}}} \quad \text{Equation 2-5}$$

whereas Re refers to the Reynolds number, the term η_{eff} refers to effective viscosity, N refers to the rotational speed of the mixer, and ρ shows density.

Chapter 2: Literature review

2.6.2 Power number (N_p)

The efficiency of impeller has been evaluated by measuring the input power (P₀). Rudolph (2007) defined power uptake as a function of various parameter including tank and impeller diameter (T and D), impeller bottom clearance (C), number of blade and blades, and liquid height (H).

$$P_0 = f(\rho, \mu, C, g, D, T, H, N, \dots) \quad \text{Equation 2-6}$$

The rate of energy dissipation within the liquid can be represented by the Power number.

$$N_p = \frac{P_0}{\rho N^3 D^5} = C \left(\frac{H}{D}\right)^a \left(\frac{T}{D}\right)^b \left(\frac{DN^2}{g}\right)^c \left(\frac{\rho ND^2}{\eta_{eff}}\right)^d \quad \text{Equation 2-7}$$

where, N_p indicates the power transferred by the shaft to the liquid, D is the propeller diameter, η_{eff} refers to the effective viscosity, N indicates the rotational speed of the impeller, ρ refers to density, P₀ indicates power consumption as be obtained from the equation below:

$$P_0 = 2\pi NM \quad \text{Equation 2-8}$$

where M is torque and calculated from the integrated pressure on impeller blade.

2.6.3 Froude number (Fr)

When a vortex exists, the Froude number is defined as based on inertial forces and gravitational force. Applying the Froude number is not a suitable technique for scaling-up a system (Rudolph et al. 2007). The result of the following equation shows the Re number is in the range of 10-1000, as a transient flow (Jaszczur, Młynarczykowska, and Demurtas 2020).

$$Fr = \frac{N^2 D}{g} \quad \text{Equation 2-9}$$

However, a combination of gas flow number and Froude number can be employed to evaluate liquid-gas flow patterns including flooding, loading, complete dispersion and their transitional states, as described in Section 3.7.1 (Paul, Atiemo-obeng, and Kresta 2004).

Chapter 2: Literature review

2.6.4 Gas flow number (Fl_g)

A gas flow dimensionless number is a term that defines the flow pattern occurring in an agitated vessel as gas bubbles rise. Nagata and Yamada (1972) have previously indicated that gas flow number is constant in a turbulent regime, whilst it calculated from the equation below in laminar flow (I. Nagata and Yamada 1972).

$$Fl_g = \frac{Q_g}{ND^3} \quad \text{Equation 2-10}$$

Gas flow number indicates the correlation between impeller pumping capacity and gas volumetric flow rate (Q_g).

2.6.5 Mixing time number (N_θ)

There are many studies that have investigated mixing time with a single impeller and have compare the degree of homogeneity. Some research has defined dimensionless mixing time number (N_θ) and related N_θ to other dimensionless numbers including Re and Fr. The dependency of mixing time number with Re and flow regime has been investigated within the literature (Tanguy and Takenaka 2005). Further, the relationship between dimensionless mixing time and impeller speed has been widely studied within research (Gogate, Beenackers, and Pandit 2000). One study has reported that mixing time positively correlates with input power, while impeller type is an insignificant factor (Paul, Atiemo-obeng, and Kresta 2004).

There is still a lack of knowledge about the effect of mechanical impeller systems coupled with sparging gas on mixing time number. Some researchers have indicated that sparging gas reduces mixing time number (Vrábel et al. 2000; Hadjiev, Sabiri, and Zanati 2006; McClintock 1997). Bouaifi and Rouston (2001) indicate that gas flow do not influence mixing time when a regime is completely dispersed (Bouaifi and Rouston 2001). Further, many researchers have suggested a correlation between mixing time numbers and impeller speed and gas flow rate

Chapter 2: Literature review

when a flow pattern is flooding or loading (Vrábel et al. 2000; Tanguy and Takenaka 2005; Hampel et al. 2007).

2.7 Power consumption

Power consumption is a key parameter in evaluating mixing performance, cost, and design. Power consumption is a reliable indicator of how much energy should be transferred to a system in order to obtain the best results. The ideal system consumes less power but provides a homogenous mixing pattern within a short time.

In a gas-liquid agitated system, a combination of different dimensionless numbers, including Froude number, gas flow number, and Weber number, should be considered in calculating the whole power uptake.

Power consumption in ungasged mixing systems with different impellers has been widely studied within the literature. Takahashi et al. (1980) have calculated the consumed power for different configuration of anchor and helical ribbon impellers (Takahashi, Arai, and Saito 1980). Carreau et al. (1993) have determined a correlation between power consumption and rheology of fluid in a vessel agitated by a helical ribbon impeller (Carreau, Chhabra, and Cheng 1993). Pakzad et al., have characterized flow pattern and measured the power consumed by a Scaba 6SRGT impeller, mounted in a cylindrical vessel filled with a Herschel-Bulkely fluid (Pakzad et al. 2012, 2013; Pakzad, Ein-Mozaffari, and Chan 2008). Additionally, power consumption has been investigated for high viscous fluid agitated by coaxial mixers (Rudolph et al. 2007; Espinosa-Solares et al. 1997; Bao et al. 2018, 2015). The power consumed in an ungasged agitated vessel can be calculated from an equation combining Reynolds number and power number (Guillaume Delaplace et al. 2006). When gas is injected inside the system, cavities form near the blades and low-pressure areas are created around the impeller, leading to bubble accumulation. Thus, the power induced by an impeller into the fluid will drop, where the performance of the reactor is reduced (W. Wang, Mao, and Yang 2006). The power consumption for gas-liquid systems is a function of gas flow rate,

Chapter 2: Literature review

rotational speed, and impeller type. Some of the correlations relating to these parameters are summarized in Table 2-2.

Table 2-2 The correlation between ungasged and gassed systems reported in literature (Luong and Volesky 1979) (Michel and Miller 1962) (Shewale and Pandit 2006)

Impeller	Fluids	Correlation	
Six-blade turbine	Water	$\frac{P_g}{P_0} = 0.497 \left(\frac{Q_g}{ND^3} \right)^{-0.38} \left(\frac{N^2 D^3 \rho_l}{\sigma} \right)^{-0.18}$	(Luong and Volesky 1979)
	CMC	$\frac{P_g}{P_0} = 0.514 \left(\frac{Q_g}{ND^3} \right)^{-0.38} \left(\frac{N^2 D^3 \rho_l}{\sigma} \right)^{-0.194}$	
Disk turbine	Water	$P_g = 0.812 \left(\frac{P_0^2 ND^3}{Q_g^{0.56}} \right)^{0.45}$	(Michel and Miller 1962)
Pitched blade turbine	Water	$P_g = 1.52 \left(\frac{P_0^2 ND^3}{Q_g^{0.56}} \right)^{0.427}$	(Shewale and Pandit 2006)

2.8 Gas holdup

In most gas-liquid systems, gas dispersion is a key parameter that impacts on the performance of mixing. Optimum gas dispersion leads to maximize heat and mass transfer, uniformity, and better mixing by improving the contact between gas and liquid. Gas hold-up is a function of gas phase volume (V_g) and total volume (V_t), characterized by gas dispersion quality. The total volume is defined as the whole volume of the system including gas and liquid volume (V_l).

$$\phi_g = \frac{V_g}{V_l + V_g} \quad \text{Equation 2-11}$$

Gas holdup has been classified into two different categories, locally and globally. The difference between the level of the liquid surface in ungasged and gassed situation is called global gas holdup. Measuring local gas holdup is a complicated task requiring accurate design and numerical validation. Much researcher have measured local gas holdup using different types of invasive methods including the suction method (Nagase and Yasui 1983), heat transfer probes (Boyer, Duquenne, and Wild 2002), as well as needle probes (W. Wang, Mao, and Yang 2006). However, these intrusive techniques may interfere with the results and change the flow

Chapter 2: Literature review

pattern. To overcome these limitations, non-invasive methods including electrical resistance tomography (ERT)(Pakzad et al. 2013), X-ray and gamma rays (Hampel et al. 2007), using high-speed cameras (Chhabra et al. 2007; Behkish et al. 2007), PIV/LIF (S. Liu, Low, and Nickerson 2009), and ultrasonic modes (Supardan et al. 2007) have become popular amongst research studies.

2.8.1 Influential factors on bubble deformation

When bubbles form, they rise vertically to overcome the buoyancy force. Gas-liquid hydrodynamics and bubble size are proportional to impeller speed, viscosity of fluid, and gas flow rate. Smaller bubbles would form by increasing the rotational speed of impeller. Bubbles have accelerated by increasing the rotational speed of impeller leading to hitting the bubbles to the blades and wall. Bubble size determines the interfacial area between phases which can directly affect the mass transfer and biogas production rate. In accordance with the importance of bubble size and distribution many researchers have examined the hydrodynamics of gas-liquid systems, particularly in agitated systems equipped with rotational impellers (Bouaifi and Roustan 2001; Hampel et al. 2007; Gumulya et al. 2016).

Further, viscosity of fluid cause deformation in bubble shapes and changing the rising velocity. Travelling bubbles fastened by increasing the viscosity resulting in longer gas holdup time. Further, higher viscosity leads to less bubble deformation and to more changes of striking and coalescence. In this case, bubble shape is nearly rounded. Additionally, high viscosity of fluid reduces the turbulence and prevents bubbles from breaking up.

Higher gas flow rate reduces the bubble deformation since bubbles rising quickly and reach to the surface in a short period of time.

Chapter 2: Literature review

2.9 Computational fluid dynamics (CFD)

CFD modelling can be applied as a powerful tool to study the hydrodynamics of an agitated multi-phase bioreactor in detail. Within the past two decades, a number of researchers have sought to simulate different aspects of hydrodynamics of agitated multiphase systems including drag force (Trad et al. 2015), mass transfer and interactions between phases (Eftaxias et al. 2020), rheological characteristics (Samandari-Masouleh et al. 2012c; Niño, Peñuela, and Gelves 2018; Fernandes del Pozo et al. 2020; Miryahyaei et al. 2020), energy demand (Houari Ameer 2015; Shahnazari, Ahmadi, and Masooleh 2017), and hydrodynamics (Gumulya et al. 2016; Fernandes del Pozo et al. 2020; J. Jiang et al. 2016a). In addition, adjustment and optimization of operating conditions through experiment can be a demanding and sometimes impossible task because of the cost and limitations involved in applying instruments and equipment. Notwithstanding these limitations, the literature suggests using CFD simulation as an alternative method in order to specify different hydrodynamic characteristics of a multiphase system (Samandari-Masouleh et al. 2012a; J. Jiang et al. 2016a; Bao et al. 2018, 2015). The influence of geometry and type of impeller on the performance of a bioreactor filled with a non-Newtonian fluid have been widely investigated in single-phase, using different CFD approaches (Torotwa and Changying 2018; Singh, Szamosi, and Siménfalvi 2020; Tobo, Bartacek, and Nopens 2020; Meister et al. 2018). Many research has been conducted on biogas production that applies different CFD approaches (Shen et al. 2013; Kamla et al. 2019). Lebranchu et al. (2017) have carried out a series of experiments and used CFD modelling to compare the biogas production of a biodigester operated with different impeller types. They reported the higher efficiency of a dual helical ribbon agitator compared to other impellers (Lebranchu et al. 2017; Houari Ameer, Kamla, and Sahel 2017). It has been reported that effect of width of a helical ribbon blade on bioreactor efficiency is insignificant (Kuncewicz and Stelmach 2017). Detailed examination by Ameer and Ghenaim (2018) has shown that the

Chapter 2: Literature review

rheological characteristics of fluid dominate the hydrodynamics of a biodigester (Houari Ameer and Ghenaim 2018). The key outcome of this work is that sludge should be considered as a non-Newtonian fluid. However, most CFD studies have ignored the rheological behaviour of sludge, due to its complex nature (Oyegbile and Akdogan 2018; Basavarajappa et al. 2015). In most of previous studies, it has been assumed that bioreactors contain a single-phase fluid, and this assumption is far from reality. The interaction between phases is an influential factor in modelling bioreactors, and it plays a key role in hydrodynamics, and gauging the efficiency of a system. Mutual dynamic interactions between gas and liquid phases, including drag forces, gas holdup, liquid viscoelastic behaviour, velocity field, and bubble size distribution, can alter the efficiency of a system. Smaller, fully dispersed bubbles expand within the interfacial area between phases and facilitate mass and heat transfer. Most CFD simulation studies have only focused on modelling the liquid phase, because CFD modelling was not specifically designed to evaluate factors related to breakage and coalescence of bubbles in detail. As a result, a combination of CFD-PBM methods has been suggested in the literature to model the interaction between phases (Dhanasekharan et al. 2005; Venneker, Derksen, and Van den Akker 2002; Niño, Peñuela, and Gelves 2018).

2.9.1 Governing equations

Previous studies have identified the Eulerian-Eulerian (E-E) multiphase approach as a suitable numerical method to solve continuity and momentum equations. This method suggests two phases as continuous (Ali and Pushpavanam 2011). The continuity and conversion of momentum equations for phase i have been reported in Equations 2-12 and 2-13.

$$\frac{\partial}{\partial t}(\alpha_i \rho_i) + \nabla \cdot (\alpha_i \rho_i v_i) = 0 \quad \text{Equation 2-12}$$

$$\frac{\partial}{\partial t}(\alpha_i \rho_i v_i) + \nabla \cdot (\alpha_i \rho_i v_i v_i) = -\alpha_i \nabla p + \alpha_i \rho_i g + \nabla \cdot \bar{\bar{T}}_i + \alpha_i \rho_i \vec{F}_i + \sum_{j=1}^n \vec{R}_{ji} \quad \text{Equation 2-13}$$

$$\alpha_i + \alpha_j = 1 \quad \text{Equation 2-14}$$

Chapter 2: Literature review

Where α_i refers to the volume fraction of the continuous phase, v_i refers to the liquid mean velocity, $\nabla \cdot \bar{T}_i$ refers to the shear stress, \bar{F}_i refers the momentum between gas and liquid phases, and \bar{R}_{ji} shows the interphase forces. The following equation shows the shear rate caused by laminar and turbulent momentum fluxes:

$$\bar{T}_i = \alpha_i(\mu_{eff})[\nabla \vec{v}_i + \vec{v}_i^T] - \left(\frac{2}{3}\right) \alpha_i(\mu_{eff})\nabla \vec{v}_i \bar{I} \quad \text{Equation 2-15}$$

The term μ_{eff} refers to the liquid effective viscosity characterised by shear induced viscosity ($\mu_{t,i}$), molecular viscosity (μ_i), and turbulence viscosity ($\mu_{b,i}$) (Sato and Sadatomi 1981).

$$\mu_{eff} = \mu_i + \mu_{t,i} + \mu_{b,i} \quad \text{Equation 2-16}$$

The gradian of cohesion, pressure, and friction alter interphase forces, which can be characterized by the classical drag model of Schiller and Naumann. Where C_D refers to the drag coefficient of a gas phase (Guan et al. 2019).

$$C_D = \begin{cases} \frac{24}{Re_b} (0.15 Re_b)^{0.687} & Re \leq 1000 \\ 0.44 & Re > 1000 \end{cases} \quad \text{Equation 2-17}$$

The $k - \varepsilon$ model is employed to explain the turbulence based on two equations. This model is a combination of the two equations below.

$$\frac{\partial}{\partial t}(\rho_m k) + \nabla \cdot (\rho_m \vec{v}_m k) = \nabla \cdot \left(\frac{\mu_{t,m}}{\delta_k} \nabla k \right) + G_{k,m} - \rho_m \varepsilon \quad \text{Equation 2-18}$$

$$\frac{\partial}{\partial t}(\rho_m \varepsilon) + \nabla \cdot (\rho_m \vec{v}_m \varepsilon) = \nabla \cdot \left(\frac{\mu_{t,m}}{\delta_\varepsilon} \nabla \varepsilon \right) + C_{1\varepsilon} G_{k,m} - C_{2\varepsilon} \rho_m \varepsilon \quad \text{Equation 2-19}$$

where ε refers the dissipation rate, k refers to turbulent kinetic energy, and G is defined as the generation of turbulent kinetic energy.

The following equations explain the properties of the mixture, where $C_\mu = 0.09$, $C_{1\varepsilon} = 1.44$, and $C_{2\varepsilon} = 1.92$ are constants, as mentioned in the literature (Ranade 2001).

$$\rho_m = \sum_{i=1}^n \alpha_i \rho_i \quad \text{Equation 2-20}$$

$$\vec{v}_m = \frac{\sum_{i=1}^n \alpha_i \rho_i \vec{v}_i}{\sum_{i=1}^n \alpha_i \rho_i} \quad \text{Equation 2-21}$$

Chapter 2: Literature review

$$\mu_{t,m} = \rho_m C_\mu \frac{k^2}{\varepsilon} \quad \text{Equation 2-22}$$

2.9.2 Population balance model (PBM)

PBM is a powerful method for predicting changes in bubble size during a mixing process (Marchisio, Vigil, and Fox 2003). Developing a comprehensive understanding about bubble breakage and coalescence is essential in understanding the hydrodynamics of two-phase systems. A combination of the CFD-PBM method has been applied in literature to predict the characteristics of an unsteady multiphase system including drag (X. Jiang, Yang, and Yang 2016), lift (Tomiyama et al. 1997) and mass transfer.

$$\frac{\partial}{\partial t} n(\vec{x}, V_b, t) + \frac{\partial}{\partial z} [n(\vec{x}, V_b, t) u_b(\vec{x}, V_b)] + \frac{\partial}{\partial V_b} [n(\vec{x}, V_b, t) \frac{\partial}{\partial t} V_b(\vec{x}, V_b)] = S(\vec{x}, V_b, t) \quad \text{Equation 2-23}$$

Whilst the first term on the left refers to the bubble density distribution function position of \vec{x} , V_b and time t . $S(\vec{x}, V_b, t)$ refer to phase interactions while u_b refers to the local velocity of bubbles.

Although extensive research has been carried out on CFD modelling of helical ribbon impellers, to the researcher's knowledge no single study exists that considers helical ribbon impellers in two-phase systems. This study focuses on CFD modelling of a helical ribbon impeller where gas is injected inside a pseudoplastic fluid.

2.10 References

- Ali, B Ashraf, and S Pushpavanam. 2011. "Analysis of Unsteady Gas – Liquid Flows in a Rectangular Tank: Comparison of Euler – Eulerian and Euler – Lagrangian Simulations." *International Journal of Multiphase Flow* 37: 268–77. <https://doi.org/10.1016/j.ijmultiphaseflow.2010.10.002>.
- Ameur, Houari. 2015. "Energy Efficiency of Different Impellers in Stirred Tank Reactors." *Energy* 93: 1980–88. <https://doi.org/10.1016/j.energy.2015.10.084>.

Chapter 2: Literature review

Ameur, Houari, Mohamed Bouzit, and Abdellah Ghenaim. 2013. "Hydrodynamics in a Vessel Stirred by Simple and Double Helical Ribbon Impellers." *Central European Journal of Engineering* 3 (1): 87–98. <https://doi.org/10.2478/s13531-012-0045-x>.

Ameur, Houari, Mohamed Bouzit, and Mustapha Helmaoui. 2011. "Numerical Study of Fluid Flow and Power Consumption in a Stirred Vessel with a CABA 6SRGT Impeller." *Chemical and Process Engineering* 32 (4): 351–66. <https://doi.org/10.2478/v10176-011-0028-0>.

Ameur, Houari, and Abdellah Ghenaim. 2018. "Mixing of Complex Fluids in a Cylindrical Tank by a Modified Anchor Impeller." *ChemistrySelect* 3 (26): 7472–77. <https://doi.org/10.1002/slct.201801047>.

Ameur, Houari, Youcef Kamla, and Djamel Sahel. 2017. "Performance of Helical Screw Impellers for Mixing of Viscous Liquids in Cylindrical Reactors." *ChemistrySelect* 2 (5): 1891–94. <https://doi.org/10.1002/slct.201602072>.

Anne-Archard, D., M Marouche, and H C Boisson. 2006. "Hydrodynamics and Metzner – Otto Correlation in Stirred Vessels for Yield Stress Fluids." *Chemical Engineering Journal* 125: 15–24. <https://doi.org/10.1016/j.cej.2006.08.002>.

Babaei, Roghayyeh, Babak Bonakdarpour, and Farhad Ein-Mozaffari. 2015. "The Use of Electrical Resistance Tomography for the Characterization of Gas Holdup inside a Bubble Column Bioreactor Containing Activated Sludge." *Chemical Engineering Journal* 268: 260–69. <https://doi.org/10.1016/j.cej.2015.01.042>.

Bao, Yuyun, Yu Lu, Qianqin Liang, Li Li, Zhengming Gao, Xiongbin Huang, and Song Qin. 2015. "Power Demand and Mixing Performance of Coaxial Mixers in a Stirred Tank with CMC Solution." *Chinese Journal of Chemical Engineering* 23 (4): 623–32. <https://doi.org/10.1016/j.cjche.2015.01.002>.

Basavarajappa, Manjunath, Teri Draper, Pal Toth, Terry A. Ring, and Sanja Miskovic. 2015. "Numerical and Experimental Investigation of Single-Phase Flow Characteristics in Stirred Tanks Using Rushton Turbine and Flotation Impeller." *Minerals Engineering* 83: 156–67. <https://doi.org/10.1016/j.mineng.2015.08.018>.

Baudez, J.C., Rahul K. Gupta, Nicky Eshtiaghi, and Paul Slatter. 2013. "The Viscoelastic Behaviour of Raw and Anaerobic Digested Sludge: Strong Similarities with Soft-Glassy Materials." *Water Research* 47 (1): 173–80. <https://doi.org/10.1016/j.watres.2012.09.048>.

Baudez, Flora Markis, Nicky Eshtiaghi, and Paul Slatter. 2011. "The Rheological Behaviour of Anaerobic Digested Sludge." *Water Research* 45 (17): 5675–80. <https://doi.org/10.1016/j.watres.2011.08.035>.

Behkish, Arsam, Romain Lemoine, Laurent Sehabiague, Rachid Oukaci, and Badie I. Morsi. 2007. "Gas Holdup and Bubble Size Behavior in a Large-Scale Slurry Bubble Column Reactor Operating with an Organic Liquid under Elevated Pressures and Temperatures." *Chemical Engineering Journal* 128 (2–3): 69–84. <https://doi.org/10.1016/j.cej.2006.10.016>.

Bhattacharjee, Pradipto K., Stephen Kennedy, Nicky Eshtiaghi, and Rajarathinam Parthasarathy. 2015. "Flow Regimes in the Mixing of Municipal Sludge Simulant Using Submerged, Recirculating Jets." *Chemical Engineering Journal* 276 (3145364): 137–44. <https://doi.org/10.1016/j.cej.2015.04.068>.

Chapter 2: Literature review

Bobade, Veena, Madalyn Cheetham, Jamal Hashim, and Nicky Eshtiaghi. 2018. "Influence of Gas Injection on Viscous and Viscoelastic Properties of Xanthan Gum." *Water Research* 134: 86–91. <https://doi.org/10.1016/j.watres.2018.01.071>.

Bouaifi, M., and M. Roustan. 2001. "Power Consumption, Mixing Time and Homogenisation Energy in Dual-Impeller Agitated Gas-Liquid Reactors." *Chemical Engineering and Processing* 40 (2): 87–95. [https://doi.org/10.1016/S0255-2701\(00\)00128-8](https://doi.org/10.1016/S0255-2701(00)00128-8).

Boyer, Christophe, Anne-marie Duquenne, and Gabriel Wild. 2002. "Open Archive TOULOUSE Archive Ouverte (OATAO) Measuring Techniques in Gas – Liquid and Gas – Liquid – Solid Reactors" 57 (02): 3185–3215.

Brito-De La Fuente, E., L. Choplin, and P. A. Tanguy. 1997. "Mixing with Helical Ribbon Impellers: Effect of Highly Shear Thinning Behaviour and Impeller Geometry." *Chemical Engineering Research and Design* 75 (1): 45–52. <https://doi.org/10.1205/026387697523381>.

Cabaret, F., L. Fradette, and P. A. Tanguy. 2008. "Gas-Liquid Mass Transfer in Unbaffled Dual-Impeller Mixers." *Chemical Engineering Science* 63 (6): 1636–47. <https://doi.org/10.1016/j.ces.2007.11.028>.

Carreau, P J, R P Chhabra, and J Cheng. 1993. "Effect of Rheological Properties on Power Consumption with Helical Ribbon Agitators." *AIChE Journal* 39 (9): 1421–30. <https://doi.org/10.1002/aic.690390902>.

Cheng, Jianya, and Pierre J. Carreau. 1994. "Aerated Mixing of Viscoelastic Fluids with Helical Ribbons Impellers." *Chemical Engineering Science* 49 (12): 1965–72. [https://doi.org/10.1016/0009-2509\(94\)80080-4](https://doi.org/10.1016/0009-2509(94)80080-4).

Chhabra, R. P., L. Bouvier, G. Delaplace, G. Cuvelier, S. Domenek, and Christophe André. 2007. "Determination of Mixing Times with Helical Ribbon Mipeller for Non-Newtonian Viscous Fluids Using an Advanced Imaging Method." *Chemical Engineering and Technology* 30 (12): 1686–91. <https://doi.org/10.1002/ceat.200700320>.

Crawford, Ronald L., and Don L. Crawford. 2006. *Bioremediation: Principles and Applications (Biotechnology Research)*. Cambridge University Press.

Curry, Nathan, and Pragasen Pillay. 2012. "Biogas Prediction and Design of a Food Waste to Energy System for the Urban Environment." *Renewable Energy* 41: 200–209. <https://doi.org/10.1016/j.renene.2011.10.019>.

Delafosse, Angélique, Marie Laure Collignon, Sébastien Calvo, Frank Delvigne, Michel Crine, Philippe Thonart, and Dominique Toye. 2014. "CFD-Based Compartment Model for Description of Mixing in Bioreactors." *Chemical Engineering Science* 106: 76–85. <https://doi.org/10.1016/j.ces.2013.11.033>.

Delaplace, Guillaume, Romuald Guerin, Jean Claude Leuliet, and R. P. Chhabra. 2006. "An Analytical Model for the Prediction of Power Consumption for Shear-Thinning Fluids with Helical Ribbon and Helical Screw Ribbon Impellers." *Chemical Engineering Science* 61 (10): 3250–59. <https://doi.org/10.1016/j.ces.2005.11.069>.

Dhanasekharan, Kumar M., Jay Sanyal, Anupam Jain, and Ahmad Haidari. 2005. "A Generalized Approach to Model Oxygen Transfer in Bioreactors Using Population Balances

Chapter 2: Literature review

and Computational Fluid Dynamics.” *Chemical Engineering Science* 60 (1): 213–18. <https://doi.org/10.1016/j.ces.2004.07.118>.

Dieulot, J.Y., G. Delaplace, R. Guerin, J.P. Brienne, and Leuliet J.C. 2002. “Laminar Mixing Performances of a Stirred Tank Equipped with Helical Ribbon Agitator Subjected to Steady and Unsteady Rotational Speed” 80 (May). <https://doi.org/10.1205/026387602317446371>.

Eftaxias, Alexandros, Vasileios Diamantis, Christos Michailidis, Katerina Stamatelatou, and Alexandros Aivasidis. 2020. “Comparison of Anaerobic Digesters Performance Treating Palmitic, Stearic and Oleic Acid: Determination of the LCFA Kinetic Constants Using ADM1.” *Bioprocess and Biosystems Engineering* 43 (7): 1329–38. <https://doi.org/10.1007/s00449-020-02328-2>.

Eshtiaghi, Nicky, Shao Dong Yap, Flora Markis, Jean Christophe Baudez, and Paul Slatter. 2012. “Clear Model Fluids to Emulate the Rheological Properties of Thickened Digested Sludge.” *Water Research* 46 (9): 3014–22. <https://doi.org/10.1016/j.watres.2012.03.003>.

Espinosa-Solares, T., E. Brito-De La Fuente, A. Tecante, and P. A. Tanguy. 1997. “Power Consumption of a Dual Turbine-Helical Ribbon Impeller Mixer in Ungassed Conditions.” *Chemical Engineering Journal* 67 (3): 215–19. [https://doi.org/10.1016/S1385-8947\(97\)00040-5](https://doi.org/10.1016/S1385-8947(97)00040-5).

Farno, Ehsan, Rajarathinam Parthasarathy, and Nicky Eshtiaghi. 2015. “Effect of Thermally-Induced Protein Solubilisation on Rheology of Activated Sludge,” no. November.

Fernandes del Pozo, David, Alain Liné, Kevin M. Van Geem, Claude Le Men, and Ingmar Nopens. 2020. “Hydrodynamic Analysis of an Axial Impeller in a Non-Newtonian Fluid through Particle Image Velocimetry.” *AIChE Journal* 66 (6). <https://doi.org/10.1002/aic.16939>.

Forster-Carneiro, T., M. Pérez, and L. I. Romero. 2008. “Influence of Total Solid and Inoculum Contents on Performance of Anaerobic Reactors Treating Food Waste.” *Bioresource Technology* 99 (15): 6994–7002. <https://doi.org/10.1016/j.biortech.2008.01.018>.

Gogate, Parag R., Anthony A.C.M. Beenackers, and Aniruddha B. Pandit. 2000. “Multiple-Impeller Systems with a Special Emphasis on Bioreactors: A Critical Review.” *Biochemical Engineering Journal* 6 (2): 109–44. [https://doi.org/10.1016/S1369-703X\(00\)00081-4](https://doi.org/10.1016/S1369-703X(00)00081-4).

Guan, Xiaoping, Xinju Li, Ning Yang, and Mingyan Liu. 2019. “CFD Simulation of Gas-Liquid Flow in Stirred Tanks: Effect of Drag Models.” *Chemical Engineering Journal*, no. xxxx. <https://doi.org/10.1016/j.cej.2019.04.134>.

Guillard, Fabrice, Christian Trägårdh, and Laszlo Fuchs. 2000. “Study on the Instability of Coherent Mixing Structures in a Continuously Stirred Tank.” *Chemical Engineering Science* 55 (23): 5657–70. [https://doi.org/10.1016/S0009-2509\(00\)00201-3](https://doi.org/10.1016/S0009-2509(00)00201-3).

Gumulya, Monica, Jyeshtharaj B. Joshi, Ranjeet P. Utikar, Geoffrey M. Evans, and Vishnu Pareek. 2016. “Bubbles in Viscous Liquids: Time Dependent Behaviour and Wake Characteristics.” *Chemical Engineering Science* 144 (2000): 298–309. <https://doi.org/10.1016/j.ces.2016.01.051>.

Chapter 2: Literature review

Hadjiev, Dimiter, Nour Eddine Sabiri, and Adel Zanati. 2006. "Mixing Time in Bioreactors under Aerated Conditions." *Biochemical Engineering Journal* 27 (3): 323–30. <https://doi.org/10.1016/j.bej.2005.08.009>.

Hampel, U., H. V. Hristov, A. Bieberle, and C. Zippe. 2007. "Application of High-Resolution Gamma Ray Tomography to the Measurement of Gas Hold-up Distributions in a Stirred Chemical Reactor." *Flow Measurement and Instrumentation* 18 (5–6): 184–90. <https://doi.org/10.1016/j.flowmeasinst.2007.06.001>.

Holliger, Christof, Madalena Alves, Diana Andrade, Irini Angelidaki, Sergi Astals, Urs Baier, Claire Bougrier, et al. 2016. "Towards a Standardization of Biomethane Potential Tests." *Water Science and Technology* 74 (11): 2515–22. <https://doi.org/10.2166/wst.2016.336>.

Houska, M. 1986. "Anchor-Agitated Systems: Power Input Correlation for Pseudoplastic and Thixotropic Fluids in Equilibrium." *AIChE Journal* 32 (1): 155–58. <https://doi.org/10.1002/aic.690320119>.

Hui, Leo K., Chad P.J. Bennington, and Guy A. Dumont. 2009. "Cavern Formation in Pulp Suspensions Using Side-Entering Axial-Flow Impellers." *Chemical Engineering Science* 64 (3): 509–19. <https://doi.org/10.1016/j.ces.2008.09.021>.

Jiang, Jiankai, Jing Wu, Souhila Poncin, and Huai Z. Li. 2016. "Effect of Hydrodynamic Shear on Biogas Production and Granule Characteristics in a Continuous Stirred Tank Reactor." *Process Biochemistry* 51 (3): 345–51. <https://doi.org/10.1016/j.procbio.2015.12.014>.

Jiang, Xuedong, Ning Yang, and Bolun Yang. 2016. "Computational Fluid Dynamics Simulation of Hydrodynamics in the Riser of an External Loop Airlift Reactor." *Particuology* 27: 95–101. <https://doi.org/10.1016/j.partic.2015.05.011>.

Kamla, Youcef, Houari Ameer, Abdelkader Karas, and Mohammed Ilies. 2019. "Performance of New Designed Anchor Impellers in Stirred Tanks." *Chemical Papers*, no. 0123456789: 2–8. <https://doi.org/10.1007/s11696-019-00902-x>.

Kaparaju, Prasad, Inmaculada Buendia, Lars Ellegaard, and Irini Angelidakia. 2008. "Effects of Mixing on Methane Production during Thermophilic Anaerobic Digestion of Manure: Lab-Scale and Pilot-Scale Studies." *Bioresource Technology* 99 (11): 4919–28. <https://doi.org/10.1016/j.biortech.2007.09.015>.

Karim, Khursheed, Gregory J. Thoma, and Muthanna H. Al-Dahhan. 2007. "Gas-Lift Digester Configuration Effects on Mixing Effectiveness." *Water Research* 41 (14): 3051–60. <https://doi.org/10.1016/j.watres.2007.03.042>.

Kariyama, Ibrahim Denka, Xiaodong Zhai, and Binxin Wu. 2018. "Influence of Mixing on Anaerobic Digestion Efficiency in Stirred Tank Digesters: A Review." *Water Research* 143: 503–17. <https://doi.org/10.1016/j.watres.2018.06.065>.

Kato, Yoshihito, Haruki Furukawa, Yasuyuki Ikeda, Toshikazu Nakanishi, Tadashi Sano, and Kenji Tomioka. 2018. "Development of a Mixing Process Using an HB-Type Impeller to Easily Achieve Scale-Up by Maintaining Geometrical Similarity" 2018.

Chapter 2: Literature review

Kennedy, Stephen, Pradipto K Bhattacharjee, Sati N Bhattacharya, Nicky Eshtiaghi, and Rajarathinam Parthasarathy. 2018. "Control of the Mixing Time in Vessels Agitated by Submerged Recirculating Jets Subject Category: Subject Areas:"

Kennedy, Stephen, Pradipto K Bhattacharjee, and Nicky Eshtiaghi. 2015. "Submerged, Recirculating Jets: Nozzle Geometry and Its Effect on Active Volume Creation in the Mixing of Municipal Sludge Simulant 1 Introduction 2 Methodology" c (3145323): 2236–41.

Kennedy, Stephen, Rajarathinam Parthasarathy, Nicky Eshtiaghi, and Sati Bhattacharya. 2014. "Liquid Jet Recirculation in a Model Digester: Flow Characteristics." In, 1–7.

Kuncewicz, Czesław, and Jacek Stelmach. 2017. "Optimization of Geometric Parameters of a Ribbon Impeller." *Chemical and Process Engineering - Inzynieria Chemiczna i Procesowa* 38 (3): 491–502. <https://doi.org/10.1515/cpe-2017-0038>.

Lebranchu, Aline, Stéphane Delaunay, Philippe Marchal, Fabrice Blanchard, Stéphane Pacaud, Michel Fick, and Eric Olmos. 2017. "Impact of Shear Stress and Impeller Design on the Production of Biogas in Anaerobic Digesters." *Bioresource Technology* 245: 1139–47. <https://doi.org/10.1016/j.biortech.2017.07.113>.

Lindmark, Johan, Eva Thorin, Rebei Bel Fdhila, and Erik Dahlquist. 2014. "Effects of Mixing on the Result of Anaerobic Digestion: Review." *Renewable and Sustainable Energy Reviews* 40: 1030–47. <https://doi.org/10.1016/j.rser.2014.07.182>.

Liu, Shuanghui, Nicholas H. Low, and Michael T. Nickerson. 2009. "Effect of PH, Salt, and Biopolymer Ratio on the Formation of Pea Protein Isolate Gum Arabic Complexes." *Journal of Agricultural and Food Chemistry* 57 (4): 1521–26. <https://doi.org/10.1021/jf802643n>.

Low, Siew Cheng, Rajarathinam Parthasarathy, Paul Slatter, and Nicky Eshtiaghi. 2013. "Improving Mixing in Anaerobic Digesters with a Jet Recirculation System." In *Improving Mixing in Anaerobic Digesters with a Jet Recirculation System* Siew, 2–6.

Luong, H.T., and B. Volesky. 1979. "Mechanical Power Requirements of Gas-Liquid Agitated Systems." *AIChE Journal* 25 (5): 893–95. <https://doi.org/10.1002/aic.690250520>.

Marchisio, Daniele L., R. Dennis Vigil, and Rodney O. Fox. 2003. "Quadrature Method of Moments for Aggregation-Breakage Processes." *Journal of Colloid and Interface Science* 258 (2): 322–34. [https://doi.org/10.1016/S0021-9797\(02\)00054-1](https://doi.org/10.1016/S0021-9797(02)00054-1).

Mcclintock, James B. 1997. "Full Papers." *October* 60 (10): 0–7. <https://doi.org/10.1002/adsc.200600473>.

Meister, Michael, Massoud Rezavand, Christian Ebner, Thomas Pümpel, and Wolfgang Rauch. 2018. "Mixing Non-Newtonian Flows in Anaerobic Digesters by Impellers and Pumped Recirculation." *Advances in Engineering Software* 115 (October 2017): 194–203. <https://doi.org/10.1016/j.advengsoft.2017.09.015>.

Meng, Fangang, Fenglin Yang, Baoqiang Shi, and Hanmin Zhang. 2008. "A Comprehensive Study on Membrane Fouling in Submerged Membrane Bioreactors Operated under Different Aeration Intensities." *Separation and Purification Technology* 59 (1): 91–100. <https://doi.org/10.1016/j.seppur.2007.05.040>.

Chapter 2: Literature review

Metcalf & Eddy, George Tchobanoglous, H. David Stensel, Ryujiro Tsuchihashi, Franklin L. Burton. 2003. *Wasterwater Engineering - Treatment and Reuse*. McGraw-Hill Education. www.mhhe.com.

Metzner, A, and R E Otto. 1957. "Agitation of Non-Newtonian Fluids." *AICHe Journal* 3 (1): 3–10. <https://doi.org/10.1002/aic.690030103>.

Michel, B. J., and S. A. Miller. 1962. "Power Requirements of Gas-liquid Agitated Systems." *AICHe Journal* 8 (2): 262–66. <https://doi.org/10.1002/aic.690080226>.

Miryahyaei, S., K. Olinga, M. Sh. Ayub, Sh. Sh. Jayaratna, M. Othman, and N. Eshtiaghi. 2020. "Rheological Measurements as Indicators for Hydrolysis Rate, Organic Matter Removal, and Dewaterability of Digestate in Anaerobic Digesters." *Journal of Environmental Chemical Engineering* 8 (4): 103970. <https://doi.org/10.1016/j.jece.2020.103970>.

Nagase, Yoichi, and Hiroo Yasui. 1983. "Fluid Motion and Mixing in a Gas-Liquid Contactor with Turbine Agitators." *The Chemical Engineering Journal* 27 (1): 37–47. [https://doi.org/10.1016/0300-9467\(83\)80044-6](https://doi.org/10.1016/0300-9467(83)80044-6).

Nagata, Isamu, and Toshiro Yamada. 1972. "Correlation and Prediction of Heats of Mixing." *Industrial and Engineering Chemistry Research* 11 (4): 1–5. <https://doi.org/10.1021/i260044a021>.

Nagata, Shinji, Masabumi Nishikawa, Tada Hisayuki, Hideo Hirabayashi, and Shinji Gotoh. 1970. "Power Consumption of Mixing Impellers Bingham Plastic Liquids." *Journal of Chemical Engineering of Japan* 3 (2): 237–43. <https://doi.org/10.1252/jcej.3.237>.

Niedzielska, A., and Cz Kuncewicz. 2005. "Heat Transfer and Power Consumption for Ribbon Impellers. Mixing Efficiency." *Chemical Engineering Science* 60 (8-9 SPEC. ISS.): 2439–48. <https://doi.org/10.1016/j.ces.2004.10.046>.

Niño, L, M Peñuela, and G R Gelves. 2018. "Gas-Liquid Hydrodynamics Simulation Using CFD in a Helical Ribbon Impeller Applied for Non-Newtonian Fluids." *International Journal of Applied Engineering Research* 13 (11): 9353–59. <http://www.ripublication.com>.

Novak, V, and F Rieger. 1975. "Homogenization Efficiency of Helical Ribbon and Anchor Agitators." *The Chemical Engineering Journal* 9: 63–70.

Oyegbile, Benjamin, and Guven Akdogan. 2018. "Hydrodynamic Characterization of Physicochemical Process in Stirred Tanks and Agglomeration Reactors." *Laboratory Unit Operations and Experimental Methods in Chemical Engineering*. <https://doi.org/10.5772/intechopen.77014>.

Paglianti, Alessandro, Sandro Pintus, and Massimiliano Giona. 2000. "Time-Series Analysis Approach for the Identification of Flooding/Loading Transition in Gas-Liquid Stirred Tank Reactors." *Chemical Engineering Science* 55 (23): 5793–5802. [https://doi.org/10.1016/S0009-2509\(00\)00125-1](https://doi.org/10.1016/S0009-2509(00)00125-1).

Pakzad, Leila, Farhad Ein-Mozaffari, and Philip Chan. 2008. "Measuring Mixing Time in the Agitation of Non-Newtonian Fluids through Electrical Resistance Tomography." *Chemical Engineering and Technology* 31 (12): 1838–45. <https://doi.org/10.1002/ceat.200800362>.

Chapter 2: Literature review

Pakzad, Leila, Farhad Ein-Mozaffari, Simant R. Upreti, and Ali Lohi. 2013. "Characterisation of the Mixing of Non-Newtonian Fluids with a Scaba 6SRGT Impeller through Ert and CFD." *Canadian Journal of Chemical Engineering* 91 (1): 90–100. <https://doi.org/10.1002/cjce.21616>.

Pakzad, Leila, Farhad Ein-mozaffari, Simant R Upreti, and Ali Lohi. 2012. "Chemical Engineering Research and Design Agitation of Herschel – Bulkley Fluids with the Scaba – Anchor Coaxial Mixers." *Chemical Engineering Research and Design* 91 (5): 761–77. <https://doi.org/10.1016/j.cherd.2012.09.008>.

Pant, H. J., V. K. Sharma, K. T. Shenoy, and T. Sreenivas. 2015. "Measurements of Liquid Phase Residence Time Distributions in a Pilot-Scale Continuous Leaching Reactor Using Radiotracer Technique." *Applied Radiation and Isotopes* 97: 40–46. <https://doi.org/10.1016/j.apradiso.2014.12.010>.

Paul, Edward L, Victor a Atiemo-obeng, and Suzanne M Kresta. 2004. *Handbook of Industrial Mixing*. <https://doi.org/10.1002/0471451452>.

Ranade, Vivek V. 2001. "Computational Flow Modeling for Chemical Reactor Engineering, Volume 5 (Process Systems Engineering)," 480. <http://www.amazon.com/Computational-Modeling-Chemical-Reactor-Engineering/dp/0125769601>.

Ratanatamskul, Chavalit, and Tawinan Saleart. 2016. "Effects of Sludge Recirculation Rate and Mixing Time on Performance of a Prototype Single-Stage Anaerobic Digester for Conversion of Food Wastes to Biogas and Energy Recovery." *Environmental Science and Pollution Research* 23 (8): 7092–98. <https://doi.org/10.1007/s11356-015-4448-0>.

Ratkovich, N., W. Horn, F. P. Helmus, S. Rosenberger, W. Naessens, I. Nopens, and T. R. Bentzen. 2013. "Activated Sludge Rheology: A Critical Review on Data Collection and Modelling." *Water Research* 47 (2): 463–82. <https://doi.org/10.1016/j.watres.2012.11.021>.

Rieger, FRANTISEK, Vaclav Novak, and HAVELKOVA Dagmar. 1986. "Homogenization Efficiency of Helical Ribbon Agitators." *The Chemical Engineering Journal* 33: 143–50. [https://doi.org/10.1016/0300-9467\(86\)80013-2](https://doi.org/10.1016/0300-9467(86)80013-2).

Rudolph, L., M. Schäfer, V. Atiemo-Obeng, and M. Kraume. 2007. "Experimental and Numerical Analysis of Power Consumption for Mixing of High Viscosity Fluids with a Co-Axial Mixer." *Chemical Engineering Research and Design* 85 (5 A): 568–75. <https://doi.org/10.1205/cherd06178>.

Ruiz-Hernando, Maria, Jordi Labanda, and Joan Llorens. 2015. "Structural Model to Study the Influence of Thermal Treatment on the Thixotropic Behaviour of Waste Activated Sludge." *Chemical Engineering Journal* 262: 242–49. <https://doi.org/10.1016/j.cej.2014.09.097>.

Samandari-Masouleh, Leila, Navid Mostoufi, A. A. Khodadadi, Y. Mortazavi, and Morteza Maghrebi. 2012a. "Kinetic Modeling of Carbon Nanotube Production and Minimization of Amorphous Carbon Overlayer Deposition in Floating Catalyst Method." *International Journal of Chemical Reactor Engineering* 10 (1): 10–12. <https://doi.org/10.1515/1542-6580.2972>.

Samandari-Masouleh, Leila, Navid Mostoufi, Abbasali Khodadadi, Yadollah Mortazavi, and Morteza Maghrebi. 2012b. "Modeling the Growth of Carbon Nanotubes in a Floating Catalyst Reactor." *Industrial and Engineering Chemistry Research* 51 (3): 1143–49. <https://doi.org/10.1021/ie201137j>.

Chapter 2: Literature review

Sato, Y, and M. Sadatomi. 1981. "Momentum and Heat Transfer in Two-Phase Bubble Flow." *International Journal of Multiphase Flow* 7: 167–77.

Shahnazari, M. R., Z. Ahmadi, and L. S. Masooleh. 2017. "Perturbation Analysis of Heat Transfer and a Novel Method for Changing the Third Kind Boundary Condition into the First Kind." *Journal of Porous Media* 20 (5): 449–60. <https://doi.org/10.1615/jpormedia.v20.i5.60>.

Shen, Fei, Libin Tian, Hairong Yuan, Yunzhi Pang, Shulin Chen, Dexun Zou, Baoning Zhu, Yanping Liu, and Xiujin Li. 2013. "Improving the Mixing Performances of Rice Straw Anaerobic Digestion for Higher Biogas Production by Computational Fluid Dynamics (CFD) Simulation." *Applied Biochemistry and Biotechnology* 171 (3): 626–42. <https://doi.org/10.1007/s12010-013-0375-z>.

Shewale, Satish D., and Aniruddha B. Pandit. 2006. "Studies in Multiple Impeller Agitated Gas-Liquid Contactors." *Chemical Engineering Science* 61 (2): 489–504. <https://doi.org/10.1016/j.ces.2005.04.078>.

Singh, Buta, Zoltán Szamosi, and Zoltán Siménfalvi. 2019. "State of the Art on Mixing in an Anaerobic Digester: A Review." *Renewable Energy* 141: 922–36. <https://doi.org/10.1016/j.renene.2019.04.072>.

Singh, Buta, Zoltán Szamosi, and Zoltán Siménfalvi. 2020. "Techniques for Evaluation of Mixing Efficiency in an Anaerobic Digester." *Solutions for Sustainable Development - Proceedings of the 1st International Conference on Engineering Solutions for Sustainable Development, ICES2D 2019 050004 (November): 139–47.* <https://doi.org/10.1201/9780367824037-19>.

Siverts-Wong, Elena, Taira Newman, Tom Chapman, and Chein-Chi Chang. 2017. "Mixing and Transport." *Water Environment Research* 89 (10): 1503–16. <https://doi.org/10.2175/106143017X15023776270548>.

Supardan, Muhammad Dani, Yoshifumi Masuda, Akinori Maezawa, and Shigeo Uchida. 2007. "The Investigation of Gas Holdup Distribution in a Two-Phase Bubble Column Using Ultrasonic Computed Tomography." *Chemical Engineering Journal* 130 (2–3): 125–33. <https://doi.org/10.1016/j.cej.2006.08.035>.

Takahashi, Koji, Kunio Arai, and Shozaburo Saito. 1980. "POWER CORRELATION FOR ANCHOR AND HELICAL." *Journal of Chemical Engineering of Japan* 13: 147–50. <https://doi.org/10.1252/jcej.13.147>.

Tangup, A, Ecole Polytechnique, and Station Centre-ville. 1996. "A New Investigation of the Metzner-Otto Concept for Anchor Mixing Impellers" 74.

Tanguy, P A, and K Takenaka. 2005. "Power and mixing time study involving a maxblend W impeller with viscous newtonian and non-newtonian fluids" 85: 1514–23.

Tixier, N., G. Guibaud, and M. Baudu. 2003. "Determination of Some Rheological Parameters for the Characterization of Activated Sludge." *Bioresource Technology* 90 (2): 215–20. [https://doi.org/10.1016/S0960-8524\(03\)00109-3](https://doi.org/10.1016/S0960-8524(03)00109-3).

Chapter 2: Literature review

Tobo, Yohannis Mitiku, Jan Bartacek, and Ingmar Nopens. 2020. "Linking CFD and Kinetic Models in Anaerobic Digestion Using a Compartmental Model Approach." *Processes* 8 (6): 1–12. <https://doi.org/10.3390/PR8060703>.

Tomiyama, A., I. Žun, H. Higaki, Y. Makino, and T. Sakaguchi. 1997. "A Three-Dimensional Particle Tracking Method for Bubbly Flow Simulation." *Nuclear Engineering and Design* 175 (1–2): 77–86. [https://doi.org/10.1016/S0029-5493\(97\)00164-7](https://doi.org/10.1016/S0029-5493(97)00164-7).

Torotwa, Ian, and Ji Changying. 2018. "A Study of the Mixing Performance of Different Impeller Designs in Stirred Vessels Using Computational Fluid Dynamics." *Designs* 2 (1): 10. <https://doi.org/10.3390/designs2010010>.

Trad, Zaineb, Christophe Vial, Jean Pierre Fontaine, and Christian Larroche. 2015. "Modeling of Hydrodynamics and Mixing in a Submerged Membrane Bioreactor." *Chemical Engineering Journal* 282: 77–90. <https://doi.org/10.1016/j.cej.2015.04.119>.

Turovskiy, Izrail S. 2006. *Processing Wastewater Sludge Processing*. <https://doi.org/10.1002/047179161X>.

Venneker, Bart C.H., Jos J. Derksen, and Harrie E.A. Van den Akker. 2002. "Population Balance Modeling of Aerated Stirred Vessels Based on CFD." *AIChE Journal* 48 (4): 673–85. <https://doi.org/10.1002/aic.690480404>.

Verhoff, F. H., M. W. Tenney, and W. F. Echelberger. 1974. "Mixing in Anaerobic Digestion." *Biotechnology and Bioengineering* 16 (6): 757–70. <https://doi.org/10.1002/bit.260160606>.

Vesvikar, Mehul S., and Muthanna Al-Dahhan. 2015. "Effect of Scale on Hydrodynamics of Internal Gas-Lift Loop Reactor-Type Anaerobic Digester Using CFD." *Chemical Product and Process Modeling* 10 (3): 179–92. <https://doi.org/10.1515/cppm-2015-0009>.

Vrábel, Peter, Rob G.J.M. Van Der Lans, Karel Ch A.M. Luyben, Lotte Boon, and Alvin W. Nienow. 2000. "Mixing in Large-Scale Vessels Stirred with Multiple Radial or Radial and Axial Up-Pumping Impellers: Modelling and Measurements." *Chemical Engineering Science* 55 (23): 5881–96. [https://doi.org/10.1016/S0009-2509\(00\)00175-5](https://doi.org/10.1016/S0009-2509(00)00175-5).

Wang, Weijing, Zai Sha Mao, and Chao Yang. 2006. "Experimental and Numerical Investigation on Gas Holdup and Flooding in an Aerated Stirred Tank with Rushton Impeller." *Industrial and Engineering Chemistry Research* 45 (3): 1141–51. <https://doi.org/10.1021/ie0503085>.

Wiedemann, Leonhard, Fosca Conti, Tomasz Janus, Matthias Sonnleitner, Wilfried Zörner, and Markus Goldbrunner. 2017. "Mixing in Biogas Digesters and Development of an Artificial Substrate for Laboratory-Scale Mixing Optimization." *Chemical Engineering and Technology* 40 (2): 238–47. <https://doi.org/10.1002/ceat.201600194>.

Wu, Jing, Hong ming Zhou, Huai zhi Li, Peng cheng Zhang, and Jie Jiang. 2009. "Impacts of Hydrodynamic Shear Force on Nucleation of Flocculent Sludge in Anaerobic Reactor." *Water Research* 43 (12): 3029–36. <https://doi.org/10.1016/j.watres.2009.04.026>.

Chapter 3: Material and methods

3.1 Reactor setup

The experiments were carried out in a flat bottom cylindrical vessel with an internal diameter of 19 cm, which is shown in Figure 3-1. The setup was fixed on top of a cast iron bench to support the motor, shaft, mixer, tank, and air entrance valve installed at the bottom. For the purpose of flow field analysis, the reactor was made from transparent plexiglass, located in a rectangular tank filled with water to eliminate the reflection of light. Height-to-diameter (Aspect ratio) was designed to be adjusted to 1.4. The working volume of the reactor was 7 litres, furnished by an aluminum dual helical ribbon (H:15 cm, D:16 cm, and W:2 cm) rotated by an electrical motor adjusted to 50-100 rpm. The driven motor was equipped with a digital monitor, torque meter and controller. The geometric configuration of the stirred system is shown in Table 3-1. The air flows coming from a compressed air pipeline, has been controlled by a regulator toward a flowmeter (Omega engineering flow meter with accuracy of $\pm 2\%$ Full Scale) ranging from 0-2.2 LPM. A hose connected the flow meter to the surface sparger with a non-return valve installed at the bottom of the tank. The surface sparger was fixed at the bottom of the tank, using 10 drilled holes of 0.00025 m diameter.

Table 3-1 The geometric configuration of the stirred system

Vessel diameter (m)	inner	Vessel height (m)	Impeller height (m)	Impeller diameter (m)	Impeller blade diameter (m)	Impeller clearance (m)	Shaft diameter (m)
D		H	h	d	di	IC	ds
0.19		0.4	0.155	0.14	0.02	0.02, 0.04, 0.06	0.015

Chapter 3: Material and methods

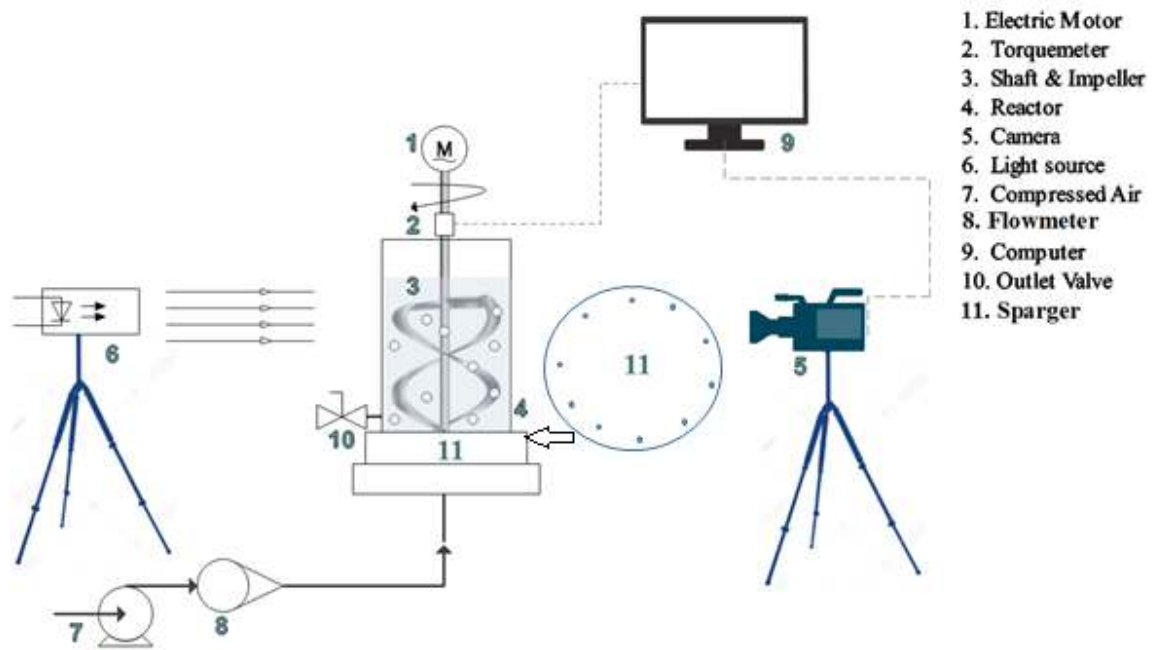


Figure 3-1: The Schematic of experimental setup

Chapter 3: Material and methods

3.2 Sample preparation

Transparent sludge simulants were provided by Rowe Company (Sydney, Australia) including PEG 400,000 with 2.25-4.5 Pa.s, 5 % in H₂O, NaCMC with a viscosity of 0.1-1 Pa.s, 2 % in H₂O, and XG from *Xanthomonas campestris* with a viscosity of 0.8-1.2 Pa.s. Further, alginate with a viscosity of 0.3-0.4 Pa.s, 1% in H₂O was supplied by Novachem Company (Australia). All these polymers have been verified as safe, extracted from natural resources and applicable within the food industry (Wasikiewicz et al. 2005).

The process of dissolving these four polymers in water was time consuming, requiring gentle agitation at 500 rpm for 12-24 hours using a magnetic stirrer. Because of the large size of the polymer molecules, it is suggested to gradually dissolve the polymers in deionized water to avoid agglomeration. Six solutions of varied concentrations (0.1, 0.5, 1, 1.5, 2, and 3 wt%) were prepared for each polymer. Following this, the samples were refrigerated and stored overnight to release any trapped bubbles.

The first series of result in Chapter 4 shows the strong similarity between rheological properties of XG and sludge compared to other polymers. However, NaCMC as a clear simulant fluid has been used in this study to facilitate the image processing procedure and PIV tests. Because XG solution clarity is poor for applying the visualization method.

3.3 Measurement of pH and zeta potential

A total of 24 samples were tested in terms of their stability and pH resistance. The major source of uncertainty in using these solutions is the likelihood of forming floccules, leading to instability. Therefore, the stability of the solution was examined by measuring Zeta potential (ζ -potential). An unstable solution shows particle surface charge between the range of -30 mv and +30 mv (Alexandru Grumezescu 2016). The Stable range of Zeta Potential is less than -30 mv and more than +30 mv. If the magnitude of particle surface charge (ζ -potential) in a solution

Chapter 3: Material and methods

shows a higher value, the likelihood of being agglomerated reduces. In this study, a Malvern zeta sizer (Malvern series ZEN 3500, Malvern Instruments Ltd., Worcester, UK) with a normal accuracy ± 0.1 mv, was used to measure ζ -potentials of solution.

The acid-base method was applied to measure mixing time in this study, where it was essential to control the level of pH tolerance of solutions. Therefore, a glass pH electrode (EUTECH, pH 700 with normal accuracy ± 0.1) was applied to evaluate the resistance of the solution to pH changes.

All experiments were repeated twice to account for human and instrument error.

3.4 Rheological measurement and test procedures

A DHR-3, TA Instruments rheometer with normal accuracy ± 0.005 was applied to measure the rheological characteristics of the solutions. The series of experiment were repeated under the same conditions, whereby poor signal/noise ratio was improved. The data collected from the rheometer was analysed to enable the formation of flow curves and to measure the level of viscoelasticity and thixotropy of solutions. The experiment was conducted in a coaxial cylinder cup (diameter 30.4 mm) and a bob (diameter 28 mm and height 42 mm) with a gap distance of 1 mm. The tests were carried out at a constant temperature of 25°C. The cup was filled with 20 ml of solution and pre-sheared for 15 min at 300 s⁻¹ in order to erase the previous memory. Following this, the samples were rested for 5 min at zero shear rate (Baudez, Slatter, and Eshtiaghi 2013). Then, the viscoelasticity of solutions was examined with amplitude sweep oscillation tests at 1 Hz through an increasing ramp of strain from 1% to 300%. By conducting the amplitude sweep oscillation tests, the solid-like (storage moduli, G') and liquid-like (loss Moduli, G'') behaviour of simulant materials can be clarified. To plot the flow curve, a flow sweep test was carried out through decreasing the ramp of shear rate from 1 to 300 s⁻¹ up to 15

Chapter 3: Material and methods

minutes (Deborah and De 2008). The gap between increasing and decreasing shear ramps identify the thixotropic level of fluid.

3.5 Mixing pattern

The performance of the impeller can be evaluated by measuring consumed power and mixing time. The ideal mixing process occurs when the complete mixed system is achieved with the shortest amount of time and minimum consumed power. Further, the intensity and duration of the mixing process plays a key role in digester throughput in terms of destroying the microorganism environment (Ward et al. 2008).

3.5.1 Mixing time

The most popular method to investigate mixing time is the Acid-Base technique (Taylor et al., n.d.; Foucault, Ascanio, and Tanguy 2004; Hari-prajitno et al. 1998; Deans, n.d.). By adding 7 ml of purple NaOH-Phenolphthalein solution to the agitated system, the solution starts to become purple. Following this 2 ml HCl acid was injected close to the central shaft on the top surface of liquid. All this process was recorded and captured with a high-speed camera (Samsung digital Camera 12 MP with dual pixel autofocus speed of 1.4 μm) for further analysis. This method makes it possible to detect the vanishing of dye throughout the system. The final point of mixing cannot be seen by just colouring method due to exitance of dye both in front and behind the point. The decolorization method can help to address this issue. In decolorization, the last point of mixing remains coloured and can be detected through the image processing method. In this study, an acid- base indicator dye was used to measure the mixing time (Paul, Atiemo-obeng, and Kresta 2004).

Chapter 3: Material and methods

3.6 Experimental design

The main objectives of the proposed study evaluate the influence of impeller speed, gas flow rate, viscosity, and impeller clearance from bottom of the tank in relation to mixing time and power consumption. Table 3-2 demonstrates the list of variables and their levels (minimum, maximum, and average), as obtained in the preliminary study.

Table 3-2 Variables applied in the optimization procedure of the impeller performance using RSM method

Symbols	Variables	Low level	Central level	High level
X ₁	Impeller speed (1/s)	50	75	100
X ₂	Gas flow rate (l/min)	0.5	1.35	2.2
X ₃	Impeller Clearance (m)	0.02	0.04	0.06
X ₄	Concentration (Wt%)	0.1	0.8	1.5

In the one-factor at one-time method (OFAT), there are unanswered questions about what the most influential factor is. Further, in this method interactions between parameters are completely neglected. To cover this gap, a full factorial method should be considered, requiring 125 tests for 3 variables. Applying statistical method would help to reduce the number of laboratory experiment and to optimize the experiment condition (Zitrom 1999).

The impacts and relationship between listed factors have been analysed through a three-factor three-level Box-Behnken method. Next, the optimization of factor levels was evaluated through response surface methodology (RSM). Accordingly, the most influential factor can be identified through this method. This process was repeated three times in order to ensure reproducibility of experiments.

This method of analyses not only reduces the number of experiments, but also optimizes interactions and quadratic effects. Equation 3-1 can be considered as a suitable choice to correlate all associated variables.

Chapter 3: Material and methods

$$Y = \beta_0 + \sum_{i=1}^3 \beta_i X_i + \sum_{i=1}^3 \beta_{ii} X_i^2 + \sum_{i=1}^3 \sum_{j=1}^3 \beta_{ij} X_i X_j + error \quad \text{Equation 3-1}$$

In this equation, Y refers to the response, for example mixing time, while β_0 , β_i , β_{ii} , and β_{ij} refer to regression coefficients. The most influential factors have been identified by drawing 3D surface plots (Zitrom 1999).

3.6.1 Installing impeller

In this part of the experiments, the helical ribbon impeller was installed inside the cylindrical reactor. The impeller shaft was rotated by an electric motor equipped with a speed controller installed outside the vessel. The power consumption was controlled between 5-8 W/m³, as recommended by the US EPA (U.S. Environmental Protection Agency, 1987). To monitor the inactive volume of fluid, 15 ml NaOH and florescent dye was well- stirred inside the digester to increase the pH until a green color appeared. Next, 20 ml of solution was collected and agitated with an adequate amount of HCl and injected near the impeller for visualization purposes. After injection, a discoloration process was observed and recorded during the time (t) by a high-speed camera.

3.6.2 Data analysis

The data gathered during the experiment was classified and analysed. Then, the results were interpreted and formed into graphs, tables, and charts using appropriate software. Some of the analysed and processed data has already been published in two high ranked scientific journals (M. Amirafabi and Khiadani Mehdi 2019a; M. Amirafabi, Khiadani, and Mohammed 2020). Additionally, the remainder of the experiments and numerical simulations are currently under review.

Chapter 3: Material and methods

3.7 CFD simulation

This study applied a combination of CFD- PBM models as well as a suitable drag model to predict the hydrodynamics of an agitated gas- liquid system. The first step involved developing 3D geometry, like what is used in experiments, with a few simplifications. Following this, the mesh was generated in five different cell sizes, ranging from coarse to small. The whole geometry was divided into three separate zones. The impeller is defined as a stagnant first body, while the tank is divided into inner and outer bodies, where the inner body rotates with the impeller speed. Each body has then been divided into a number of small and non-overlapping grids, called mesh. After defining the boundary conditions, five mesh were imported to the solver to study the mesh independency and grid sensitivity analysis.

The second phase of CFD modelling is putting the grid into the solver where the fluid variable, operating parameters, and physical boundary conditions are defined. The optimum operating conditions were determined from statistical analysis of previous experiments (M. Amirafabi, Khiadani, and Mohammed 2020). Rotational speed was examined in three different rotational speeds of 25, 75, and 150 rpm when the gas flow rate was equal to 1.8 LPM and concentration at %0.5 Wt. Next, the governing equations were solved for each cell using a suitable numerical algorithm. Recent studies suggest this discrete method is a successful technique to solve the PBM model (Hounslow, Ryall, and Marshall 1988).

Results including velocity field, pressure, and concentration were obtained during this procedure and extracted by post CFD software.

Finally, the CFD simulation predictions were compared with PIV results to verify the CFD model. The findings were reported, analysed, and plotted to compare to experiment results using the post CFD software.

This study divided bubble diameters to five different intervals in order to evaluate bubble deformation. The range of minimum and maximum bubble diameter can be investigated in a

Chapter 3: Material and methods

series of experiment by image processing analysis. This study follows the imaging or photographing techniques identified within the literature to measure local bubble size and find average size in an agitated vessel (Pant et al. 2015; Hirata, Nienow, and Moore 1994; Laakkonen, Moilanen, et al. 2005; Vlaev and Martinov 1998).

3.8 PIV measurements

3.8.1 PIV setup

The velocity field and bubble movement of agitated multiphase system were recorded and visualized using the Particle Image Velocimetry (PIV) technique. The 2D surface of the system was vertically divided into two zones to eliminate shadows. Figure 3-2 schematically shows how the PIV system works. The total number of images recorded by a PIV is 600, where seven samples were captured every second. In this work, an in-line dual-pulsed Nd:YAG laser (make: Dantec Dynamics, model: Dual Power 200-15) with 200mJ/pulse at $\lambda=532\text{nm}$ has been applied. Images were captured by a monochromatic CCD camera (make: Dantec Dynamics, model: Flow Sense EO 16M-9) with a resolution of 4920 x 3280 pixels and coupled with a Carl Zeiss (T*1.4/50) lens with a 50mm focal length. The data was analysed and processed by Dynamic Studio 5.1 software. To counter the effects of rising bubbles and noises through the system, a filter lens and fluorescent polymer particles (PMMA-RhB-Frak-Particles) with a mean average diameter of 20-25 μm were applied. The movement of these fluorescent particles visualized the trajectory of liquid during the mixing process.

Chapter 3: Material and methods

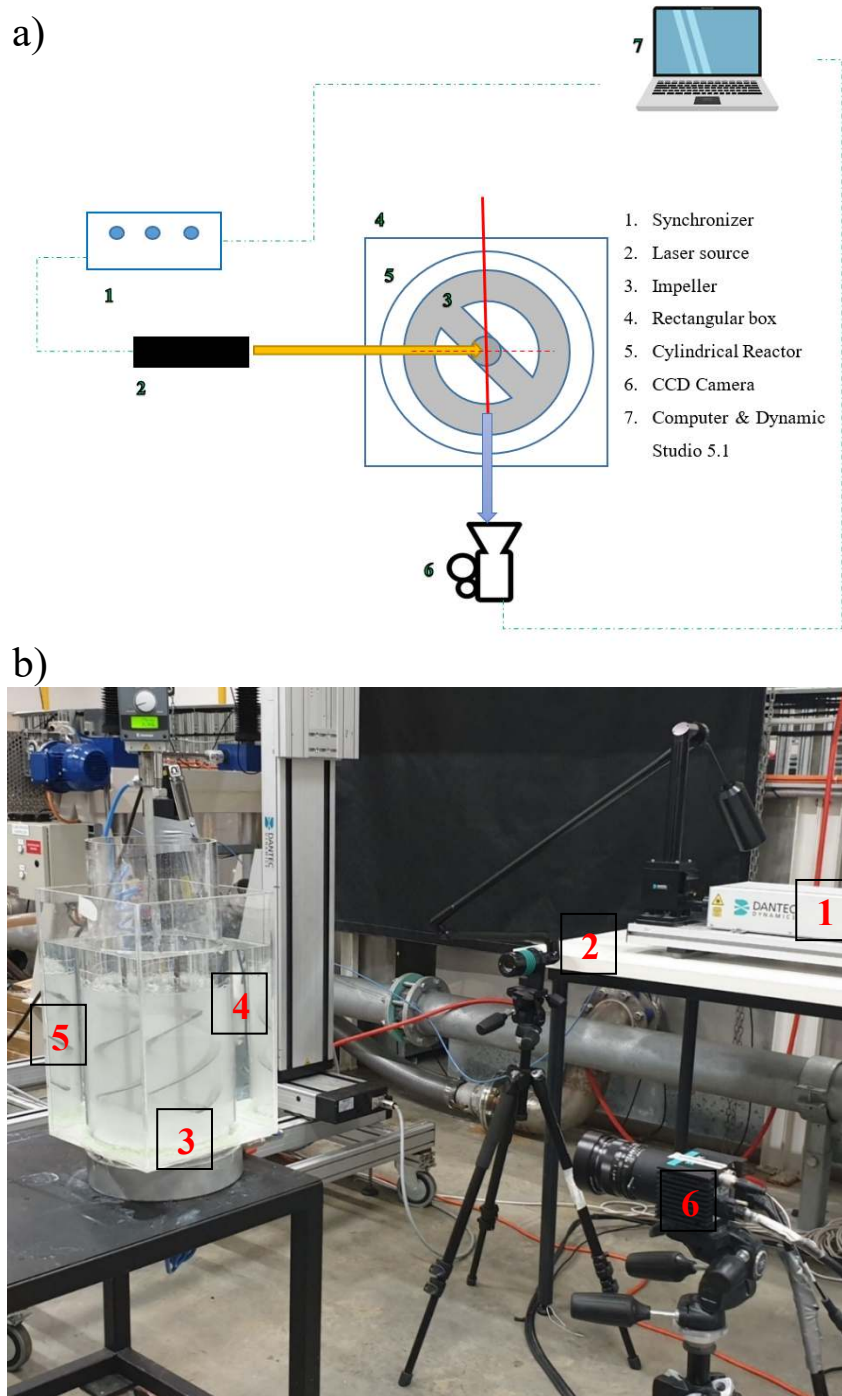


Figure 3-2 a) Schematic diagram of PIV system; and b) Real experimental setup.

3.9 References

Alexandru Grumezescu. 2016. Emulsions- Nanotechnology in the Agri-Food Industry. Edited by Patricia Osborn. Vol. 3. Elsevier. <https://doi.org/10.1002/9783527634798>.

Chapter 3: Material and methods

Amirafabi, Maryam, and Khiadani Mehdi. 2019. "Transparent Polymers to Emulate the Rheological Properties of Primary, Activated, and Digested Sludge Authors:" *Chemical Engineering Research and Design*. <https://doi.org/10.1016/j.mex.2019.03.017>.

Amirafabi, Maryam, Mehdi Khiadani, and Hussein A. Mohammed. 2020. "Performance of a Dual Helical Ribbon Impeller in a Two-Phase (Gas-Liquid) Stirred Tank Reactor." *Chemical Engineering and Processing - Process Intensification* 148: 107811. <https://doi.org/10.1016/j.cep.2020.107811>.

Baudez, J.C., Paul Slatter, and Nicky Eshtiaghi. 2013. "The Impact of Temperature on the Rheological Behaviour of Anaerobic Digested Sludge." *Chemical Engineering Journal*. <https://doi.org/10.1016/j.cej.2012.10.099>.

Deans, Sean. n.d. "Techniques for Mixing and Scaling in Mechanically Agitated Vessels."

Deborah, Intermediate, and Numbers De. 2008. *Rheology for Chemists*. *Rheology for Chemists*. <https://doi.org/10.1039/9781847558046>.

Foucault, By Støphane, Gabriel Ascanio, and Philippe A Tanguy. 2004. "Coaxial Mixer Hydrodynamics with Newtonian and Non-Newtonian Fluids," no. 3. <https://doi.org/10.1002/ceat.200401996>.

Hari-prajitno, Dana W A T I, P Ved, The Centre, and B Birmingham. 1998. "Gas-Liquid Mixing Studies with Multiple Up- and Down- Pumping Hydrofoil Impellers: Power Characteristics and Mixing Time" 76.

Hirata, Yushi, Alvin W. Nienow, and Iain P.T. Moore. 1994. "Estimation of Cavern Sizes in a Shear-Thinning Plastic Fluid Agitated by a Rushton Turbine Based on LDA Measurements." *Journal of Chemical Engineering of Japan*. <https://doi.org/10.1252/jcej.27.235>.

Hounslow, M. J., R. L. Ryall, and V. R. Marshall. 1988. "A Discretized Population Balance for Nucleation, Growth, and Aggregation." *AIChE Journal* 34 (11): 1821–32. <https://doi.org/10.1002/aic.690341108>.

Laakkonen, Marko, P. Moilanen, T. Miettinen, K. Saari, M. Honkanen, P. Saarenrinne, and J. Aittamaa. 2005. "Local Bubble Size Distributions in Agitated Vessel Comparison of Three Experimental Techniques." *Chemical Engineering Research and Design* 83 (1 A): 50–58. <https://doi.org/10.1205/cherd.04122>.

Pant, H. J., V. K. Sharma, K. T. Shenoy, and T. Sreenivas. 2015. "Measurements of Liquid Phase Residence Time Distributions in a Pilot-Scale Continuous Leaching Reactor Using Radiotracer Technique." *Applied Radiation and Isotopes* 97: 40–46. <https://doi.org/10.1016/j.apradiso.2014.12.010>.

Paul, Edward L, Victor a Atiemo-obeng, and Suzanne M Kresta. 2004. *Handbook of Industrial Mixing*. <https://doi.org/10.1002/0471451452>.

Taylor, Publisher, Reza Afshar Ghotli, Abdul A A Raman, and Shaliza Ibrahim. n.d. "LIQUID-LIQUID MIXING IN STIRRED VESSELS: A REVIEW Liquid-Liquid Mixing in Stirred Vessels: A Review," no. January 2014: 37–41. <https://doi.org/10.1080/00986445.2012.717313>.

Vlaev, Serafim D., and Martin Martinov. 1998. "Non-Uniformity of Gas Dispersion in Turbine-Generated Viscoelastic Circulation Flow." *Canadian Journal of Chemical Engineering* 76 (3): 405–12. <https://doi.org/10.1002/cjce.5450760309>.

Chapter 3: Material and methods

Ward, Alastair J., Phil J. Hobbs, Peter J. Holliman, and David L. Jones. 2008. "Optimisation of the Anaerobic Digestion of Agricultural Resources." *Bioresource Technology* 99 (17): 7928–40. <https://doi.org/10.1016/j.biortech.2008.02.044>.

Wasikiewicz, Jaroslaw M., Fumio Yoshii, Naotsugu Nagasawa, Radoslaw A. Wach, and Hiroshi Mitomo. 2005. "Degradation of Chitosan and Sodium Alginate by Gamma Radiation, Sonochemical and Ultraviolet Methods." *Radiation Physics and Chemistry* 73 (5): 287–95. <https://doi.org/10.1016/j.radphyschem.2004.09.021>.

Zitrom, Veronica C. 1999. "One-Factor-at-a-Time Versus Designed Experiments." *The American Statistician* 53 (2): 126–31. <https://doi.org/10.2307/2685731>.

Contents lists available at [ScienceDirect](https://www.sciencedirect.com)

Chemical Engineering Research and Design

journal homepage: www.elsevier.com/locate/cherd


Transparent polymers to emulate the rheological properties of primary, activated, and digested sludge

Maryam Amiraftabi, Mehdi Khiadani*

School of Engineering, Edith Cowan University, 270 Joondalup Drive, Joondalup, Perth, WA 6027, Australia

ARTICLE INFO

Article history:

Received 24 December 2018

Received in revised form 19

February 2019

Accepted 28 March 2019

Available online 18 April 2019

Keywords:

Sludge rheological characteristics

Simulant fluids

Xanthan gum

Flow curve

Viscoelastic modulus

ABSTRACT

Understanding the rheological characteristics of sludge is important for design and operation of water and wastewater treatment units including stirrers, mixers, pumps, and separators. Studying the rheological characteristics of real sludge involves health risks and complexity due to opaque nature of sludge and its time evolution caused by microbial activity and aging. Researchers have applied various simulants such as clay, minerals, and gels to prepare synthetic sludge and to perform a lab-scale study on rheological properties and flow behaviour of real sludge. Some of previous studies have ignored the stability and rheological characteristics of simulant fluids, which might lead to less reliable results. Therefore, selection of a safe, cheap and stable alternative that can mimic rheological behaviour of real sludge is still open and challenging. The proposed study examined the pH sensitivity, zeta potential characteristics and rheological properties of sodium carboxymethyl cellulose, polyethylene glycol, sodium alginate, and xanthan gum as popular model fluids with different concentrations (0.1, 0.5, 1, 1.5, 2, and 3 wt%) in details. A comparison of rheological properties of these fluids with the rheology of different types of sludge indicated that xanthan gum is a preferred simulant fluid that mimic the behaviour of sludge for the shear rate below 100 s^{-1} . Analysis of zeta potential and pH sensitivity indicates that xanthan gum is also a resistant solution to pH changes and agglomeration. In addition, it replicates sludge behaviour in terms of viscosity, flow curve, and Herschel–Bulkely parameters. Nevertheless, xanthan gum does not support thixotropy and viscoelastic characteristics of sludge.

© 2019 Institution of Chemical Engineers. Published by Elsevier B.V. All rights reserved.

1. Introduction

Increasing amounts of annually produced wastewater due to rapid population growth and accelerated urbanization pose negative effects on both the environment and human health. This rapid urbanization applies pressure on municipal wastewater treatment plants to increase the capacity and to reduce the size of treatment units. Wastewater treatment authorities are now focused on optimizing the design and efficiency of wastewater treatment units to minimize the amount of produced sludge. Therefore, studies of the rheological and hydrodynamic behaviour of municipal sludge including viscosity, flow behaviour, viscoelasticity, and thixotropy have become an important

topic from both an industry and research perspective (Baroutian et al., 2013; Dai et al., 2014; Feng et al., 2017; Liu et al., 2016; Markis et al., 2014; Miryahyaei et al., 2018; Oz et al., 2014; Ratkovich et al., 2013; Zhang et al., 2016). Some experimental works have proved that rheology of fluid influences design factors, capital costs and performance of sludge processing units (Baudez et al., 2007; Feng et al., 2017; Liu et al., 2016; Papa et al., 2015; Ratkovich et al., 2013; Spinosa and Lotito, 2003). An example of these variables are the contribution of rheology to pressure drop in pipelines, energy consumption and fouling in membrane bioreactors, aeration tanks and, anaerobic digesters, head loss in pumps and surface area in heat exchangers (Amiraftabi et al., 2014; Ratkovich et al., 2013).

* Corresponding author.

E-mail addresses: m.amiraftabi@ecu.edu.au (M. Amiraftabi), m.khiadani@ecu.edu.au (M. Khiadani).
<https://doi.org/10.1016/j.cherd.2019.03.040>

0263-8762/© 2019 Institution of Chemical Engineers. Published by Elsevier B.V. All rights reserved.

Table 1 – Summary of previous studies that have used simulant fluids to mimic primary sludge (PS), activated sludge (AS), and digested sludge (DS).

Materials	Sludge	Appearance	Purpose	Reference
Suspensions of kaolin and quartz sand in water	AS	Turbid solution	To study yield stress of sludge	Spinosa and Lotito (2003)
Lanthanum chloride (LaCl ₃), polyethyleneimine, and poly[[3(methacryloylamino)-propyl]-trimethylammonium chloride)	AS/DS	–	Investigation of deswelling and flocculation of sludge	Legrand et al. (1998)
Suspension of glass bead and carbopol gel	DS	Transparent	Simulation of elastic rheological properties of sludge	Eshtiaghi et al. (2013)
Sulfate polystyrene latex particles suspended in sodium alginate	AS	Transparent	To understand bioflocculation of sludge	Sanin and Vesilind (1996)
Kaolin suspensions	AS	Turbid solution	Analysis of organic material and sludge distribution pattern	Dieudé-Fauvel et al. (2016)
Carbopol, laponite, and carboxymethyl cellulose sodium salt (NaCMC)	DS	Transparent	Investigation of rheological properties of thickened digested sludge	Eshtiaghi et al. (2012)
Xanthan gum	DS	Transparent	To visualize rheological behaviour of sludge when gas is injected	Bobade et al. (2018)
Xanthan gum	DS	Transparent	To improve mixing performance inside the digester	Kennedy (2017)
Xanthan gum	DS	Transparent	Visualization of the recirculation pattern inside the digester	Kennedy et al. (2014)
Sodium carboxymethyl cellulose (NaCMC), polyethylene glycol (PEG), acrylamide-based Polysinth0 (PS), and xanthan gum	DS	Transparent	To improve mixing pattern inside biogas digester	Wiedemann et al. (2017)

Despite great achievements in characterizing the rheological behaviour of sludge as a non-Newtonian fluid, there are still some barriers for effectively exploring the nature of sludge as the by-product of wastewater treatment plants. One of these barriers is time-dependent changes could take place in microbial conditions and activities of real sludge which make it impractical to transport to laboratory as this might not mimic the behaviour of sludge obtained at where it is originated ([Baudez and Coussot, 2001](#); [Dai et al., 2014](#); [Guibaud et al., 2004](#)). Additionally, sludge is a complex product that contains various organic and inorganic compounds making analytical study difficult. Further, real sludge is unhygienic and may contain protozoa, bacteria and viruses which can spread different types of diseases. Therewith, in some countries working with real sludge requires approval from health and safety authorities as a means of addressing these handling and microbiological concerns ([Baudez et al., 2007](#); [Spinosa and Vignoles, 2013](#); [Spinosa, 2016](#)).

Since managing, handling, and disposing of sludge is a challenging and demanding task, researchers have been investigating safe and easy alternatives (e.g. preparation of synthetic sludge) to facilitate an in-depth research on sludge ([Baudez et al., 2007](#); [Bobade et al., 2018](#); [Eshtiaghi et al., 2013, 2012](#); [Wiedemann et al., 2017](#)). Therefore, working with a model fluid that mimic sludge characteristics is desirable and can significantly assist in optimizing water and wastewater treatment process ([Baudez et al., 2007](#); [Besra et al., 2000](#)). A summary of previous studies with focus on the use of simulant/model fluids to study sludge behaviour is presented in [Table 1](#).

Several researchers have focused on producing synthetic sludge using various mineral substances such as calcite, talc, limestone, kaolin, and barium sulphate as one of the sludge main component ([Dieudé-Fauvel et al., 2016](#); [Legrand et al., 1998](#); [Spinosa and Lotito, 2003](#)). Whilst kaolin has frequently been used in previous studies ([Dieudé-Fauvel et al., 2016](#); [Sanin, 2002](#)), [Baudez et al.](#) explained that kaolin solution is not a suitable model fluid for simulating viscoelastic behaviour of sludge ([Baudez et al., 2013a](#)). [Eshtiaghi et al.](#) explored the rheological behaviour of sodium carboxymethyl cellulose (NaCMC), carbopol gel and laponite clay solutions as shear-thinning fluids with yield stress ([Eshtiaghi et al., 2013, 2012](#)). Previous studies have concluded that NaCMC is a suitable material to mimic the thickened digested sludge in

higher shear rates and carbopol can be used as a simulant fluid to predict the behaviour of thickened sludge in short time operation including pumping ([Eshtiaghi et al., 2013, 2012](#); [Flemming and Wingender, 2010](#); [Forster, 2008](#)).

Recently, xanthan gum (XG) has been applied as a proxy simulant fluid to study the shear behaviour of digested sludge ([Bobade et al., 2018](#); [Kennedy et al., 2015, 2014](#); [Kennedy, 2017](#)). [Wiedemann et al.](#) used different types of polymers including Walocel30000, NaCMC, polyethylene glycol (PEG), acrylamide-based Polysinth0 (PS), and XG and concluded NaCMC is the most suitable material ([Wiedemann et al., 2017](#)).

Most of previous literature used glassy and clear polymers to visualize qualitatively the flow pattern inside aerobic and anaerobic digesters through colorimetry method ([Bobade et al., 2018](#); [Kennedy, 2017](#); [Kennedy et al., 2014](#); [Wiedemann et al., 2017](#)). This non-intrusive technique is based on injection of pH sensitive fluorescent dyes or tracer into reactors followed by adding hydrochloric acid (HCl) and sodium hydroxide (NaOH) to change the pH of solution. Therefore, simulant fluid resistance to pH changes is one of the most critical criterion that need to be considered for selecting a simulant.

Following the discussion elaborated above, the proposed study pores over the pH stability, zeta potential analysis, and rheological properties of several suggested simulant fluids applied as model fluids in previous studies and compared with rheological behaviour of different types of municipal sludge. First, a review is carried out to explore some physical characteristics and composition of different types of municipal sludge including primary, activated and digested sludge. Municipal sludge is described as an odorous suspension including water (80%), trapped gas bubbles, and solid particles (20%). The solid particles consist of various components such as proteins, polysaccharides, lipids, minerals, bacteria, microorganisms and other dissolved materials ([Neyens and Baeyens, 2003](#); [Oz et al., 2014](#)). Primary, activated (secondary) and digested sludge originate from settling tank, aeration system and digester, respectively ([Baroutian et al., 2013](#); [Markis et al., 2014](#)). They differ in their composition, type of microorganisms, temperature, shape and size of solid particles, and pH. Some researchers have demonstrated that polysaccharides mainly form the structure of activated sludge ([Seviour et al., 2012, 2009](#)), while lipopolysaccharides

and proteins are the main polymers constituent of digested sludge (Baroutian et al., 2013; Flemming and Wingender, 2010; Forster, 2008; Neyens et al., 2004).

Although several previous studies have applied different types of polymers as synthetic sludge, there is no evidence for the suitability of these simulants to mimic the sludge rheology. Therefore, this study first explores and compares the rheological behaviour of four different types of polymers including NaCMC, PEG, sodium alginate (Alg), and XG for the concentration in the range of 0.5–3 wt%. To achieve this purpose, the viscosity and flow curve of NaCMC, PEG, Alg, and XG have been measured by applying the shear rates of low to medium range. Additionally, parameters of Herschel–Bulkely equation have been calculated for primary, activated and digested sludge using existing data in the literatures. Then, a comparison has been made between the rheological properties of real sludge and simulant fluids. Further, this study applied complimentary viscoelastic and thixotropic tests on the most suitable polymer and highlighted the applicable range of shear rate and concentration. The result of this study could be used to select and apply a safe, cheap, stable and clear simulant fluid, assisting researchers and practitioners to study the rheological and hydrodynamic behaviour of municipal sludge.

2. Materials and methods

2.1. Sample preparation

Technical polymer powders including NaCMC with viscosity of 0.4–1 Pa s, 2% in H₂O, PEG 400,000 with 2.25–4.5 Pa s, 5% in H₂O, and XG from *Xanthomonas campestris* with viscosity of 0.8–1.2 Pa s, were purchased from Rowe Company (Sydney, Australia). Both XG and NaCMC are organic matters originating from bacteria (*Xanthomonas campestris*) and cellulose, respectively, while poly ethylene glycol is a clear synthetic polymer widely applied in food industry. Additionally, Alg with viscosity 0.3–0.4 Pa s, 1% in H₂O was purchased from Novachem Company (Australia). This biopolymer is also a natural substance extracted from the cell wall of brown seaweed (Wasikiewicz et al., 2005).

Polymer powder requires time to dissolve in dionized water completely. As the gel networks became strong and form a paste for the concentration beyond 3 wt%, the solutions were only prepared in concentrations 0.1, 0.5, 1, 1.5, 2, and 3 wt% by dissolving the powders in ultrapure water. Homogenous solutions were prepared by gently stirring the solutions at 500 rpm for 12–24 h using a magnetic stirrer. All samples were refrigerated overnight at 4 ° to make sure the trapped air bubbles (if any) are removed from the solution.

2.2. Measurement of pH and zeta potential

The preliminary tests were carried out to evaluate the resistance of solution to pH changes. The pH values of simulant polymers were measured using a glass pH electrode (EUTECH, pH 700).

Zeta potential (ζ -potential) is a quantitative factor for quantifying the magnitude of particle surface charge and consequently the stability of particle in a continuous medium. A particle with a ζ -potential outside the range of –30 mv and +30 mv is considered stable. The higher value of ζ -potential means there is stronger repulsion force between particles which prevents agglomeration. Therefore, ζ -potential plays a pivotal role in the theory of aggregation stability. In this study, ζ -potentials of different polymers were measured using Malvern zeta sizer (Malvern series ZEN 3500, Malvern Instruments Ltd., Worcester, UK).

2.3. Rheological measurement and test procedures

The rheological characteristics of polymers including flow curve, viscoelasticity, thixotropy at various concentrations were measured by DHR-3, TA Instruments rheometer equipped with a coaxial cylinder cup having a diameter 30.4 mm, bob diameter 28 mm, bob height 42 mm, and gap distance 1 mm. In addition, a Peltier system was used to keep the temperature constant at 25 °C during the tests.

After loading the cup with 20 mL of solutions and reaching the equilibrium temperature, samples were pre-sheared up to 300 s⁻¹ for 15 min to fade the previous memory completely, followed by 5 min rest at zero shear rate (Baudez et al., 2013b). Next, amplitude sweep oscillation tests were carried out at 1 Hz through an increasing ramp of strain from 1% to 300% to measure the viscoelastic characteristics including solid-like (storage moduli, G') and liquid-like (loss Moduli, G'') behaviour of simulant materials. The flows sweep test was carried out under the imposed decreasing ramp of shear rate from 1 to 300 s⁻¹ up to 15 min for different concentration of polymers (Goodwin and Hughes, 2008). Then the measured shear stress and viscosity were plotted versus shear rate. The enclosed area between shear stress as a function of ramp of shear rate shows the thixotropic degree of the fluid.

Since low shear rates and laminar flow are more favourable in most biological process units including pumps, pipelines, reactors and mixers to provide a suitable environment for microbial activities, the rheological behaviour of polymers at higher shear rate was not investigated (Baroutian et al., 2013). Further, Baudez et al. concluded that digested sludge could show unusual rheological behaviour in higher shear stress and shear rates (Baudez et al., 2011). Therefore, this study has only focused on comparing the rheological behaviour of sludge and polymers for shear rates of less than 300 s⁻¹.

2.4. Non-Newtonian flow models

The proposed study applied the most frequently used non-Newtonian equations to model the rheological behaviour of sludge. The fundamental basis of these mathematical equations is the correlation between yield stress (τ_y), apparent viscosity and shear rate ($\dot{\gamma}$). In these equations, n is considered as the flow behaviour index which shows the degree and the type of non-Newtonian fluid, which for $n > 1$, the fluid is shear-thickening; for $0 < n < 1$, the fluid is shear-thinning and for $n = 1$, the fluid is Newtonian. In addition, k is the fluid consistency index, τ_y shows the critical shear stress (yield stress), and (τ) is shear stress (Brehmer et al., 2012; Wu et al., 2011). Hong et al., explained non-Newtonian equations in detail which are listed below (Hong et al., 2018).

$$\tau = k\dot{\gamma}^n \quad (\text{Power – law/Ostwald – de Waele model}) \quad (1)$$

This model does not consider the yield stress which is one of the most significant properties of sludge system.

$$\tau = \tau_y + k\dot{\gamma} \quad (\text{Bingham model}) \quad (2)$$

This model is a linear equation which cannot emulate the sludge flow curve in higher concentration where the shear

stress as a function of increasing shear rates changes exponentially (Baroutian et al., 2013; Eshtiaghi et al., 2013).

$$\tau = \tau_y + k\dot{\gamma}^n \quad (\text{Herschel – Bulkely model}) \quad (3)$$

The Herschel–Bulkely takes into consideration the yield stress and non-linearity between shear rate and shear stress of sludge (Baroutian et al., 2013; Baudez, 2008; Eshtiaghi et al., 2012). Herschel–Bulkley equation is the modified form of Power-law model emphasizing more on the solid concentration of sludge as a shear thinning fluid (Baudez et al., 2011). Therefore, this equation can mimic not only yield stress and shear-thinning characteristics of sludge but also the rheological behaviour of sludge under both stagnant and flowing conditions (Baroutian et al., 2013).

Additionally, although power-law, Herschel–Bulkley and Bingham models follow the same trend in lower concentration ranges, only Hershel–Bulkley and Power-law demonstrate the exponential behaviour of sludge in high concentrations (Baudez et al., 2011).

3. Results and discussion

3.1. Polymer resistance to pH changes

Some previous studies have considered transparency as a critical criterion for selecting simulant fluids. Application of transparency is in colorimetry where they injected pH sensitive dyes to visualize particle trajectory and flow pattern (Bobade et al., 2018; Kennedy, 2017; Kennedy et al., 2014; Wiedemann et al., 2017). The sensitivity of polymers to pH should be examined before using this method as pH variation influence the rheological properties and natural gel network structure of polymers (Alemdar et al., 2005). This study examined the pH effects on resistance of selected polymers by adding sodium hydroxide (NaOH) and hydrochloric acid (HCl) dropwise. Fig. 1(a) indicate the pH for the selected simulant fluids without and with pH adjustment, respectively. The results show that the viscosity of PEG and Alg changes dramatically with increasing or decreasing the pH. While the viscosity of XG and NaCMC shows strong stability to pH changes (for pH = 5–8).

Fig. 1(a) shows viscosity as a function of shear rate for different pH values (from 5 to 8) for XG 1 wt%. The results indicate that the viscosity of XG solution is stable over the tested range of pH. Some studies have also pointed out that the pH resistance of XG is due to its gel network structure (Baxter et al., 2008; Gilani et al., 2011; Santos et al., 2000). Therefore, the results suggest that PEG, Alg are not suitable sludge simulant where acid or alkaline are added to the system.

3.2. Zeta-potential analysis

Previous studies considered pH as the main factor that affects the number of charged reactive groups on the surface of polymers (Liu et al., 2009). Hence, a correlation between pH and ζ -potential is expected (Wang et al., 2017). Fig. 1(b) presents the ζ -potential of different simulant fluids and compares their ζ -potential as a function of pH. The results show that Alg and XG are relatively stable over different range of pH (5–8) caused by high and negative values of ζ -potential (below -30 mv). While the ζ -potential of PEG and NaCMC are within an unstable range (-30 mv to $+30$ mv). Consequently, PEG and NaCMC are at the

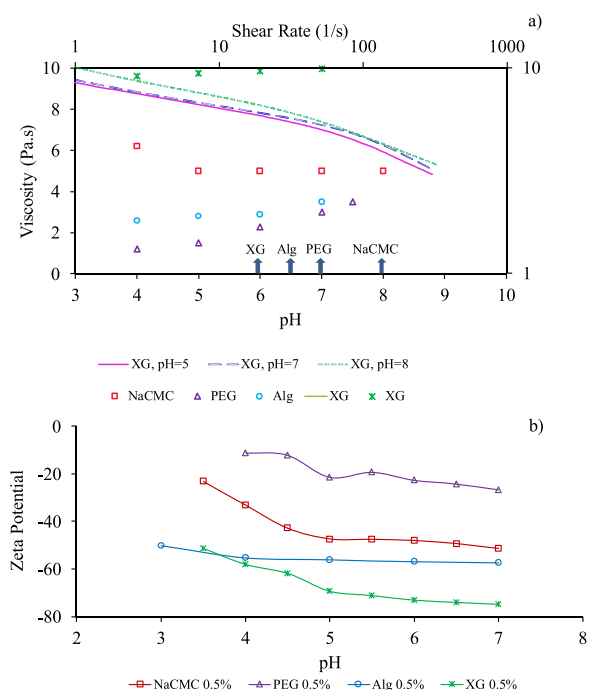


Fig. 1 – (a) Marker represent change of viscosity with pH for NaCMC, PEG, Alg, and XG (0.5 wt%), lines represent change of viscosity with shear rate for XG (0.5 wt%) for pH = 5, 7, and 8, vertical arrows show the neutralized pH for different polymers for 1 wt% concentration), (b) zeta potential of different simulant materials as a function of pH (shown with markers).

high risk of agglomeration because the ζ -potential of solution is located in the unstable range.

3.3. Shear-thinning behaviour of selected polymers

Fig. 2 presents viscosity versus shear rate in the range 0.01 – 300 s^{-1} for NaCMC, PEG, Alg and XG. The results show that these polymers have shear-thinning behaviour since viscosity is inversely proportional to shear rate. A similar behaviour has also been reported for different types of sludge (Ameur et al., 2011; Karim et al., 2004; Yang et al., 2009). Corresponding, Bhattacharya (1981) demonstrated the shear-thinning behaviour for primary and digested sludge with total solid concentration between 3 wt% and 8 wt%. Change in viscosity of polymers is due to internal molecular forces, molecular interactions and external resultant force-torque (Baudez et al., 2011; Benchabane and Bekkour, 2008; Eshtiaghi et al., 2013, 2012). Shear thinning behaviour can be attributed to disentanglement and orientation of the polymer coils set alongside the direction of the flow leading to a sharp increase in the elastic strain (Baudez et al., 2011; Benchabane and Bekkour, 2008; Eshtiaghi et al., 2013, 2012).

Further, Fig. 2 demonstrates that diluted solutions of NaCMC (Fig. 2(a)), PEG (Fig. 2(b)), and Alg (Fig. 2(c)) below 0.5 wt% concentration behave like Newtonian fluids until 10 s^{-1} . The main reason for this is the domination of water rheological properties inside the solutions. However, increasing polymer concentration elevates intensive non-Newtonian behaviour. As the solution concentration increases, polymer coils interpenetrate and form stronger networks, which leads to an increase in the viscosity of studied polymers (Baudez et al., 2011; Benchabane and Bekkour, 2008; Eshtiaghi et al., 2013, 2012). In contrast, as demonstrated in Fig. 2(d) this behaviour

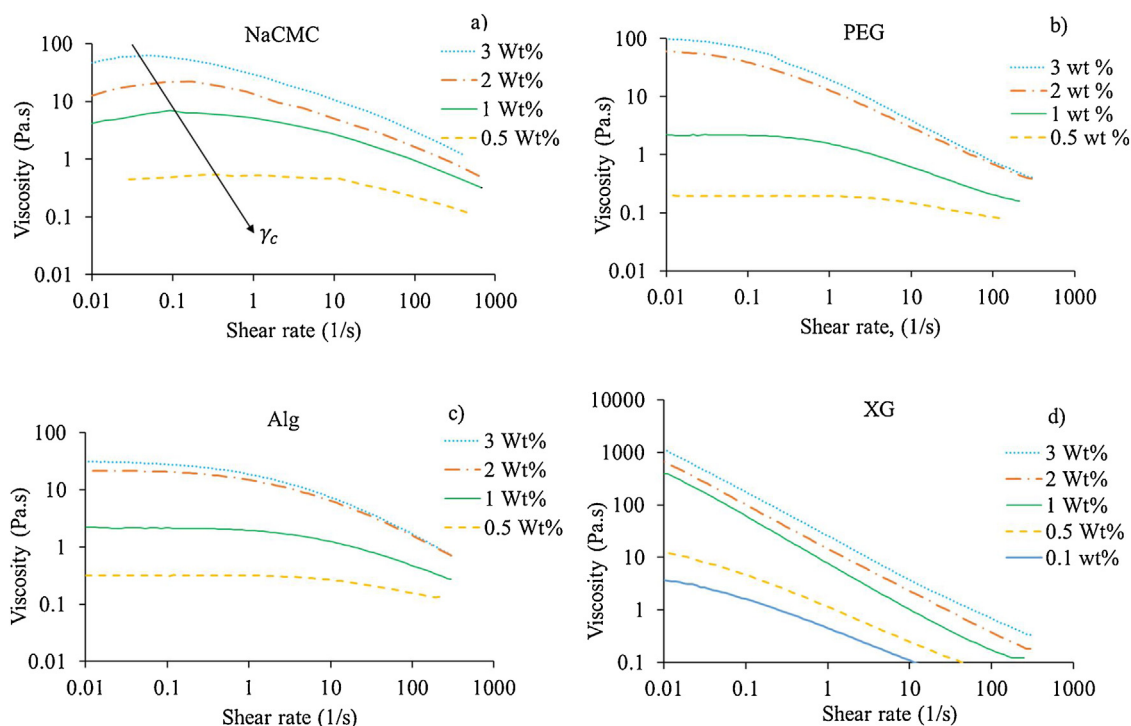


Fig. 2 – Viscosity versus shear rate for NaCMC, PEG, Alg, and XG for different concentrations where γ_c in (a) is the critical shear stress.

is absent in diluted solutions of XG. Furthermore, Fig. 2(a) represents a sigmoid curve in concentrations higher than 1 wt% for NaCMC. The point of inflection of the curve for higher concentrations indicates that the fluid behaviour changes from shear-thickening to shear-thinning. Some studies have observed a similar behaviour for NaCMC (Benchabane and Bekkour, 2008), while others have reported uniform ascending change of viscosity versus shear rate (Eshtiahi et al., 2012; Wiedemann et al., 2017). Sigmoid curves in all concentrations of NaCMC reflect the initial shear-thickening behaviour below critical shear stress (γ_c). Similarly, previous studies have reported that the initial shear-thickening behaviour is due to formation of entanglements of coils, a stiffer inner structure, and increase in intermolecular interactions (Benchabane and Bekkour, 2008).

3.4. Comparison between the flow behaviour of sludge and polymers

Many studies have focused on flow curve of real sludge as it is a reliable indicator for sludge rheological behaviour (Bhattacharya, 1981; Dai et al., 2014; Dieudé-Fauvel et al., 2016; Eshtiahi et al., 2012, 2003; Guibaud et al., 2004; Kennedy, 2017; Liu et al., 2016). Flow curve provides basic information for handling, processing, pumping, phase separation, sedimentation and stirring of non-Newtonian fluids. In this study, flow curves are plotted to compare rheological characteristics of selected polymers with different types of sludge. The flow curves of NaCMC and sludge for different concentrations are plotted in Fig. 3. Fig. 3(a) and (b) show that the flow behaviour of NaCMC and primary and digested sludge are different. Fig. 3(c) shows that the flow behaviour of digested sludge is also different from NaCMC excluding NaCMC with 2 wt% concentration within the range of 10–300 s⁻¹. At this concentration, NaCMC behaves similar to digested sludge 3.23 wt%. This similarity was also reported by Eshtiahi et al., who con-

sidered NaCMC as a suitable simulant material for digested sludge 3.23 wt%.

Fig. 4 compares the rheological behaviour of PEG with primary, activated and digested sludge. The results in this figure show that there is no significant similarity between the flow curve of PEG with primary, activated, and digested sludge. The most striking observation emerging from the data comparison is the similarity observed between flow behaviour of digested sludge 3.23 wt% and PEG 2 wt%. Additionally, primary sludge 6.5 wt% and PEG 1 wt% concentrations have similar behaviour in a limited range of shear rate according to the results shown in Fig. 4(a).

Fig. 5 compares the flow curve of Alg with primary, activated and digested sludge. According to these results, Alg and sludge show different flow behaviour, however, there are some similarities in a limited range of shear rate in which Alg 2 wt% can mimic digested sludge 8 wt% and primary sludge 4.24 wt% for the shear rate of 10–300 s⁻¹.

Fig. 6 compares the flow curves of XG with different types of sludge. The result indicates that the shear stress of XG and different types of sludge increase nonlinearly over the increasing shear rate. Contrary to other polymers, these results indicate that there is a strong similarity between the flow curve of XG and different types of sludge for the shear rate of 1–100 s⁻¹. However, Fig. 6(a) and (c) demonstrate insignificant inconsistencies between the rheological behaviour of XG with concentration between 0.1–3 wt% and primary sludge (3.7–6.5 TS%) and digested sludge (1.85–3.23%) within 10% difference. These similarities are also summarized in Table 2. A possible explanation is the difference between semi-solid network and molecular structures of XG and primary and digested sludge. Primary sludge is a highly thixotropic colloidal suspension containing suspended solid particles (Baudez et al., 2013b; Markis et al., 2016) and digested sludge consists of lipopolysaccharides and proteins (Baudez et al., 2013b). Contrastingly, XG is a polysaccharide with a gel struc-

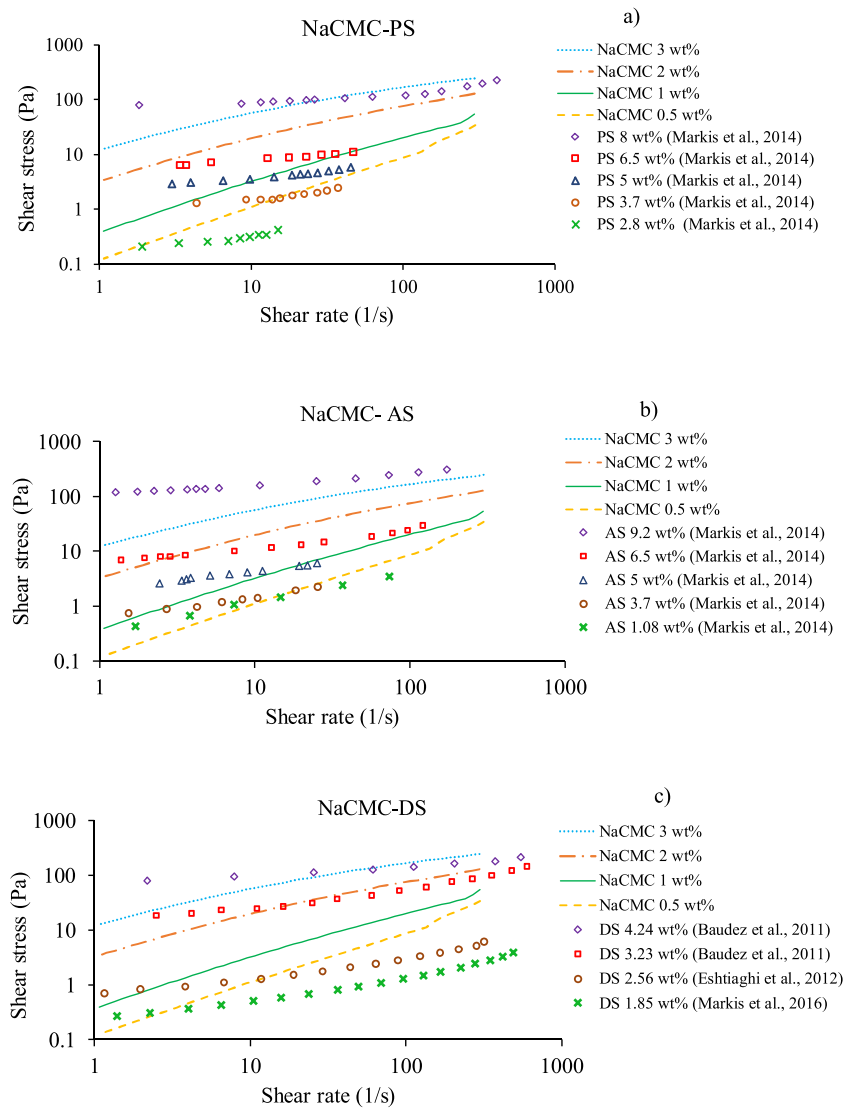


Fig. 3 – Comparison of NaCMC flow behaviour with: (a) primary, (b) activated, and (c) digested sludge.

Table 2 – Recommended xanthan gum concentrations for primary, activated and digested sludge of different TS%.

Sludge type	TS%	Xanthan gum concentration (wt%)	Shear rate limit (s ⁻¹)
Primary sludge	6.50%	1.10%	1–100
	5.00%	0.55%	1–100
	3.70%	0.25%	1–100
Activated sludge	6.50%	1.25%	1–100
	3.70%	0.75%	1–100
	2.80%	0.25%	1–100
	1.08%	0.20%	1–100
Digested sludge	3.23%	2.00%	1–100
	2.56%	0.20%	1–100
	1.85%	0.10%	1–100

ture network similar to that of activated sludge (Seviour et al., 2012, 2009). Fig. 6(b) shows that the flow behaviour of XG is closely comparable to activated sludge. The main reason for this close similarity is that both activated sludge and XG consist of long chain polysaccharides containing hydrogen bonds which can form a gel structure network (Seviour et al., 2012, 2009).

Further, for the shear rates more than 100 s⁻¹, the slope of XG flow curve changes due to the creation of vortex. Therefore, findings of this study are limited to shear rate 100 s⁻¹. Additionally, Fig. 6(c) shows that XG cannot be used as a simulant fluid for digested sludge for concentrations larger than 4 wt%.

With regards to the above results, XG is ranked as a preferred simulant fluid to mimic different types of sludge, particularly activated sludge. Subsequently, an attempt was made to draw a correlation between concentrations of XG and TS% of sludge. Table 2 summarizes the relationship between TS% and concentration of XG corresponding to a shear rate smaller than 100 s⁻¹ for primary, activated and digested sludge. These results facilitate selection of an appropriate concentration of XG for simulating a particular sludge. Other concentrations could be estimated by interpolation.

3.5. Comparison between Herschel–Bulkely parameters of sludge and polymers

Herschel–Bulkely is a widely accepted equation for estimating the rheological behaviour of primary, activated and digested sludge (Eshtiaghi et al., 2013; Kennedy et al., 2016). Table 3 shows the parameters of Herschel–Bulkely equation were calculated for extracted data from literature for primary, activated and digested sludge. The R-square values have

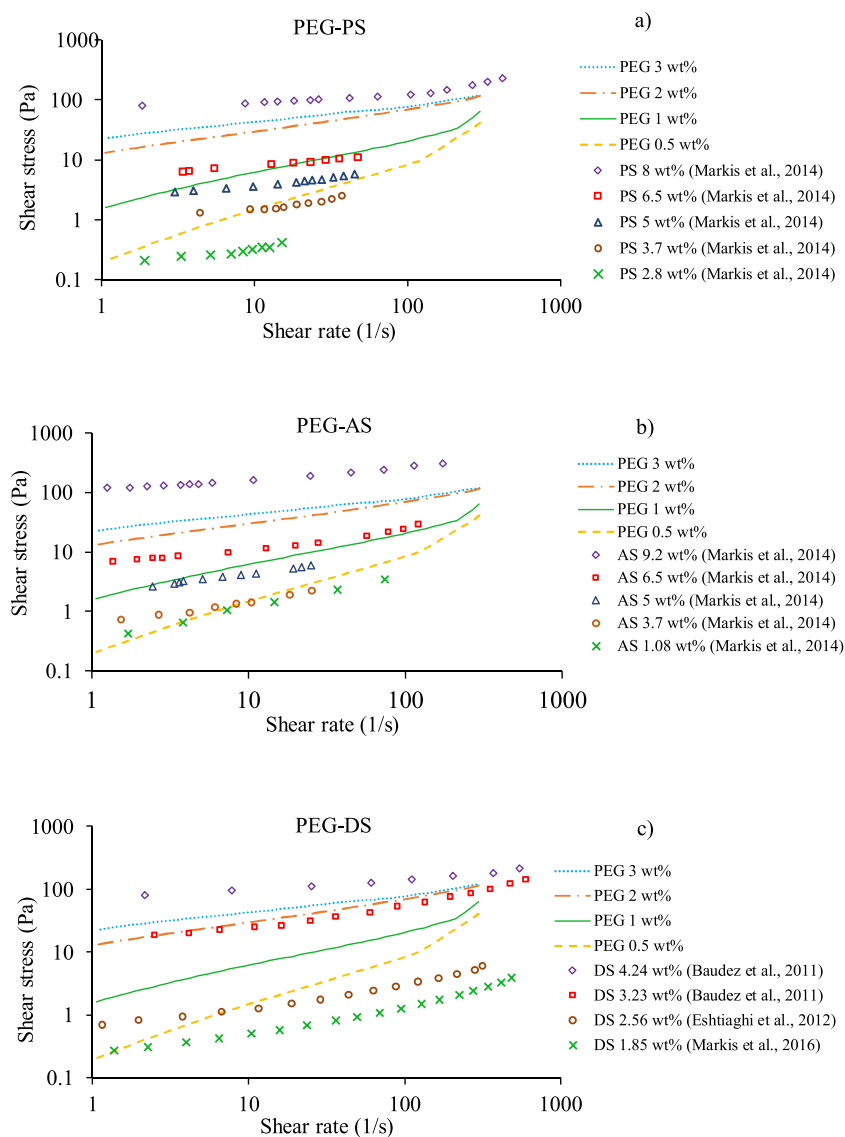


Fig. 4 – Comparison of PEG flow behaviour with: (a) primary, (b) activated, and (c) digested sludge.

Table 3 – Herschel-Bulkely parameters for primary, activated, and digested sludge.

Type of sludge	TS (%)	Parameters			R ²	Reference
		k	n	τ_y		
Primary sludge	2.80%	0.02	0.90	0.16	0.98	Markis et al. (2014)
	3.70%	0.09	0.75	0.87	0.97	Markis et al. (2014)
	5.00%	0.38	0.59	2.12	0.99	Markis et al. (2014)
	6.50%	0.79	0.52	15.04	0.99	Markis et al. (2014)
	8.00%	9.34	0.38	67.26	0.96	Markis et al. (2014)
Activated sludge	1.08%	0.24	0.61	0.15	0.99	Sanin (2002)
	3.70%	0.65	0.59	1.56	0.98	Markis et al. (2014)
	5.00%	1.22	0.56	3.20	0.99	Markis et al. (2014)
	6.50%	1.45	0.55	5.31	0.99	Markis et al. (2014)
	9.20%	22.20	0.44	95.02	0.99	Markis et al. (2014)
Digested sludge	1.85%	0.02	0.79	0.31	0.99	Baudez et al. (2011)
	2.56%	0.10	0.68	0.70	0.99	Baudez et al. (2011)
	3.23%	5.31	0.48	2.30	0.98	Eshtiaghi et al. (2012)
	4.24%	17.91	0.34	57.19	0.99	Markis et al. (2016)

been estimated to measure the degree of interrelation and dependence between variables. The results demonstrate a correlation between TS% and the Herschel-Bulkely parameters. Additionally, there is an increase in the fluid consistency index (k) and yield stress (τ) when the sludge total solid

concentration increases. However, flow behaviour index (n) is inversely proportional to TS%. Higher values of k and τ , and a lower value of n , demonstrates the higher viscosity which is directly correlated with higher total solid percentage.

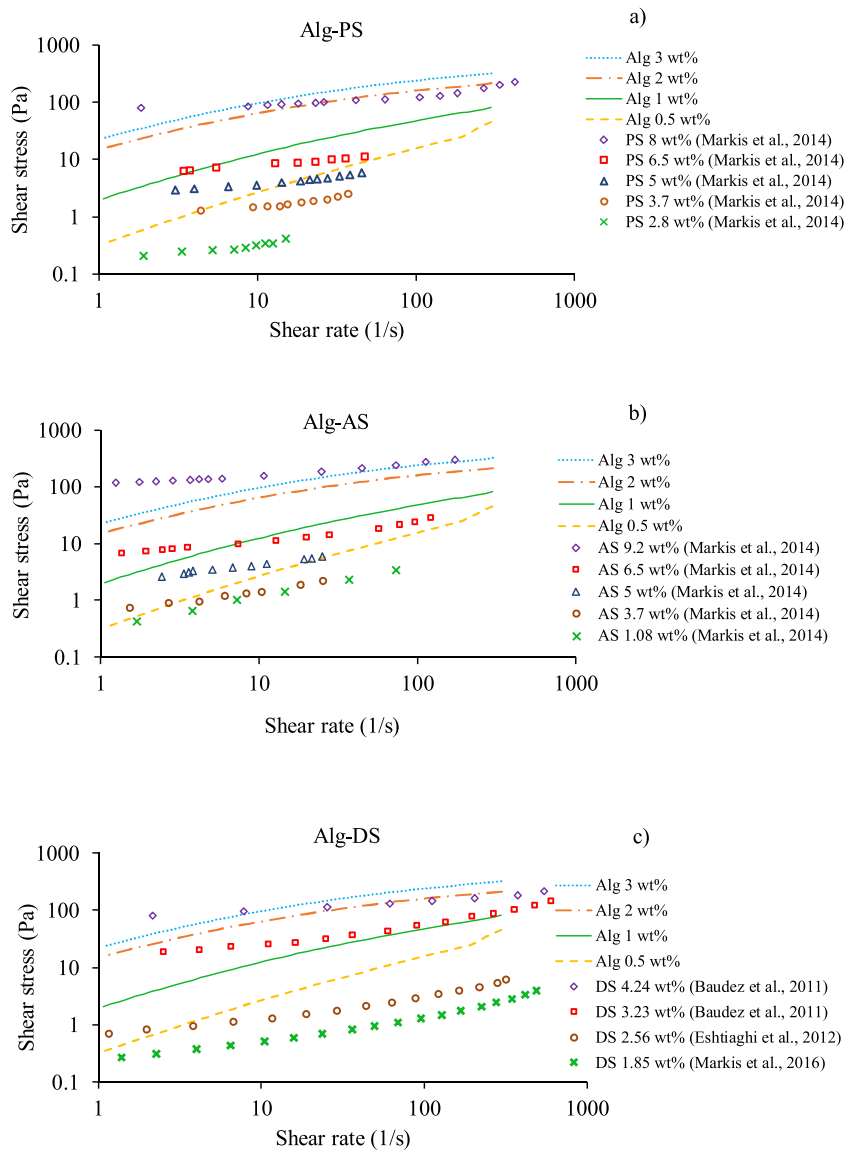


Fig. 5 – Comparison of Alg flow behaviour with: (a) primary, (b) activated, and (c) digested sludge.

Table 4 – Model parameters for polymers of different concentrations.

Polymer	Fitted model	Concentration (wt%)	Parameters			R ²
			k	n	τ_y	
NaCMC	Power-law	0.5%	0.13	0.92	–	0.99
		1%	0.46	0.82	–	0.99
		2%	6.08	0.54	–	0.99
		3%	21.37	0.44	–	0.99
Alginate	Power-law	0.5%	0.29	0.87	–	0.98
		1%	1.17	0.70	–	0.99
		2%	27.35	0.37	–	0.98
		3%	32.81	0.27	–	0.98
PEG	Power-law	0.5%	0.12	0.95	–	0.98
		1%	0.78	0.73	–	0.95
		2%	11.90	0.39	–	0.99
		3%	18.53	0.32	–	0.99
XG	Herschel–Bulkely	0.5%	0.35	0.62	2.26	0.99
		1%	0.90	0.50	3.40	0.99
		2%	6.64	0.32	8.54	0.99
		3%	6.99	0.24	19.06	0.99

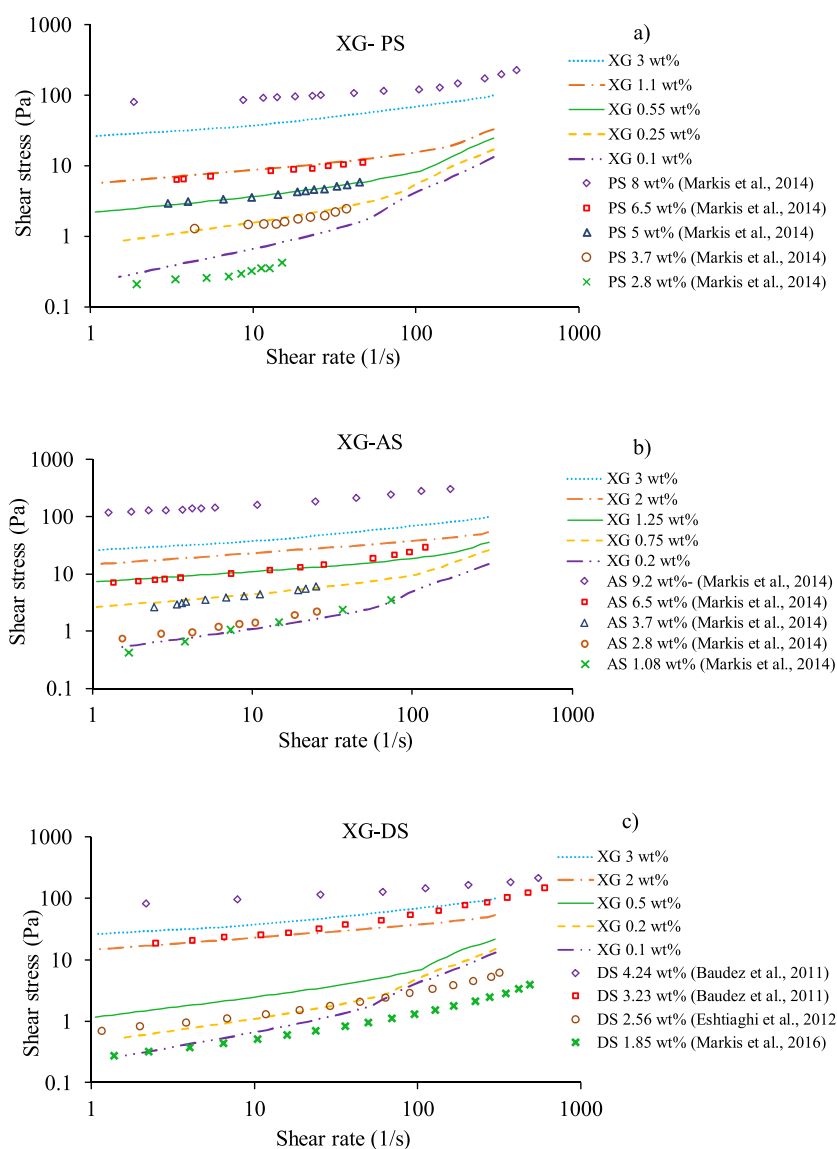


Fig. 6 – Comparison of XG flow behaviour with: (a) primary, (b) activated, and (c) digested sludge.

Similarly, calculated Herschel–Bulkely parameters for NaCMC, PEG, Alg, and XG, and are summarized in Table 4. The R-square method has been used to evaluate the accuracy of obtained data. The results indicate that n is less than unity for the used polymers, which suggest they are pseudo-plastic fluids. Moreover, the best fitted non-Newtonian model for NaCMC, PEG, Alg is power-law, whereas XG follows the Herschel–Bulkely equation. As mentioned earlier, the main difference between power-law and Herschel–Bulkely is the yield stress, where XG requires an initial yield stress (γ_c) to flow. This yield stress could be originated from a large number of hydrogen bonds in XG gel-like structure (Kennedy et al., 2015). Also, sludge can flow when their stress overcome critical yield stress (Baroutian et al., 2013; Baudez, 2008; Eshtiaghi et al., 2012). Therefore, both XG and sludge are considered an elastic materials and flow after breaking their internal structure network. Altogether, the summarized results in Table 4 suggests that XG among all other polymers is the preferred simulant to mimic the shear stress, yield stress, and viscosity of sludge.

3.6. Comparison between the viscoelastic behaviour of digested sludge and XG

This section compares viscoelastic behaviour of XG with digested sludge. Due to lack of experimental data for viscoelastic behaviour of primary and activated sludge in literature, this study focused on viscoelastic behaviour of digested sludge. Fig. 7 shows the viscoelastic curve and its stress response (storage modulus (G') and loss modulus (G'')) as a function of strain) for different concentration of XG and digested sludge (3.23 wt %). Similar to viscosity and flow curve as shown in Table 2, it is expected that moduli of XG 2 wt% and digested sludge with 3.23 wt% TS show similar behaviour. However, the result in Fig. 7 show that XG is unable to replicate the viscoelasticity of digested sludge. Further study is required to investigate the viscoelasticity of primary, secondary, and digested sludge. The elastic modulus G' and G'' remain almost constant when strain increases followed by a sudden break in the gel network structures. Additionally, the storage modulus is larger than the loss modulus, which means

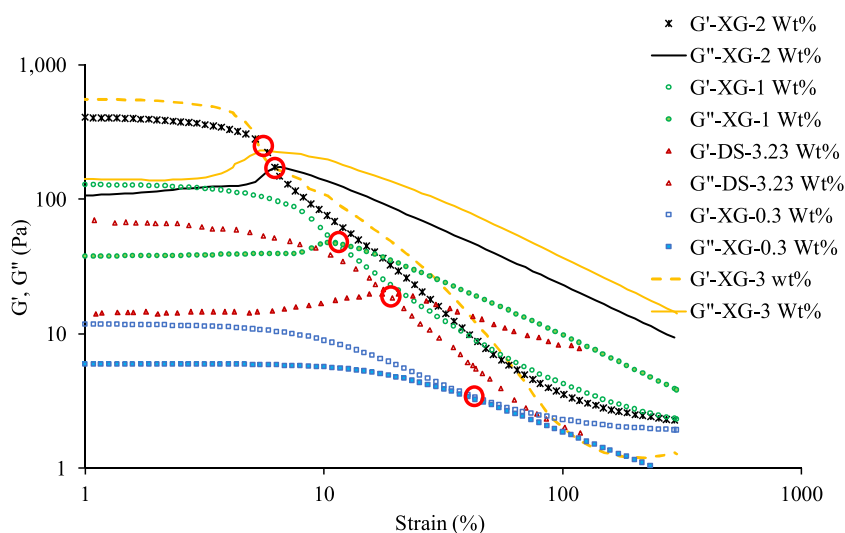


Fig. 7 – Storage modulus (G') and loss modulus (G'') as a function of strain for different concentration of xanthan gum and digested sludge (3.23 wt%). The red circles are the break down points in that $G' = G''$. (For interpretation of the references to colour in this figure legend, the reader is referred to the web version of this article).

the gel structure dominates external forces before reaching the cross-over point ($G' = G''$). This point is the intersection where mechanical forces break down the microstructure of the gel. Previous studies have also reported similar trends for digested sludge (Baudez et al., 2013a; Feng et al., 2015, 2014). Fig. 7 also indicates that in higher concentrations, cross-over points shift to a lower strain. The main reason for this is that the increased sensitivity of strain in higher concentration enhances breaking structure of the gel networks. Eshtiaghi et al. (2013, 2012) also reported similar behaviour for digested sludge, where it was proved that the structure of digested sludge is increasingly sensitive to strain when solid particles are added. Overall, the results in Fig. 7 shows that XG cannot exactly fit into the viscoelastic curve of digested sludge. Therefore, there is some errors in viscoelastic behaviour if we use XG as a simulant fluid.

3.7. Comparison between the thixotropic behaviour of activated sludge and XG

Primary, activated and digested sludge are classified as thixotropic materials, meaning that the viscosity of these sludge depend not only on temperature and shear rate but also on time (Baroutian et al., 2013; Baudez et al., 2013a; Lotito et al., 1997; Markis et al., 2014). After increasing the shear rate, its internal network requires some time to reform and return to its equilibrium state. The flow curve of thixotropic material does not follow an exact path on the network breakdown and rebuilding due to the stabilization of its structure between these two. The enclosed area between the two shear stress curves shaped by fluctuation of shear rates, forms a hysteresis loop which represents the energy consumed to break the structure of the network (Perret et al., 1996). Fig. 8 compares the hysteresis loop for activated sludge with 2.8 wt% TS (Markis et al., 2014) with the corresponding XG concentration of 0.25 wt% that is obtained from Table 2. Moreover, the results show that although the flow curves of XG and activated sludge follow the same trend over the increasing shear rates, their broken structures do not recover in the same way. For this reason, it can be concluded that XG unable mimic the thixotropic behaviour of activated sludge. In other words, activated sludge is an extremely thixotropic material, while

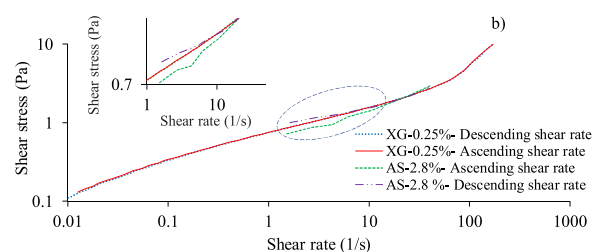


Fig. 8 – Comparison of hysteresis loop of xanthan gum 0.25 wt% with activated sludge (AS) 2.8 wt%. The enclosed area for xanthan gum is too small, while the gaps between shear ramps for activated sludge is extremely wide.

thixotropy of XG is not significant. There is a lack of experimental data for thixotropy of digested and primary sludge in the literatures, therefore this study just focused on thixotropic behaviour of activated sludge.

4. Conclusions

The purpose of this study was to investigate the rheological properties of four different types of shear-thinning polymers used as surrogate to replicate the rheological behaviour of various types of sludge. Zeta potential characterization, pH analysis, flow curve, viscoelasticity, and thixotropy were measured to draw comparison between simulant fluids and different types of sludge. Although xanthan gum, carboxyl methyl cellulose, polyethylene glycol and sodium alginate have been widely applied in previous studies, only a small number of rheological tests have been performed to characterise these simulant fluids. The proposed study shines a new light on the feasibility of using these simulant polymers through investigation of differences and similarities with sludge. Additionally, transparent simulant fluids are widely used to visualize the flow patterns and particle trajectory through colorimetry method required to change pH dramatically. The proposed study investigated the pH resistance and zeta potential of these polymers as this has barely been studied in the literature. This study highlights that only xanthan gum in low to medium shear rates (less than 100 s^{-1}) offers similarity to sludge. The flow curve and viscosity of xanthan

gum is closely similar to activated sludge and the reason for this might be the similar molecular and internal network structures. In addition, among these four types of polymers only xanthan gum follows the Herschel–Bulkely model as the most suitable equation for mimicking the behaviour of different types of sludge. However, xanthan gum and sludge seems to not show similar behaviour in terms of thixotropy and viscoelasticity. Thus, more study can be conducted to investigate the similarity between thixotropy and viscoelasticity of XG and different types of sludge.

The results of this study assist to select and apply a safe, cheap, stable and clear simulant fluid to study the rheological and hydrodynamic behaviours of sludge.

References

- Alemdar, A., Güngör, N., Ece, O.I., Atici, O., 2005. The rheological properties and characterization of bentonite dispersions in the presence of non-ionic polymer PEG. *J. Mater. Sci.* 40, 171–177, <http://dx.doi.org/10.1007/s10853-005-5703-4>.
- Ameur, H., Bouzit, M., Helmaoui, M., 2011. Numerical study of fluid flow and power consumption in a stirred vessel with a CABA 6SRGT impeller. *Int. J. Chem. Process. Eng. Res.* 32, 351–366, <http://dx.doi.org/10.2478/v10176-011-0028-0>.
- Amiraftebi, M.S., Mostoufi, N., Hosseinzadeh, M., Mehrnia, M.R., 2014. Reduction of membrane fouling by innovative method (injection of air jet). *J. Environ. Health Sci. Eng.* 12, 1–8, <http://dx.doi.org/10.1186/s40201-014-0128-0>.
- Baroutian, S., Eshtiaghi, N., Gapes, D.J., 2013. Rheology of a primary and secondary sewage sludge mixture: dependency on temperature and solid concentration. *Bioresour. Technol.* 140, 227–233, <http://dx.doi.org/10.1016/j.biortech.2013.04.114>.
- Baudez, J.-C., 2008. The sludge rheology exhibited a strong dependency on SRT and reactor's temperature. *Appl. Rheol.* 18.
- Baudez, J.-C., Coussot, P., 2001. Rheology of aging, concentrated, polymeric suspensions: application to pasty sewage sludges. *J. Rheol. (N. Y. N. Y.)* 45, 1123–1139, <http://dx.doi.org/10.1122/1.1392298>.
- Baudez, J.C., Ginisty, P., Peuchot, C., Spinosa, L., 2007. The preparation of synthetic sludge for lab testing. *Water Sci. Technol.* 56, 67–74, <http://dx.doi.org/10.2166/wst.2007.714>.
- Baudez, J.C., Markis, F., Eshtiaghi, N., Slatter, P., 2011. The rheological behaviour of anaerobic digested sludge. *Water Res.* 45, 5675–5680, <http://dx.doi.org/10.1016/j.watres.2011.08.035>.
- Baudez, J.C., Gupta, R.K., Eshtiaghi, N., Slatter, P., 2013a. The viscoelastic behaviour of raw and anaerobic digested sludge: strong similarities with soft-glassy materials. *Water Res.* 47, 173–180, <http://dx.doi.org/10.1016/j.watres.2012.09.048>.
- Baudez, J.C., Slatter, P., Eshtiaghi, N., 2013b. The impact of temperature on the rheological behaviour of anaerobic digested sludge. *Chem. Eng. J.*, <http://dx.doi.org/10.1016/j.cej.2012.10.099>.
- Baxter, R., Hastings, N., Law, A., Glass, E.J., 2008. *Food stabilisers, thickeners and gelling agent. Anim. Genet.*
- Benchabane, A., Bekkour, K., 2008. Rheological properties of carboxymethyl cellulose (CMC) solutions. *Colloid Polym. Sci.* 286, 1173–1180, <http://dx.doi.org/10.1007/s00396-008-1882-2>.
- Besra, L., Sengupta, D.K., Roy, S.K., 2000. Particle characteristics and their influence on dewatering of kaolin, calcite and quartz suspensions. *Int. J. Miner. Process.* 59, 89–112, [http://dx.doi.org/10.1016/S0301-7516\(99\)00065-4](http://dx.doi.org/10.1016/S0301-7516(99)00065-4).
- Bhattacharya, S.N., 1981. Flow characteristics of primary and digested sewage sludge. *Rheol. Acta* 20, 288–298, <http://dx.doi.org/10.1007/BF01678030>.
- Bobade, V., Cheetham, M., Hashim, J., Eshtiaghi, N., 2018. Influence of gas injection on viscous and viscoelastic properties of Xanthan gum. *Water Res.* 134, 86–91, <http://dx.doi.org/10.1016/j.watres.2018.01.071>.
- Brehmer, M., Eppinger, T., Kraume, M., 2012. Influence of rheology on the flow pattern in stirred biogas plants. *Chem. Ing. Tech.* 84, 2048–2056, <http://dx.doi.org/10.1002/cite.201200062>.
- Dai, X., Gai, X., Dong, B., 2014. Rheology evolution of sludge through high-solid anaerobic digestion. *Bioresour. Technol.* 174, 6–10, <http://dx.doi.org/10.1016/j.biortech.2014.09.122>.
- Dieudé-Fauvel, E., Héritier, P., Roux, J.C., 2016. Impact of sludge mechanical behaviour on spatial distribution parameters obtained with centrifugal spreader: preliminary study. *Eng. Agric. Environ. Food* 9, 242–249, <http://dx.doi.org/10.1016/j.eaef.2016.01.003>.
- Eshtiaghi, N., Markis, F., Yap, S.D., Baudez, J.C., Slatter, P., 2003. Rheological characterisation of municipal sludge: a review. *Sport Mark. Q.* 12, 206–216, <http://dx.doi.org/10.1016/j.buildenv.2013.04.022>. This.
- Eshtiaghi, N., Yap, S.D., Markis, F., Baudez, J.C., Slatter, P., 2012. Clear model fluids to emulate the rheological properties of thickened digested sludge. *Water Res.* 46, 3014–3022, <http://dx.doi.org/10.1016/j.watres.2012.03.003>.
- Eshtiaghi, N., Markis, F., Baudez, J.C., Slatter, P., 2013. Proxy model materials to simulate the elastic properties of digested municipal sludge. *Water Res.* 47, 557–5563, <http://dx.doi.org/10.1016/j.watres.2013.06.027>.
- Feng, G., Liu, L., Tan, W., 2014. Effect of thermal hydrolysis on rheological behavior of municipal sludge. *Ind. Eng. Chem. Res.* 53, 11185–11192, <http://dx.doi.org/10.1021/ie501488q>.
- Feng, G., Guo, Y., Tan, W., 2015. Effects of thermal hydrolysis temperature on physical characteristics of municipal sludge. *Water Sci. Technol.* 72, 2018–2026, <http://dx.doi.org/10.2166/wst.2015.425>.
- Feng, G.H., Ma, H., Bai, T., Guo, Y., 2017. Rheology characteristics of activated sludge and thermal treated sludge at different process temperature. *Water Sci. Technol.* 00, 1–8, <http://dx.doi.org/10.2166/wst.2016.501>.
- Flemming, H.C., Wingender, J., 2010. Relevance of microbial extracellular polymeric substances (EPSs) - Part I: structural and ecological aspects. *Nat. Rev. Microbiol.* 8, 623–633, <http://dx.doi.org/10.1038/nrmicro2415>.
- Forster, C.F., 2008. Bound water in sewage sludges and its relationship to sludge surfaces and sludge viscosities. *J. Chem. Technol. Biotechnol.* 33, 76–84, <http://dx.doi.org/10.1002/jctb.280330107>.
- Gilani, S.L., Najafpour, G.D., Heydarzadeh, H.D., Zare, H., 2011. Kinetic models for xanthan gum production using *Xanthomonas campestris* from molasses. *Chem. Ind. Chem. Eng. Q.* 17, 179–187, <http://dx.doi.org/10.2298/CICEQ101030002G>.
- Goodwin, Jim W., Hughes, R.W., 2008. Rheology for chemists. In: *The Theology for Chemists*. Royal Society of Chemistry, <http://dx.doi.org/10.1039/9781847558046>, ISBN code: 978-0-85404-839-7.
- Guibaud, G., Dollet, P., Tixier, N., Dagot, C., Baudu, M., 2004. Characterisation of the evolution of activated sludges using rheological measurements. *Process Biochem.* 39, 1803–1810, <http://dx.doi.org/10.1016/j.procbio.2003.09.002>.
- Hong, E., Yeneneh, A.M., Sen, T.K., Ang, H.M., Kayaalp, A., 2018. A comprehensive review on rheological studies of sludge from various sections of municipal wastewater treatment plants for enhancement of process performance. *Adv. Colloid Interface Sci.* 257, 19–30, <http://dx.doi.org/10.1016/j.cis.2018.06.002>.
- Karim, K., Varma, R., Vesvikar, M., Al-Dahhan, M.H., 2004. Flow pattern visualization of a simulated digester. *Water Res.* 38, 3659–3670, <http://dx.doi.org/10.1016/j.watres.2004.06.009>.
- Kennedy, S., 2017. *Improving the Mixing Performance of Anaerobic Digesters in Wastewater Treatment*.
- Kennedy, S., Parthasarathy, R., Eshtiaghi, N., Bhattacharya, S., 2014. *Liquid Jet Recirculation in a Model Digester: Flow Characteristics*, pp. 1–7.
- Kennedy, J.R.M., Kent, K.E., Brown, J.R., 2015. Rheology of dispersions of xanthan gum, locust bean gum and mixed biopolymer gel with silicon dioxide nanoparticles. *Mater. Sci. Eng. C* 48, 347–353, <http://dx.doi.org/10.1016/j.msec.2014.12.040>.

- Kennedy, S., Bhattacharjee, P.K., Eshtiaghi, N., Parthasarathy, R., 2016. Accelerating the spread of the active mixing region in a sludge simulant using submerged jets. *Chem. Eng. Res. Des.* 114, 331–340, <http://dx.doi.org/10.1016/j.cherd.2016.08.030>.
- Legrand, V., Hourdet, D., Audebert, R., Snidaro, D., 1998. Deswelling and flocculation of gel networks: application to sludge dewatering. *Water Res.* 32, 3662–3672, [http://dx.doi.org/10.1016/S0043-1354\(98\)00133-X](http://dx.doi.org/10.1016/S0043-1354(98)00133-X).
- Liu, S., Low, N.H., Nickerson, M.T., 2009. Effect of pH, salt, and biopolymer ratio on the formation of pea protein isolate gum arabic complexes. *J. Agric. Food Chem.* 57, 1521–1526, <http://dx.doi.org/10.1021/jf802643n>.
- Liu, J., Yu, D., Zhang, J., Yang, M., Wang, Y., Wei, Y., Tong, J., 2016. Rheological properties of sewage sludge during enhanced anaerobic digestion with microwave-H₂O₂ pretreatment. *Water Res.* 98, 98–108, <http://dx.doi.org/10.1016/j.watres.2016.03.073>.
- Lotito, V., Spinosa, L., Mininni, G., Antonacci, R., 1997. The rheology of sewage sludge at different steps of treatment. *Water Sci. Technol.* 36, 79–85, [http://dx.doi.org/10.1016/S0273-1223\(97\)00672-0](http://dx.doi.org/10.1016/S0273-1223(97)00672-0).
- Markis, F., Baudez, J.C., Parthasarathy, R., Slatter, P., Eshtiaghi, N., 2014. Rheological characterisation of primary and secondary sludge: impact of solids concentration. *Chem. Eng. J.* 253, 526–537, <http://dx.doi.org/10.1016/j.cej.2014.05.085>.
- Markis, F., Baudez, J.C., Parthasarathy, R., Slatter, P., Eshtiaghi, N., 2016. Predicting the apparent viscosity and yield stress of mixtures of primary, secondary and anaerobically digested sewage sludge: simulating anaerobic digesters. *Water Res.* 100, 568–579, <http://dx.doi.org/10.1016/j.watres.2016.05.045>.
- Miryahyaei, S., Olinga, K., Muthalib, F.A.A., Das, T., Aziz, M.S.A., Othman, M., Baudez, J.C., Batstone, D., Eshtiaghi, N., 2018. Impact of rheological properties of substrate on anaerobic digestion and digestate dewaterability: new insights through rheological and physico-chemical interaction. *Water Res.*, <http://dx.doi.org/10.1016/j.watres.2018.11.049>.
- Neyens, E., Baeyens, J., 2003. A review of thermal sludge pre-treatment processes to improve dewaterability. *J. Hazard. Mater.* 98, 51–67, [http://dx.doi.org/10.1016/S0304-3894\(02\)00320-5](http://dx.doi.org/10.1016/S0304-3894(02)00320-5).
- Neyens, E., Baeyens, J., Dewil, R., De Heyder, B., 2004. Advanced sludge treatment affects extracellular polymeric substances to improve activated sludge dewatering. *J. Hazard. Mater.* 106, 83–92, <http://dx.doi.org/10.1016/j.jhazmat.2003.11.014>.
- Oz, N.A., Uzun, A.C., Uzun, A.C., 2014. Comparing the Influence of Low Power Ultrasonic and Microwave Pre-treatments on the Solubilisation and Semi-continuous Anaerobic Digestion of Waste Activated Sludge., <http://dx.doi.org/10.1016/j.ultsonch.2014.04.018>.
- Papa, M., Pedrazzani, R., Nembrini, S., Bertanza, G., 2015. Should rheological properties of activated sludge be measured? *Appl. Rheol.* 25, <http://dx.doi.org/10.3933/APPLRHEOL-25-24590>.
- Perret, D., Locat, J., Martignoni, P., 1996. Thixotropic behavior during shear of a fine-grained mud from Eastern Canada. *Eng. Geol.* 43, 31–44, [http://dx.doi.org/10.1016/0013-7952\(96\)00031-2](http://dx.doi.org/10.1016/0013-7952(96)00031-2).
- Ratkovich, N., Horn, W., Helmus, F.P., Rosenberger, S., Naessens, W., Nopens, I., Bentzen, T.R., 2013. Activated sludge rheology: a critical review on data collection and modelling. *Water Res.* 47, 463–482, <http://dx.doi.org/10.1016/j.watres.2012.11.021>.
- Sanin, D.F., 2002. Effect of solution physical chemistry on the rheological properties of activated sludge. *Water SA* 28, 207–212, <http://dx.doi.org/10.4314/wsa.v28i2.4886>.
- Sanin, F.D., Vesilind, P.A., 1996. Synthetic sludge: a physical/chemical model in understanding bioflocculation. *Water Environ. Res.* 68, 927–933, <http://dx.doi.org/10.2175/106143096X127938>.
- Santos, V.E., Casas, J.A., Go, E., 2000. *Xanthan Gum: Production, Recovery, and Properties*, vol. 18.
- Seviour, T., Pijuan, M., Nicholson, T., Keller, J., Yuan, Z., 2009. Gel-forming exopolysaccharides explain basic differences between structures of aerobic sludge granules and floccular sludges. *Water Res.* 43, 4469–4478, <http://dx.doi.org/10.1016/j.watres.2009.07.018>.
- Seviour, T., Yuan, Z., van Loosdrecht, M.C.M., Lin, Y., 2012. Aerobic sludge granulation: a tale of two polysaccharides? *Water Res.* 46, 4803–4813, <http://dx.doi.org/10.1016/j.watres.2012.06.018>.
- Spinosa, L., 2016. Standardized characterization procedures: a necessary support to regulations. *Water Sci. Technol.* 74, 220–228, <http://dx.doi.org/10.2166/wst.2016.201>.
- Spinosa, L., Lotito, V., 2003. A simple method for evaluating sludge yield stress. *Adv. Environ. Res.* 7, 655–659, [http://dx.doi.org/10.1016/S1093-0191\(02\)00041-2](http://dx.doi.org/10.1016/S1093-0191(02)00041-2).
- Spinosa, L., Vignoles, C., 2013. *Developments of European Standardisation on Sludge: Guidelines for Good Practice 1* 10., pp. 55–61.
- Wang, H.F., Ma, Y.J., Wang, H.J., Hu, H., Yang, H.Y., Zeng, R.J., 2017. Applying rheological analysis to better understand the mechanism of acid conditioning on activated sludge dewatering. *Water Res.* 122, 398–406, <http://dx.doi.org/10.1016/j.watres.2017.05.002>.
- Wasikiewicz, J.M., Yoshii, F., Nagasawa, N., Wach, R.A., Mitomo, H., 2005. Degradation of chitosan and sodium alginate by gamma radiation, sonochemical and ultraviolet methods. *Radiat. Phys. Chem.* 73, 287–295, <http://dx.doi.org/10.1016/j.radphyschem.2004.09.021>.
- Wiedemann, L., Conti, F., Janus, T., Sonnleitner, M., Zörner, W., Goldbrunner, M., 2017. Mixing in biogas digesters and development of an artificial substrate for laboratory-scale mixing optimization. *Chem. Eng. Technol.* 40, 238–247, <http://dx.doi.org/10.1002/ceat.201600194>.
- Wu, X.hui, Wang, F., Sun, D.X., Yang, W.H., 2011. Rheology and flow characteristic of urban untreated sewage for cooling and heating source. *Exp. Therm. Fluid Sci.* 35, 612–617, <http://dx.doi.org/10.1016/j.expthermflusci.2010.11.009>.
- Yang, F., Bick, A., Shandalov, S., Brenner, A., Oron, G., 2009. Yield stress and rheological characteristics of activated sludge in an airlift membrane bioreactor. *J. Membr. Sci.* 334, 83–90, <http://dx.doi.org/10.1016/j.memsci.2009.02.022>.
- Zhang, J., Haward, S.J., Wu, Z., Dai, X., Tao, W., Li, Z., 2016. Evolution of rheological characteristics of high-solid municipal sludge during anaerobic digestion. *Appl. Rheol.*, 26, <http://dx.doi.org/10.3933/APPLRHEOL-26-32973>.

Chapter 4: Transparent polymers to emulate the rheological properties of primary, activated, and digested sludge

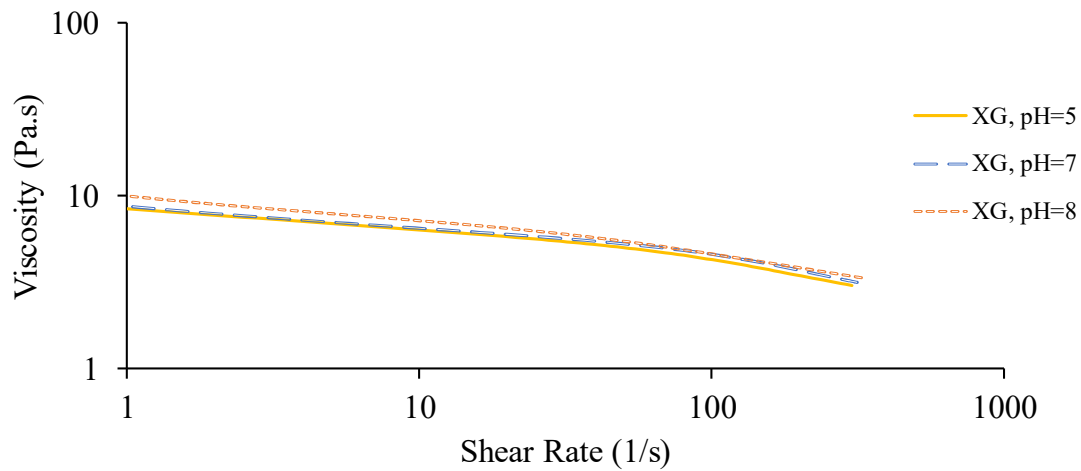


Figure 4-2 Effect of pH changes on viscosity of XG with concentration of 0.5% wt%.

4.4.2 Zeta-potential analysis

Previous studies considered pH as the main factor that affects the number of charged reactive groups on the surface of polymers (S. Liu, Low, and Nickerson 2009). Hence, a correlation between pH and ζ -potential is expected (H. F. Wang et al. 2017). Figure 4-3 presents the ζ -potential of different simulant fluids and compares their ζ -potential as a function of pH. Fig. 4-3 shows Alg and XG relative stability over different rang of pH caused by high and negative values of ζ -potential (below -30 mv). While the ζ -potential of PEO and NaCMC are within an unstable range (-30 mv- +30 mv). Consequently, PEO and NaCMC are at the high risk of agglomeration because the ζ -potential of solution is located in the unstable range.

Chapter 4: Transparent polymers to emulate the rheological properties of primary, activated, and digested sludge

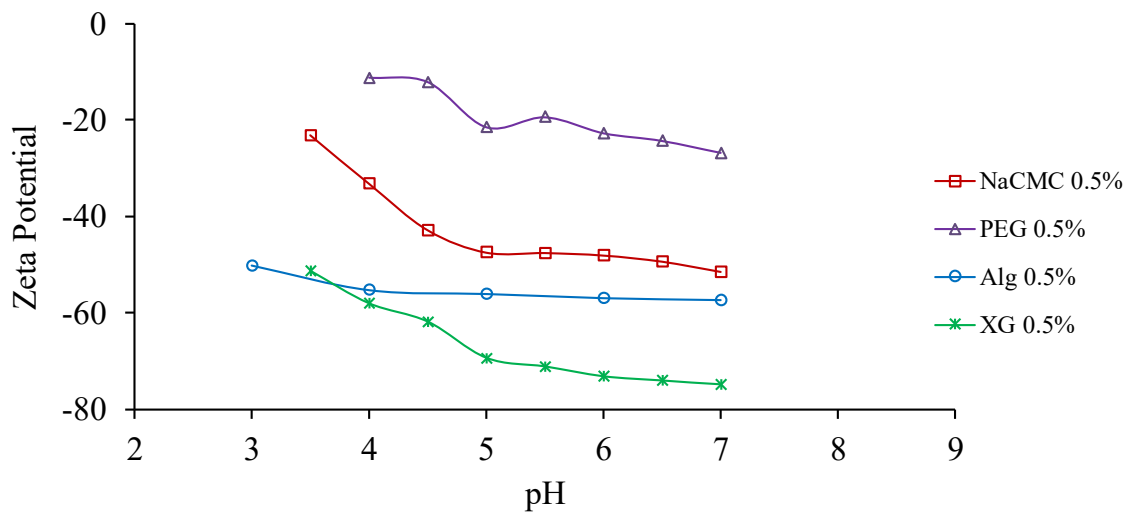


Figure 4-3 Zeta potential of different simulant materials as a function of pH.

4.4.3 Shear-thinning behaviour of selected polymers

Figure 4-4 presents viscosity versus shear rate in the range 0.01- 300s⁻¹ for NaCMC, PEG, Alg and XG. The results show that these polymers have shear-thinning behaviour since viscosity is inversely proportional to shear rate. A similar behaviour has also been reported for different types of sludge (Houari Ameer, Bouzit, and Helmaoui 2011; Karim et al. 2004; F. Yang et al. 2009). Corresponding, Markis et. al. (2014) demonstrated the shear-thinning behaviour for primary and digested sludge with total solid concentration between 3 wt% and 8 wt%. Change in viscosity of polymers is due to internal molecular forces, molecular interactions and external resultant force-torque (Baudez et al. 2011; Benchabane and Bekkour 2008; Eshtiaghi et al. 2013, 2012). Shear thinning behaviour can be attributed to disentanglement and orientation of the polymer coils set alongside the direction of the flow leading to a sharp increase in the elastic strain (Baudez et al. 2011; Benchabane and Bekkour 2008; Eshtiaghi et al. 2013, 2012).

Further, Fig. 4-4 demonstrates that diluted solutions of NaCMC (Fig. 4-4 a), PEG (Fig. 4-4 b), and Alg (Fig. 4-4 c) below 0.5 wt% concentration behave like Newtonian fluids. The main reason for this is the domination of water rheological properties inside the solutions. However,

Chapter 4: Transparent polymers to emulate the rheological properties of primary, activated, and digested sludge

increasing polymer concentration elevates intensive non-Newtonian behaviour. As the solution concentration increases, polymer coils interpenetrate and form stronger networks, which leads to an increase in the viscosity of studied polymers (Baudez et al. 2011; Benchabane and Bekkour 2008; Eshtiaghi et al. 2013, 2012).

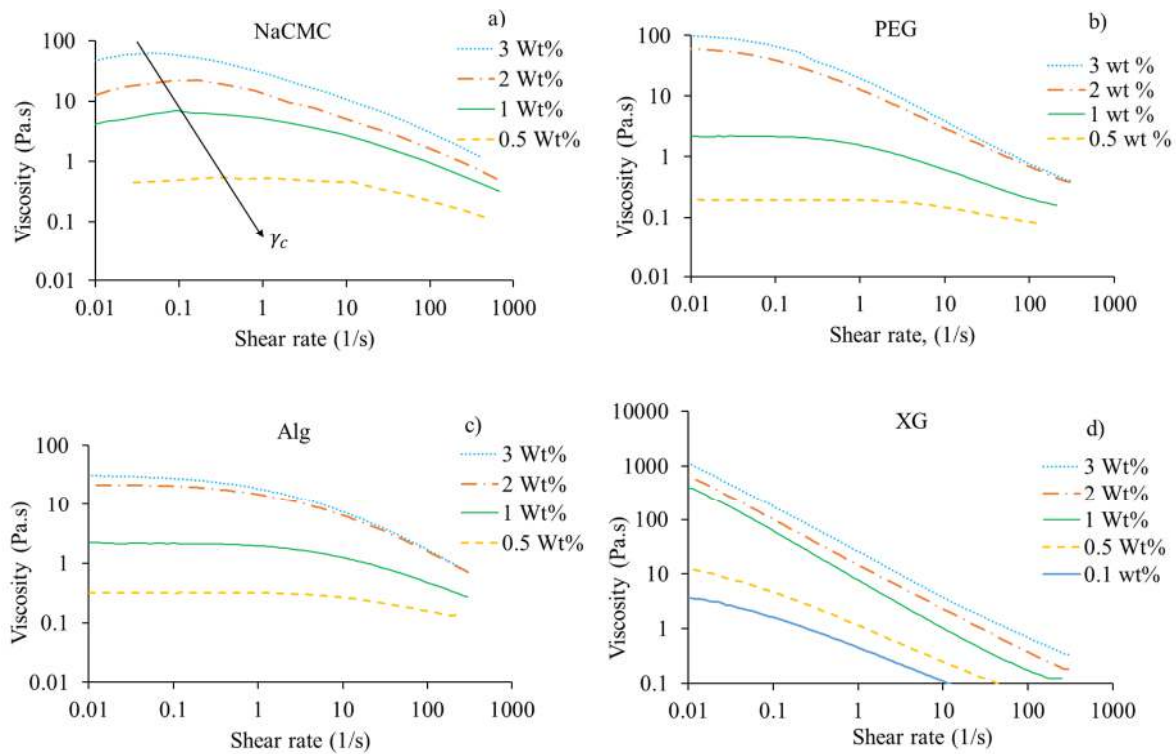


Figure 4-4 Viscosity versus shear rate for NaCMC, PEG, Alg, and XG for different concentrations where γ_c in (a) is the critical shear stress.

In contrast, as demonstrated in Fig. 4-4(d) this behaviour is absent in diluted solutions of XG. Furthermore, Fig. 4-4 (a) represents a sigmoid curve in concentrations higher than 1wt% for NaCMC. The point of inflection of the curve for higher concentrations indicates that the fluid behaviour changes from shear-thickening to shear-thinning. Some studies have observed a similar behaviour for NaCMC (Benchabane and Bekkour 2008), while others have reported uniform ascending change of viscosity versus shear rate (Wiedemann et al. 2017; Eshtiaghi et al. 2012). Sigmoid curves in all concentrations of NaCMC reflect the initial shear-thickening

Chapter 4: Transparent polymers to emulate the rheological properties of primary, activated, and digested sludge

behaviour below critical shear stress (γ_c). Similarly, previous studies have reported that the initial shear-thickening behaviour is due to formation of entanglements of coils, a stiffer inner structure, and increase in intermolecular interactions (Benchabane and Bekkour 2008).

4.4.4 Comparison between the flow behaviour of sludge and polymers

Many studies have focused on flow curve of real sludge as it is a reliable indicator for sludge rheological behaviour (Eshtiaghi et al. 2012; Bhattacharya 1981; Dieudé-Fauvel, Héritier, and Roux 2016; Dai, Gai, and Dong 2014; Guibaud et al. 2004; S. Kennedy 2017; J. Liu et al. 2016). Flow curve provides basic information for handling, processing, pumping, phase separation, sedimentation and stirring of non-Newtonian fluids. In this study, flow curves are plotted to compare rheological characteristics of selected polymers with different types of sludge. The flow curves of NaCMC and sludge for different concentrations are plotted in Fig. 4-5. Figure 4-5(a) and (b) show that the flow behaviour of NaCMC and primary and digested sludge are different. Figure 4-5(c) shows that the flow behaviour of digested sludge is also different from NaCMC excluding NaCMC with 2 wt% concentration. At this concentration, NaCMC behaves similar to digested sludge 3.23 wt%. This similarity was also reported by Eshtiaghi et al., who considered NaCMC as a suitable simulant material for digested sludge 3.23 wt%.

Chapter 4: Transparent polymers to emulate the rheological properties of primary, activated, and digested sludge

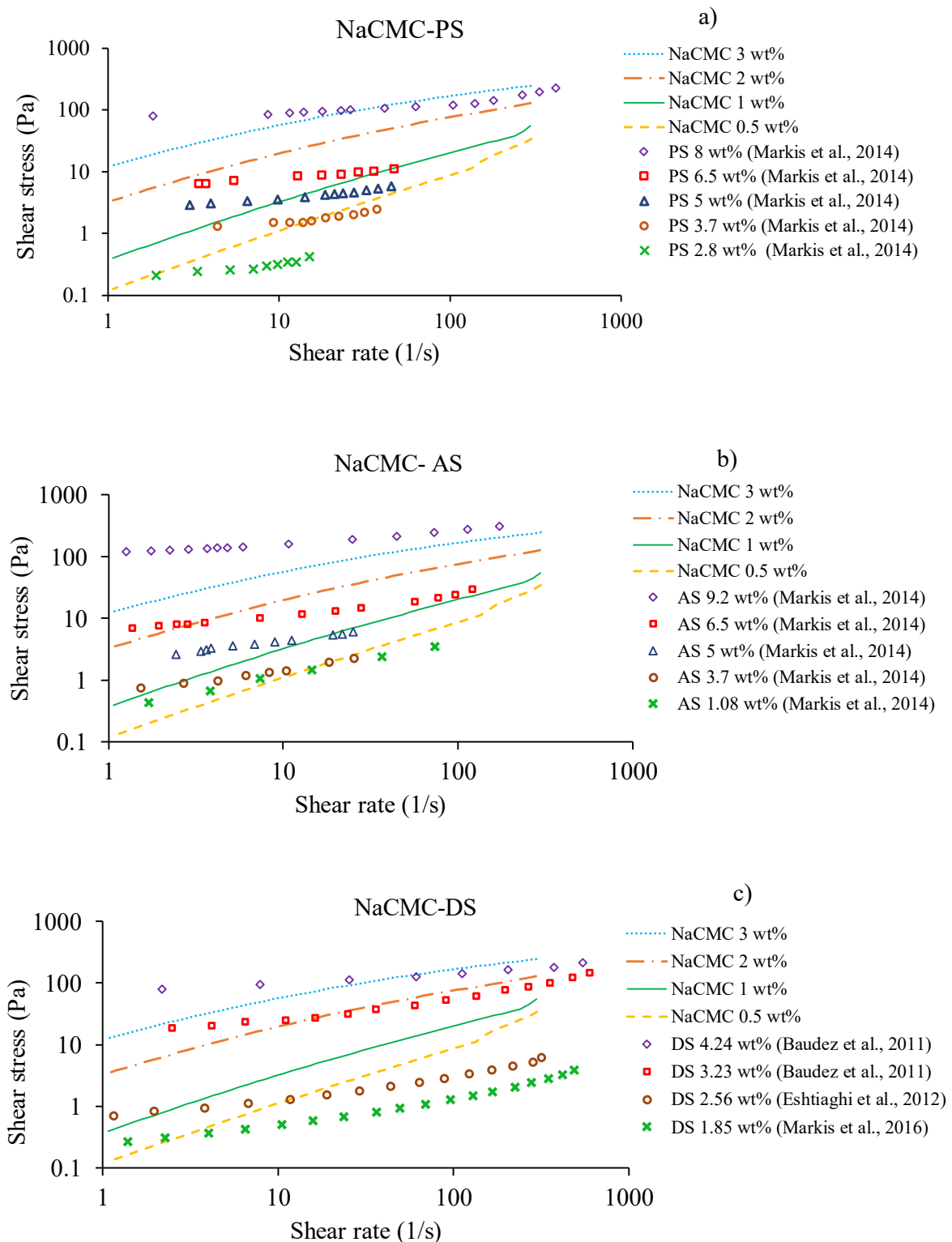


Figure 4-5 Comparison of NaCMC flow behaviour with: (a) primary, (b) activated, and (c) digested sludge.

Chapter 4: Transparent polymers to emulate the rheological properties of primary, activated, and digested sludge

Figure 4-6 compares the rheological behaviour of PEG with primary, activated, and digested sludge.

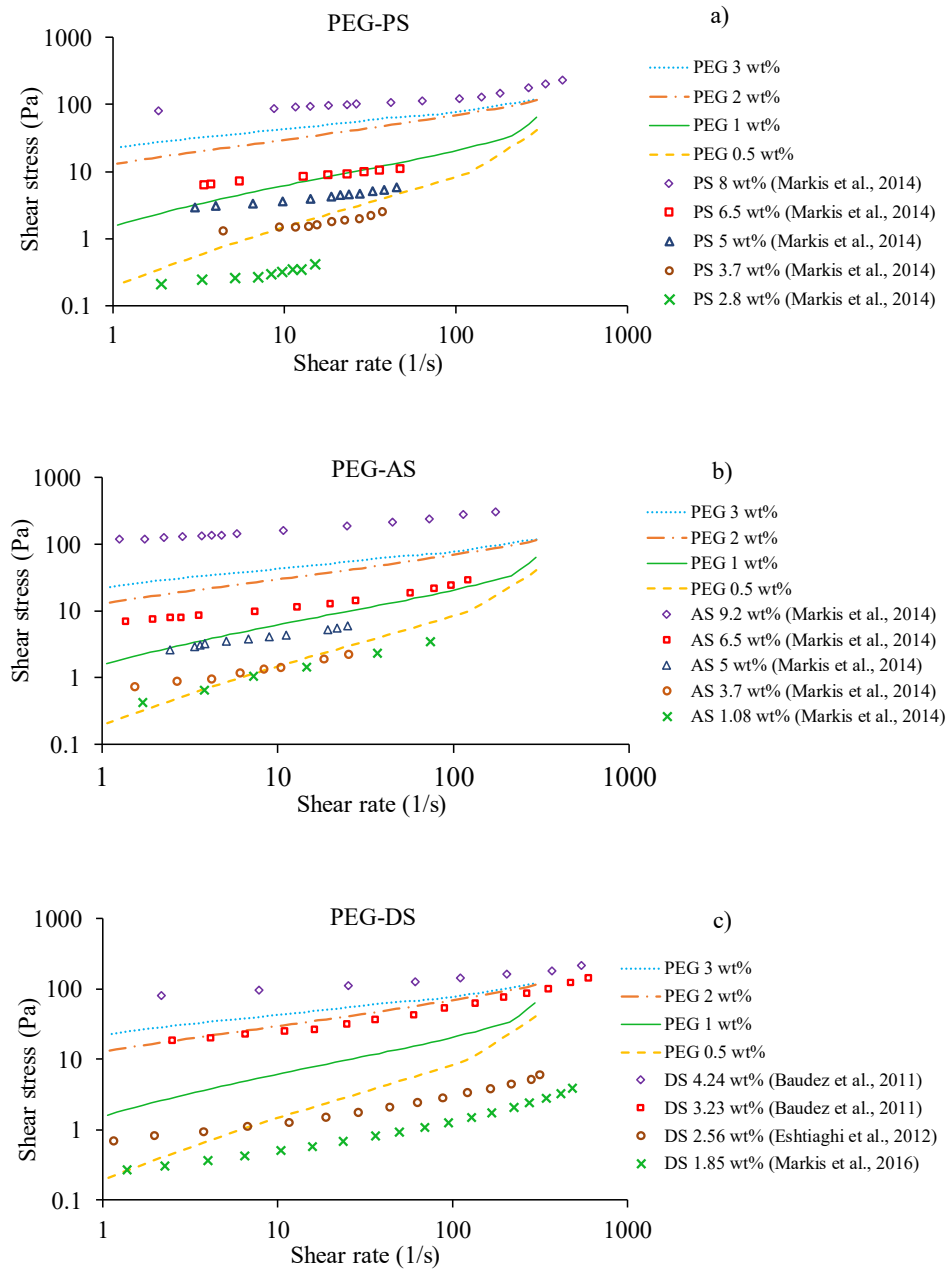


Figure 4-6 Comparison of PEG flow behaviour with: (a) primary, (b) activated, and (c) digested sludge.

The results in this figure show that there is no significant similarity between the flow curve of PEG with primary, activated, and digested sludge. The most striking observation emerging from the data comparison is the similarity observed between flow behaviour of digested sludge

Chapter 4: Transparent polymers to emulate the rheological properties of primary, activated, and digested sludge

3.23 wt% and PEG 2 wt%. Additionally, primary sludge 6.5 wt% and PEG 1 wt% concentrations have similar behaviour in a limited range of shear rate according to the results shown in Fig. 4-6 (a).

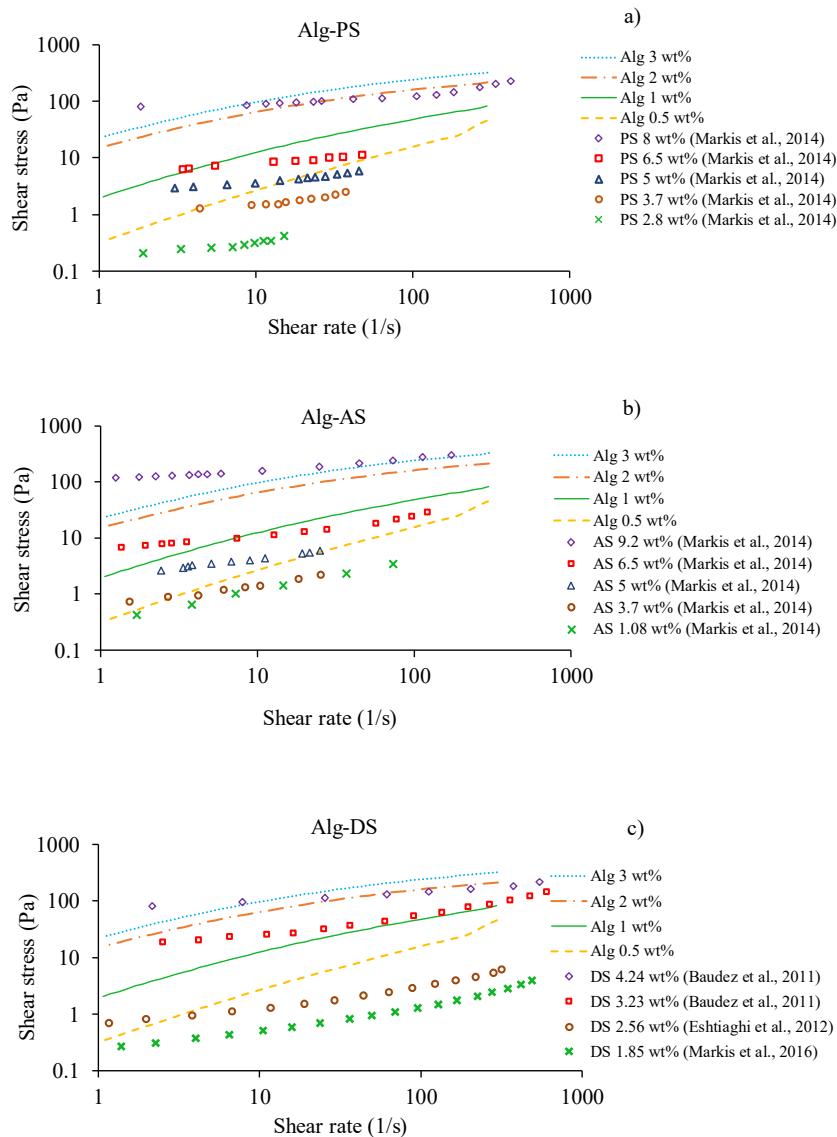


Figure 4-7 Comparison of Alg flow behaviour with: (a) primary, (b) activated, and (c) digested sludge

Figure 4-7 compares the flow curve of Alg with primary, activated, and digested sludge. According to these results, Alg and sludge show different flow behaviour, however, there are

Chapter 4: Transparent polymers to emulate the rheological properties of primary, activated, and digested sludge

some similarities in a limited range of shear rate in which Alg 2 wt% can mimic digested sludge 8 wt% and primary sludge 4.24 wt% for the shear rate of 10-300s⁻¹.

Figure 4-8 compares the flow curves of XG with different types of sludge. The result indicates that the shear stress of XG and different types of sludge increase nonlinearly over the increasing shear rate. Contrary to other polymers, these results indicate that there is a strong similarity between the flow curve of XG and different types of sludge for the shear rate of 1-100 s⁻¹. However, Fig. 4-8 (a) and (c) demonstrate insignificant inconsistencies between the rheological behaviour of XG and primary and digested sludge (10% difference). A possible explanation is the difference between semi-solid network and molecular structures of XG and primary and digested sludge. Primary sludge is a highly thixotropic colloidal suspension containing suspended solid particles (Flora Markis et al. 2016; Baudez, Slatter, and Eshtiaghi 2013) and digested sludge consists of lipopolysaccharides and proteins (Baudez, Slatter, and Eshtiaghi 2013). Contrastingly, XG is a polysaccharide with a gel structure network similar to that of activated sludge (Seviour et al. 2009, 2012). Fig. 4-8 (b) shows that the flow behaviour of XG is closely comparable to activated sludge. The main reason for this close similarity is that both activated sludge and XG consist of long chain polysaccharides containing hydrogen bonds which can form a gel structure network (Seviour et al. 2009, 2012).

Chapter 4: Transparent polymers to emulate the rheological properties of primary, activated, and digested sludge

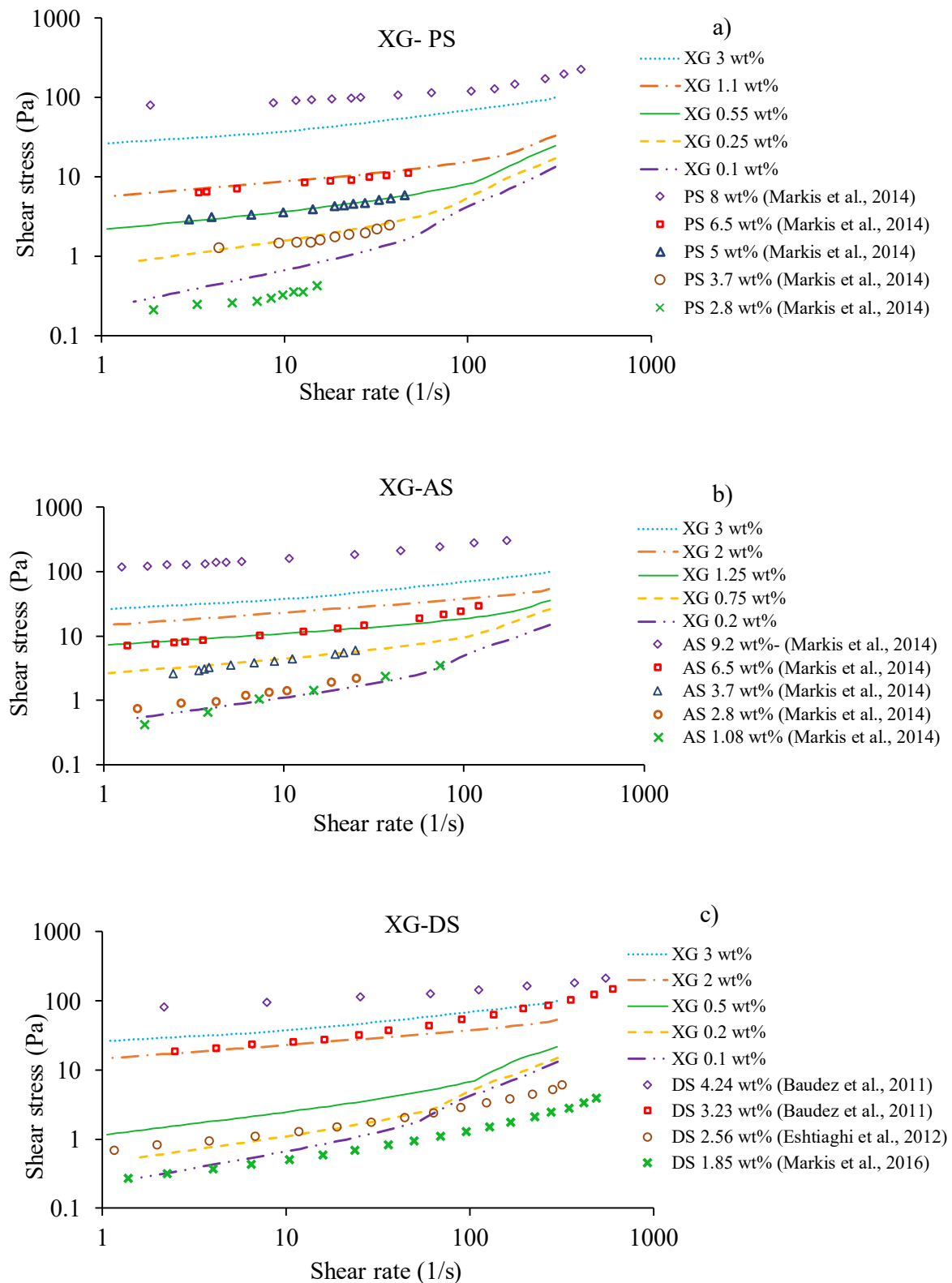


Figure 4-8 Comparison of XG flow behaviour with: (a) primary, (b) activated, and (c) digested sludge

Chapter 4: Transparent polymers to emulate the rheological properties of primary, activated, and digested sludge

Further, for the shear rates more than 100 s^{-1} , the slope of XG flow curve changes due to the creation of vortex. Therefore, findings of this study are limited to shear rate 100 s^{-1} . Additionally, Fig. 4-8(c) shows that XG cannot be used as a simulant fluid for digested sludge for concentrations larger than 4 wt%.

With regards to the above results, XG is ranked as a preferred simulant fluid to mimic different types of sludge, particularly activated sludge. Subsequently, an attempt was made to draw a correlation between concentrations of XG and TS% of sludge. Table 4-3 summarizes the relationship between TS% and concentration of XG corresponding to a shear rate smaller than 100 s^{-1} for primary, activated, and digested sludge. These results facilitate selection of an appropriate concentration of XG for simulating a particular sludge. Other concentrations could be estimated by interpolation.

Table 4-3 Recommended xanthan gum concentrations for primary, activated and digested sludge of different TS%.

Sludge type	TS%	Xanthan gum concentration (wt%)	Shear rate limit (s^{-1})
Primary sludge	6.50%	1.10%	1-100
	5.00%	0.55%	1-100
	3.70%	0.25%	1-100
Activated sludge	6.50%	1.25%	1-100
	3.70%	0.75%	1-100
	2.80%	0.25%	1-100
	1.08%	0.20%	1-100
Digested sludge	3.23%	2.00%	1-100
	2.56%	0.20%	1-100
	1.85%	0.10%	1-100

4.4.5 Comparison between Herschel- Bulkely parameters of sludge and

Chapter 4: Transparent polymers to emulate the rheological properties of primary, activated, and digested sludge

polymers

Herschel-Bulkley is a widely accepted equation for estimating the rheological behaviour of primary, activated and digested sludge (Eshtiaghi et al. 2013; S. Kennedy et al. 2016). Table 4-4 shows the parameters of Herschel-Bulkley equation were calculated for extracted data from literature for primary, activated, and digested sludge. The R-square values have been estimated to measure the degree of interrelation and dependence between variables. The results demonstrate a correlation between TS% and the Herschel-Bulkley parameters. Additionally, there is an increase in the fluid consistency index (k) and yield stress (τ_y) when the sludge total solid concentration increases.

Table 4-4 Herschel-Bulkley parameters for primary, activated, and digested sludge.

Type of sludge	TS (%)	Parameters			R ²	Reference
		k	n	τ_y		
Primary Sludge	2.80%	0.02	0.90	0.16	0.98	(Flora; Markis et al. 2014)
	3.70%	0.09	0.75	0.87	0.97	(Flora; Markis et al. 2014)
	5.00%	0.38	0.59	2.12	0.99	(Flora; Markis et al. 2014)
	6.50%	0.79	0.52	15.04	0.99	(Flora; Markis et al. 2014)
	8.00%	9.34	0.38	67.26	0.96	(Flora; Markis et al. 2014)
Activated Sludge	1.08%	0.24	0.61	0.15	0.99	(D. F. Sanin 2002)
	3.70%	0.65	0.59	1.56	0.98	(Flora; Markis et al. 2014)
	5.00%	1.22	0.56	3.20	0.99	(Flora; Markis et al. 2014)
	6.50%	1.45	0.55	5.31	0.99	(Flora; Markis et al. 2014)
	9.20%	22.20	0.44	95.02	0.99	(Flora; Markis et al. 2014)
Digested Sludge	1.85%	0.02	0.79	0.31	0.99	(Baudez et al. 2011)
	2.56%	0.10	0.68	0.70	0.99	(Baudez et al. 2011)
	3.23%	5.31	0.48	2.30	0.98	(Eshtiaghi et al. 2012)
	4.24%	17.91	0.34	57.19	0.99	(Flora Markis et al. 2016)

Chapter 4: Transparent polymers to emulate the rheological properties of primary, activated, and digested sludge

However, flow behaviour index (n) is inversely proportional to TS%. Higher values of k and τ_y , and a lower value of n , demonstrates the higher viscosity which is directly correlated with higher total solid percentage.

Similarly, Herschel-Bulkley parameters have been calculated for NaCMC, PEG, Alg, and XG and are summarised in Table 4-5. The R-Square method has been used to evaluate the accuracy of obtained data. The results indicate that $n < 1$ for the used polymers, which suggest these polymers are pseudo-plastic fluids.

Table 4-5 Model parameters for polymers of different concentrations.

Polymer	Fitted model	Concentration (wt%)	Parameters			R ²
			k	n	τ_y	
NaCMC	Power-law	0.5%	0.13	0.92	-	0.99
		1%	0.46	0.82	-	0.99
		2%	6.08	0.54	-	0.99
		3%	21.37	0.44	-	0.99
Alginate	Power-law	0.5%	0.29	0.87	-	0.98
		1%	1.17	0.70	-	0.99
		2%	27.35	0.37	-	0.98
		3%	32.81	0.27	-	0.98
PEG	Power-law	0.5%	0.12	0.95	-	0.98
		1%	0.78	0.73	-	0.95
		2%	11.90	0.39	-	0.99
		3%	18.53	0.32	-	0.99
XG	Herschel-Bulkley	0.5%	0.35	0.62	2.26	0.99
		1%	0.90	0.50	3.40	0.99
		2%	6.64	0.32	8.54	0.99
		3%	6.99	0.24	19.06	0.99

Moreover, the best fitted non-Newtonian model for NaCMC, PEG, Alg is power-law, whereas XG follows the Herschel-Bulkley equation. As mentioned earlier, the main difference between power-law and Herschel-Bulkley is the yield stress, where XG requires an initial yield stress (γ_c) to flow. This yield stress could be originated from a large number of hydrogen bonds in

Chapter 4: Transparent polymers to emulate the rheological properties of primary, activated, and digested sludge

XG gel-like structure (J. R. M. Kennedy, Kent, and Brown 2015). Also, sludge can flow when their stress overcome critical yield stress (Baroutian, Eshtiaghi, and Gapes 2013; Baudez 2008; Eshtiaghi et al. 2012). Therefore, both XG and sludge are considered an elastic materials and flow after breaking their internal structure network. Altogether, the summarized results in Tables 4-4 and 4-5 suggest that XG among all other polymers is the preferred simulants to mimic the shear stress, yield stress, and viscosity of sludge.

4.4.6 Comparison between the viscoelastic behaviour of digested sludge and XG

This section compares the other rheological properties of XG including thixotropy and viscoelastic behaviour to digested sludge. Due to lack of experimental data for viscoelastic behaviour of primary and activated sludge in literature, this study focused on viscoelastic behaviour of digested sludge. Figure 4-9 shows the viscoelastic curve and its stress response (storage modulus (G') and loss modulus (G'')) as a function of strain) for different concentration of XG and digested sludge (3.23 wt%). The elastic modulus G' and G'' remain almost constant when strain increases followed by a sudden break in the gel network structures. Additionally, the storage modulus is larger than the loss modulus, which means the gel structure dominates external forces before reaching the cross-over point ($G'=G''$). This point is the intersection where mechanical forces break down the microstructure of the gel. Previous studies have also reported similar trends for digested sludge (Feng, Guo, and Tan 2015; Feng, Liu, and Tan 2014; Baudez et al. 2013). Figure 4-9 also indicates that in higher concentrations, cross-over points shift to a lower strain. The main reason for this is that the increased sensitivity of strain in higher concentration enhances breaking structure of the gel networks. Eshtiaghi et al., (2013, 2012) also reported similar behaviour for digested sludge, where it was proved that the structure of digested sludge is increasingly sensitive to strain when solid particles are added. Overall,

Chapter 4: Transparent polymers to emulate the rheological properties of primary, activated, and digested sludge

the results in Fig. 4-9 shows that XG is not a suitable material to mimic the viscoelastic behaviour of digested sludge.

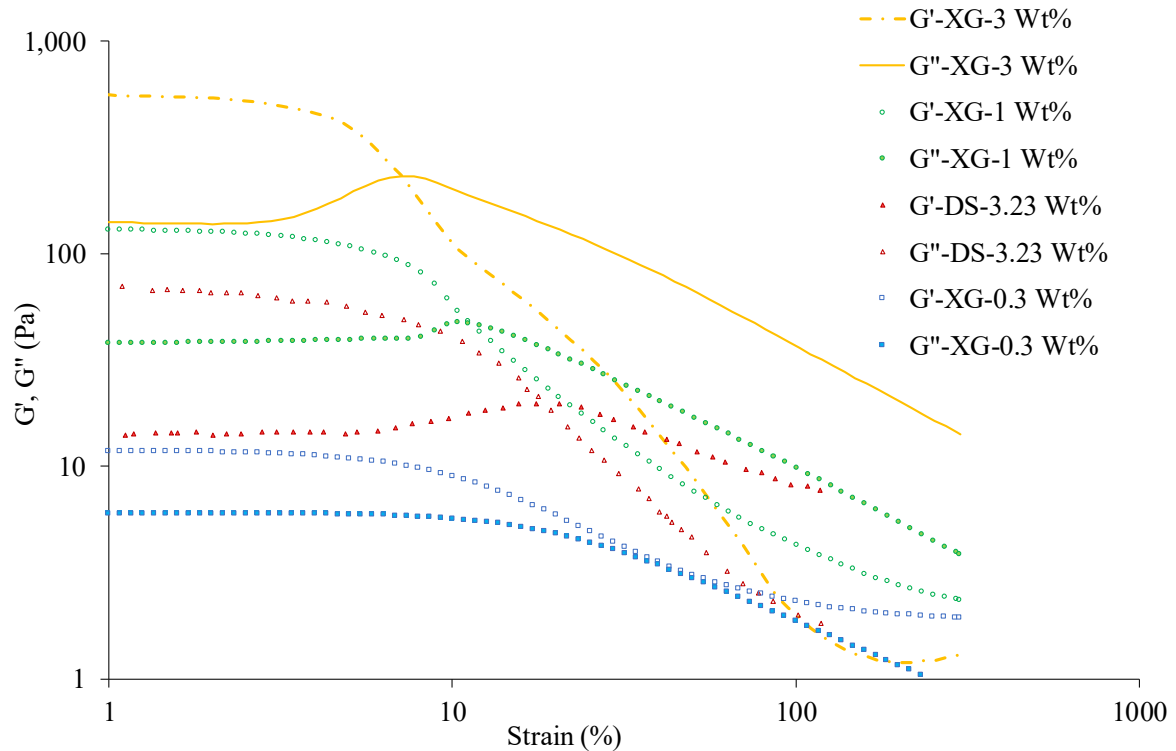


Figure 4-9 Storage modulus (G') and loss modulus (G'') as a function of strain for different concentration of xanthan gum and digested sludge (3.23 wt%)

Figure 4-10 presents the cross-over points for various concentrations of XG. This confirms the presence of a three-dimensional network in higher concentrations. Additionally, this figure shows that the break down points shift upward as XG concentration increases.

Chapter 4: Transparent polymers to emulate the rheological properties of primary, activated, and digested sludge

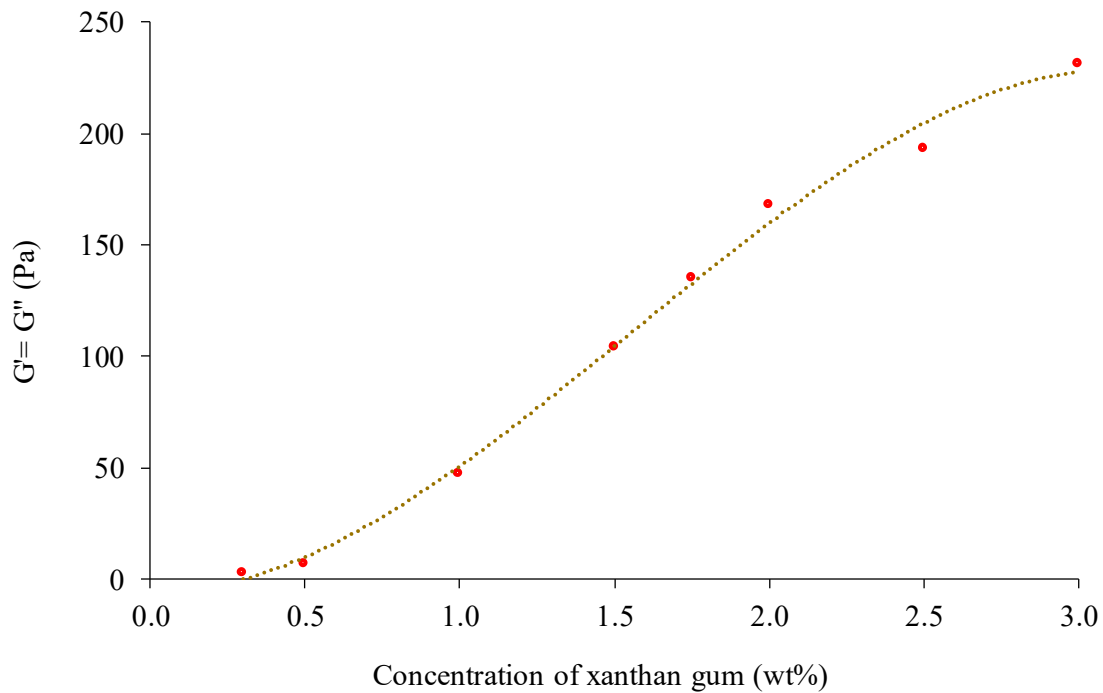


Figure 4-10 Dependency of cross-over points ($G' = G''$) to xanthan gum concentration at 25°C and one Hz

4.4.7 Comparison between the thixotropic behaviour of activated sludge and XG

Primary, activated and digested sludge are classified as thixotropic materials, meaning that the viscosity of these sludge depend not only on temperature and shear rate but also on time (Lotito et al. 1997; Flora; Markis et al. 2014; Baudez et al. 2013; Baroutian, Eshtiaghi, and Gapes 2013). After increasing the shear rate, its internal network requires some time to reform and return to its equilibrium state. The flow curve of thixotropic material does not follow an exact path on the network breakdown and rebuilding due to the stabilization of its structure between these two. The enclosed area between the two shear stress curves shaped by fluctuation of shear rates, forms a hysteresis loop which represents the energy consumed to break the structure of the network (Perret, Locat, and Martignoni 1996). Figure 4-11 compares the hysteresis loop for activated sludge with 2.8 wt% TS (Flora; Markis et al. 2014) with the corresponding XG

Chapter 4: Transparent polymers to emulate the rheological properties of primary, activated, and digested sludge

concentration of 0.25 wt% that is obtained from Table 4-5. Moreover, the results show that although the flow curves of XG and activated sludge follow the same trend over the increasing shear rates, their broken structures do not recover in the same way. For this reason, it is concluded that XG cannot mimic the thixotropic behaviour of activated sludge. There is a lack of experimental data for thixotropy of digested and primary sludge in the literatures, therefore this study just focused on thixotropic behaviour of activated sludge.

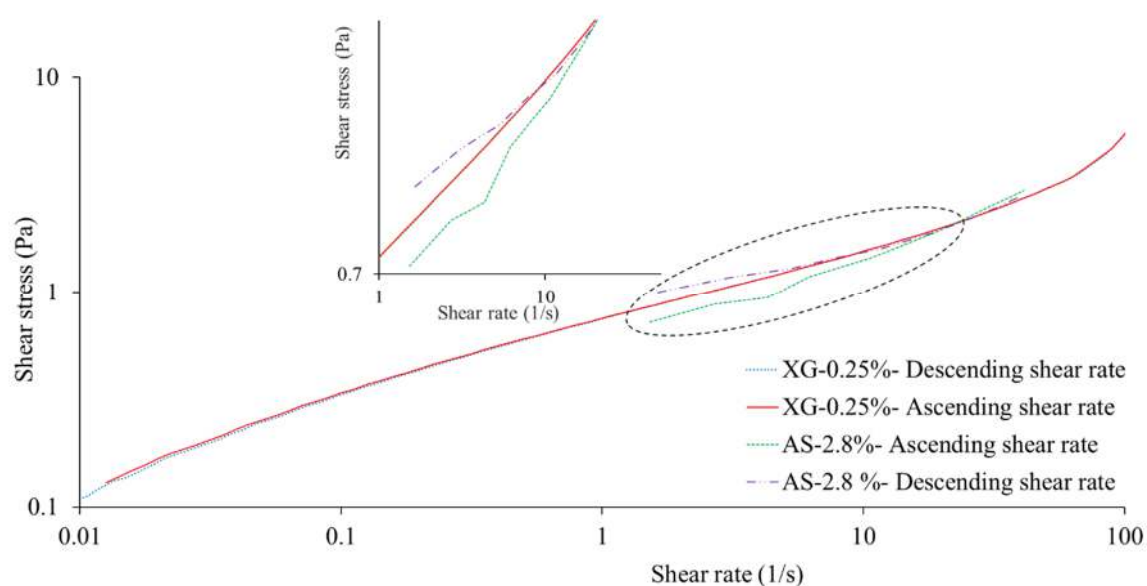


Figure 4-11 Comparison of hysteresis loop of xanthan gum 0.3 wt% with activated sludge (AS) 2.8 wt%

4.5 Conclusions

The purpose of this study was to investigate the rheological properties of four different types of shear-thinning polymers used as surrogate to replicate the rheological behaviour of various types of sludge. Zeta potential characterization, pH analysis, flow curve, viscoelasticity, and thixotropy were measured to draw comparison between simulant fluids and different types of sludge. Although xanthan gum, carboxyl methyl cellulose, polyethylene glycol and sodium alginate have been widely applied in previous studies, only a small number of rheological tests have been performed to characterise these simulant fluids. The proposed study shines a new

Chapter 4: Transparent polymers to emulate the rheological properties of primary, activated, and digested sludge

light on the feasibility of using these simulant polymers through investigation of differences and similarities with sludge. Additionally, transparent simulant fluids are used widely to visualize the flow patterns and particle trajectory through colorimetry method required to change pH dramatically. The proposed study investigates the pH resistance and zeta potential of these polymers which have been studied barely in available literature. This study highlights that only xanthan gum in low to medium shear rates (less than 100 s⁻¹) offers similarity to sludge. The flow curve and viscosity of xanthan gum is closely similar to activated sludge and the reason for this might be the similar molecular and internal network structures. In addition, among these four types of polymers only xanthan gum follows the Herschel-Bulkley model as the most suitable equation for mimicking the behaviour of different types of sludge. However, xanthan gum and sludge do not show similar behaviour in terms of thixotropy and viscoelasticity.

The results of this study assist to select and apply a safe, cheap, stable, and clear simulant fluid to study the rheological and hydrodynamic behaviours of sludge.

4.6 References

- Alemdar, A., N. Güngör, O. I. Ece, and O. Atici. 2005. "The Rheological Properties and Characterization of Bentonite Dispersions in the Presence of Non-Ionic Polymer PEG." *Journal of Materials Science* 40 (1): 171–77. <https://doi.org/10.1007/s10853-005-5703-4>.
- Alexandru Grumezescu. 2016. *Emulsions- Nanotechnology in the Agri-Food Industry*. Edited by Patricia Osborn. Vol. 3. Elsevier. <https://doi.org/10.1002/9783527634798>.
- Ameur, Houari, Mohamed Bouzit, and Mustapha Helmaoui. 2011. "Numerical Study of Fluid Flow and Power Consumption in a Stirred Vessel with a CABA 6SRGT Impeller." *Chemical and Process Engineering* 32 (4): 351–66. <https://doi.org/10.2478/v10176-011-0028-0>.
- Amiraftebi, Maryam Sadat, Navid Mostoufi, Mostafa Hosseinzadeh, and Mohammad Reza Mehrnia. 2014. "Reduction of Membrane Fouling by Innovative Method (Injection of Air Jet)." *Journal of Environmental Health Science and Engineering* 12 (1): 1–8. <https://doi.org/10.1186/s40201-014-0128-0>.
- Baroutian, Saeid, Nicky Eshtiaghi, and Daniel J. Gapes. 2013. "Rheology of a Primary and Secondary Sewage Sludge Mixture: Dependency on Temperature and Solid Concentration." *Bioresource Technology* 140: 227–33. <https://doi.org/10.1016/j.biortech.2013.04.114>.

Chapter 4: Transparent polymers to emulate the rheological properties of primary, activated, and digested sludge

Baudez. 2008. "The Sludge Rheology Exhibited a Strong Dependency on SRT and Reactor's Temperature." *Applied Rheology* 18 (1).

Baudez, J.C., and Philippe Coussot. 2001. "Rheology of Aging, Concentrated, Polymeric Suspensions: Application to Pasty Sewage Sludges." *Journal of Rheology* 45 (5): 1123–39. <https://doi.org/10.1122/1.1392298>.

Baudez, J.C., Pascal Ginisty, Christophe Peuchot, and Ludovico Spinosa. 2007. "The Preparation of Synthetic Sludge for Lab Testing." *Water Science and Technology* 56 (9): 67–74. <https://doi.org/10.2166/wst.2007.714>.

Baudez, J.C., Rahul K. Gupta, Nicky Eshtiaghi, and Paul Slatter. 2013. "The Viscoelastic Behaviour of Raw and Anaerobic Digested Sludge: Strong Similarities with Soft-Glassy Materials." *Water Research* 47 (1): 173–80. <https://doi.org/10.1016/j.watres.2012.09.048>.

Baudez, J.C., Paul Slatter, and Nicky Eshtiaghi. 2013. "The Impact of Temperature on the Rheological Behaviour of Anaerobic Digested Sludge." *Chemical Engineering Journal*. <https://doi.org/10.1016/j.cej.2012.10.099>.

Baudez, Flora Markis, Nicky Eshtiaghi, and Paul Slatter. 2011. "The Rheological Behaviour of Anaerobic Digested Sludge." *Water Research* 45 (17): 5675–80. <https://doi.org/10.1016/j.watres.2011.08.035>.

Baxter, R., N. Hastings, A. Law, and E. J. Glass. 2008. *Food Stabilisers, Thickeners and Gelling Agent*. Animal Genetics. Vol. 39.

Benchabane, Adel, and Karim Bekkour. 2008. "Rheological Properties of Carboxymethyl Cellulose (CMC) Solutions." *Colloid and Polymer Science* 286 (10): 1173–80. <https://doi.org/10.1007/s00396-008-1882-2>.

Besra, L., D. K. Sengupta, and S. K. Roy. 2000. "Particle Characteristics and Their Influence on Dewatering of Kaolin, Calcite and Quartz Suspensions." *International Journal of Mineral Processing* 59 (2): 89–112. [https://doi.org/10.1016/S0301-7516\(99\)00065-4](https://doi.org/10.1016/S0301-7516(99)00065-4).

Bhattacharya, S. N. 1981. "Flow Characteristics of Primary and Digested Sewage Sludge." *Rheologica Acta* 20: 288–98. <https://doi.org/https://doi.org/10.1007/BF01678030>.

Bobade, Veena, Madalyn Cheetham, Jamal Hashim, and Nicky Eshtiaghi. 2018. "Influence of Gas Injection on Viscous and Viscoelastic Properties of Xanthan Gum." *Water Research* 134: 86–91. <https://doi.org/10.1016/j.watres.2018.01.071>.

Brehmer, Manuel, Thomas Eppinger, and Matthias Kraume. 2012. "Influence of Rheology on the Flow Pattern in Stirred Biogas Plants." *Chemie-Ingenieur-Technik* 84 (11): 2048–56. <https://doi.org/10.1002/cite.201200062>.

Dai, Xiaohu, Xin Gai, and Bin Dong. 2014. "Rheology Evolution of Sludge through High-Solid Anaerobic Digestion." *Bioresource Technology* 174: 6–10. <https://doi.org/10.1016/j.biortech.2014.09.122>.

Deborah, Intermediate, and Numbers De. 2008. *Rheology for Chemists*. *Rheology for Chemists*. <https://doi.org/10.1039/9781847558046>.

Chapter 4: Transparent polymers to emulate the rheological properties of primary, activated, and digested sludge

Dieudé-Fauvel, E., P. Héritier, and J. C. Roux. 2016. "Impact of Sludge Mechanical Behaviour on Spatial Distribution Parameters Obtained with Centrifugal Spreader: Preliminary Study." *Engineering in Agriculture, Environment and Food* 9 (3): 242–49. <https://doi.org/10.1016/j.eaef.2016.01.003>.

Eshtiaghi, Nicky, Flora Markis, Jean Christophe Baudez, and Paul Slatter. 2013. "Proxy Model Materials to Simulate the Elastic Properties of Digested Municipal Sludge." *Water Research* 47 (15): 557–5563. <https://doi.org/10.1016/j.watres.2013.06.027>.

Eshtiaghi, Nicky, Flora Markis, Shao\ Dong Yap, and Paul Baudez, Jean-Christophe Slatter. 2003. "Rheological Characterisation of Municipal Sludge: A Review." *Sport Marketing Quarterly* 12 (4): 206–16. <https://doi.org/10.1016/j.buildenv.2013.04.022>.This.

Eshtiaghi, Nicky, Shao Dong Yap, Flora Markis, Jean Christophe Baudez, and Paul Slatter. 2012. "Clear Model Fluids to Emulate the Rheological Properties of Thickened Digested Sludge." *Water Research* 46 (9): 3014–22. <https://doi.org/10.1016/j.watres.2012.03.003>.

Feng, Guohong, Yabing Guo, and Wei Tan. 2015. "Effects of Thermal Hydrolysis Temperature on Physical Characteristics of Municipal Sludge." *Water Science and Technology* 72 (11): 2018–26. <https://doi.org/10.2166/wst.2015.425>.

Feng, Guohong, Liyan Liu, and Wei Tan. 2014. "Effect of Thermal Hydrolysis on Rheological Behavior of Municipal Sludge." *Industrial and Engineering Chemistry Research* 53 (27): 11185–92. <https://doi.org/10.1021/ie501488q>.

Feng, Guohong, He Ma, Bai Tiantian, and Yabing Guo. 2017. "Rheology Characteristics of Activated Sludge and Thermal Treated Sludge at Different Process Temperature." *Water Science & Technology* 00: 1–8. <https://doi.org/10.2166/wst.2016.501>.

Flemming, Hans Curt, and Jost Wingender. 2010. "Relevance of Microbial Extracellular Polymeric Substances (EPSs) - Part I: Structural and Ecological Aspects." *Nature Reviews Microbiology* 8 (9): 623–33. <https://doi.org/10.1038/nrmicro2415>.

Forster, C. F. 2008. "Bound Water in Sewage Sludges and Its Relationship to Sludge Surfaces and Sludge Viscosities." *Journal of Chemical Technology and Biotechnology. Biotechnology* 33 (1): 76–84. <https://doi.org/10.1002/jctb.280330107>.

Gilani, S.L., G.D. Najafpour, H.D. Heydarzadeh, and H. Zare. 2011. "Kinetic Models for Xanthan Gum Production Using *Xanthomonas Campestris* from Molasses." *Chemical Industry and Chemical Engineering Quarterly* 17 (2): 179–87. <https://doi.org/10.2298/CICEQ101030002G>.

Guibaud, G., P. Dollet, N. Tixier, C. Dagot, and M. Baudu. 2004. "Characterisation of the Evolution of Activated Sludges Using Rheological Measurements." *Process Biochemistry* 39 (11): 1803–10. <https://doi.org/10.1016/j.procbio.2003.09.002>.

Imeson, Alan. 1997. *Thickening and Gelling Agents for Food*. Springer Science & Business Media. [https://doi.org/10.1016/0924-2244\(93\)90161-3](https://doi.org/10.1016/0924-2244(93)90161-3).

Karim, Khursheed, Rajneesh Varma, Mehul Vesvikar, and M. H. Al-Dahhan. 2004. "Flow Pattern Visualization of a Simulated Digester." *Water Research* 38 (17): 3659–70. <https://doi.org/10.1016/j.watres.2004.06.009>.

Kennedy, Jordan R.M., Katherine E. Kent, and Jennifer R. Brown. 2015. "Rheology of Dispersions of Xanthan Gum, Locust Bean Gum and Mixed Biopolymer Gel with Silicon Dioxide Nanoparticles." *Materials Science and Engineering C* 48: 347–53. <https://doi.org/10.1016/j.msec.2014.12.040>.

Chapter 4: Transparent polymers to emulate the rheological properties of primary, activated, and digested sludge

Kennedy, Stephen, Pradipto K Bhattacharjee, Nicky Eshtiaghi, and Rajarathinam Parthasarathy. 2016. "Accelerating the Spread of the Active Mixing Region in a Sludge Simulant Using Submerged Jets." *Chemical Engineering Research and Design* 114: 331–40. <https://doi.org/10.1016/j.cherd.2016.08.030>.

Kennedy, Stephen, Rajarathinam Parthasarathy, Nicky Eshtiaghi, and Sati Bhattacharya. 2014. "Liquid Jet Recirculation in a Model Digester: Flow Characteristics." In, 1–7.

Legrand, V., D. Hourdet, R. Audebert, and D. Snidaro. 1998. "Deswelling and Flocculation of Gel Networks: Application to Sludge Dewatering." *Water Research* 32 (12): 3662–72. [https://doi.org/10.1016/S0043-1354\(98\)00133-X](https://doi.org/10.1016/S0043-1354(98)00133-X).

Liu, Jibao, Dawei Yu, Jian Zhang, Min Yang, Yawei Wang, Yuansong Wei, and Juan Tong. 2016. "Rheological Properties of Sewage Sludge during Enhanced Anaerobic Digestion with Microwave-H₂O₂ pretreatment." *Water Research* 98 (November 2017): 98–108. <https://doi.org/10.1016/j.watres.2016.03.073>.

Liu, Shuanghui, Nicholas H. Low, and Michael T. Nickerson. 2009. "Effect of PH, Salt, and Biopolymer Ratio on the Formation of Pea Protein Isolate Gum Arabic Complexes." *Journal of Agricultural and Food Chemistry* 57 (4): 1521–26. <https://doi.org/10.1021/jf802643n>.

Lotito, V., L. Spinosa, G. Mininni, and R. Antonacci. 1997. "The Rheology of Sewage Sludge at Different Steps of Treatment." *Water Science and Technology* 36 (11): 79–85. [https://doi.org/10.1016/S0273-1223\(97\)00672-0](https://doi.org/10.1016/S0273-1223(97)00672-0).

Markis, Flora, Jean Christophe Baudez, Rajarathinam; Parthasarathy, Paul Slatter, and Nicky Eshtiaghi. 2014. "Rheological Characterisation of Primary and Secondary Sludge: Impact of Solids Concentration." *Chemical Engineering Journal* 253: 526–37. <https://doi.org/10.1016/j.cej.2014.05.085>.

Markis, Flora, Jean Christophe Baudez, Rajarathinam Parthasarathy, Paul Slatter, and Nicky Eshtiaghi. 2016. "Predicting the Apparent Viscosity and Yield Stress of Mixtures of Primary, Secondary and Anaerobically Digested Sewage Sludge: Simulating Anaerobic Digesters." *Water Research* 100: 568–79. <https://doi.org/10.1016/j.watres.2016.05.045>.

Miryahyaei, S., K. Olinga, F.A.Abdul Muthalib, T. Das, M.S.Ab Aziz, M. Othman, J.C. Baudez, D. Batstone, and N. Eshtiaghi. 2018. "Impact of Rheological Properties of Substrate on Anaerobic Digestion and Digestate Dewaterability: New Insights through Rheological and Physico-Chemical Interaction." *Water Research*, no. November. <https://doi.org/10.1016/j.watres.2018.11.049>.

Moeller, Gabriela, and Luis Gilberto Torres. 1997. "Rheological Characterization of Primary and Secondary Sludges Treated by Both Aerobic and Anaerobic Digestion." *Bioresource Technology* 61 (3): 207–11. [https://doi.org/10.1016/S0960-8524\(97\)00061-8](https://doi.org/10.1016/S0960-8524(97)00061-8).

Neyens, E., and J. Baeyens. 2003. "A Review of Thermal Sludge Pre-Treatment Processes to Improve Dewaterability." *Journal of Hazardous Materials* 98 (1–3): 51–67. [https://doi.org/10.1016/S0304-3894\(02\)00320-5](https://doi.org/10.1016/S0304-3894(02)00320-5).

Neyens, Elisabeth, Jan Baeyens, Raf Dewil, and Bart De Heyder. 2004. "Advanced Sludge Treatment Affects Extracellular Polymeric Substances to Improve Activated Sludge Dewatering." *Journal of Hazardous Materials* 106 (2–3): 83–92. <https://doi.org/10.1016/j.jhazmat.2003.11.014>.

Oz, Nilgun Ayman, Alev Cagla Uzun, and A C Uzun. 2014. "Comparing the Influence of Low Power Ultrasonic and Microwave Pre-Treatments on the Solubilisation and Semi-Continuous Anaerobic Digestion of Waste Activated Sludge," no. April. <https://doi.org/10.1016/j.ultsonch.2014.04.018>.

Chapter 4: Transparent polymers to emulate the rheological properties of primary, activated, and digested sludge

- Papa, Matteo, Roberta Pedrazzani, Stefano Nembrini, and Giorgio Bertanza. 2015. "Should Rheological Properties of Activated Sludge Be Measured?" *Applied Rheology* 25 (2). <https://doi.org/10.3933/APPLRHEOL-25-24590>.
- Perret, D., J. Locat, and P. Martignoni. 1996. "Thixotropic Behavior during Shear of a Fine-Grained Mud from Eastern Canada." *Engineering Geology* 43 (1): 31–44. [https://doi.org/10.1016/0013-7952\(96\)00031-2](https://doi.org/10.1016/0013-7952(96)00031-2).
- Practice, Good. 2013. "Developments of European Standardisation on Sludge: Guidelines for Good Practice 1" 10 (1): 55–61.
- Ratkovich, N., W. Horn, F. P. Helmus, S. Rosenberger, W. Naessens, I. Nopens, and T. R. Bentzen. 2013. "Activated Sludge Rheology: A Critical Review on Data Collection and Modelling." *Water Research* 47 (2): 463–82. <https://doi.org/10.1016/j.watres.2012.11.021>.
- Sanin, Dilek F. 2002a. "Effect of Solution Physical Chemistry on the Rheological Properties of Activated Sludge." *Water SA* 28 (2): 207–12. <https://doi.org/10.4314/wsa.v28i2.4886>.
- Sanin, F Dilek, and P Aarne Vesilind. 1996. "Synthetic Sludge: A Physical/Chemical Model in Understanding Bioflocculation." *Water Environment Research* 68 (5): 927–33. <https://doi.org/10.2175/106143096X127938>.
- Santos, V E, J A Casas, and E Go. 2000. "Xanthan Gum: Production, Recovery , and Properties" 18.
- Seviour, Thomas, Maite Pijuan, Timothy Nicholson, Jürg Keller, and Zhiguo Yuan. 2009. "Gel-Forming Exopolysaccharides Explain Basic Differences between Structures of Aerobic Sludge Granules and Floccular Sludges." *Water Research* 43 (18): 4469–78. <https://doi.org/10.1016/j.watres.2009.07.018>.
- Seviour, Thomas, Zhiguo Yuan, Mark C.M. van Loosdrecht, and Yuemei Lin. 2012. "Aerobic Sludge Granulation: A Tale of Two Polysaccharides?" *Water Research* 46 (15): 4803–13. <https://doi.org/10.1016/j.watres.2012.06.018>.
- Spinosa, L., and Vincenzo Lotito. 2003. "A Simple Method for Evaluating Sludge Yield Stress." *Advances in Environmental Research* 7 (3): 655–59. [https://doi.org/10.1016/S1093-0191\(02\)00041-2](https://doi.org/10.1016/S1093-0191(02)00041-2).
- Spinosa, Ludovico. 2016. "Standardized Characterization Procedures: A Necessary Support to Regulations." *Water Science and Technology* 74 (1): 220–28. <https://doi.org/10.2166/wst.2016.201>.
- Wang, Hou Feng, Yun Jie Ma, Hua Jie Wang, Hao Hu, Hai Yang Yang, and Raymond J. Zeng. 2017. "Applying Rheological Analysis to Better Understand the Mechanism of Acid Conditioning on Activated Sludge Dewatering." *Water Research* 122: 398–406. <https://doi.org/10.1016/j.watres.2017.05.002>.
- Wasikiewicz, Jaroslaw M., Fumio Yoshii, Naotsugu Nagasawa, Radoslaw A. Wach, and Hiroshi Mitomo. 2005. "Degradation of Chitosan and Sodium Alginate by Gamma Radiation, Sonochemical and Ultraviolet Methods." *Radiation Physics and Chemistry* 73 (5): 287–95. <https://doi.org/10.1016/j.radphyschem.2004.09.021>.
- Wiedemann, Leonhard, Fosca Conti, Tomasz Janus, Matthias Sonnleitner, Wilfried Zörner, and Markus Goldbrunner. 2017. "Mixing in Biogas Digesters and Development of an Artificial Substrate for Laboratory-Scale Mixing Optimization." *Chemical Engineering and Technology* 40 (2): 238–47. <https://doi.org/10.1002/ceat.201600194>.

Chapter 4: Transparent polymers to emulate the rheological properties of primary, activated, and digested sludge

Wu, Xue hui, Fei Wang, De Xing Sun, and Wei Hao Yang. 2011. "Rheology and Flow Characteristic of Urban Untreated Sewage for Cooling and Heating Source." *Experimental Thermal and Fluid Science* 35 (4): 612–17. <https://doi.org/10.1016/j.expthermflusci.2010.11.009>.

Yang, Fei, Amos Bick, Semion Shandalov, Asher Brenner, and Gideon Oron. 2009. "Yield Stress and Rheological Characteristics of Activated Sludge in an Airlift Membrane Bioreactor." *Journal of Membrane Science* 334 (1–2): 83–90. <https://doi.org/10.1016/j.memsci.2009.02.022>.

Zhang, Jingsi, Simon J. Haward, Zhigen Wu, Xiaohu Dai, Wenquan Tao, and Zhuo Li. 2016. "Evolution of Rheological Characteristics of High-Solid Municipal Sludge during Anaerobic Digestion." *Applied Rheology* 26 (3). <https://doi.org/10.3933/ApplRheol-26-32973>.

1-1-2020

Performance of a dual helical ribbon impeller in a two-phase (gas-liquid) stirred tank reactor

Maryam Amiraftabi
Edith Cowan University

Mehdi Khiadani
Edith Cowan University

Hussein A. Mohammed
Edith Cowan University

Follow this and additional works at: <https://ro.ecu.edu.au/ecuworkspost2013>



Part of the [Engineering Commons](#)

[10.1016/j.cep.2020.107811](https://doi.org/10.1016/j.cep.2020.107811)

Amiraftabi, M., Khiadani, M., & Mohammed, H. A. (2020). Performance of a dual helical ribbon impeller in a two-phase (gas-liquid) Stirred Tank Reactor. *Chemical Engineering and Processing: Process Intensification*, 148, Article 107811.

<https://doi.org/10.1016/j.cep.2020.107811>

This Journal Article is posted at Research Online.

<https://ro.ecu.edu.au/ecuworkspost2013/7652>



Performance of a dual helical ribbon impeller in a two-phase (gas-liquid) stirred tank reactor

Maryam Amiraftebi, Mehdi Khiadani*, Hussein A. Mohammed

School of Engineering, Edith Cowan University, 270 Joondalup Drive, Joondalup, Perth, WA, 6027, Australia

ARTICLE INFO

Keywords:

Dual helical ribbon impeller
Gas-liquid stirred tank reactor
Power consumption
Mixing time
Bubble behaviour
Response surface methodology

ABSTRACT

The performance of a dual helical ribbon impeller in a gassed stirred tank reactor filled with a shear-thinning polymer has been investigated experimentally in this study. Sodium carboxymethyl cellulose with different concentrations were applied to change the viscosity and rheological behaviour of working fluid. Titration reaction between HCl and NaOH then took place inside the reactor under controlled pH, evaluating the influence of a dual helical ribbon impeller on the performance of a two-phase agitated reactor. The impact of impeller rotational speed, gas flow rate, viscosity, and clearance to the bottom on power uptake and mixing time are explored. The results thus reveal that the presence of bubbles reduces both required power uptake and mixing time to reach an endpoint reaction. Contrary to expectations, this study indicates that increasing the impeller's speed beyond a certain level, not only fails to further reduction in mixing time, whilst the power uptake increases exponentially.

Furthermore, for the first time, this study suggest that power number is inversely proportional to the square root of Reynolds number when systems are equipped with a dual helical ribbon impeller. The response surface method and quadratic numerical models are applied to suggest models in order to calculate the mixing time and power consumption.

1. Introduction

Stirred tank reactors (STRs¹) are one of the most widely used pieces of equipment in process industries. Gas-liquid STRs are involved in many chemical and biochemical processes including various multiphase reactions, polymerization, fermentation, foam food processing, production of antibiotics, and digestion [1–6]. The efficient and cost-effective heat and mass transfer and homogeneity of dispersed phase and nutrients are the main objectives of these multiphase mixing processes [7]. To date, various methods have been developed and introduced to enhance the mixing performance of gas-liquid reactors that contain shear-thinning fluids [8–13]. An increase in rotational speed seems to be one promising method that prevents the development of unmixed regions, of forming nutrient segregations and non-uniformity of the dispersed phase. Although using a high rotational speed in some cases might reduce mixing times, it also reduces the productivity of microorganisms in biological units, and the performance of final products, where it similarly increases the operational costs of chemical processes. The main explanation for this limitation is that some materials and microorganisms are extremely shear-sensitive. For example, a high

rotational speed disturbs the environment in which microorganisms seed and grow [11,12,14]. Microorganism cannot tolerate momentum, heat, and mass variations in their living environment, where high rotational speed or nonhomogeneous environments may consequently lead to switching metabolic pathways [7]. In cases where the shear sensitivity of substrate is an issue for reactor performance, using low rotational speed impellers has been suggested within the literature [14,15].

Using an ordinary small impeller including a Rushton turbine and pitched blade in a vessel filled with a non-Newtonian fluid has been shown to be inefficient and causes stagnant regions [16]. This phenomenon occurs because the central impeller fails to generate effective momentum and a sufficient shear rate in regions which are located far from the impeller itself. Close-clearance impellers including gate, anchor, screw and helical ribbon have been identified as ideal impellers by literature to complete mixing in a single-phase agitated systems involving non-Newtonian fluids [14]. Close-clearance impellers provide an almost tangential shear rate in the whole system, especially near the wall of the vessel which remains stagnant when non-Newtonian fluids rotate with an ordinary impeller [17]. In close-clearance agitator, the

* Corresponding author.

E-mail addresses: m.amiraftebi@ecu.edu.au (M. Amiraftebi), m.khiadani@ecu.edu.au (M. Khiadani), Hussein.mohammed@ecu.edu.au (H.A. Mohammed).

¹ Stirred Tank Reactor (STR)

Nomenclature			
A	Cross sectional area (m ²)	N _p	Power number (Dimensionless)
AR	Aspect Ratio	n	Flow index behaviour
D	Vessel inner diameter (m)	P ₀	Input power (W)
d	Impeller Diameter (m)	P _g	Power consumption after injection of gas (W)
d _i	Impeller blade diameter (m)	Q _p	Upward pumping rate by fluid (Lpm)
d _s	Shaft diameter (m)	Q _{AX}	Pumping rate by rising bubbles (Lpm)
Flg	Gas flow number	Re	Reynold number (Dimensionless)
g	Gravitational acceleration (m/s ²)	RSM	Response surface methodology
G _f	Gas Flow Rate (Lpm)	STR	Stirred Tank Reactor
H	Depth of Fluid (m)	u _g	Superficial gas velocity (m/s)
h	Impeller Height (m)	wt%	Weight percentage (%)
HCl	Hydrochloric Acid	X	Variables
IC	Impeller Clearance	Y	RSM Response
K	Consistency Index (Pa.s ⁿ)	β ₀	RSM regression coefficients
K _s	Metzner and Otto's constant	β _i	RSM regression coefficients
M _{Adjusted}	Actual torque required to rotate the shaft (N.m)	β _{ii}	RSM interaction coefficient
M _{display}	Torque displayed by torquemeter (N.m)	β _{ij}	RSM interaction coefficient
M _{friction}	Friction torque (N.m)	γ _g	Gas shear rates (1/s)
N	Impeller Rotational Speed (rpm)	γ _l	Liquid shear rates (1/s)
NaCMC	Sodium Carboxymethyl Cellulose	γ̄ _T	Average shear rates (1/s)
NaOH	Sodium hydroxide	η	Average apparent viscosity (Pa.s)
		ρ	Density (kg/m ³)
		τ	Average shear stress (N/m ²)

high shear rate region is located between the wall and impeller blade, where the impeller sweeps wall and returns the stagnant volume of fluid into the bulk.

Power consumption and levels of homogeneity are two main factors affecting the design of an efficient reactor, have been investigated widely in the literature [7,14,16]. Power consumption determines the cost efficiency of using stirred tank reactors in process industries. Similarly, mixing time is an indicator of homogeneity in stirrers. Ameur and Bouzit [18] have indicated that a helical ribbon is the most efficient impeller, reducing mixing time when a fluid is shear-thinning. Delafosse et al. [19] have defined the mixing time as the time interval between the injection of the tracer and 95 % of the full homogeneity degree. They further indicated that the mixing time is a function of impeller geometry and tracer injection methods. The power consumption and mixing time have been investigated by Bao et al. [17], with different coaxial mixers for two different non-Newtonian fluids. The above author concluded that a combination of Paddler and helical ribbon impellers reduce the mixing time significantly.

To date, various methods including conductivity, thermal refractive index, redox ionic reaction, and decolouration have been developed and introduced to measure mixing time in agitated systems [20–25]. However, all of these techniques depend on the location of deliberately placed detectors, lights and cameras [26–28]. Titration has typically been applied as one of the most common techniques to evaluate mixing time in agitated vessels without any physical interference [27,28]. This non-intrusive technique has been used to measure the degree of homogenization and qualitatively to visualize the flow pattern including the formation of caverns, stagnant regions, and dead zones. Since the titration method is based on human observation, complementary approaches like the image processing method have been developed to reduce errors related to human eyesight [26,29]. Titration acid-base reaction has been used in this study to explore mixing times.

Apart from studies investigating the efficiency of agitators working in single-phase systems, there is a general lack of research on the performance of multiphase STRs filled with shear thinning fluid. Bouaif and Roustan [30] developed a dimensionless correlation between power consumption and mixing time in an aerated mixing system equipped with multi-impellers. Machon and Jahoda [31] have studied the effect of aeration on the mixing process in a multi-impeller vessel, where they concluded that aeration improves homogeneity and reduces

the mixing time significantly. Further, Hashemi et al. [32] have measured bubble characteristics and gas holdup in mixing systems equipped with a combination of an anchor and central impeller. Some researchers have indicated that the presence of gas in gas-liquid systems enhances the homogeneity of the system and reduces mixing time [33–35]. Furthermore, many studies have shown that the gas flow rate and impeller speeds play a pivotal role in forming different flow patterns [36,37]. By changing the gas flow rate and rotational speed of an impeller, various flow patterns can be observed including flooding, loading, and complete dispersion [38,39]. In flooding pattern, gas bubbles rise quickly, thus the impeller speed fails to influence the bubble behaviour. The loading regime occurs when the gas flow rate decreases or the impeller speed increases. In this case, bubbles accumulate and become trapped behind the impeller or around the impeller shaft. The optimum scenario for gas-liquid systems is complete dispersion, where the gas bubble is well-distributed in the whole volume of the vessel [40]. A well-distributed mixing system holds bubbles inside for sufficient time in order to maintain bubbles and optimize heat and mass transfer [39].

A dual helical ribbon is a close-clearance impeller used in low Reynolds number under laminar and transient flow regimes to agitate shear sensitive non-Newtonian fluids. Dual helical ribbon impellers have been extensively studied in single-phase to evaluate the effect of geometry, rheology, kinematics (impeller speed), and impeller design on mixing time, homogeneity, and power uptake [41–47]. Chavan and Ulbrecht [47] have suggested a model based on geometry predicting power consumption for different types of helical ribbon impellers in the liquid phase. The influence of viscosity, viscoelasticity, and pseudoplasticity on the performance of an agitated system equipped with helical ribbon and helical ribbon screw impellers has been investigated by Brito-De La Fuente et al. [48]. They developed a model which indicates the deviation of pseudoplasticity from Newtonian power uptake for a helical ribbon impeller. Their findings are consistent with the general equation reported by Mentzor and Otto [41], although more research is needed to study the Mentzor- Otto correlation for strongly shear-thinning fluids.

Many reactions occur in gas-liquid phases, where, the presence of bubbles inside systems is unavoidable. Accordingly, researchers have shown an increased interest in the behaviour of bubbles and their influence on the flow pattern. Apart from Espinosa-Solares et al. [7] and

Cheng and Carreau [45] who have reported the influence of the presence of bubbles on power consumption of dual helical ribbons, previous studies are limited to single phase agitated systems. Therefore, little is known about the influence of impeller speed, gas flow rate, impeller clearance, and viscosity on mixing time and power consumption of multiphase agitated reactors driven by a dual helical ribbon impeller. Further, it is not clear how these factors are related to the desired mixing time and cost-effective power uptake when gassed STRs are filled with shear-thinning fluids. Additionally, there has been little information about the generalized correlation between power consumption and Reynolds number when a reactor tank is equipped with a dual helical ribbon impeller. Furthermore, little is known about the impacts of sparging gas into the system agitated with a helical ribbon impeller and it is not clear that rising bubbles has a positive or negative impact on the mixing performance.

Thus, the major objective of this study is to investigate the mixing performance of a helical ribbon impeller when the bubbles are dispersed, and the fluid phase is non-Newtonian. Further, this study evaluates the impacts of impeller speed, gas flow rate, impeller clearance from the bottom, and viscosity on mixing time and power consumption. It is believed that the empirical findings in this study would provide a new understanding of the flow pattern in the mixing process of gas-liquid STRs. The findings confirm that the association between impeller speed, gas flow rate, impeller clearance, and viscosity on the mixing time and power uptake. Data gathered from the experiments have identified that increases in impeller speed and gas flow rate are not always connected with reducing the mixing time and power consumption. Therefore, this study suggests a valuable correlation between Reynolds number and power number which remarkably influence the design, planning, and cost of gas-liquid reactors involving in process industries. The relationships between mixing time and power consumption with impeller speed, gas flow rate, impeller clearance, and viscosity have been suggested by ANOVA test. Therefore, the optimum response can be predicted in various operating conditions by using these two statistical equations achieved through response surface methodology (RSM²).

2. Materials and methods

2.1. Experimental setup

A transparent flat bottom and open-top cylindrical STR with an aluminium central shaft is studied, where the driven force of the stirrer is supplied by an electric motor. This type of system is widely used in mineral processing and oil storage. The³ aspect ratio (AR: height to diameter) of the reactor has been determined to be 1.4. This ratio is kept in the range of 1–3 when an insoluble gas exists in the system where higher heat and mass transfer is the main requirement. The geometric configuration of the experimental set up is presented in Table 1 and shown in Fig. 1.

Gas flow was supplied at the bottom of the stirred tank equipped with a surface sparger consists of 10 equally spaced holes drilled on the periphery of the surface, each having a diameter of 0.00025 m. The compressed air is supplied to the system through a central air system and a flowmeter (Omega engineering flow meter with accuracy of ± 2 % Full Scale) with the range of 0–2.2 LPM is applied to control the airflow.

The calculated Reynolds number (Eq. 9) in the current experiment was between 10–1000, therefore, the flow regime was considered as a transient flow. While this study focuses on the transient regime, the combination of both laminar and turbulent flows exist in the system. This means that inertial forces dominate in turbulent regime, while

viscous forces overcome in laminar flow.

In this study, NaCMC was used as working fluid due to its optical transparency and resistance to pH changes [49]. The reactor was filled up to 0.27 m of its height with NaCMC solution in four different concentrations of 0.1, 0.5, 1, and 1.5 wt%.

2.2. Acid-base reaction

Acid-Base titration reaction as an ordinary method of measuring the mixing time has been applied in this work for two different purposes [20–25]. The first one is to make it possible to see the evolution of colourful mixed region throughout the reactor as the impeller rotates. The second one is to find the mixing time by controlling the normality and volume of acid, base, and pH of the NaCMC solution. Adding the purple solution of NaOH and phenolphthalein into the agitated reactor followed by acid injection helps to visualize the chaotic movement of colour particles, homogenization process, and the formed vortices.

According to the previous study, to monitor fluid chaotic movement, 7 ml NaOH of 2 N and phenolphthalein indicator was injected closed the rotating shaft near the surface inside the reactor to raise pH value until the working fluid colour turns into purple in all regions. The reaction was recorded using a high-speed camera (Samsung digital Camera 12 M P with speed of 1.4 μm including dual-pixel autofocus) for further evaluation. Then, 5 ml of HCl solution was injected at the same location (near the impeller shaft) to decolourize the working fluid and the growth of decolouration of the working fluid was observed and recorded by the camera [20–25].

In this paper, mixing time is considered as the time taken for the 95 % of complete mixing where the solution was homogenous. Mixing time is determined by using RGB method and post processing software (ImageJ). This method is presented and described in literature in a systematic and detailed way [50,51].

Each experiment was repeated three times under the same conditions to ensure the consistency of the results. Additionally, the normality and volume of the required solution of acid and base were verified by titration before each set of experiments.

2.3. Torquemeters

The dissipated power of an impeller is correlated with impeller speed and rheological properties of liquid in which agitator is carried out. In this study, the power uptake by a mixing system was measured by a commercial torquemeter (GUNT system with ± 0.1 N.m). The consumed power and the adjusted torque were calculated from Eq. 11 and Eq. 12, respectively.

2.4. Rheometer

The viscoelastic characteristics of the polymer solutions was measured with a DHR-3, TA rheometer with normal accuracy ± 0.005 , equipped with a coaxial cylinder cup with a diameter of 0.304 m, bob diameter of 0.28 m, bob height of 0.42 m, and gap distance of 0.001 m. Further, the temperature was controlled to 25 °C with a Peltier system during the tests.

Oscillation tests were carried out with increasing and decreasing ramp of strain from 1 to 300 % and vice versa at a constant frequency of 1 Hz in order to collect 30 points per decade. To remove the molecular network memory completely, the sample was pre-sheared at 300 s^{-1} up to 15 min, after loading the cup and reaching to the equilibrium stage. Then, this procedure was followed by a 5 min rest at zero shear rate [49].

2.5. Theoretical considerations

Flow regime, formation, and distribution of bubbles, and fluid rheological behaviour inside STRs are affected by the pumping rate of

² Response surface methodology (RSM)

³ Aspect Ratio (AR)

Table 1
The geometric configuration of the stirred system.

Vessel inner diameter (m)	Vessel height (m)	Impeller height (m)	Impeller diameter (m)	Impeller blade diameter (m)	Impeller clearance (m)	Shaft diameter (m)
D	H	h	d	di	IC	ds
0.19	0.4	0.155	0.14	0.02	0.02, 0.04, 0.06	0.015

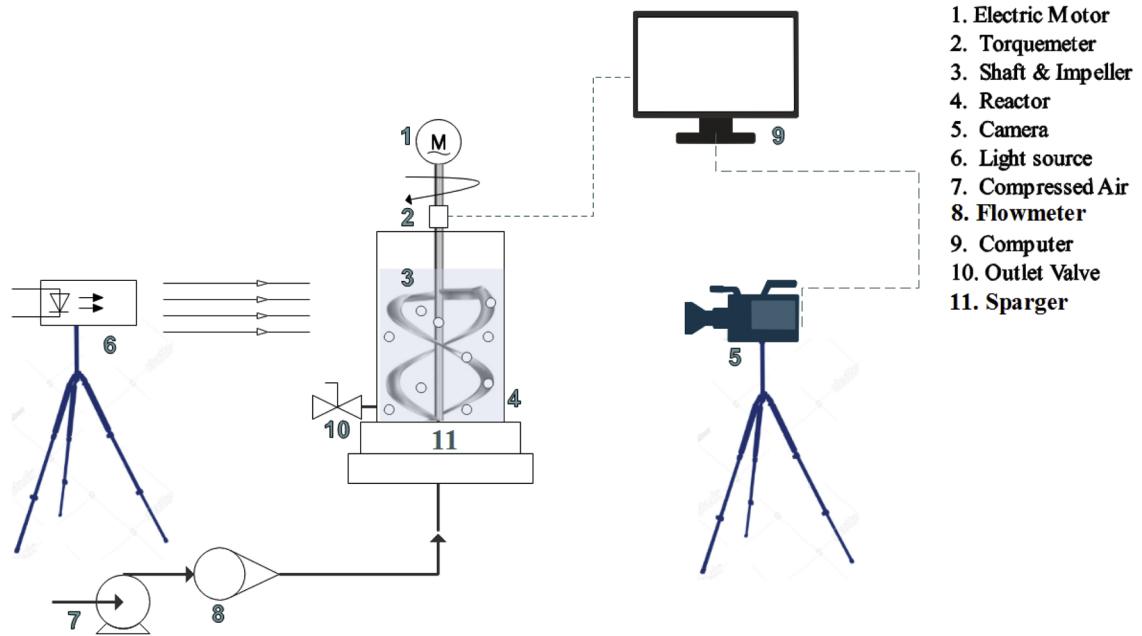


Fig. 1. Schematic of experimental setup.

the agitator which Q_p ⁴ is upward pumping rate by fluid (Lpm) and Q_{AX} ⁵ is the volume rate of liquid pumping upwards by rising bubbles (Lpm) [34]. Smith [34] has suggested the following two equations to predict the flow regime of gas-liquid agitated systems. If $Q_{AX} \neq Q_p$, the reactor flow pattern in loading/ flooding transition is not desirable.

$$Q_{AX} \propto (G_f g H^5) \quad (1)$$

$$Q_p \propto (N d^3) \quad (2)$$

where H is the depth of fluid in the reactor (m), G_f is the gas flow rate (LPM), D is the diameter of impeller (m), N is the impeller rotational speed (rpm), and g is the gravitational acceleration constant (m/s²).

This study examines Q_p and Q_{AX} for various impeller speeds and different gas flow rates combined with visual observation in order to assure the flow regime undergoes complete dispersion inside the reactor.

In gas-liquid agitation reactors, the maximum shear rate is imposed by the rotary mechanical part. However, rising gas bubbles can also have some impact on the fluid bulk. In this case, the average total shear rate can be calculated from;

$$\dot{\gamma}_T = \sqrt{\dot{\gamma}_g^2 + \dot{\gamma}_l^2} \quad (3)$$

where, $\dot{\gamma}_l$ is liquid shear rates (1/s), $\dot{\gamma}_g$ is gas shear rates (1/s), and $\dot{\gamma}_T$ is average total shear rates (1/s).

According to Metzner and Otto's correlation [52] the average shear rate for shear-thinning fluids inside an agitated system ($\dot{\gamma}_l$) can be defined as follows:

$$\dot{\gamma}_l = K_s N \quad (4)$$

where $\dot{\gamma}_l$ is the average shear rate in a stirred vessel depending on the impeller geometry and characteristics reflecting in Metzner and Otto's constant (K_s) [52]. Additionally, the strong dependency of K_s to fluid rheology has been widely investigated in the literature. Some researchers have indicated that flow index behaviour (n) is proportional to K_s [53], while others report the decreasing value of K_s is correlated to increasing flow index behaviour [54,55].

Additionally, the gas shear rates ($\dot{\gamma}_g$) can be calculated by Hashikawa's correlation [56], which shows the effect of bubble motion on liquid and defined as;

$$\dot{\gamma}_g = 1500 u_g \quad (5)$$

$$u_g = \frac{G_f}{A} \quad (6)$$

where u_g is the superficial gas velocity (m/s) which is consider equal to 1500 m/s as a proportional constant and A is Cross sectional area (m²).

η ⁶ is the average apparent viscosity (Pa.s) and can be calculated by the correlation between the $\dot{\gamma}_T$ and τ ⁷ as a shear stress (N/m²).

$$\eta = \frac{\tau}{\dot{\gamma}_T} = \frac{\tau}{\sqrt{(K_s N)^2 + (1500 u_g)^2}} \quad (7)$$

Further, a previous study noted NaCMC as a shear-thinning fluid that follows the Power-Law equation [49].

$$\tau = K \dot{\gamma}_l^n = K (K_s N)^n \quad (8)$$

where n is the flow index, K is the consistency index (Pa.sⁿ). All these rheological parameters have been investigated in a previous study [49], where the rheological factors for NaCMC are summarized in Table 2.

Eq. 9 shows the Reynolds number for a stirred system. Substitution of the Power-Law model in Eq. 8 leads to obtaining Reynolds number

Table 2
The rheological parameters of NaCMC [49].

Concentration (wt%)	n (-)	K (Pa.s ⁿ)
0.1	0.98	0.08
0.5	0.92	0.13
1	0.82	0.46
1.5	0.58	4.3

for a dual helical ribbon. Fuente et al. [48] have reported $K_s = 32.9$ – 35.7 for a dual helical ribbon impeller in a shear-thinning fluid, whereas n is close to 1.

$$Re = \frac{\rho N d^2}{\eta} \quad (9)$$

In most recent studies, the mixing time as an indicator of homogeneity has been measured in different approaches including local and general mixing time [57]. Within the realm of macromixing, bulk mixing time t(s) is the time taken for the complete mixing, where the solution is homogenous.

The Power number represents the rate of energy dissipation within the liquid and the power consumption by impeller in a specific rotational speed. Ungassed power number as the most important parameters in coaxial mixers have been studied widely [58,59].

$$N_p = \frac{P_0}{\rho N^3 d^5} \quad (10)$$

where ρ is density (kg/m³).

P_0 as input power (W) is one of the main parameters evaluating the efficiency of ungassed impeller which can be calculated by using the following formula [60–62]:

$$P_0 = 2. \pi. N. M_{Adjusted} \quad (11)$$

Furthermore, Bourne and Butler [63] have proven that there is a correlation between Reynolds number and Power number in single phase viscose fluid. Finally, torque should be obtained from the following formula:

$$M_{Adjusted} = M_{display} - M_{friction} \quad (12)$$

$M_{Adjusted}$ ⁸ is the actual torque required to rotate the shaft (N.m). It can be calculated from the subtracting the friction torque ($M_{friction}$ ⁹) from what is monitored on the power meter ($M_{display}$ ¹⁰) (N.m). If the impeller rotates in the open air, the magnitude of torque will be considered as friction torque.

2.6. Response surface method

Response surface method (RSM) approach was used to predict the mixing time and power consumption under different operating conditions. The main objective of the RMS is e to identify the correlation between variables including impeller speed, gas flow rate, impeller clearance, and viscosity as well as responses including mixing time and power consumption. For this purpose, the Box-Behnken method is used to design the experiments. Next, the response surface methodology (RSM) is applied to optimize the factor levels and find the most influential parameters. For each experiment, three replicates are considered to ensure the reproducibility of the experiments. The correlation is defined as:

$$Y = \beta_0 + \sum_{i=1}^3 \beta_i X_i + \sum_{i=1}^3 \beta_{ii} X_i^2 + \sum_{i=1}^3 \sum_{j=2}^3 \beta_{ij} X_i X_j + error \quad (13)$$

⁴ Upward pumping rate (Q_p)

⁵ Volume rate of liquid pumping upwards (Q_{AX})

⁶ Average apparent viscosity (η)

⁷ Shear stress (τ)

⁸ Actual torque required to rotate the shaft ($M_{Adjusted}$)

⁹ Friction torque ($M_{friction}$)

¹⁰ Torque displayed by torque meter ($M_{display}$)

Table 3
Variables used in RSM method to optimize the mixer performance and uncertainty analysis for different variables.

Symbols	Variables	Low level	Central level	High level	Instrument	Systematic Uncertainty (± %)	Random Uncertainty (± %)	Total Uncertainty (± %)
X ₁	Impeller speed (1/s)	50	75	100	Torquemeter	–	1	1.00
X ₂	Gas flow rate (Lpm)	0.5	1.35	2.2	Flow meter	1.5	0.66	1.64
X ₃	Impeller clearance (m)	0.02	0.04	0.06	Ruler	0.5	0.83	0.97
X ₄	Concentration (wt %)	0.1	0.8	1.5	Scale	0.1	0.32	0.34

In this equation, X shows variables, Y indicates the response such as mixing time, while β_0^{11} , β_i^{12} , β_{ii}^{13} , and β_{ij}^{14} are regression coefficients and interaction terms. Different 3D surface plots are plotted to find the most influential factor when the other factor are at optimized level [64].

The list of variables and their maximum and minimum levels are summarized in Table 3. These maximum and minimum levels are selected based on the preliminary study.

Further, uncertainty analysis has been done for measured and calculated data, as well as instrument accuracy. The result of uncertainty analysis is summarized in Table 3.

3. Results and discussion

In this study, the impeller speed, gas flow rate, impeller clearance from the bottom, and viscosity are considered as principal factors influencing the mixing process of a shear thinning fluid. It is worth noting that the maximum impeller speed in the current investigation was limited to 100 rpm. This limitation was considered because of the extreme shear sensitivity of some materials and microorganisms [11,65].

As mentioned earlier, the experiments were carried out in the optimal range where the hydrodynamics of a gas-liquid system is completely dispersed. The influence of gas flow rates of 0.5–2.2 Lpm is examined when the system is agitated by a dual helical ribbon impeller between 50–100 rpm under transient flow regime. Generally, the effects of bubble motion, impeller speed, gas flow rate, and viscosity on power consumption and mixing time are discussed and interpreted in this section.

3.1. Mixing pattern

The two-dimensional cross-section of the mixing pattern in the vessel when the reaction between acid and base occurs is shown in Fig. 2.

The visual evidence presented in this section shows that initially, the radial movement of fluid bulk is stronger than the axial movement for a dual helical ribbon. The impeller drives fluid towards the walls of the vessel where the shear rate is at the maximum, where little movement of fluid can be observed in the axial direction near the central shaft. Then, fluid moves downward alongside the cylinder wall. Following this, the axial movements become stronger and the top surface becomes clear. Decolouration of the purple fluid shows that the maximum mixing in this type of impeller happens close to the clearance between the wall and impeller where the high shear imposes on the fluid film as well as areas near to the inner edge of the blade. Whilst, there is still an unmixed zone located at the bottom of the tank, the efficiency of the impeller in the region near the wall is significant. Therefore, the mixing time is controlled by the mixing pattern of the low-shear central regions located far from the blade edges. A possible explanation for these results may be the reduction in viscosity when the

high shear rate region rotates near the inner and outer edges of the blade. The enclosed volume of fluid between impeller and wall as well as the bulk of fluids around the inner edge of the blade can be considered as a low viscosity film which can be easily influenced by this type of impeller. Generally, these regions are introduced as a stagnant zone in other types of impellers.

Although extensive research has been carried out on the effects of dual helical ribbon impellers on single phase flow pattern, few studies have paid attention to the influence of chaotic bubble motion on multi phases mixing process [56]. Fig. 3 indicates the qualitative mixing pattern over time when air bubbles are introduced. Rising a bubble from bottom of the tank imposes shear rate to the bulk of the fluid. As a result, the viscosity of the shear-thinning fluid is reduced to some extent depending on the gas flow rate, general gas hold-up, and rheology of the fluid. The more reduction in viscosity, the more desirable results are achieved including less energy consumption and shorter mixing time. Since bubbles are dispersed everywhere, the mixed area near the central shaft can gradually develop, which enhances the mixing performance of the dual helical ribbon impeller.

Fig. 3 indicates that in a low rotational speed helical ribbon impeller, the formed bubbles rise without significant breakage or coalescence. They are trapped behind the impeller blade and form a film of gas which follows the impeller patterns to reach the free surface. The interesting point here is the enhancement of the uniformity of homogenization and dispersion of liquid inside the system. In the presence of bubbles, after the injection of acid, clear liquid not only moves toward the clearance of the vessel and impeller but also gradually penetrates downward. Although this requires more investigation, this phenomenon could be interpreted by increasing the internal liquid shear stress as a result of bubbles motions. In completely disperse mixing patterns, bubbles disperse completely in the whole system, even in stagnant regions. The presence of bubbles in the stagnant zones increases the shear stress resulting in the breakdown of the NaCMC internal network [49]. Weakening the network structure of shear-thinning fluids increases both molecular and bulk diffusions resulting in enhancement of the mixing process.

3.2. Impact of impeller speed

The impact of various rotational speeds on the performance of the mixing system has been studied widely in the literature. Results show that an increase in rotational speed reduces the time of mixing and improves the homogeneity of heat, mass, and nutrient [7,10,37,66,67].

Fig. 4a and b depict both mixing time and power consumption over various rotational speeds for different concentration of NaCMC solutions. The results indicate that a higher rotational speed leads to shortened mixing time, while power uptake increases exponentially. The results indicate that an increase in rotational speed up to 75 rpm could reduce the mixing time of viscous fluid to some extent.

Fig. 4a shows the expected time to reach homogeneity in different impeller rotational speeds. For the same rotational speed, the more concentrated solution the more time required to reach homogenous conditions, where the natural gel structure of polymer requires more energy and time to destroy. Therefore, the diluted solution requires less time in a lower rotational speed to reach a certain level of homogeneity. Further, it can be noted that the homogeneity graphs are exponential

¹¹ RSM regression coefficients (β_0)

¹² RSM regression coefficients (β_i)

¹³ RSM interaction coefficient (β_{ij})

¹⁴ RSM interaction coefficient (β_{ij})

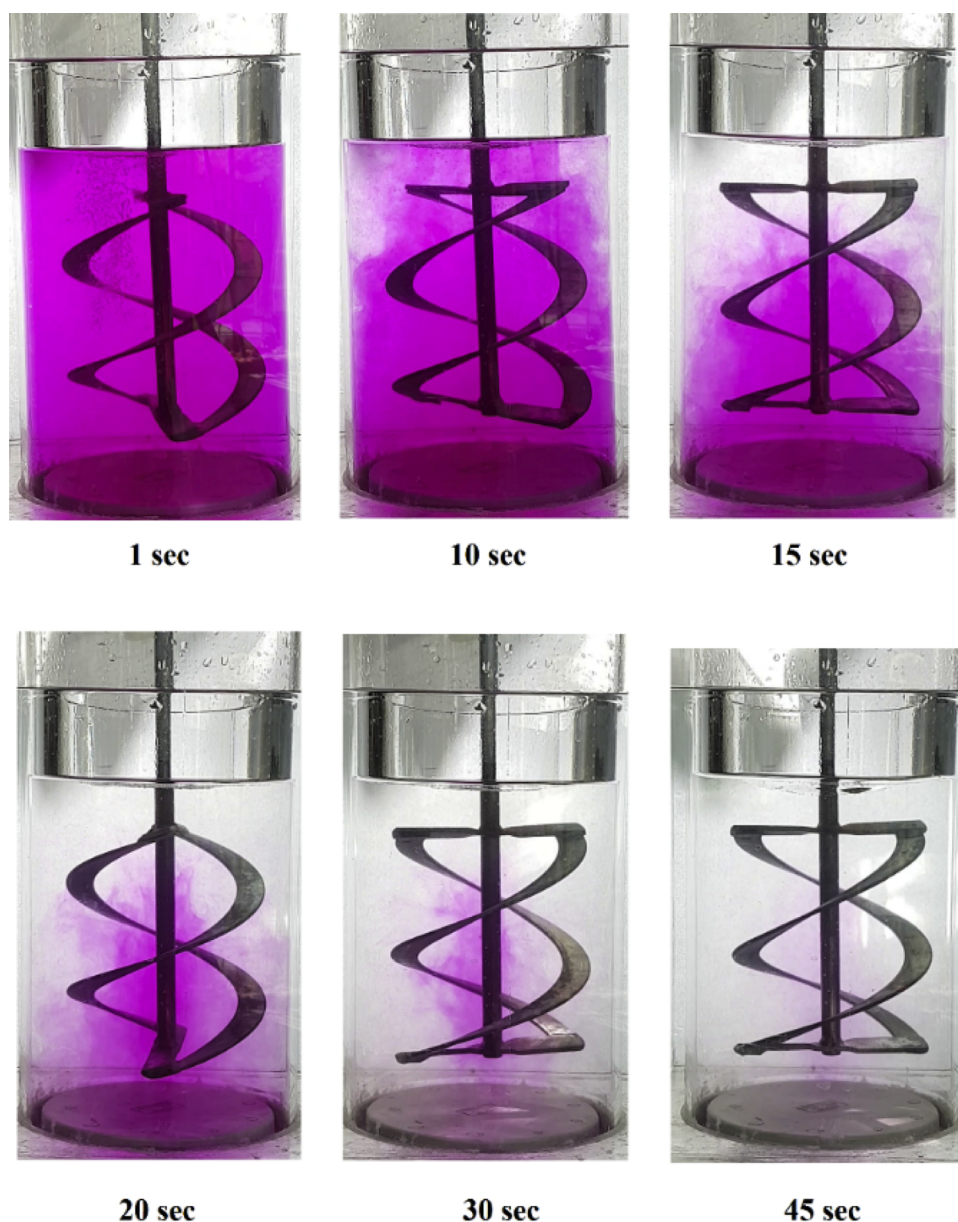


Fig. 2. The evolution of mixed area inside the reactor when the impeller speed is 75 rpm and concentration of NaCMC solution is 1 %.

which become level off at the end. Thus, it seems that the system has become homogenous in somewhere between rotational speed of 0–50 rpm when the concentration of NaCMC solution is 0.1 %.

However, increasing the rotational speed beyond 75 rpm not only has insignificant contribution in reducing the mixing time but also exponentially increases power consumption. This finding suggests that increasing the impeller speed up to optimum value could enhance the performance of the mixing system. Whilst, after this certain level, the power consumption increases sharply with a limited positive contribution to mixing performance.

Two different dimensionless terms have been defined to investigate the extra power consumed by the impeller compared to mixing time reduction. The first term is the extra power consumed when the impeller speed increases from 75 to 85 and 100 rpm and the second term is the decrease of the mixing time when the impeller speed increases to 85 and 100 rpm.

Fig. 5 represents these two dimensionless terms for different

concentrations of NaCMC. According to this figure, a remarkable increase is observed in the percentage of power uptake compared to the reduction in the percentage of mixing time when the solution is more concentrated. For example, when impeller speed changes from 85 to 100 rpm in a concentration of 1.5 % solution, the power consumption has been increased by 60 %, while the mixing time decreased by 10 %. This finding is vital in terms of cost efficiency and scaling up the system.

3.3. Influence of bubble motion

The mixing time versus gas flow rate for gassed cases in both stirred and non-stirred conditions is shown in Fig. 6. Hollow markers show the mixing time in different gas flow rates for various concentrations of NaCMC solutions when the impeller speed is 75 rpm. Filled markers demonstrate the mixing time under the same operating conditions when the impeller is off (impeller speed = 0 rpm). The results in this figure reveal that the gas flow rate is an influential factor in mixing time when

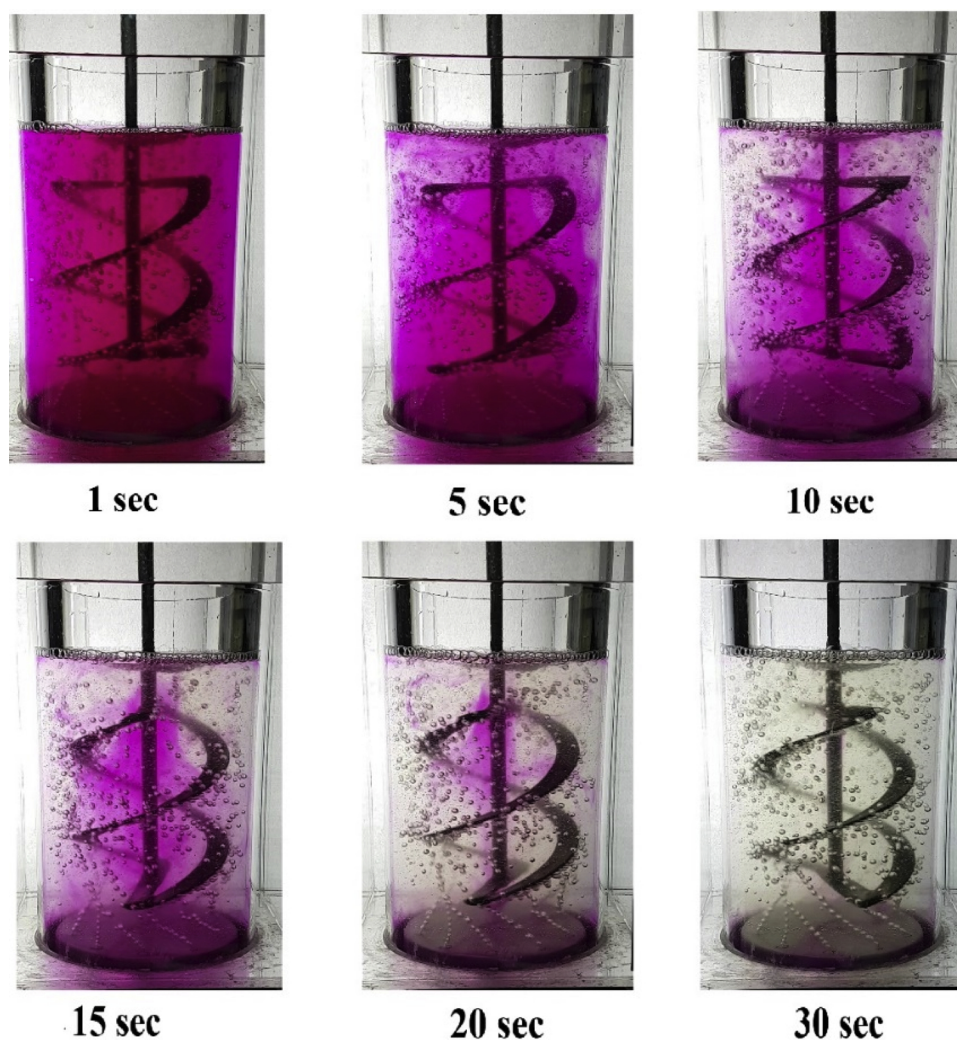


Fig. 3. The evolution of mixed area inside the aerated reactor when the impeller speed is 75 rpm and concentration of NaCMC solution is 1 %.

the mechanical agitator is not working. Increasing the gas flow rate from 0.5 to 2.2 LPM could reduce the mixing time to half in non-stirred systems. However, hollow markers show that the mechanical agitator is more influential on mixing time compared to the gas flow rate.

Some previous studies suggest that for a system with a Rushton turbine and PBD- anchor, the gas flow rate increases the mixing time [36,37]. It has been argued that in high gas flow rate, the buoyancy force overcomes the hydrodynamics of system and the gas-liquid system flooded [36,37]. Other researchers, however, have reported an improvement in the mixing performance by the presence of bubbles inside the system [33–35]. This inconsistency may be due to the complex hydrodynamics of gas-liquid agitated flow patterns. The variety of hydrodynamics in gas-liquid STRs can be almost considered as a function of impeller type, rheology of fluid, gas flow rate, impeller speed, and bubble size [39].

3.4. Power consumption

Power uptake is another influential design parameter representing the economic performance of a mixing system. The power consumption of the impeller should be taken into account when the cost efficiency of a mixing process is important. Power consumption displays the performance of the agitating process depending on the geometry of impeller and physical properties of the fluid [68]. The power consumption

measurement has been carried out on NaCMC solution with different concentrations of 0.1, 0.5, 1, and 1.5 wt% for five different impeller speeds of 50, 65, 75, 85, and 100 rpm.

Fig. 7a indicates the power uptake by impeller versus Reynolds number for the rotational speed of 50, 65, 75, 85, and 100 rpm for different concentration of NaCMC solutions. The greater the viscoelasticity of the fluid, the greater the energy required to achieve complete mixing. It can be observed that an increase in viscosity shifts the power curve to the lower Reynolds numbers and higher energy consumption.

Fig. 7b displays the dimensionless energy consumption (N_p) as a function of Reynolds number (Re) or power curve for a dual helical ribbon in five different rotational speeds of 50, 65, 75, 85 and 100 rpm and constant gas flow rate of 1 LPM. The power curve is unique for each impeller type. The single most striking observation to emerge from the plotted data is the relationship between N_p and Re , which for the first time this result has been presented. Regression analysis was used to predict the correlation between these two parameters which is importantly repeated for all concentrations of NaCMC, whereas the flow regime is transient. This practical correlation has been reported in Eq. 14. It is noticed that this practical correlation is unique and demonstrating how a dual helical ribbon impeller performs in a transient two phases flow regime.

$$N_p \cdot Re^\beta = \alpha \text{ or } N_p = 918.9Re^{-0.5} \quad (14)$$

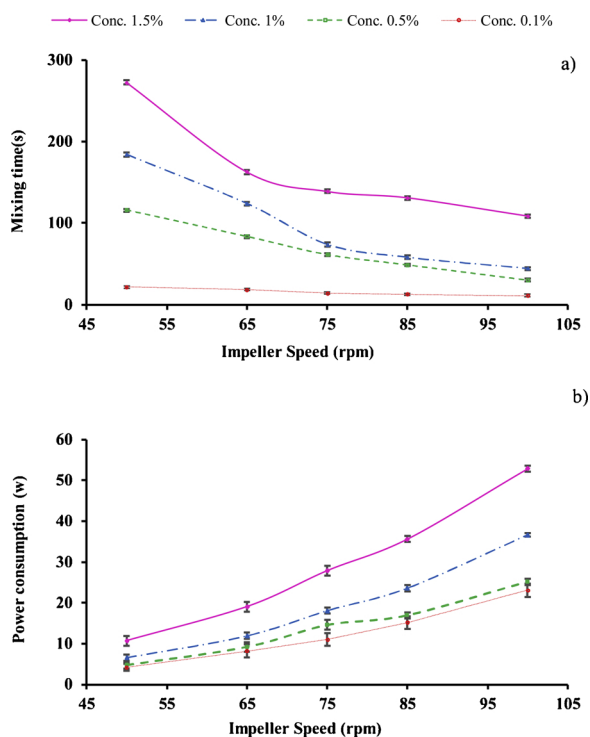


Fig. 4. a) Mean mixing time and b) mean power consumption with error bars over impeller speed in different concentration of NaCMC solutions.

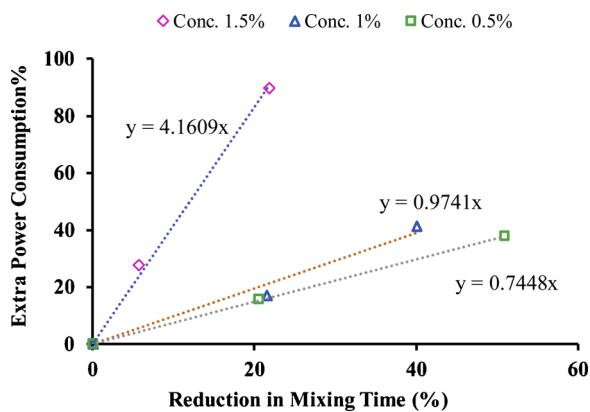


Fig. 5. Comparison between the percentage of power consumption and percentage of enhancing mixing time.

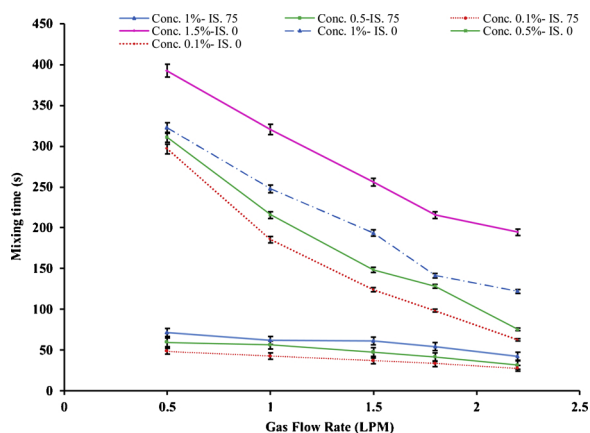


Fig. 6. Comparison between the mean gassed mixing time with error bars in both stirred and non-stirred conditions.

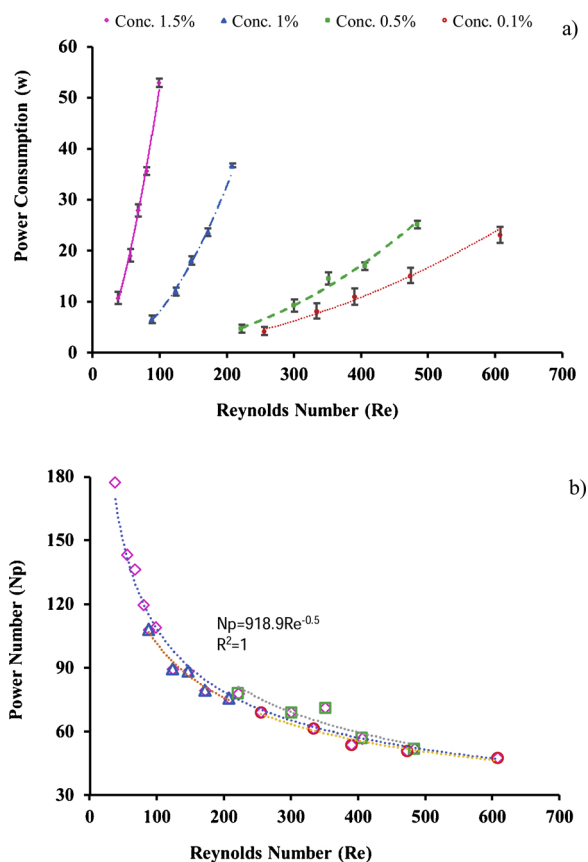


Fig. 7. a) Mean power curve and b) Power number (Np) vs. Reynolds number (Re) for a dual helical ribbon in five different rotational speeds for various concentrations of NaCMC.

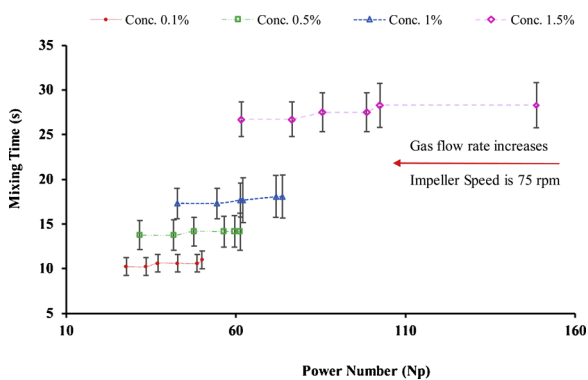


Fig. 8. Influence of gas injection on mean mixing time with error bars over power number (Np).

where, $\beta = 0.5$ and $\alpha = 918.9$ are constant for a dual helical ribbon impeller in different concentration of NaCMC solutions from 0.1 wt% to 1.5 wt%.

What is surprising here is that the trend of the power curve is not influenced by changes in concentration. Patel et al. [69] have indicated that $Re \cdot N_p$ is a constant value for the Scaba and the A320 impellers in single-phase flow. They also mentioned that the power number changes slightly based on Reynolds number in transient flow for the Scaba and the A320 impeller in single-phase flow. However, this correlation has not previously been found for a dual helical ribbon impeller in gas-liquid interactions.

Additionally, Fig. 8 shows the power consumption as a function of mixing time at a constant impeller speed of 75 rpm. These results show the effect of bubble motion on mixing time and power consumption.

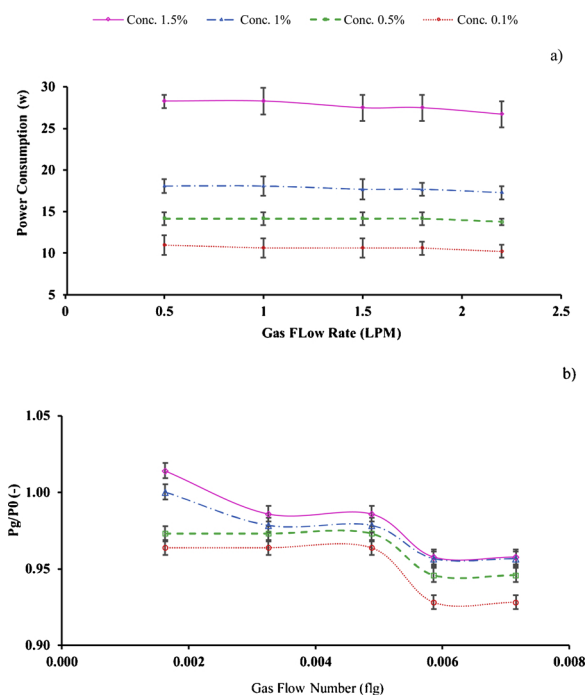


Fig. 9. The role of bubble motion around the impeller on mean power consumption.

Interestingly, a decrease in power consumption was observed when gas was injected into the system. This 5–7 % reduction in power consumption could be due to the presence of bubbles inside the reactor. The reduction in power uptake by sparging bubbles in a mixing system has also been observed by other researchers [30,70]. This finding can be interpreted through the formation of gas pockets (cavities) underneath the impeller streamlining the blade movement and reducing fluid drag resulting in lower power consumption. Further, reducing the viscosity of shear thinning fluid as a result of axial and rotational

Table 4
Plan for ANOVA analysis.

Order	Impeller speed (N)	Gas flow rate (Gf)	Impeller Clearance (IC) ^a	Concentration (C)	Mixing Time	Power consumption
	rpm	LPM	m	wt%	s	W
1	100	0.5	0.04	0.8	57	30.8
2	75	0.5	0.04	1.5	102.4	27.88
3	75	1.35	0.02	0.1	34	10.6
4	75	0.5	0.04	0.1	48.7	10.6
5	75	1.35	0.06	0.1	45.5	10.6
6	75	1.35	0.06	1.5	91.1	27.1
7	75	0.5	0.02	0.8	65.5	16.3
8	75	2.2	0.04	0.1	27.8	10.2
9	75	1.35	0.02	1.5	88	27.1
10	50	1.35	0.06	0.8	63.25	6.5
11	75	2.2	0.02	0.8	31.5	15.3
12	50	1.35	0.02	0.8	42.8	6.5
13	100	1.35	0.04	1.5	95.8	52.8
14	75	2.2	0.06	0.8	42.8	15.3
15	75	0.5	0.06	0.8	75.8	16.3
16	100	1.35	0.06	0.8	46.5	32.46
17	75	1.35	0.04	0.8	57.1	15.1
18	50	2.2	0.04	0.8	39	6.54
19	50	1.35	0.04	0.1	49.8	4.45
20	75	2.2	0.04	1.5	61.7	26.31
21	100	1.35	0.04	0.1	23.9	20.94
22	100	2.2	0.04	0.8	26	31.4
23	50	0.5	0.04	0.8	68.8	6.28
24	100	1.35	0.02	0.8	46.5	30.9
25	50	1.35	0.04	1.5	90.7	11.8

^a Impeller Clearance (IC).

Table 5
Results of ANOVA test for Quadratic model.

Response	Mixing time		Power consumption	
	F-value	P-value	F-value	P-value
Model	45.37	< 0.0001*	128.1	< 0.0001*
A-Impeller Speed	14.52	0.0034*	1138.3	< 0.0001*
B-Gas Flow rate	151.38	< 0.0001*	0.4454	0.5197 ^{ns}
C-Concentration	379.81	< 0.0001*	513.47	< 0.0001*
D-Impeller Clearance	13.54	0.0042*	0.1121	0.7447 ^{ns}
AB	0.0182	0.8953 ^{ns}	0.016	0.9019 ^{ns}
AC	12.17	0.0058*	82.98	< 0.0001*
AD	5.29	0.0442*	0.3362	0.5749 ^{ns}
BC	4.96	0.051 ^{ns}	0.1891	0.6729 ^{ns}
BD	0.0127	0.9126 ^{ns}	0	1 ^{ns}
CD	0.8933	0.3669 ^{ns}	0	1 ^{ns}
A ²	2.48	0.1466 ^{ns}	20.95	0.001*
B ²	2.95	0.1165 ^{ns}	0.0326	0.8603 ^{ns}
C ²	12.92	0.0049*	19.56	0.0013*
D ²	0.2279	0.6433 ^{ns}	0.206	0.6596 ^{ns}

*: Not significant at $P < 0.05$, ns: Significant at $P > 0.05$.
P – value and F – value: Indicator of significance decision.

bubble movements can be considered as another influential factor.

In addition, Fig. 8 depicts that both power consumption and mixing time are highly affected by the viscosity of the fluid. The higher the viscosity of the fluid, the more power required to achieve complete mixing. Therefore, when the viscosity of the shear-thinning fluid increases, more power and time are required to achieve desirable mixing.

These results differ from most published studies that reported bubble motion causes an increase in power consumption of an aerated stirred system [30,70]. However, the present results are in agreement with Cheng and Carreau's [45] findings which show the presence of bubbles leads to a reduction of power consumption by the impeller.

Fig. 9a and b clearly describes the role of gas flow rate on power consumption where the impeller rotational speed is constant at 75 rpm. According to Fig. 9a, an increase in gas flow rate from 1 to 2.2 LPM reduces the mixing power to some extent. Further Fig. 9b, represents the ratio of power uptake by impeller when the gas sparged (P_g), watt,

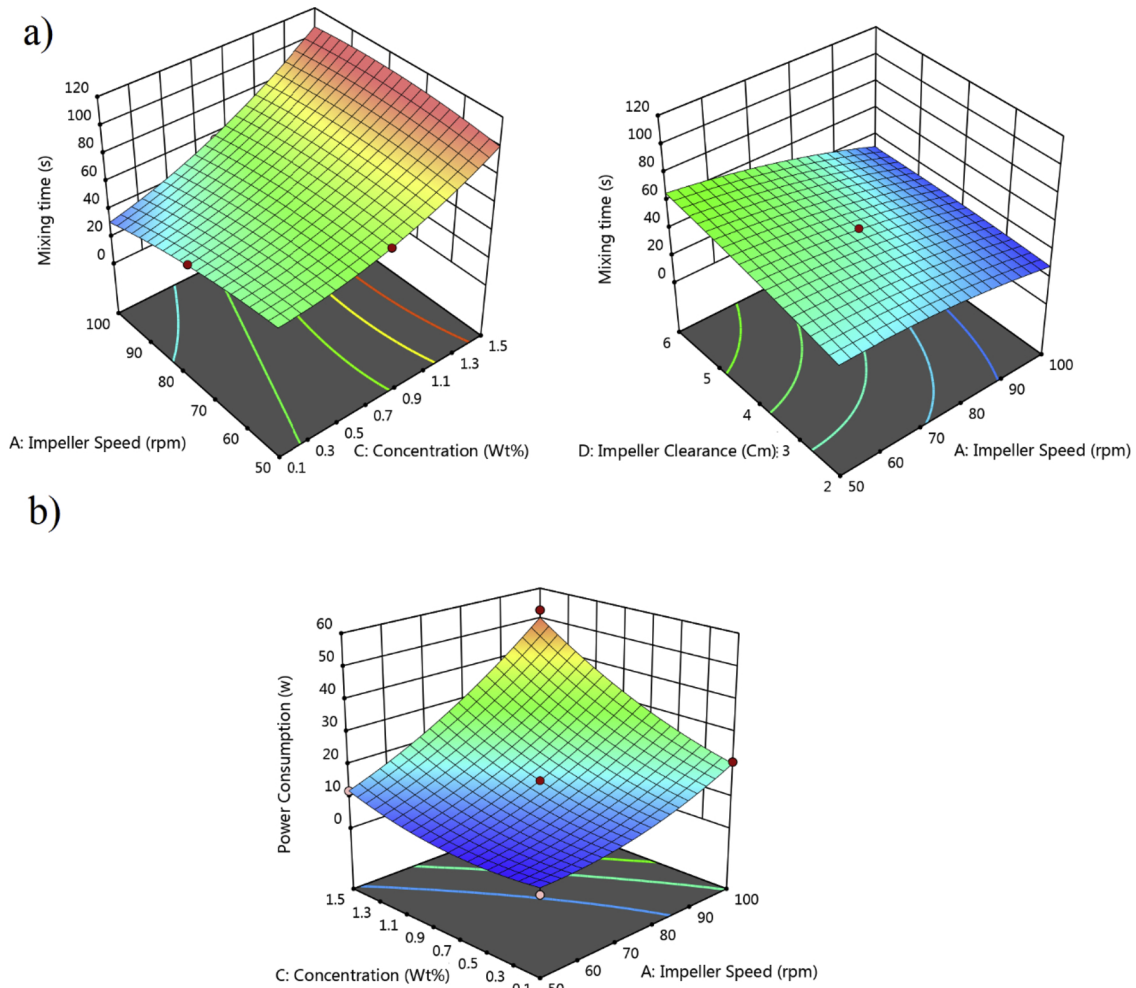


Fig. 10. Influential interaction model parameters analysed by ANOVA test.

to the power consumption of single-phase system (P_0), watt, over the gas flow number (flg^{15}) which shows the flow developing in the impeller zone independent to impeller geometry.

This figure shows that power consumption experiences a significant fall after a certain value of gas flow rate. Dispersed bubbles can reduce the viscosity of the fluid around the blade to some extent and reduce the power uptake. By increasing the impeller speed, the bubbles disperse everywhere in the fluid bulk and some of them still follow the impeller path. As a result, the impeller has the maximum level of contact with the air bubbles trapped behind the blade which slightly decrease the power consumption of the aerated system compared to single-phase one.

3.5. Statistical analysis

This proposed study investigates the impacts of four listed factors shown in Table 3 through the three-level Box-Behnken method [71]. Then, the response surface methodology (RSM) is applied to optimize and to find the most influential factors and their interactions. Table 4 summarizes the plan, the number of experiments and variables applied in RSM.

The result of statistical analysis suggests strong correlations between responses and all independent and dependent variables lead to Eq. 15 and Eq. 16.

$$\begin{aligned}
 \text{Mixing time} = & -1.26 + 0.88N + 5.5Gf - 11.31C + 13.56IC \\
 & - 0.014N \times Gf + 0.44N \times \text{conc.} - 0.1N \times IC \\
 & - 8.3Gf \times \text{conc.} + 0.14Gf \times IC - 1.5\text{Conc.} \times IC \\
 & + 0.0067N^2 - 6.3Gf^2 + 19.4C^2 - 0.32IC^2 (\text{Adjusted R2} \\
 & = 0.9628)
 \end{aligned} \quad (15)$$

$$\begin{aligned}
 \text{Power Consumption} = & 28.53 - 0.67N - 0.75Gf - 1.25IC - 24.58C \\
 & + 0.004N \times Gf + 0.35N \times C + 0.007N \times IC \\
 & - 0.49Gf \times C + 3.9E^{-16}Gf \times IC - 1.07^{-15}C \times IC \\
 & + 0.0058IS^2 + 0.2Gf^2 + 7.23C^2 \\
 & + 0.09IC^2 (\text{Adjusted R2} = 0.9867)
 \end{aligned} \quad (16)$$

where N is the impeller speed, Gf is the gas flow rate, C is the concentration of the solution, and IC is the impeller clearance.

Further, the result of ANOVA test has been summarized in Table 5 for the response surface quadratic model. This table demonstrates P-values and F-values for all variables. In this case, A, B, C, D, AC, AD, BC, A^2 , and C^2 are significant model parameters.

The Model F-values of 45.37 for mixing time and 128.1 for power consumption confirm that the proposed Eq. 14 and Eq. 15 are reliable and remarkably accurate to predict the mixing time and power consumption in different operating conditions. These equations have significant practical value for industrial designing, operating, and cost studying of STRs.

To sum up, the statistical analysis indicates that impeller speed, gas

¹⁵ Gas flow number (flg)

flow rate, impeller clearance, and viscosity influence the mixing time and power consumption, respectively.

Further, analysis of interactions between variables and the model coefficients are displayed in three-dimensional response surfaces and are shown in Fig. 10a, b. This figure displays the significant interaction model parameters based on P-value < 0.05. Fig. 10a shows the most influential interactions on mixing time including impeller speed-concentration, and impeller clearance-impeller speed. Additionally, according to P-value, the most influential model parameter on power consumption is interaction of concentration-impeller speed as shown in Fig. 10b.

4. Conclusions

Collectively, this study outlines the role of a helical ribbon impeller on mixing performance and cost of operation of a gassed STR. The range of gas flow rate and impeller speed has been adjusted in the preliminary study. In addition, this work provides a conceptual understanding of the flow pattern inside a gassed reactor equipped with a dual helical ribbon impeller and filled with a shear thinning fluid. The findings of this study suggest that increasing the rotational speed more than 75 rpm not only fails to reduce mixing time but also increases the power consumption. It can be concluded that the optimum rotational speed should be selected with caution because boosting impeller speed may impose the extra operating cost while the efficiency of mixing remains unchanged. Additionally, aeration enhances power uptake and mixing time to some extent. Further, based on the experimental data in this study, two equations are proposed using ANOVA test to predict the mixing time and power uptake for a helical ribbon impeller in different operating conditions. The statistical analysis demonstrates the significant role of viscosity and impeller speed on the mixing performance. Suggesting a practical correlation between Reynolds and power numbers, this study provides unique and valuable results that can be applied to process industries.

Declaration of Competing Interest

The authors declare that there are no conflicts of interest.

Appendix A. Supplementary data

Supplementary material related to this article can be found, in the online version, at doi:<https://doi.org/10.1016/j.cep.2020.107811>.

References

- [1] L. Samandari-Masouleh, N. Mostoufi, A. Khodadadi, Y. Mortazavi, M. Maghrebi, Modeling the growth of carbon nanotubes in a floating catalyst reactor, *Ind. Eng. Chem. Res.* 51 (2012) 1143–1149, <https://doi.org/10.1021/ie2011137j>.
- [2] L. Samandari-Masouleh, N. Mostoufi, A.A. Khodadadi, Y. Mortazavi, M. Maghrebi, Kinetic modeling of carbon nanotube production and minimization of amorphous carbon overlayer deposition in floating catalyst method, *Int. J. Chem. React. Eng.* 10 (2012) 10–12, <https://doi.org/10.1515/1542-6580.2972>.
- [3] S. Miryahaie, K. Olinga, F.A. Abdul Muthalib, T. Das, M.S. Ab Aziz, M. Othman, J.C. Baudez, D. Batstone, N. Eshtiagh, Impact of rheological properties of substrate on anaerobic digestion and digestate dewaterability: new insights through rheological and physico-chemical interaction, *Water Res.* 150 (2019) 56–67, <https://doi.org/10.1016/j.watres.2018.11.049>.
- [4] M. Schrimpf, J. Esteban, T. Rösler, A.J. Vorholt, W. Leitner, Intensified reactors for gas-liquid-Liquid multiphase catalysis: from chemistry to engineering, *Chem. Eng. J.* 372 (2019) 917–939, <https://doi.org/10.1016/j.cej.2019.03.133>.
- [5] F. Almeida, F. Rocha, A. Ferreira, Analysis of liquid flow and mixing in an oscillatory flow reactor provided with 2D smooth periodic constrictions, *U. Porto J. Eng.* 4 (2018) 1–15, https://doi.org/10.24840/2183-6493_004.002.0001.
- [6] E.K. Nauha, Z. Kálal, J.M. Ali, V. Alopaeus, Compartmental modeling of large stirred tank bioreactors with high gas volume fractions, *Chem. Eng. J.* 334 (2018) 2319–2334, <https://doi.org/10.1016/j.cej.2017.11.182>.
- [7] T. Espinosa-Solares, E. Brito-De La Fuente, A. Tecante, L. Medina-Torres, P.A. Tanguy, Mixing time in rheologically evolving model fluids by hybrid dual mixing systems, *Chem. Eng. Res. Des.* 80 (2002) 817–823, <https://doi.org/10.1205/026387602321143345>.
- [8] L. Pakzad, F. Ein-mozaffari, S.R. Upreti, A. Lohi, Chemical engineering research and design agitation of Herschel – bulkley fluids with the Scaba – anchor coaxial mixers, *Chem. Eng. Res. Des.* 91 (2012) 761–777, <https://doi.org/10.1016/j.cherd.2012.09.008>.
- [9] L. Pakzad, F. Ein-Mozaffari, S.R. Upreti, A. Lohi, Characterisation of the mixing of non-newtonian fluids with a scaba 6SRGT impeller through ert and CFD, *Can. J. Chem. Eng.* 91 (2013) 90–100, <https://doi.org/10.1002/cjce.21616>.
- [10] L. Pakzad, F. Ein-Mozaffari, P. Chan, Measuring mixing time in the agitation of non-Newtonian fluids through electrical resistance tomography, *Chem. Eng. Technol.* 31 (2008) 1838–1845, <https://doi.org/10.1002/ceat.200800362>.
- [11] D.J. Lamberto, F.J. Muzzio, P.D. Swanson, A.L. Tonkovich, Using time-dependent RPM to enhance mixing in stirred vessels, *Chem. Eng. Sci.* 51 (1996) 733–741, [https://doi.org/10.1016/0009-2509\(95\)00203-0](https://doi.org/10.1016/0009-2509(95)00203-0).
- [12] T. Espinosa-Solares, E. Brito-De La Fuente, A. Tecante, P.A. Tanguy, Power consumption of a dual turbine-helical ribbon impeller mixer in ungassed conditions, *Chem. Eng. J.* 67 (1997) 215–219, [https://doi.org/10.1016/S1385-8947\(97\)00040-5](https://doi.org/10.1016/S1385-8947(97)00040-5).
- [13] M.S. Amirafabi, N. Mostoufi, M. Hosseinzadeh, M.R. Mehrnia, Reduction of membrane fouling by innovative method (injection of air jet), *J. Environ. Health Sci. Eng.* 12 (2014) 1–8, <https://doi.org/10.1186/s40201-014-0128-0>.
- [14] J. Jiang, J. Wu, S. Poncin, H.Z. Li, Effect of hydrodynamic shear on biogas production and granule characteristics in a continuous stirred tank reactor, *Process Biochem.* 51 (2016) 345–351, <https://doi.org/10.1016/j.procbio.2015.12.014>.
- [15] K. Takahashi, Mixing of pseudoplastic liquid in a vessel equipped with a variety of helical ribbon impellers, *J. Chem. Eng. Jpn.* 45 (1979) 63–68.
- [16] Y.Y. Tsui, Y.C. Hu, Flow characteristics in mixers agitated by helical ribbon blade impeller, *Eng. Appl. Comput. Fluid Mech.* 5 (2011) 416–429, <https://doi.org/10.1080/19942060.2011.11015383>.
- [17] Y. Bao, Y. Lu, Q. Liang, L. Li, Z. Gao, X. Huang, S. Qin, Power demand and mixing performance of coaxial mixers in a stirred tank with CMC solution, *Chinese J. Chem. Eng.* 23 (2015) 623–632, <https://doi.org/10.1016/j.cjche.2015.01.002>.
- [18] H. Ameer, M. Bouzit, Mixing in shear thinning fluids, *Braz. J. Chem. Eng.* 29 (2012) 349–358, <https://doi.org/10.1590/S0104-66322012000200015>.
- [19] A. Delafosse, M.L. Collignon, S. Calvo, F. Delvigne, M. Crine, P. Thonart, D. Teye, CFD-based compartment model for description of mixing in bioreactors, *Chem. Eng. Sci.* 106 (2014) 76–85, <https://doi.org/10.1016/j.ces.2013.11.033>.
- [20] P. Taylor, R.A. Ghotli, A.A.A. Raman, S. Ibrahim, LIQUID-LIQUID MIXING IN STIRRED VESSELS : A REVIEW Liquid-Liquid Mixing in Stirred Vessels : A Review, (n.d.) 37–41. doi:10.1080/00986445.2012.717313.
- [21] B.S. Foucault, G. Ascanio, P.A. Tanguy, Coaxial Mixer Hydrodynamics With Newtonian and Non-newtonian Fluids, (2004), <https://doi.org/10.1002/ceat.200401996>.
- [22] D.W.A.T.I. Hari-prajitno, P. Ved, T. Centre, B. Birmingham, Gas-Liquid Mixing Studies With Multiple up- and Down- Pumping Hydrofoil Impellers : Power Characteristics and Mixing Time, (1998), p. 76.
- [23] Y. Kato, H. Furukawa, Y. Ikeda, T. Nakanishi, T. Sano, K. Tomioka, Development of a mixing process using an HB-type impeller to easily achieve scale-up by maintaining geometrical similarity, *Int. J. Chem. Eng.* 2018 (2018).
- [24] Y. Bao, Y. Lu, Q. Liang, L. Li, Z. Gao, X. Huang, S. Qin, Power demand and mixing performance of coaxial mixers in a stirred tank with CMC solution Chinese Journal of Chemical Engineering Power demand and mixing performance of coaxial mixers in a stirred tank with CMC solution, *Chin. J. Chem. Eng.* (2018), <https://doi.org/10.1016/j.cjche.2015.01.002>.
- [25] S. Deans, Techniques for Mixing and Scaling in Mechanically Agitated Vessels, (n. d.).
- [26] T. Kouda, H. Yano, F. Yoshinaga, M. Kaminoyama, M. Kamiwano, Characterization of non-newtonian behavior during mixing of bacterial cellulose in a bioreactor, *J. Ferment. Bioeng.* 82 (1996) 382–386, [https://doi.org/10.1016/0922-338X\(96\)89155-0](https://doi.org/10.1016/0922-338X(96)89155-0).
- [27] D. Hari-prajitno, V.P. Mishra, K. Takenaka, W. Bujalski, A.W. Nienow, J. McKemmie, Gas-liquid mixing studies with multiple up- and down-pumping hydrofoil impellers: power characteristics and mixing time, *Can. J. Chem. Eng.* 76 (1998) 1056–1068, <https://doi.org/10.1002/cjce.5450760612>.
- [28] K. Takahashi, N. Sugawara, Y. Takahata, Mixing time in an agitated vessel equipped with large impeller, *J. Chem. Eng. Jpn.* 48 (2015) 513–517, <https://doi.org/10.1252/jcej.14we192>.
- [29] L. Lehrer, Mixing Time Prediction, *Gas.* 2, (1983), p. 2 <http://www.mech.eng.unimelb.edu.au/people/staffresearch/AFMSSite/8/Lehrer2.pdf>.
- [30] M. Bouaifi, M. Roustan, Power consumption, mixing time and homogenisation energy in dual-impeller agitated gas-liquid reactors, *Chem. Eng. Process.* 40 (2001) 87–95, [https://doi.org/10.1016/S0255-2701\(00\)00128-8](https://doi.org/10.1016/S0255-2701(00)00128-8).
- [31] B.V. Machon, M. Jahoda, Liquid homogenization in aerated multi-impellers stirred vessel, *Chem. Eng. Technol.* 23 (2012), https://doi.org/10.1201/b11330-2_1-1.
- [32] N. Hashemi, F. Ein-Mozaffari, S.R. Upreti, D.K. Hwang, Experimental investigation of the bubble behavior in an aerated coaxial mixing vessel through electrical resistance tomography (ERT), *Chem. Eng. J.* 289 (2016) 402–412, <https://doi.org/10.1016/j.cej.2015.12.077>.
- [33] S.C. Low, D. Allitt, N. Eshtiagh, R. Parthasarathy, Measuring active volume using electrical resistance tomography in a gas-sparged model anaerobic digester, *Chem. Eng. Res. Des.* 130 (2018) 42–51, <https://doi.org/10.1016/j.cherd.2017.11.039>.
- [34] A. Einsele, R.K. Flinn, Influence of gas flow rates and gas holdup on blending efficiency in stirred tanks - industrial & engineering chemistry process design and development (ACS publications), *Ind. Eng. Chem.* (1980) 600–603.
- [35] N. Blakebrough, K. Sambamurthy, Mass transfer and mixing rates in fermentation vessels, *Biotechnol. Bioeng.* 8 (1966) 25–42, <https://doi.org/10.1002/bit.260080104>.

- [36] B.V. Machon, M. Jahoda, Liquid homogenization in aerated multi-impeller stirred vessel, *Technol. Med. Sci.* 23 (2012), <https://doi.org/10.1201/b11330-2> 1–1.
- [37] N. Hashemi, F. Ein-Mozaffari, S.R. Upreti, D.K. Hwang, Analysis of mixing in an aerated reactor equipped with the coaxial mixer through electrical resistance tomography and response surface method, *Chem. Eng. Res. Des.* 109 (2016) 734–752, <https://doi.org/10.1016/j.cherd.2016.03.028>.
- [38] J.C. Baudez, Physical aging and thixotropy in sludge rheology, *Appl. Rheol.* 18 (2007) 1–8.
- [39] J.M. Smith, *Dispersion of gases in liquids: the hydrodynamics of gas dispersion in low viscosity liquids*, *Mix. Liq. by Mech. Agit.* (1985) 342.
- [40] A. Paglianti, S. Pintus, M. Giona, Time-series analysis approach for the identification of flooding/loading transition in gas-liquid stirred tank reactors, *Chem. Eng. Sci.* 55 (2000) 5793–5802, [https://doi.org/10.1016/S0009-2509\(00\)00125-1](https://doi.org/10.1016/S0009-2509(00)00125-1).
- [41] R.P. Chhabra, L. Bouvier, G. Delaplace, G. Couvelier, S. Domenek, C. André, Determination of mixing times with helical ribbon mixer for non-Newtonian viscous fluids using an advanced imaging method, *Chem. Eng. Technol.* 30 (2007) 1686–1691, <https://doi.org/10.1002/ceat.200700320>.
- [42] P. Ayazi Shamlou, M.F. Edwards, Power consumption of helical ribbon mixers in viscous newtonian and non-newtonian fluids, *Chem. Eng. Sci.* 40 (1985) 1773–1781, [https://doi.org/10.1016/0009-2509\(85\)80040-3](https://doi.org/10.1016/0009-2509(85)80040-3).
- [43] F. Rieger, V. Novak, H. Dagmar, Homogenization efficiency of helical ribbon agitators, *Chem. Eng. J.* 33 (1986) 143–150, [https://doi.org/10.1016/0300-9467\(86\)80013-2](https://doi.org/10.1016/0300-9467(86)80013-2).
- [44] H. Ameur, Y. Kamla, D. Sahel, Performance of helical ribbon and screw impellers for mixing viscous fluids in cylindrical reactors, *Chemeng. J.* 2 (2018) 1–9, <https://doi.org/10.3390/chemengineering2020026>.
- [45] J. Cheng, P.I. Carreau, Aerated mixing of viscoelastic fluids with helical ribbon impellers, *Chem. Eng. Sci.* 49 (1994) 1965–1972.
- [46] K. Takahashi, T. Yokota, H. Konno, Power consumption of helical ribbon agitators in highly viscous pseudoplastic liquids, *J. Chem. Eng. Jpn.* 17 (1984) 657–659, <https://doi.org/10.1252/jcej.17.657>.
- [47] V.V. Chavan, J. Ulbrecht, Power correlations for close-clearance helical impellers in non-newtonian liquids, *Ind. Eng. Chem. Process Des. Dev.* 12 (1973) 472–476, <https://doi.org/10.1021/i260048a015>.
- [48] E. Brito-De La Fuente, L. Choplin, P.A. Tanguy, Mixing with helical ribbon impellers: effect of highly shear thinning behaviour and impeller geometry, *Chem. Eng. Res. Des.* 75 (1997) 45–52, <https://doi.org/10.1205/026387697523381>.
- [49] M. Amirafabi, Khiadani Mehdi, Transparent polymers to emulate the rheological properties of primary, activated, and digested sludge authors, *Chem. Eng. Res. Des.* (2019), <https://doi.org/10.1016/j.mex.2019.03.017>.
- [50] G. Delaplace, L. Bouvier, A. Moreau, R. Guérin, J.C. Leuliet, Determination of mixing time by colourimetric diagnosis - Application to a new mixing system, *Exp. Fluids* 36 (2004) 437–443, <https://doi.org/10.1007/s00348-003-0741-7>.
- [51] F. Cabaret, S. Bonnot, L. Fradette, P.A. Tanguy, Mixing time analysis using colorimetric methods and image processing, *Ind. Eng. Chem. Res.* 46 (2007) 5032–5042, <https://doi.org/10.1021/ie0613265>.
- [52] A.B. Metzner, R.E. Otto, Agitation of non-Newtonian fluids, *AIChE J.* 3 (1957) 3–10, <https://doi.org/10.1002/aic.690030103>.
- [53] R. Baxter, N. Hastings, A. Law, E.J. Glass, *Food Stabilisers, Thickeners and Gelling Agent*, (2008).
- [54] S. Nagata, M. Nishikawa, T. Hisayuki, H. Hirabayashi, S. Gotoh, Power consumption of mixing impellers Bingham plastic liquids, *J. Chem. Eng. Jpn.* 3 (1970) 237–243, <https://doi.org/10.1252/jcej.3.237>.
- [55] M. Houska, Anchor-agitated systems : power input correlation for pseudoplastic and thixotropic fluids in equilibrium, *AIChE J.* 32 (1986) 155–158, <https://doi.org/10.1002/aic.690320119>.
- [56] J. Cheng, P.J. Carreau, Aerated mixing of viscoelastic fluids with helical ribbons impellers, *Chem. Eng. Sci.* 49 (1994) 1965–1972, [https://doi.org/10.1016/0009-2509\(94\)80080-4](https://doi.org/10.1016/0009-2509(94)80080-4).
- [57] M. Moo-Young, K. Tichar, F.A.L. Dullien, The blending efficiencies of some impellers in batch mixing, *AIChE J.* 18 (1972) 178–182, <https://doi.org/10.1002/aic.690180133>.
- [58] H. Ameur, Energy efficiency of different impellers in stirred tank reactors, *Energy* 93 (2015) 1980–1988, <https://doi.org/10.1016/j.energy.2015.10.084>.
- [59] J. Wu, Y. Zhu, L. Pullum, The effect of impeller pumping and fluid, *Can. J. Chem. Eng.* 79 (2001) 177–186, <https://doi.org/10.1002/cjce.5450790201>.
- [60] E.L. Paul, V. A. Atiemo-obeng, S.M. Kresta, *Handbook of Industrial Mixing*, (2004), <https://doi.org/10.1002/0471451452>.
- [61] J. Wu, H. ming Zhou, H. zhi Li, P. cheng Zhang, J. Jiang, Impacts of hydrodynamic shear force on nucleation of flocculent sludge in anaerobic reactor, *Water Res.* 43 (2009) 3029–3036, <https://doi.org/10.1016/j.watres.2009.04.026>.
- [62] M. hui Xie, J. ye Xia, Z. Zhou, G. zhong Zhou, J. Chu, Y. ping Zhuang, S. liang Zhang, H. Noorman, Power consumption, local and average volumetric mass transfer coefficient in multiple-impeller stirred bioreactors for xanthan gum solutions, *Chem. Eng. Sci.* 106 (2014) 144–156, <https://doi.org/10.1016/j.ces.2013.10.032>.
- [63] H. Bourne, J.R. Buttler, Power consumption of helical ribbon impellers in viscose liquids, *Process Saf. Environ. Prot.* 47 (1969).
- [64] V.C. Zitrom, One-factor-at-a-time versus designed experiments, *Am. Stat.* 53 (1999) 126–131, <https://doi.org/10.2307/2685731>.
- [65] L. Wiedemann, F. Conti, T. Janus, M. Sonnleitner, W. Zörner, M. Goldbrunner, Mixing in biogas digesters and development of an artificial substrate for laboratory-scale mixing optimization, *Chem. Eng. Technol.* 40 (2017) 238–247, <https://doi.org/10.1002/ceat.201600194>.
- [66] X.H. Yang, W.L. Zhu, Viscosity properties of sodium carboxymethylcellulose solutions, *Cellulose* 14 (2007) 409–417, <https://doi.org/10.1007/s10570-007-9137-9>.
- [67] D. Patel, F. Ein-Mozaffari, M. Mehrvar, Improving the dynamic performance of continuous-flow mixing of pseudoplastic fluids possessing yield stress using Maxblend impeller, *Chem. Eng. Res. Des.* 90 (2012) 514–523, <https://doi.org/10.1016/j.cherd.2011.08.022>.
- [68] M. Fújasová, V. Linek, T. Moucha, E. Prokopová, Energy demands of different impeller types in gas – liquid dispersions, *Sep. Purif. Technol.* 39 (2004) 123–131, <https://doi.org/10.1016/j.seppur.2003.12.015>.
- [69] D. Patel, F. Ein-Mozaffari, M. Mehrvar, Improving the dynamic performance of continuous-flow mixing of pseudoplastic fluids possessing yield stress using Maxblend impeller, *Chem. Eng. Res. Des.* 90 (2012) 514–523, <https://doi.org/10.1016/j.cherd.2011.08.022>.
- [70] A. Bombáč, M. Žumer, I. Žun, Power consumption in mixing and aerating of shear thinning fluid in a stirred vessel, *Chem. Biochem. Eng. Q.* 21 (2007) 131–138.
- [71] S.L.C. Ferreira, R.E. Bruns, H.S. Ferreira, G.D. Matos, J.M. David, G.C. Brandão, E.G.P. da Silva, L.A. Portugal, P.S. dos Reis, A.S. Souza, W.N.L. dos Santos, Box-Behnken design: an alternative for the optimization of analytical methods, *Anal. Chim. Acta* 597 (2007) 179–186, <https://doi.org/10.1016/j.aca.2007.07.011>.

Chapter 5: Performance of a dual helical ribbon impeller in a two-phase (gas-liquid) stirred tank reactor

$$Re = \frac{\rho N d^2}{\eta} \quad \text{Equation 5-9}$$

In most recent studies, the mixing time as an indicator of homogeneity has been measured in different approaches including local and general mixing time (Moo-Young, Tichar, and Dullien 1972). Within the realm of macromixing, bulk mixing time t (s) is the time taken for the complete mixing, where the solution is homogenous.

The Power number represents the rate of energy dissipation within the liquid and the power consumption by impeller in a specific rotational speed. Ungassed power number as the most important parameters in coaxial mixers have been studied widely (Houari Ameer 2015; Jie Wu, Zhu, and Pullum 2001).

$$N_p = \frac{P_0}{\rho N^3 d^5} \quad \text{Equation 5-10}$$

where ρ is density (kg/m^3).

P_0 as input power (W) is one of the main parameters evaluating the efficiency of ungassed impeller which can be calculated by using the following formula (Paul, Atiemo-obeng, and Kresta 2004; Jing Wu et al. 2009; Xie et al. 2014):

$$P_0 = 2. \pi. N. M_{Adjusted} \quad \text{Equation 5-11}$$

Furthermore, Bourne and Butler (Bourne, J.R.; Buttler 1969) have proven that there is a correlation between Reynolds number and Power number in single phase viscous fluid. Finally, torque should be obtained from the following formula:

$$M_{Adjusted} = M_{display} - M_{friction} \quad \text{Equation 5-12}$$

$M_{Adjusted}$ is the actual torque required to rotate the shaft (N.m). It can be calculated from subtracting the friction torque ($M_{friction}$) from what is monitored on the power meter ($M_{display}$)

(N.m). If the impeller rotates in the open air, the magnitude of torque will be considered as friction torque.

5.3.6 Response Surface Method

Response surface method (RSM) approach was used to predict the mixing time and power consumption under different operating conditions. The main objective of the RMS is to identify the correlation between variables including impeller speed, gas flow rate, impeller clearance, and viscosity as well as responses including mixing time and power consumption. For this purpose, the Box-Behnken method is used to design the experiments. Next, the response surface methodology (RSM) is applied to optimize the factor levels and find the most influential parameters. For each experiment, three replicates are considered to ensure the reproducibility of the experiments. The correlation is defined as:

$$Y = \beta_0 + \sum_{i=1}^3 \beta_i X_i + \sum_{i=1}^3 \beta_{ii} X_i^2 + \sum_{i=1}^3 \sum_{j=2}^3 \beta_{ij} X_i X_j + error \quad \text{Equation 5-13}$$

In this equation, X shows variables, Y indicates the response such as mixing time, while β_0 , β_i , β_{ii} , and β_{ij} are regression coefficients and interaction terms. Different 3D surface graphs are plotted to find the most influential factor when the other factors are set at optimized level (Zitrom 1999).

The list of variables and their maximum and minimum levels are summarized in Table 5-3.

These maximum and minimum levels are selected based on the preliminary study.

Further, uncertainty analysis has been done for measured and calculated data, as well as instrument accuracy. The result of uncertainty analysis is summarized in Table 5-3.

Table 5-3 Variables used in RSM method to optimize the mixer performance and uncertainty analysis for different variables.

Symbols	Variables	Low level	Central level	High level	Instrument	Systematic Uncertainty (± %)	Random Uncertainty (± %)	Total Uncertainty (± %)
---------	-----------	-----------	---------------	------------	------------	------------------------------	--------------------------	-------------------------

X₁	Impeller speed (1/s)	50	75	100	Torquemeter	-	1	1.00
X₂	Gas flow rate (Lpm)	0.5	1.35	2.2	Flow meter	1.5	0.66	1.64
X₃	Impeller clearance (m)	0.02	0.04	0.06	Ruler	0.5	0.83	0.97
X₄	Concentration (wt %)	0.1	0.8	1.5	Scale	0.1	0.32	0.34

5.4 Results and discussion

In this study, the impeller speed, gas flow rate, impeller clearance from the bottom, and viscosity are considered as principal factors influencing the mixing process of a shear thinning fluid. It is worth noting that the maximum impeller speed in the current investigation was limited to 100 rpm. This limitation was considered because of the extreme shear sensitivity of some materials and microorganisms (Lamberto et al. 1996; Wiedemann et al. 2017).

As mentioned earlier, the experiments were carried out in the optimal range where the hydrodynamics of a gas-liquid system is completely dispersed. The influence of gas flow rates of 0.5-2.2 Lpm is examined when the system is agitated by a dual helical ribbon impeller between 50 to 100 rpm under transient flow regime. Generally, the effects of bubble motion, impeller speed, gas flow rate, and viscosity on power consumption and mixing time are discussed and interpreted in this section.

5.4.1 Mixing pattern

The two-dimensional cross-section of the mixing pattern in the vessel when the reaction between acid and base occurs is shown in Figure 5-2.

The visual evidence presented in this section shows that initially, the radial movement of fluid bulk is stronger than the axial movement for a dual helical ribbon. The impeller drives fluid towards the walls of the vessel where the shear rate is at the maximum, where little movement of fluid can be observed in the axial direction near the central shaft. Then, fluid moves downward alongside the cylinder wall. Following this, the axial movements become stronger and the top surface becomes clear. Decolouration of the purple fluid shows that the maximum

Chapter 5: Performance of a dual helical ribbon impeller in a two-phase (gas-liquid) stirred tank reactor

mixing in this type of impeller happens close to the clearance between the wall and impeller where the high shear imposes on the fluid film as well as areas near to the inner edge of the blade. Whilst there is still an unmixed zone located at the bottom of the tank, the efficiency of the impeller in the region near the wall is significant. Therefore, the mixing time is controlled by the mixing pattern of the low-shear central regions located far from the blade edges. A possible explanation for these results may be the reduction in viscosity when the high shear rate region rotates near the inner and outer edges of the blade. The enclosed volume of fluid between impeller and wall as well as the bulk of fluids around the inner edge of the blade can be considered as a low viscosity film which can be easily influenced by this type of impeller. Generally, these regions are introduced as a stagnant zone in other types of impellers.

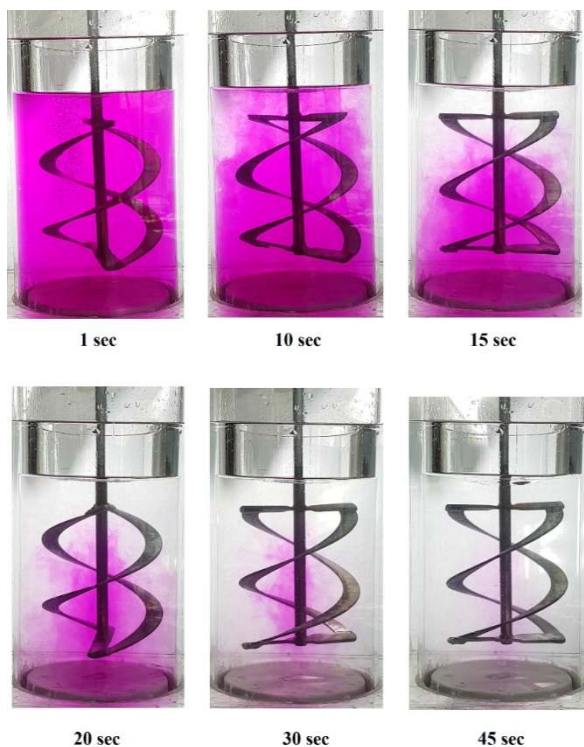


Figure 5-2 The evolution of mixed area inside the reactor when the impeller speed is 75 rpm and concentration of NaCMC solution is 1%.

Although extensive research has been carried out on the effects of dual helical ribbon impellers on single phase flow pattern, few studies have paid attention to the influence of chaotic bubble motion on multi phases mixing process (Cheng and Carreau 1994). Figure 5-3 indicates the

Chapter 5: Performance of a dual helical ribbon impeller in a two-phase (gas-liquid) stirred tank reactor

qualitative mixing pattern over time when air bubbles are introduced. Rising a bubble from bottom of the tank imposes shear rate to the bulk of the fluid. As a result, the viscosity of the shear-thinning fluid is reduced to some extent depending on the gas flow rate, general gas hold-up, and rheology of the fluid. The more reduction in viscosity, the more desirable results are achieved including less energy consumption and shorter mixing time. Since bubbles are dispersed everywhere, the mixed area near the central shaft can gradually develop, which enhances the mixing performance of the dual helical ribbon impeller.

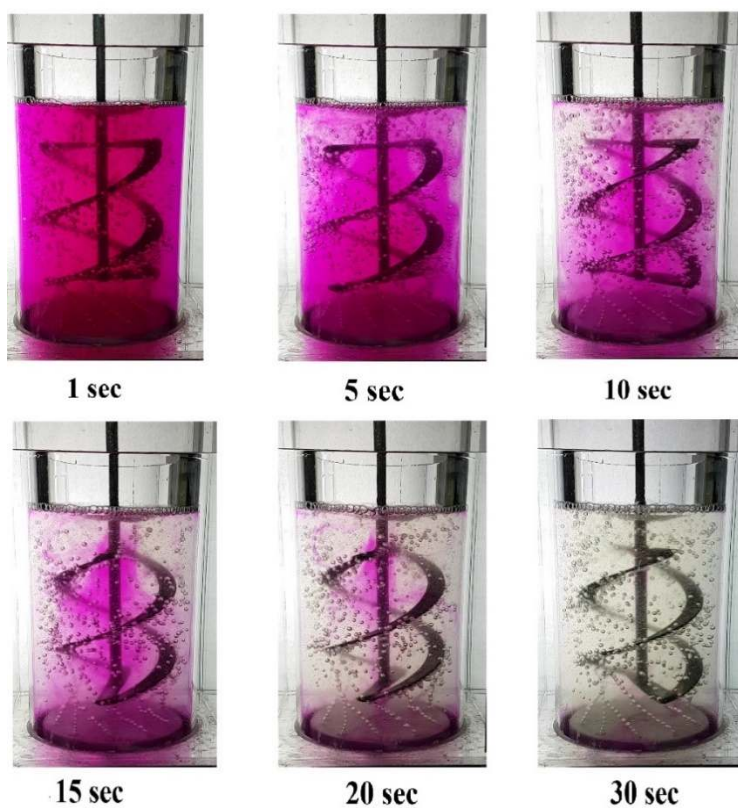


Figure 5-3 The evolution of mixed area inside the aerated reactor when the impeller speed is 75 rpm and concentration of NaCMC solution is 1%.

Figure 5-3 indicates that in a low rotational speed helical ribbon impeller, the formed bubbles rise without significant breakage or coalescence. They are trapped behind the impeller blade and form a film of gas which follows the impeller patterns to reach the free surface. The interesting point here is the enhancement of the uniformity of homogenization and dispersion of liquid inside the system. In the presence of bubbles, after the injection of acid, clear liquid

not only moves toward the clearance of the vessel and impeller but also gradually penetrates downward. Although this requires more investigation, this phenomenon could be interpreted by increasing the internal liquid shear stress as a result of bubbles motions. In completely disperse mixing patterns, bubbles disperse completely in the whole system, even in stagnant regions. The presence of bubbles in the stagnant zones increases the shear stress resulting in the breakdown of the NaCMC internal network (M. Amiraftebi and Khiadani Mehdi 2019a). Weakening the network structure of shear-thinning fluids increases both molecular and bulk diffusions resulting in enhancement of the mixing process.

5.4.2 Impact of impeller speed

The impact of various rotational speeds on the performance of the mixing system has been studied widely in the literature. Results show that an increase in rotational speed reduces the time of mixing and improves the homogeneity of heat, mass, and nutrient (X. H. Yang and Zhu 2007; Patel, Ein-Mozaffari, and Mehrvar 2012a; Pakzad, Ein-Mozaffari, and Chan 2008; Hashemi et al. 2016a; Espinosa-Solares et al. 2002).

Figure 5-4a and 5-4b depict both mixing time and power consumption over various rotational speeds for different concentration of NaCMC solutions. The results indicate that a higher rotational speed leads to shortened mixing time, while power uptake increases exponentially. The results indicate that an increase in rotational speed up to 75 rpm could reduce the mixing time of viscous fluid to some extent.

Figure 5-4 a shows the expected time to reach homogeneity in different impeller rotational speeds. For the same rotational speed, the more concentrated solution the more time required to reach homogenous conditions, where the natural gel structure of polymer requires more energy and time to destroy. Therefore, the diluted solution requires less time in a lower rotational speed to reach a certain level of homogeneity. Further, it can be noted that the

Chapter 5: Performance of a dual helical ribbon impeller in a two-phase (gas-liquid) stirred tank reactor

homogeneity graphs are exponential which become level off at the end. Thus, it seems that the system has become homogenous in somewhere between rotational speed of 0-50 rpm when the concentration of NaCMC solution is 0.1%.

However, increasing the rotational speed beyond 75 rpm not only has insignificant contribution in reducing the mixing time but also exponentially increases power consumption. This finding suggests that increasing the impeller speed up to optimum value could enhance the performance of the mixing system. Whilst, after this certain level, the power consumption increases sharply with a limited positive contribution to mixing performance. This threshold level has been reported previously by literature for different types of digesters (McLeod, Othman, and Parthasarathy 2019).

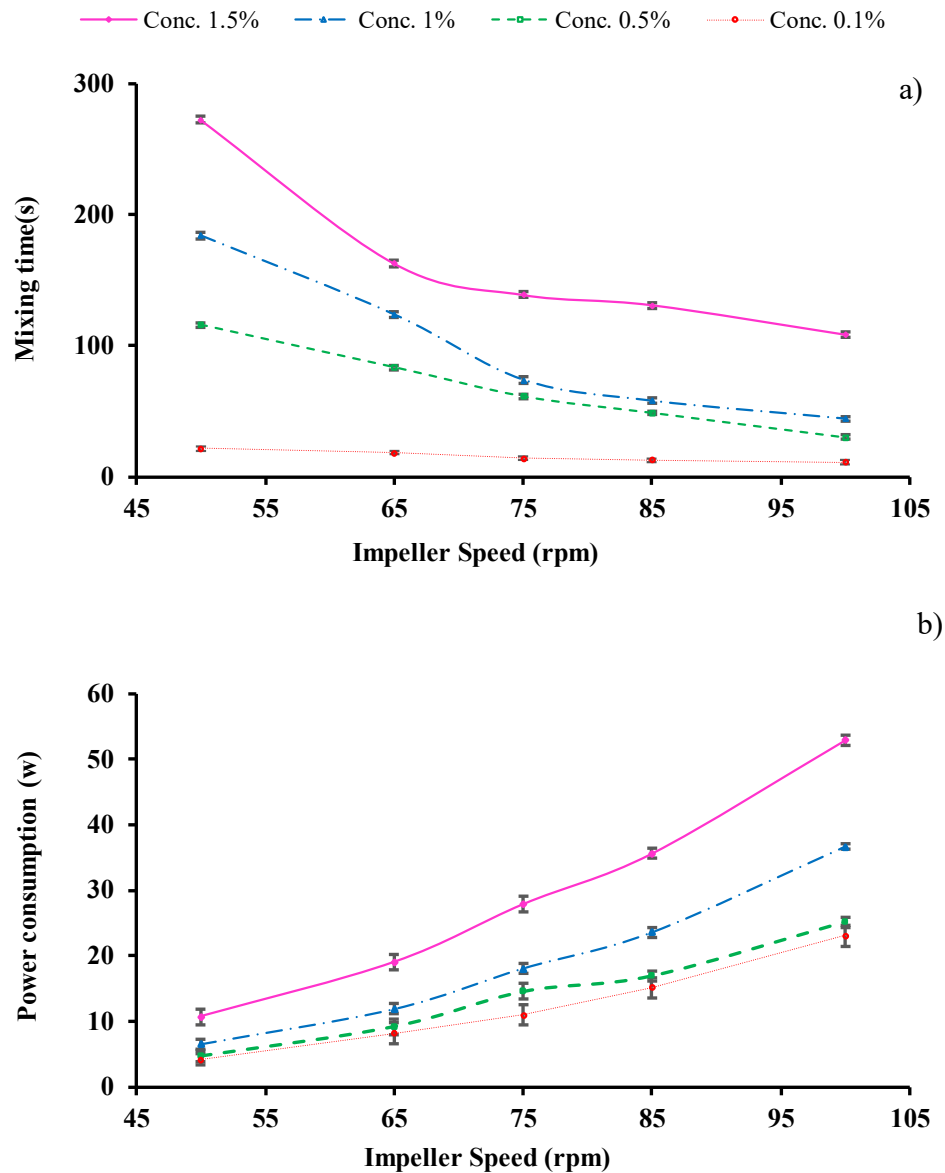


Figure 5-4 a) Mean mixing time and b) mean power consumption with error bars over impeller speed in different concentration of NaCMC solutions.

Two different dimensionless terms have been defined to investigate the extra power consumed by the impeller compared to mixing time reduction. The first term is the extra power consumed when the impeller speed increases from 75 to 85 and 100 rpm and the second term is the decrease of the mixing time when the impeller speed increases to 85 and 100 rpm.

Figure 5-5 represents these two dimensionless terms for different concentrations of NaCMC. According to this figure, a remarkable increase is observed in the percentage of power uptake

compared to the reduction in the percentage of mixing time when the solution is more concentrated. For example, when impeller speed changes from 85 to 100 rpm in a concentration of 1.5% solution, the power consumption has been increased by 60%, while the mixing time decreased by 10%. This finding is vital in terms of cost efficiency and scaling up the system.

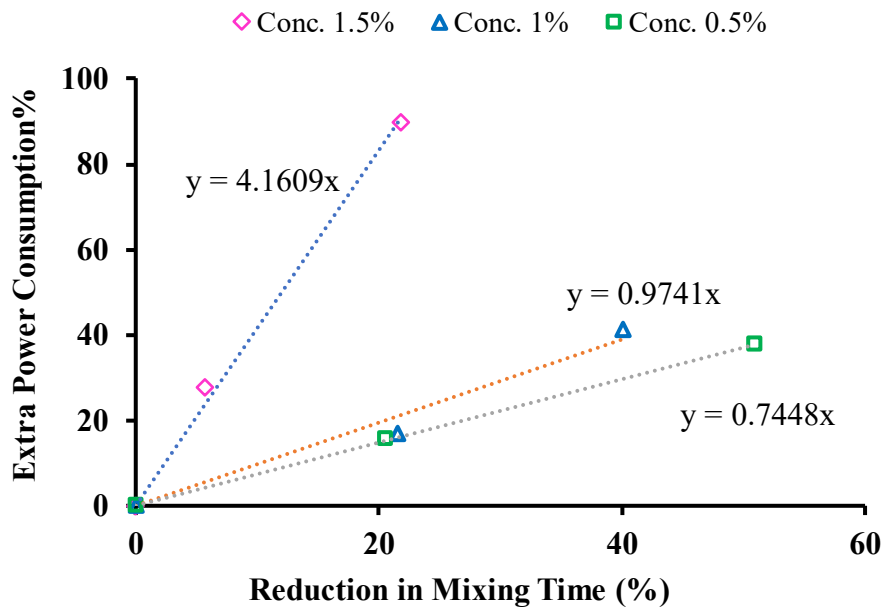


Figure 5-5 Comparison between the percentage of power consumption and percentage of enhancing mixing time.

5.4.3 Influence of bubble motion

The mixing time versus gas flow rate for gassed cases in both stirred and non-stirred conditions is shown in Figure 5-6. Hollow markers show the mixing time in different gas flow rates for various concentrations of NaCMC solutions when the impeller speed is 75 rpm. Filled markers demonstrate the mixing time under the same operating conditions when the impeller is off (impeller speed=0 rpm). The results in this figure reveal that the gas flow rate is an influential factor in mixing time when the mechanical agitator is not working. Increasing the gas flow rate from 0.5 to 2.2 LPM could reduce the mixing time to half in non-stirred systems. However,

Chapter 5: Performance of a dual helical ribbon impeller in a two-phase (gas-liquid) stirred tank reactor

hollow markers show that the mechanical agitator is more influential on mixing time compared to the gas flow rate.

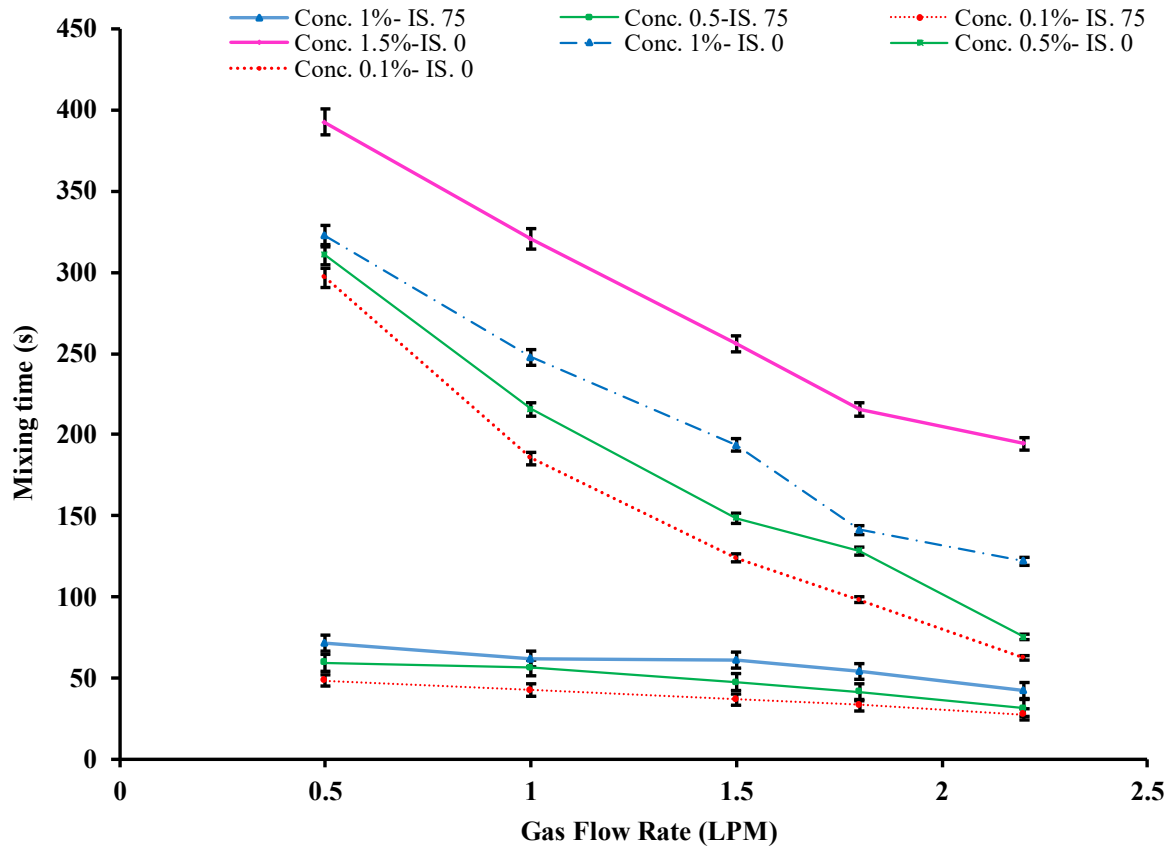


Figure 5-6 Comparison between the mean gassed mixing time with error bars in both stirred and non-stirred conditions

Some previous studies suggest that for a system with a Rushton turbine and PBD- anchor, the gas flow rate increases the mixing time (B. V Machon and Jahoda 2012; Hashemi et al. 2016a). It has been argued that in high gas flow rate, the buoyancy force overcomes the hydrodynamics of system and the gas-liquid system flooded (Hashemi et al. 2016a). Other researchers, however, have reported an improvement in the mixing performance by the presence of bubbles inside the system (Low et al. 2018; Einsele and Flinn 1980; Blakebrough and Sambamurthy 1966). Further, Xu. Et, al. (2018) indicated that injection of gas could improve the mixing performance (Xu et al. 2018). This inconsistency may be due to the complex hydrodynamics

of gas-liquid agitated flow patterns. The variety of hydrodynamics in gas-liquid STRs can be almost considered as a function of impeller type, rheology of fluid, gas flow rate, impeller speed, and bubble size (Smith 1985).

5.4.4 Power consumption

Power uptake is another influential design parameter representing the economic performance of a mixing system. The power consumption of the impeller should be taken into account when the cost efficiency of a mixing process is important. Power consumption displays the performance of the agitating process depending on the geometry of impeller and physical properties of the fluid (Fujasová et al. 2004). The power consumption measurement has been carried out on NaCMC solution with different concentrations of 0.1, 0.5, 1, and 1.5 wt% for five different impeller speeds of 50, 65, 75, 85, and 100 rpm.

Figure 5-7 a indicates the power uptake by impeller versus Reynolds number for the rotational speed of 50, 65, 75, 85, and 100 rpm for different concentration of NaCMC solutions. The greater the viscoelasticity of the fluid, the greater the energy required to achieve complete mixing. It can be observed that an increase in viscosity shifts the power curve to the lower Reynolds numbers and higher energy consumption.

Figure 5-7 b displays the dimensionless energy consumption (N_p) as a function of Reynolds number (Re) or power curve for a dual helical ribbon in five different rotational speeds of 50, 65, 75, 85 and 100 rpm and constant gas flow rate of 1 LPM.

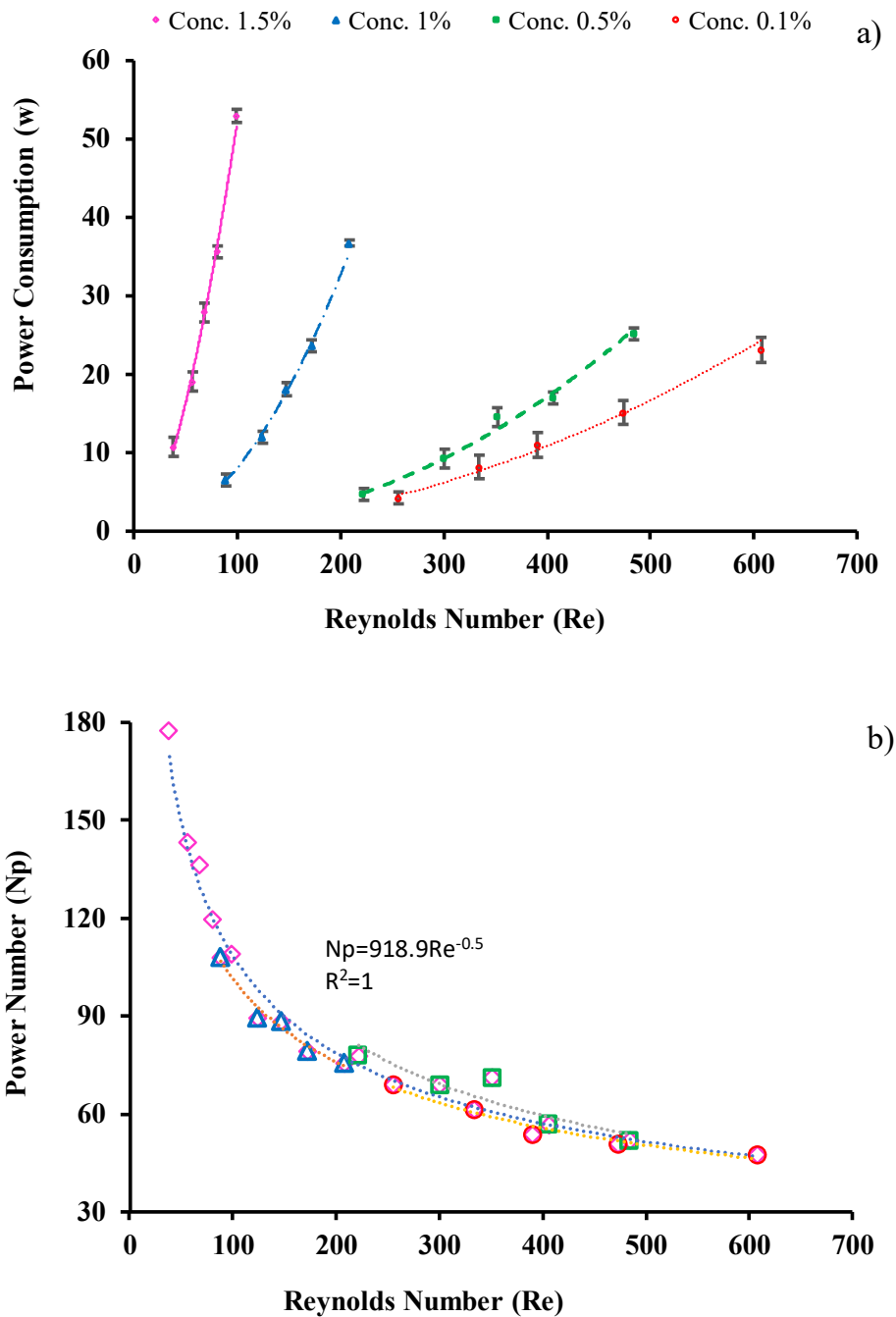


Figure 5-7 a) Mean power curve and b) Power number (N_p) vs. Reynolds number (Re) for a dual helical ribbon in five different rotational speeds for various concentrations of NaCMC.

The power curve is unique for each impeller type. The single most striking observation to emerge from the plotted data is the relationship between N_p and Re , which for the first time this result has been presented. Regression analysis was used to predict the correlation between these two parameters which is importantly repeated for all concentrations of NaCMC, whereas

Chapter 5: Performance of a dual helical ribbon impeller in a two-phase (gas-liquid) stirred tank reactor

the flow regime is transient. This practical correlation has been reported in Equation 5-14. It is noticed that this practical correlation is unique and demonstrating how a dual helical ribbon impeller performs in a transient two phases flow regime.

$$N_p \cdot Re^\beta = \alpha \quad \text{or} \quad N_p = 918.9 Re^{-0.5} \quad \text{Equation 5-14}$$

where, $\beta=0.5$ and $\alpha=918.9$ are constant for a dual helical ribbon impeller in different concentration of NaCMC solutions from 0.1 wt% to 1.5 wt%.

What is surprising here is that the trend of the power curve is not influenced by changes in concentration. Patel et al. (Patel, Ein-Mozaffari, and Mehrvar 2012b) have indicated that $Re \cdot N_p$ is a constant value for the Scaba and the A320 impellers in single-phase flow. They also mentioned that the power number changes slightly based on Reynolds number in transient flow for the Scaba and the A320 impeller in single-phase flow. However, this correlation has not previously been found for a dual helical ribbon impeller in gas-liquid interactions.

Additionally, Figure 5-8 shows the power consumption as a function of mixing time at a constant impeller speed of 75 rpm. These results show the effect of bubble motion on mixing time and power consumption. Interestingly, a decrease in power consumption was observed when gas was injected into the system. This 5-7% reduction in power consumption could be due to the presence of bubbles inside the reactor. The reduction in power uptake by sparging bubbles in a mixing system has also been observed by other researchers (Bouaifi and Roustan 2001; Bombač, Žumer, and Žun 2007). This finding can be interpreted through the formation of gas pockets (cavities) underneath the impeller streamlining the blade movement and reducing fluid drag resulting in lower power consumption. Further, reducing the viscosity of shear thinning fluid as a result of axial and rotational bubble movements can be considered as another influential factor.

In addition, Figure 5-8 depicts that both power consumption and mixing time are highly affected by the viscosity of the fluid. The higher the viscosity of the fluid, the more power

Chapter 5: Performance of a dual helical ribbon impeller in a two-phase (gas-liquid) stirred tank reactor

required to achieve complete mixing. Therefore, when the viscosity of the shear-thinning fluid increases, more power and time are required to achieve desirable mixing.

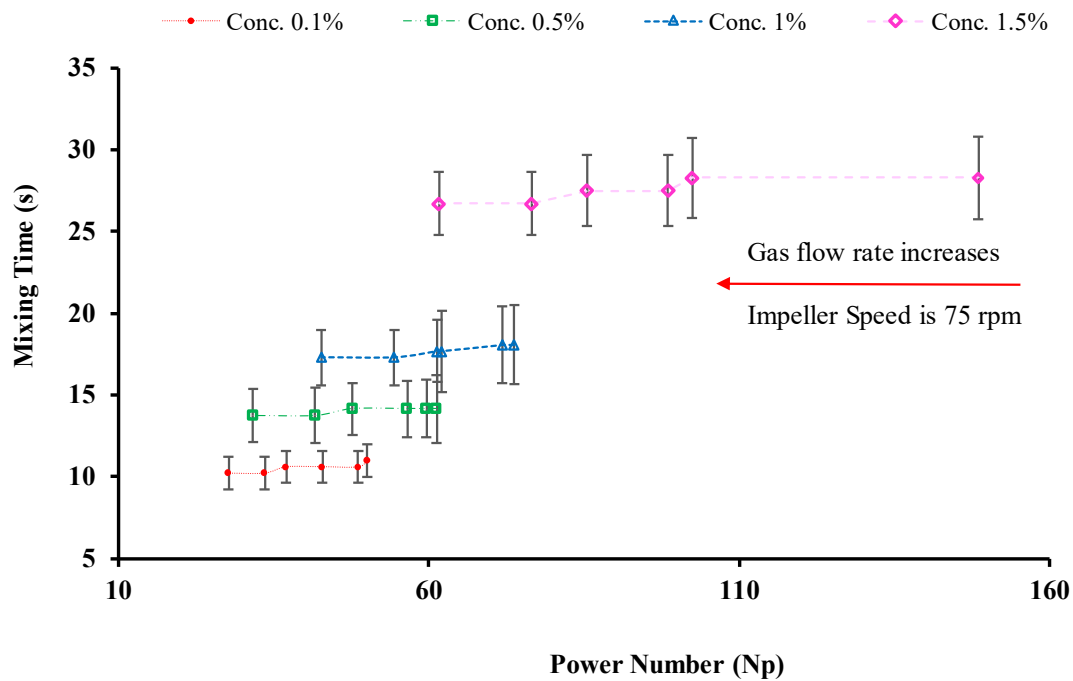


Figure 5-8 Influence of gas injection on mean mixing time with error bars over power number (N_p)

These results differ from most published studies that reported bubble motion causes an increase in power consumption of an aerated stirred system (Bouaifi and Roustan 2001; Bombač, Žumer, and Žun 2007). However, the present results are in agreement with Cheng and Carreau's (Cheng and Carreau 1994) findings which show the presence of bubbles leads to a reduction of power consumption by the impeller.

Figure 5-9 a and 5-9 b clearly describes the role of gas flow rate on power consumption where the impeller rotational speed is constant at 75 rpm.

Chapter 5: Performance of a dual helical ribbon impeller in a two-phase (gas-liquid) stirred tank reactor

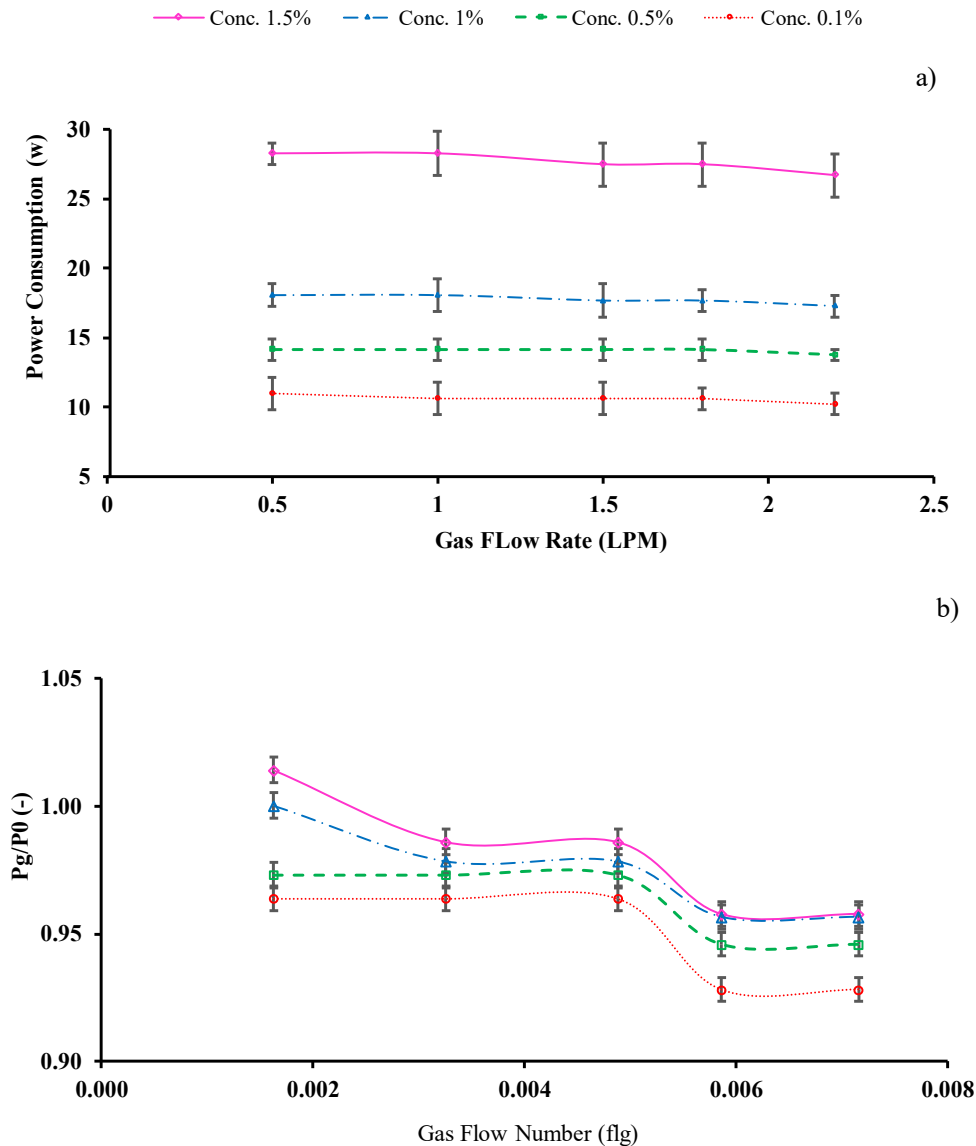


Figure 5-9 The role of bubble motion around the impeller on mean power consumption

According to Fig. 5-9 a, an increase in gas flow rate from 1 to 2.2 LPM reduces the mixing power to some extent. Further, Fig. 5-9 b, represents the ratio of power uptake by impeller when the gas sparged (P_g), watt, to the power consumption of single-phase system (P_0), watt, over the gas flow number (flg) which shows the flow developing in the impeller zone independent to impeller geometry.

This figure shows that power consumption experiences a significant fall after a certain value of gas flow rate. Dispersed bubbles can reduce the viscosity of the fluid around the blade to

some extent and reduce the power uptake. By increasing the impeller speed, the bubbles disperse everywhere in the fluid bulk and some of them still follow the impeller path. As a result, the impeller has the maximum level of contact with the air bubbles trapped behind the blade which slightly decrease the power consumption of the aerated system compared to single-phase one.

5.4.5 Statistical analysis

This proposed study investigates the impacts of four listed factors shown in Table 5-3 through the three-level Box-Behnken method (Ferreira et al. 2007). Then, the response surface methodology (RSM) is applied to optimize and to find the most influential factors and their interactions. Table 5-4 summarizes the plan, the number of experiments and variables applied in RSM.

The result of statistical analysis suggests strong correlations between responses and all independent and dependent variables lead to Equation 5-15 and Eq. 5-16.

$$\begin{aligned} \text{Mixing time} = & -1.26 + 0.88 N + 5.5 Gf - 11.31 C + 13.56 IC - 0.014 N \times Gf + \\ & 0.44 N \times conc. - 0.1 N \times IC - 8.3 Gf \times conc. + 0.14 Gf \times IC - 1.5 Conc. \times IC + \\ & 0.0067 N^2 - 6.3 Gf^2 + 19.4 C^2 - 0.32 IC^2 \text{ (Adjusted } R^2=0.9628) \end{aligned} \quad \text{Equation 5-15}$$

$$\begin{aligned} \text{Power Consumption} = & 28.53 - 0.67 N - 0.75 Gf - 1.25 IC - 24.58 C + 0.004 N \times \\ & Gf + 0.35 N \times C + 0.007 N \times IC - 0.49 Gf \times C + 3.9E^{-16} Gf \times IC - 1.07^{-15} C \times IC + \\ & 0.0058 IS^2 + 0.2 Gf^2 + 7.23 C^2 + 0.09 IC^2 \quad \text{(Adjusted } R^2=0.9867) \end{aligned} \quad \text{Equation 5-15}$$

Table 5-4 Plan for ANOVA analysis

Order	Impeller speed (N)	Gas flow rate (Gf)	Impeller Clearance (IC)	Concentration (C)	Mixing Time	Power consumption
	rpm	LPM	m	wt%	s	W
1	100	0.5	0.04	0.8	57	30.8
2	75	0.5	0.04	1.5	102.4	27.88

Chapter 5: Performance of a dual helical ribbon impeller in a two-phase (gas-liquid) stirred tank reactor

3	75	1.35	0.02	0.1	34	10.6
4	75	0.5	0.04	0.1	48.7	10.6
5	75	1.35	0.06	0.1	45.5	10.6
6	75	1.35	0.06	1.5	91.1	27.1
7	75	0.5	0.02	0.8	65.5	16.3
8	75	2.2	0.04	0.1	27.8	10.2
9	75	1.35	0.02	1.5	88	27.1
10	50	1.35	0.06	0.8	63.25	6.5
11	75	2.2	0.02	0.8	31.5	15.3
12	50	1.35	0.02	0.8	42.8	6.5
13	100	1.35	0.04	1.5	95.8	52.8
14	75	2.2	0.06	0.8	42.8	15.3
15	75	0.5	0.06	0.8	75.8	16.3
16	100	1.35	0.06	0.8	46.5	32.46
17	75	1.35	0.04	0.8	57.1	15.1
18	50	2.2	0.04	0.8	39	6.54
19	50	1.35	0.04	0.1	49.8	4.45
20	75	2.2	0.04	1.5	61.7	26.31
21	100	1.35	0.04	0.1	23.9	20.94
22	100	2.2	0.04	0.8	26	31.4
23	50	0.5	0.04	0.8	68.8	6.28
24	100	1.35	0.02	0.8	46.5	30.9
25	50	1.35	0.04	1.5	90.7	11.8

where N is the impeller speed, Gf is the gas flow rate, C is the concentration of the solution, and IC is the impeller clearance.

Further, the result of ANOVA test has been summarized in Table 5-5 for the response surface quadratic model. This table demonstrates P-values and F-values for all variables. In this case, A, B, C, D, AC, AD, BC, A², and C² are significant model parameters.

Table 5-5 Results of ANOVA test for Quadratic model

Response	Mixing time		Power consumption	
	F-value	P-value	F-value	P-value
Model	45.37	< 0.0001*	128.1	< 0.0001*
A-Impeller Speed	14.52	0.0034*	1138.3	< 0.0001*
B-Gas Flow rate	151.38	< 0.0001*	0.4454	0.5197 ^{ns}
C-Concentration	379.81	< 0.0001*	513.47	< 0.0001*
D-Impeller Clearance	13.54	0.0042*	0.1121	0.7447 ^{ns}
AB	0.0182	0.8953 ^{ns}	0.016	0.9019 ^{ns}
AC	12.17	0.0058*	82.98	< 0.0001*
AD	5.29	0.0442*	0.3362	0.5749 ^{ns}

Chapter 5: Performance of a dual helical ribbon impeller in a two-phase (gas-liquid) stirred tank reactor

BC	4.96	0.051 ^{ns}	0.1891	0.6729 ^{ns}
BD	0.0127	0.9126 ^{ns}	0	1 ^{ns}
CD	0.8933	0.3669 ^{ns}	0	1 ^{ns}
A²	2.48	0.1466 ^{ns}	20.95	0.001 [*]
B²	2.95	0.1165 ^{ns}	0.0326	0.8603 ^{ns}
C²	12.92	0.0049 [*]	19.56	0.0013 [*]
D²	0.2279	0.6433 ^{ns}	0.206	0.6596 ^{ns}

*: Not significant at P<0.05, ns: Significant at P>0.05

P-value and F-value: Indicator of significance decision

The Model F-values of 45.37 for mixing time and 128.1 for power consumption confirm that the proposed Equation 5-15 and Equation 5-16 are reliable and remarkably accurate to predict the mixing time and power consumption in different operating conditions. These equations have significant practical value for industrial designing, operating, and cost studying of STRs. To sum up, the statistical analysis indicates that impeller speed, gas flow rate, impeller clearance, and viscosity influence the mixing time and power consumption, respectively.

Chapter 5: Performance of a dual helical ribbon impeller in a two-phase (gas-liquid) stirred tank reactor

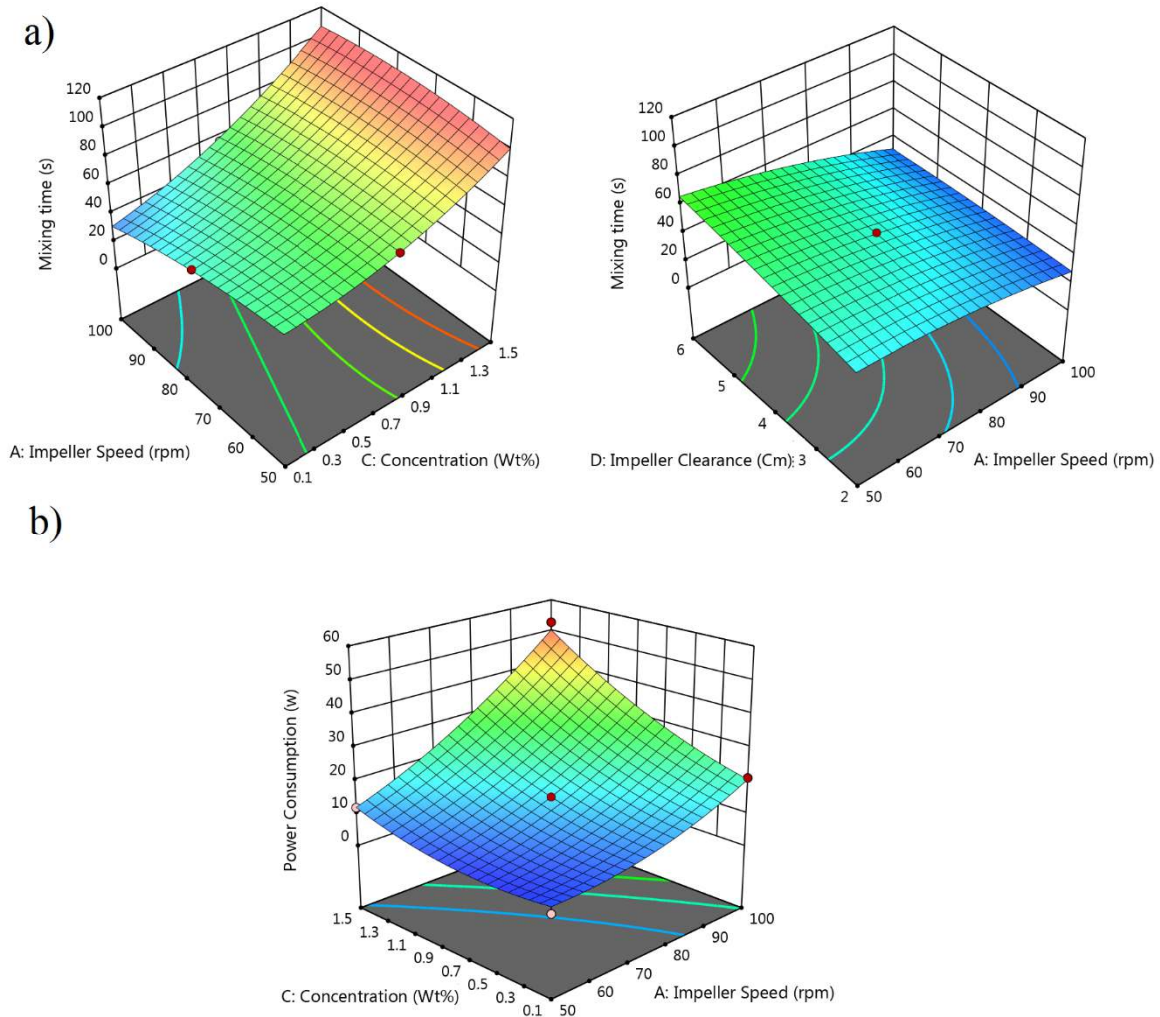


Figure 5-10 Influential interaction model parameters analysed by ANOVA test.

Further, analysis of interactions between variables and the model coefficients are displayed in three-dimensional response surfaces and are shown in Figure 5-10 a, b. This figure displays the significant interaction model parameters based on P-value <0.05 . Fig. 5-10 a shows the most influential interactions on mixing time including impeller speed-concentration, and impeller clearance-impeller speed. Additionally, according to P-value, the most influential model parameter on power consumption is interaction of concentration-impeller speed as shown in Fig. 5-10 b.

5.5 Conclusions

Collectively, this study outlines the role of a helical ribbon impeller on mixing performance and cost of operation of a gassed STR. The range of gas flow rate and impeller speed has been adjusted in the preliminary study. In addition, this work provides a conceptual understanding of the flow pattern inside a gassed reactor equipped with a dual helical ribbon impeller and filled with a shear thinning fluid. The findings of this study suggest that increasing the rotational speed more than 75 rpm not only fails to reduce mixing time but also increases the power consumption. It can be concluded that the optimum rotational speed should be selected with caution because boosting impeller speed may impose the extra operating cost while the efficiency of mixing remains unchanged. Additionally, aeration enhances power uptake and mixing time to some extent. Further, based on the experimental data in this study, two equations are proposed using ANOVA test to predict the mixing time and power uptake for a helical ribbon impeller in different operating conditions. The statistical analysis demonstrates the significant role of viscosity and impeller speed on the mixing performance. Suggesting a practical correlation between Reynolds and power numbers, this study provides unique and valuable results that can be applied to process industries.

5.6 References

- Almeida, F., F. Rocha, and A. Ferreira. 2018. "Analysis of Liquid Flow and Mixing in an Oscillatory Flow Reactor Provided with 2D Smooth Periodic Constrictions." *U.Porto Journal of Engineering* 4 (2): 1–15. https://doi.org/10.24840/2183-6493_004.002_0001.
- Ameur, H., and M. Bouzit. 2012. "Mixing in Shear Thinning Fluids." *Brazilian Journal of Chemical Engineering* 29 (2): 349–58. <https://doi.org/10.1590/S0104-66322012000200015>.
- Ameur, Houari. 2015. "Energy Efficiency of Different Impellers in Stirred Tank Reactors." *Energy* 93: 1980–88. <https://doi.org/10.1016/j.energy.2015.10.084>.
- Ameur, Houari, Youcef Kamla, and Djamel Sahel. 2017. "Performance of Helical Screw Impellers for Mixing of Viscous Liquids in Cylindrical Reactors." *ChemistrySelect* 2 (5): 1891–94. <https://doi.org/10.1002/slct.201602072>.

Chapter 5: Performance of a dual helical ribbon impeller in a two-phase (gas-liquid) stirred tank reactor

Amiraftebi, Maryam, and Khiadani Mehdi. 2019. "Transparent Polymers to Emulate the Rheological Properties of Primary, Activated, and Digested Sludge Authors." *Chemical Engineering Research and Design*. <https://doi.org/10.1016/j.mex.2019.03.017>.

Amiraftebi, Maryam Sadat, Navid Mostoufi, Mostafa Hosseinzadeh, and Mohammad Reza Mehrnia. 2014. "Reduction of Membrane Fouling by Innovative Method (Injection of Air Jet)." *Journal of Environmental Health Science and Engineering* 12 (1): 1–8. <https://doi.org/10.1186/s40201-014-0128-0>.

Ayazi Shamlou, P., and M. F. Edwards. 1985. "Power Consumption of Helical Ribbon Mixers in Viscous Newtonian and Non-Newtonian Fluids." *Chemical Engineering Science* 40 (9): 1773–81. [https://doi.org/10.1016/0009-2509\(85\)80040-3](https://doi.org/10.1016/0009-2509(85)80040-3).

Bao, Yuyun, Yu Lu, Qianqin Liang, Li Li, Zhengming Gao, Xiongbing Huang, and Song Qin. 2015. "Power Demand and Mixing Performance of Coaxial Mixers in a Stirred Tank with CMC Solution." *Chinese Journal of Chemical Engineering* 23 (4): 623–32. <https://doi.org/10.1016/j.cjche.2015.01.002>.

Baudez, J.C. 2007. "Physical Aging and Thixotropy in Sludge Rheology." *Applied Rheology* 18 (1): 1–8.

Baxter, R., N. Hastings, A. Law, and E. J. Glass. 2008. *Food Stabilisers, Thickeners and Gelling Agent*. Animal Genetics. Vol. 39.

Blakebrough, N., and K. Sambamurthy. 1966. "Mass Transfer and Mixing Rates in Fermentation Vessels." *Biotechnology and Bioengineering* 8 (1): 25–42. <https://doi.org/10.1002/bit.260080104>.

Bombač, A, M Žumer, and I Žun. 2007. "Power Consumption in Mixing and Aerating of Shear Thinning Fluid in a Stirred Vessel." *Chemical and Biochemical Engineering Quarterly* 21 (2): 131–38.

Bouaifi, M., and M. Roustan. 2001. "Power Consumption, Mixing Time and Homogenisation Energy in Dual-Impeller Agitated Gas-Liquid Reactors." *Chemical Engineering and Processing* 40 (2): 87–95. [https://doi.org/10.1016/S0255-2701\(00\)00128-8](https://doi.org/10.1016/S0255-2701(00)00128-8).

Chapter 5: Performance of a dual helical ribbon impeller in a two-phase (gas-liquid) stirred tank reactor

Bourne, J.R.; Buttler, H. 1969. "Power Consumption of Helical Ribbon Impellers in Viscose Liquids." *Transactions of the Institution of Chemical Engineers* 47.

Brito-De La Fuente, E., L. Choplin, and P. A. Tanguy. 1997. "Mixing with Helical Ribbon Impellers: Effect of Highly Shear Thinning Behaviour and Impeller Geometry." *Chemical Engineering Research and Design* 75 (1): 45–52. <https://doi.org/10.1205/026387697523381>.

Cabaret, François, Sylvain Bonnot, Louis Fradette, and Philippe A. Tanguy. 2007. "Mixing Time Analysis Using Colorimetric Methods and Image Processing." *Industrial and Engineering Chemistry Research* 46 (14): 5032–42. <https://doi.org/10.1021/ie0613265>.

Chavan, Virendra V., and Jaromir Ulbrecht. 1973. "Power Correlations for Close-Clearance Helical Impellers in Non-Newtonian Liquids." *Industrial and Engineering Chemistry Process Design and Development* 12 (4): 472–76. <https://doi.org/10.1021/i260048a015>.

Cheng, Jianya, and Pierre I Carreau. 1994. "Aerated Mixing of Viscoelastic Fluids with Helical Ribbon Impellers." *Chemical Engineering Science* 49 (12): 1965–72.

Chhabra, R. P., L. Bouvier, G. Delaplace, G. Cuvelier, S. Domenek, and Christophe André. 2007. "Determination of Mixing Times with Helical Ribbon Mipeller for Non-Newtonian Viscous Fluids Using an Advanced Imaging Method." *Chemical Engineering and Technology* 30 (12): 1686–91. <https://doi.org/10.1002/ceat.200700320>.

Deans, Sean. n.d. "Techniques for Mixing and Scaling in Mechanically Agitated Vessels."

Delafosse, Angélique, Marie Laure Collignon, Sébastien Calvo, Frank Delvigne, Michel Crine, Philippe Thonart, and Dominique Toye. 2014. "CFD-Based Compartment Model for Description of Mixing in Bioreactors." *Chemical Engineering Science* 106: 76–85. <https://doi.org/10.1016/j.ces.2013.11.033>.

Delaplace, G., L. Bouvier, A. Moreau, R. Guérin, and J. C. Leuliet. 2004. "Determination of Mixing Time by Colourimetric Diagnosis - Application to a New Mixing System." *Experiments in Fluids* 36 (3): 437–43. <https://doi.org/10.1007/s00348-003-0741-7>.

Einsele, Arthur, and Robert K. Flinn. 1980. "Influence of Gas Flow Rates and Gas Holdup on Blending Efficiency in Stirred Tanks - Industrial & Engineering Chemistry Process Design and Development (ACS Publications)." *Industrial and Engineering Chemistry*, 600–603.

Chapter 5: Performance of a dual helical ribbon impeller in a two-phase (gas-liquid) stirred tank reactor

Espinosa-Solares, T., E. Brito-De La Fuente, A. Tecante, L. Medina-Torres, and P. A. Tanguy. 2002. "Mixing Time in Rheologically Evolving Model Fluids by Hybrid Dual Mixing Systems." *Chemical Engineering Research and Design* 80 (8): 817–23. <https://doi.org/10.1205/026387602321143345>.

Espinosa-Solares, T., E. Brito-De La Fuente, A. Tecante, and P. A. Tanguy. 1997. "Power Consumption of a Dual Turbine-Helical Ribbon Impeller Mixer in Ungassed Conditions." *Chemical Engineering Journal* 67 (3): 215–19. [https://doi.org/10.1016/S1385-8947\(97\)00040-5](https://doi.org/10.1016/S1385-8947(97)00040-5).

Ferreira, S. L.C., R. E. Bruns, H. S. Ferreira, G. D. Matos, J. M. David, G. C. Brandão, E. G.P. da Silva, et al. 2007. "Box-Behnken Design: An Alternative for the Optimization of Analytical Methods." *Analytica Chimica Acta* 597 (2): 179–86. <https://doi.org/10.1016/j.aca.2007.07.011>.

Foucault, By Støphane, Gabriel Ascanio, and Philippe A Tanguy. 2004. "Coaxial Mixer Hydrodynamics with Newtonian and Non-Newtonian Fluids," no. 3. <https://doi.org/10.1002/ceat.200401996>.

Fujasová, Mária, Václav Linek, Tomáš Moucha, and Eva Prokopová. 2004. "Energy Demands of Different Impeller Types in Gas – Liquid Dispersions." *Separation and Purification Technology* 39: 123–31. <https://doi.org/10.1016/j.seppur.2003.12.015>.

Hari-prajitno, Dana W A T I, P Ved, The Centre, and B Birmingham. 1998. "Gas-Liquid Mixing Studies with Multiple Up- and Down- Pumping Hydrofoil Impellers: Power Characteristics and Mixing Time" 76.

Hari-Prajitno, Danawati, Ved P. Mishra, Katsuhide Takenaka, Waldemar Bujalski, Alvin W. Nienow, and Jack McKemmie. 1998. "Gas-Liquid Mixing Studies with Multiple up- and down-Pumping Hydrofoil Impellers: Power Characteristics and Mixing Time." *Canadian Journal of Chemical Engineering* 76 (6): 1056–68. <https://doi.org/10.1002/cjce.5450760612>.

Hashemi, Nasim, Farhad Ein-Mozaffari, Simant R. Upreti, and Dae Kun Hwang. 2016a. "Analysis of Mixing in an Aerated Reactor Equipped with the Coaxial Mixer through Electrical Resistance Tomography and Response Surface Method." *Chemical Engineering Research and Design* 109: 734–52. <https://doi.org/10.1016/j.cherd.2016.03.028>.

Chapter 5: Performance of a dual helical ribbon impeller in a two-phase (gas-liquid) stirred tank reactor

Houska, M. 1986. "Anchor-Agitated Systems: Power Input Correlation for Pseudoplastic and Thixotropic Fluids in Equilibrium." *AIChE Journal* 32 (1): 155–58. <https://doi.org/10.1002/aic.690320119>.

Jiang, Jiankai, Jing Wu, Souhila Poncin, and Huai Z. Li. 2016. "Effect of Hydrodynamic Shear on Biogas Production and Granule Characteristics in a Continuous Stirred Tank Reactor." *Process Biochemistry* 51 (3): 345–51. <https://doi.org/10.1016/j.procbio.2015.12.014>.

Kouda, Tohru, Hisato Yano, Fumihiro Yoshinaga, Meguru Kaminoyama, and Mitsuo Kamiwano. 1996. "Characterization of Non-Newtonian Behavior during Mixing of Bacterial Cellulose in a Bioreactor." *Journal of Fermentation and Bioengineering* 82 (4): 382–86. [https://doi.org/10.1016/0922-338X\(96\)89155-0](https://doi.org/10.1016/0922-338X(96)89155-0).

Lamberto, D. J., F. J. Muzzio, P. D. Swanson, and A. L. Tonkovich. 1996. "Using Time-Dependent RPM to Enhance Mixing in Stirred Vessels." *Chemical Engineering Science* 51 (5): 733–41. [https://doi.org/10.1016/0009-2509\(95\)00203-0](https://doi.org/10.1016/0009-2509(95)00203-0).

Lehrer, LH. 1983. "Mixing Time Prediction." *Gas*. [http://www.mech.eng.unimelb.edu.au/people/staffresearch/AFMS site/8/Lehrer2.pdf](http://www.mech.eng.unimelb.edu.au/people/staffresearch/AFMS%20site/8/Lehrer2.pdf).

Low, Siew Cheng, Douglas Allitt, Nicky Eshtiaghi, and Rajarathinam Parthasarathy. 2018. "Measuring Active Volume Using Electrical Resistance Tomography in a Gas-Sparged Model Anaerobic Digester." *Chemical Engineering Research and Design* 130: 42–51. <https://doi.org/https://doi.org/10.1016/j.cherd.2017.11.039>.

Machon, By V, and Milan Jahoda. 2012. "Liquid Homogenization in Aerated Multi-Impeller Stirred Vessel." *Technology and Medical Sciences* 23: 1–1. <https://doi.org/10.1201/b11330-2>.

Machon, By V, and Milan Jahoda. 2012. "Liquid Homogenization in Aerated Multi-Impellers Stirred Vessel." *Chemical Engineering and Technology* 23: 1–1. <https://doi.org/10.1201/b11330-2>.

McLeod, James D., Maazuz Z. Othman, and Rajarathinam Parthasarathy. 2019. "Process Intensification of Anaerobic Digestion: Influence on Mixing and Process Performance." *Bioresource Technology* 274: 533–40. <https://doi.org/10.1016/j.biortech.2018.12.011>.

Chapter 5: Performance of a dual helical ribbon impeller in a two-phase (gas-liquid) stirred tank reactor

Metzner, A B, and R E Otto. 1957. "Agitation of Non-Newtonian Fluids." *AICHE J.* 3 (1): 3–10. <https://doi.org/10.1002/aic.690030103>.

Miryahyaei, S., K. Olinga, F. A. Abdul Muthalib, T. Das, M. S. Ab Aziz, M. Othman, J. C. Baudez, D. Batstone, and N. Eshtiaghi. 2019. "Impact of Rheological Properties of Substrate on Anaerobic Digestion and Digestate Dewaterability: New Insights through Rheological and Physico-Chemical Interaction." *Water Research* 150: 56–67. <https://doi.org/10.1016/j.watres.2018.11.049>.

Moo-Young, M., K. Tichar, and F. A.L. Dullien. 1972. "The Blending Efficiencies of Some Impellers in Batch Mixing." *AICHE Journal* 18 (1): 178–82. <https://doi.org/10.1002/aic.690180133>.

Nagata, Shinji, Masabumi Nishikawa, Tada Hisayuki, Hideo Hirabayashi, and Shinji Gotoh. 1970. "Power Consumption of Mixing Impellers Bingham Plastic Liquids." *Journal of Chemical Engineering of Japan* 3 (2): 237–43. <https://doi.org/10.1252/jcej.3.237>.

Nauha, Elina K., Zbyněk Kálal, Jama Mohamed Ali, and Ville Alopaeus. 2018. "Compartmental Modeling of Large Stirred Tank Bioreactors with High Gas Volume Fractions." *Chemical Engineering Journal* 334: 2319–34. <https://doi.org/10.1016/j.cej.2017.11.182>.

Paglianti, Alessandro, Sandro Pintus, and Massimiliano Giona. 2000. "Time-Series Analysis Approach for the Identification of Flooding/Loading Transition in Gas-Liquid Stirred Tank Reactors." *Chemical Engineering Science* 55 (23): 5793–5802. [https://doi.org/10.1016/S0009-2509\(00\)00125-1](https://doi.org/10.1016/S0009-2509(00)00125-1).

Pakzad, Leila, Farhad Ein-Mozaffari, and Philip Chan. 2008. "Measuring Mixing Time in the Agitation of Non-Newtonian Fluids through Electrical Resistance Tomography." *Chemical Engineering and Technology* 31 (12): 1838–45. <https://doi.org/10.1002/ceat.200800362>.

Pakzad, Leila, Farhad Ein-Mozaffari, Simant R. Upreti, and Ali Lohi. 2013. "Characterisation of the Mixing of Non-Newtonian Fluids with a Scaba 6SRGT Impeller through Ert and CFD." *Canadian Journal of Chemical Engineering* 91 (1): 90–100. <https://doi.org/10.1002/cjce.21616>.

Pakzad, Leila, Farhad Ein-mozaffari, Simant R Upreti, and Ali Lohi. 2012. "Chemical Engineering Research and Design Agitation of Herschel – Bulkley Fluids with the Scaba –

Chapter 5: Performance of a dual helical ribbon impeller in a two-phase (gas-liquid) stirred tank reactor

Anchor Coaxial Mixers.” *Chemical Engineering Research and Design* 91 (5): 761–77. <https://doi.org/10.1016/j.cherd.2012.09.008>.

Patel, Dineshkumar, Farhad Ein-Mozaffari, and Mehrab Mehrvar. 2012a. “Improving the Dynamic Performance of Continuous-Flow Mixing of Pseudoplastic Fluids Possessing Yield Stress Using Maxblend Impeller.” *Chemical Engineering Research and Design* 90 (4): 514–23. <https://doi.org/10.1016/j.cherd.2011.08.022>.

Paul, Edward L, Victor a Atiemo-obeng, and Suzanne M Kresta. 2004. *Handbook of Industrial Mixing*. <https://doi.org/10.1002/0471451452>.

Rieger, FRANTISEK, Vaclav Novak, and HAVELKOVA Dagmar. 1986. “Homogenization Efficiency of Helical Ribbon Agitators.” *The Chemical Engineering Journal* 33: 143–50. [https://doi.org/10.1016/0300-9467\(86\)80013-2](https://doi.org/10.1016/0300-9467(86)80013-2).

Samandari-Masouleh, Leila, Navid Mostoufi, A. A. Khodadadi, Y. Mortazavi, and Morteza Maghrebi. 2012a. “Kinetic Modeling of Carbon Nanotube Production and Minimization of Amorphous Carbon Overlayer Deposition in Floating Catalyst Method.” *International Journal of Chemical Reactor Engineering* 10 (1): 10–12. <https://doi.org/10.1515/1542-6580.2972>.

Samandari-Masouleh, Leila, Navid Mostoufi, Abbasali Khodadadi, Yadollah Mortazavi, and Morteza Maghrebi. 2012b. “Modeling the Growth of Carbon Nanotubes in a Floating Catalyst Reactor.” *Industrial and Engineering Chemistry Research* 51 (3): 1143–49. <https://doi.org/10.1021/ie201137j>.

Schrimpf, Marco, Jesús Esteban, Thorsten Rösler, Andreas J Vorholt, and Walter Leitner. 2019. “Intensified Reactors for Gas-Liquid-Liquid Multiphase Catalysis: From Chemistry to Engineering.” *Chemical Engineering Journal* 372 (March): 917–39. <https://doi.org/10.1016/j.cej.2019.03.133>.

Smith, John M. 1985. “Dispersion of Gases in Liquids: The Hydrodynamics of Gas Dispersion in Low Viscosity Liquids.” In *Mixing of Liquids by Mechanical Agitation*, 1st ed., 342. Routledge.

Takahashi, Koji. 1979. “Mixing of Pseudoplastic Liquid in a Vessel Equipped with a Variety of Helical Ribbon Impellers” 45 (1978): 63–68.

Chapter 5: Performance of a dual helical ribbon impeller in a two-phase (gas-liquid) stirred tank reactor

Takahashi, Koji, Naoki Sugawara, and Yasuyuki Takahata. 2015. "Mixing Time in an Agitated Vessel Equipped with Large Impeller." *Journal of Chemical Engineering of Japan* 48 (7): 513–17. <https://doi.org/10.1252/jcej.14we192>.

Takahashi, Koji, Toshiyuki Yokota, and Hiroataka Konno. 1984. "Power Consumption of Helical Ribbon Agitators in Highly Viscous Pseudoplastic Liquids." *Journal of Chemical Engineering of Japan* 17 (6): 657–59. <https://doi.org/10.1252/jcej.17.657>.

Taylor, Publisher, Reza Afshar Ghotli, Abdul A A Raman, and Shaliza Ibrahim. n.d. "Liquid-Liquid Mixing In Stirred Vessels: A Review Liquid-Liquid Mixing in Stirred Vessels: A Review," no. January 2014: 37–41. <https://doi.org/10.1080/00986445.2012.717313>.

Tsui, Yeng Yung, and Yu Chang Hu. 2011. "Flow Characteristics in Mixers Agitated by Helical Ribbon Blade Impeller." *Engineering Applications of Computational Fluid Mechanics* 5 (3): 416–29. <https://doi.org/10.1080/19942060.2011.11015383>.

Wiedemann, Leonhard, Fosca Conti, Tomasz Janus, Matthias Sonnleitner, Wilfried Zörner, and Markus Goldbrunner. 2017. "Mixing in Biogas Digesters and Development of an Artificial Substrate for Laboratory-Scale Mixing Optimization." *Chemical Engineering and Technology* 40 (2): 238–47. <https://doi.org/10.1002/ceat.201600194>.

Wu, Jie, Yonggang Zhu, and Lionel Pullum. 2001. "The Effect of Impeller Pumping and Fluid." *The Canadian Journal of Chemical Engineering* 79: 177–86. <https://doi.org/10.1002/cjce.5450790201>.

Wu, Jing, Hong ming Zhou, Huai zhi Li, Peng cheng Zhang, and Jie Jiang. 2009. "Impacts of Hydrodynamic Shear Force on Nucleation of Flocculent Sludge in Anaerobic Reactor." *Water Research* 43 (12): 3029–36. <https://doi.org/10.1016/j.watres.2009.04.026>.

Xie, Ming hui, Jian ye Xia, Zhen Zhou, Guo zhong Zhou, Ju Chu, Ying ping Zhuang, Si liang Zhang, and Henk Noorman. 2014. "Power Consumption, Local and Average Volumetric Mass Transfer Coefficient in Multiple-Impeller Stirred Bioreactors for Xanthan Gum Solutions." *Chemical Engineering Science* 106: 144–56. <https://doi.org/10.1016/j.ces.2013.10.032>.

Xu, Qian, Pradipto K. Bhattacharjee, Doug Allitt, Nicky Eshtiaghi, and Rajarathinam Parthasarathy. 2018. "Evolution of Flow Regimes in Non-Newtonian Liquids under Gas

Chapter 5: Performance of a dual helical ribbon impeller in a two-phase (gas-liquid) stirred tank reactor

Sparging.” *Chemical Engineering Science* 176: 153–56.
<https://doi.org/10.1016/j.ces.2017.10.034>.

Yang, Xiao Hong, and Wei Ling Zhu. 2007. “Viscosity Properties of Sodium Carboxymethylcellulose Solutions.” *Cellulose* 14 (5): 409–17. <https://doi.org/10.1007/s10570-007-9137-9>.

Zitrom, Veronica C. 1999. “One-Factor-at-a-Time Versus Designed Experiments.” *The American Statistician* 53 (2): 126–31. <https://doi.org/10.2307/2685731>.



CFD-PBM and experimental investigation of a shear thinning fluid in a gas-liquid tank agitated by a helical ribbon impeller

Maryam Amiraftebi, Mehdi Khiadani^{*}, Hussein A. Mohammed, Arslan Arshad

School of Engineering, Edith Cowan University, 270 Joondalup Drive, Joondalup, Perth, WA 6027, Australia

ARTICLE INFO

Keywords:

CFD-PBM method
Stirred tank reactor
Non-Newtonian fluids
Mixing performance
Dual helical ribbon impeller

ABSTRACT

This study focuses on hydrodynamic characteristics of a shear thinning fluid agitated in a 3D multiphase reactor using a dual helical ribbon impeller. A combination of Computational Fluid Dynamics (CFD) simulation and Population Balance Model (PBM) were employed to study the gas-liquid interactions at various impeller speeds. The standard $k - \epsilon$ model and Eulerian multiphase approach were used to predict better quantities of turbulent flow parameters and its characteristics. Particle Image Velocimetry (PIV) was used to measure the velocity field for the model validation. Simulation results indicated that the bubble breakage and coalescence rate was intensified due to an increase in rotational speed. However, bubble breakage is still the dominant phenomenon since the bubbles would hit the walls and blades due to the turbulent intensity. Further, the helical ribbon impeller significantly reduces the viscosity of the fluid and improves the mixing efficiency that is confirming the authors' previous experimental results. Furthermore, formation of static vortices adversely affects the efficiency of mixing process proving that an increase in impeller speed does not necessarily enhance the mixing performance.

Further, the helical ribbon impeller significantly reduced the viscosity of the fluid and enhanced mixing efficiency, thereby confirming the authors' previous experimental results.

1. Introduction

The mixing process of non-Newtonian multiphase systems is important as it influences the efficiency of aerobic/anaerobic digesters, and polymerization and fermentation reactors. Mixing parameters should be adjusted under optimum operating conditions to keep a balance between several contradictory factors. The higher rotational speed of the impeller offers many advantages including the uniformity of heat and mass transfer between phases, well distribution of gas-phase as the speed controlling parameter, and higher loading capacity. While an increase in the rotational speed of the impeller not only disturbs the microbial environment, also it raises the operating and maintenance costs. Difficulties arise when an attempt is made to study the hydrodynamical behaviours of phases in detail and to find the optimum operating conditions in order to maximise the efficiency of a bioreactor. Because of that many researchers in this field have paid attention to study hydrodynamical aspects of multiphase bioreactors including gas-liquid hydrodynamics [1–4], drag force [5], mass transfer and gas-liquid interactions [6], energy consumption [7,8], and rheological properties [3,9–11]. Adjusting and monitoring these parameters is demanding and

sometimes impossible tasks as it involved some limitations. Expensive instrument and equipment, experimental limitation, the opaque nature of sludge, and complicated multiphase flow patterns make the practical study of multiphase mixing systems impossible. Notwithstanding these limitations, computational fluid dynamics (CFD) simulation as an alternative approach shining a new light on these debates through theoretical and mathematical approaches.

Rotational speed and type of impeller are predominant factors controlling the hydrodynamics of bioreactors, and uniformity of heat and mass transfer between phases. Close-clearance impellers have been known as an ideal and well performed type of blades, enhancing the bulk mixing of highly viscose fluid in single-phase bioreactors [1,12,13]. Lebranchu et al., 2015 [14] concluded that a dual helical ribbon impeller in comparison with other types improves the performance of aerated reactor up to 50%. They also indicated that the rheological behaviour of fluid is influenced by various parameters including temperature, pH, and concentration gradient. Further, different CFD approaches have been designed to determine the effect of geometry and type of dual helical ribbon impellers on the mixing performance of single-phase fluid. Kamla et al., 2019 [9] investigated the effect of geometry and the number of blades on the performance of an anaerobic

^{*} Corresponding author.

E-mail addresses: m.amiraftebi@ecu.edu.au (M. Amiraftebi), m.khiadani@ecu.edu.au (M. Khiadani), Hussein.mohammed@ecu.edu.au (H.A. Mohammed), A.Arshad@ecu.edu.au (A. Arshad).

<https://doi.org/10.1016/j.seppur.2021.118855>

Received 5 December 2020; Received in revised form 12 April 2021; Accepted 23 April 2021

Available online 3 May 2021

1383-5866/© 2021 Elsevier B.V. All rights reserved.

Nomenclature		
A	cross sectional area (m ²)	$n(\vec{x}, V_b, t)$ bubble density distribution function at the time of t and position of $\vec{x}.V_b$
AR	aspect ratio	PBM population balanced model
C	equation constant	PIV particle image velocimetry
CFD	computational fluid dynamics	\vec{R}_{ji} interphase force
C _D	drag coefficient	Re Reynold number (Dimensionless)
D	vessel inner diameter (cm)	RSM response surface methodology
d	impeller diameter (cm)	STR stirred tank reactor
d _i	impeller blade diameter (cm)	$S(\vec{x}, V_b, t)$ source term of breakage/coalescence
d _s	shaft diameter (mm)	t time (s)
E-E	Eulerian-Eulerian	u _b local velocity of bubbles (m/s)
\vec{F}_i	momentum transferred from bubbles to the liquid phase	wt% weight percentage (%)
g	gravitational acceleration (m/s ²)	α_i volume fraction of the continuous phase
G	generation of turbulent kinetic energy	ϵ dissipation rate
H _L	depth of fluid (cm)	γ_g gas shear rates (1/s)
h	impeller height (cm)	γ_l liquid shear rates (1/s)
IC	impeller clearance	$\dot{\gamma}_T$ average shear rates (1/s)
IS	impeller speed	μ_{eff} effective viscosity (Pa s)
K	consistency index (Pa s ⁿ)	μ_i molecular viscosity (Pa s)
k	turbulent kinetic energy (m ² /s ²)	$\mu_{t,i}$ shear induced viscosity (Pa s)
K_{ji}	exchange coefficient for bubbly phase	$\mu_{b,i}$ turbulence viscosity (Pa s)
MRF	multiple reference frame	v_i liquid mean velocity (m/s)
N	impeller rotational speed (rpm)	ρ density (kg/m ³)
NaCMC	sodium carboxymethyl cellulose	τ average shear stress (N/m ²)
n	flow index behaviour	

digester filled with activated sludge. They found that an increase in the number of helical blades enhances the mixing efficiency. In addition, the performance of helical screw impellers in single phase flow was simulated by Ameer et al. [15]. Further, Kunczewicz and Stelmach, 2016 [10] noted that the effect of the width of the helical ribbon impeller on power consumption can be ignored. Additionally, Mihailova et al., 2018 [11] optimised the overall performance of a new design impeller as a combination of helical ribbon and screw impellers. Ameer and Ghenaïm, 2018 [15] made a comparison between the performance of the helical ribbon and screw impellers. They indicated that the rheological behaviour of working fluid dominates the level of power consumption and hydrodynamics of the system. The complexity of the rheological behaviour of materials has forced most of the studies to ignore the rheological properties in their research [16,17]. This complexity stems from the temperature and shear rate dependence of viscosity [18,19]. In the current study, Sodium Carboxyl Methyl Cellulose (NaCMC) as a transparent non-Newtonian fluid was applied to simulate the rheological characteristics of shear-thinning fluids inside the reactor [19].

Further, the flow pattern of multiphase bioreactor has not been well understood since most literature have investigated the hydrodynamics of a single-phase reactor. While the efficiency of gas-liquid system is affected by the dynamic behaviours of both gas and liquid phases including gas holdup, the size distribution of bubbles, liquid phase velocity field, and viscosity. Clearly, the formation and interaction (breakage and coalescence) of rising bubbles and gas holdup determine the reaction rate, interfacial area, and mass transfer resistance. It is reasonable to state that higher interaction between phases is achieved by smaller fully dispersed bubbles, therefore, the breakage phenomenon is beneficial to the bioreactor performance. So, it is paramount to

investigate the performance of gas-liquid mixing system by considering the detailed knowledge of bubble size and distribution, hydrodynamics, and flow field. To predict the size distribution and breakage/coalescence rates, a combination of Population Balance Model (PBM) as a semi-empirical equation and CFD has been suggested in the literature [10,20,21]. Therefore, this study applied the discrete method to solve the PBM model as a successful method in predicting the size and distribution of bubbles [22]. Operating conditions are adjusted based on the previous experimental study [23]. The impacts of various rotational speeds, gas flow rates, impeller clearance from the bottom, and concentration on mixing time and power consumption have all been investigated. The results are presented for rotational speeds of 25, 50, and 75 rpm for a gas flow rate of 1.8 LPM, with an impeller clearance of 4 cm and concentration of 0.5 wt%, which is an optimum concentration to replicate municipal digested sludge [23].

This study seeks to obtain data that will assist in highlighting the effect of impeller rotational speeds on (i) hydrodynamics and viscosity of a shear-thinning liquid, and (ii) the bubble size distribution and gas holdup. Geometry and boundary conditions were defined based on the experimental setup. The grid sensitivity analysis was carried out for five different meshes. Further, the numerical model was verified separately for both phases including liquid and gas to compare; (i) CFD results with PIV tests for flow field and velocity magnitude of the liquid phase, (ii) the predicted bubble velocity obtained by CFD with the experimental average gas velocity achieved through image processing technique for the initial gas flow rates of 0.5 and 2 LPM.

Table 1

The geometric configuration of the stirred tank.

Vessel inner diameter (m)	Vessel height (m)	Impeller height (m)	Impeller diameter (m)	Impeller blade diameter (m)	Impeller clearance (m)	Shaft diameter (m)
D	H	h	d	d _i	IC	d _s
0.19	0.4	0.155	0.14	0.02	0.02, 0.04, 0.06	0.015

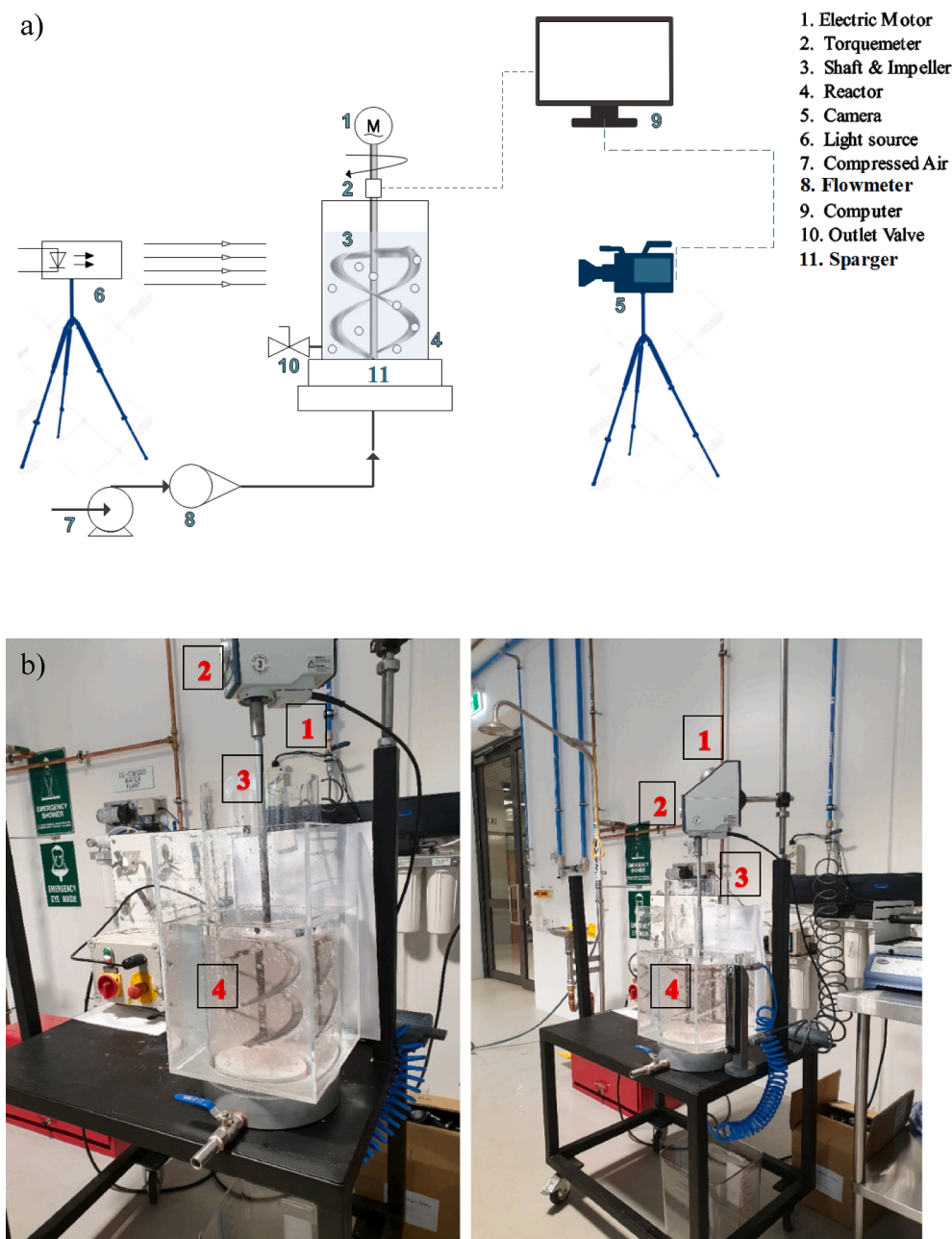


Fig. 1. (a) Schematic diagram of high-speed camera, light source, and two-phase bioreactor; and (b) Experimental setup.

2. Experimental methodology

2.1. Two-phase stirred tank reactor configuration

The experiments were conducted in a 7 L plexiglass unbaffled cylindrical vessel having 190 mm inner diameter equipped with a dual helical ribbon impeller. The system configurations and geometric details are presented in Table 1 and Fig. 1, respectively. The aspect ratio of the system (liquid level (H_L) to reactor diameter (D)) is 1.4 [24]. The central shaft is made of aluminum connected a variable speed electric motor. To avoid the light reflection during the tests and also facilitating the PIV measurements, the vessel is enclosed with a clear rectangular box. The box is filled with water to the level of liquid inside the vessel during PIV measurements.

The gas distributor was a showerhead type sparger made of PVC with 10 holes of 0.25 mm drilled on its periphery at an equal distance. The distributor was screwed at the base of the vessel connected to the air

supply hose through a rotameter type flowmeter (Omega engineering, UK with an accuracy of $\pm 2\%$). The gap between the top of the sparger and the bottom of the impeller was 40 mm.

During the operation, the impeller rotational speed and aeration rate are kept constant at an optimum range of 75 rpm and 1.8 LPM, respectively. These optimum operating values were obtained using the response surface methodology (RSM) approach mentioned in the authors' previous study [23]. RSM approach was applied to identify correlations between operating conditions including impeller speed, gas flow rate, impeller clearance, and viscosity with responses such as mixing time and power consumption of impeller. Further, the optimum working conditions were identified to minimize the mixing time and power consumption.

Power uptake was calculated from the torque measured by a digital torque meter (GUNT system with an accuracy of ± 0.1 N m). To calculate mixing time, a combination of decolorization and image processing methods was applied. Reynolds number calculated between 10 and

Table 2
Rheological characteristics of NaCMC y[19].

Concentration (wt%)	n (-)	K (Pa s ⁿ)
0.1	0.98	0.08
0.5	0.92	0.13
1	0.82	0.46
1.5	0.58	4.3

1000 based on effective viscosity [23]. Therefore, the flow regime in this study was a mix of turbulent and laminar flows.

2.2. Rheological properties of working fluid (NaCMC)

NaCMC has been applied as a safe and clear proxy simulant to emulate the shear behavior of digested sludge in an anaerobic digester. This polymer can replicate the rheological characteristics of digested

sludge in the range of shearing rate between 10 and 300 s⁻¹. Technical NaCMC Powder has been purchased from Rowe Company (Sydney, Australia)[19].

The rheological characteristics of NaCMC including viscoelastic, sweep, and thixotropic tests (1–300%), were carried out by a DHR-3, TA rheometer with normal accuracy ± 0.005 [25] and recorded in Table 2. The rheology was measured by a coaxial cylinder cup with a diameter of 0.304 m, bob diameter of 0.28 m, bob height of 0.42 m, and a gap distance of 0.001 m. Further, a Peltier system was controlled and kept the temperature at 25 °C during the tests [19,23]. The pH resistance of working fluid was tested by measuring pH by Glass pH electrode (EUTECH, pH 700) and ζ -potentials through a Malvern zeta sizer (Malvern series ZEN 3500, Malvern Instruments Ltd., Worcester, UK, ± 1 mv).

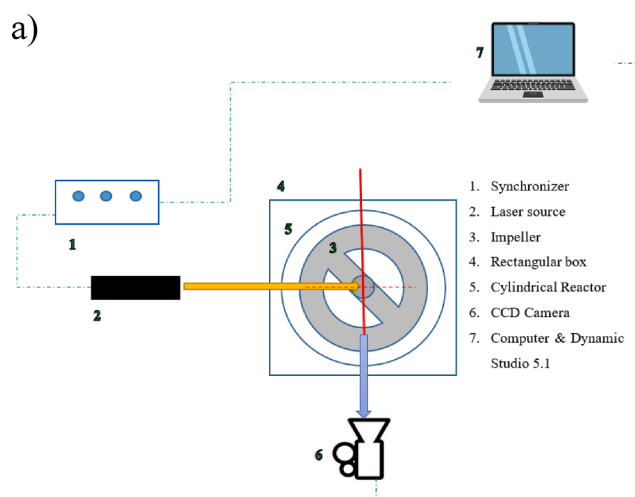


Fig. 2. (a) Schematic view of PIV system, and two-phase reactor; and (b) Experimental setup for PIV measurements.

2.3. PIV measurements

2.3.1. PIV set-up

The particle Image Velocimetry (PIV) technique was used to visualize the instantaneous velocity field of the liquid phase induced by rotary impeller and bubble movement. It was applied for a vertical cut of the system divided into two quarters to avoid shadow regions as indicated in Fig. 2. Approximately, 600 images were captured at 7 images per second per experiment. The laser source was an in-line dual-pulsed Nd:YAG laser (Dantec Dynamics, model: Dual Power 200–15) having 200 mJ/pulse at $\lambda = 532$ nm. A monochromatic CCD camera (Flow Sense EO 16M-9) having a resolution of 4920×3280 pixels which was equipped with a Carl Zeiss (T*1.4/50) lens having a 50 mm focal length was used for image acquisition. Dynamic Studio 5.1 software was used to analyse and process the images. To visualise the liquid phase trajectory, filter lenses and fluorescent polymer particles (PMMA-RhB-Frak-Particles) with a mean average diameter of 20–25 μm were used to reduce the effect of sparging gas.

3. Numerical simulation

3.1. Governing equations

The Eulerian-Eulerian (E-E) multiphase approach [26] was implemented in this study to simulate the three-dimensional geometry of the experimental rig. In this approach, both continuous and disperse phases were considered as continuous interpenetrating media based on their volume fractions. This was followed by solving the continuity and momentum equations using E-E approach for both two phases. Eqs. (1) and (2) show the continuity and conversion of momentum for phase (i), respectively:

Power-Law equation ($\mu = K \cdot \dot{\gamma}^n$) is often used to model the rheological characteristics of non-Newtonian fluids [19], whereas, $\dot{\gamma}$ (s^{-1}) shows shear rate, μ (Pa s) indicates viscosity of fluid, n (–) and K (Pa s^n) shows the flow and the consistency indexes, respectively.

$$\frac{\partial}{\partial t}(\alpha_i \rho_i) + \nabla \cdot (\alpha_i \rho_i \mathbf{v}_i) = 0 \quad (1)$$

where α_i is the volume fraction of the continuous phase and \mathbf{v}_i is the liquid mean velocity.

$$\frac{\partial}{\partial t}(\alpha_i \rho_i \mathbf{v}_i) + \nabla \cdot (\alpha_i \rho_i \mathbf{v}_i \mathbf{v}_i) = -\alpha_i \nabla p + \alpha_i \rho_i \mathbf{g} + \nabla \cdot \tilde{T}_i + \alpha_i \rho_i \vec{F}_i + \sum_{j=1}^n \vec{R}_{ji} \quad (2)$$

$$\alpha_i + \alpha_j = 1 \quad (3)$$

where $\nabla \cdot \tilde{T}_i$ indicates the shear stress caused by laminar or turbulent momentum fluxes calculated from the following equation:

$$\tilde{T}_i = \alpha_i (\mu_{\text{eff}}) \left[\nabla \vec{v}_i + \vec{\nabla}_i^T \right] - \left(\frac{2}{3} \right) \alpha_i (\mu_{\text{eff}}) \nabla \vec{v}_i \vec{1} \quad (4)$$

where μ_{eff} shows the liquid effective viscosity which is the result of molecular viscosity (μ_i), shear induced viscosity ($\mu_{t,i}$), and turbulence viscosity ($\mu_{b,i}$) [27].

$$\mu_{\text{eff}} = \mu_i + \mu_{t,i} + \mu_{b,i} \quad (5)$$

\vec{F}_i shows the momentum transferred from bubbles to the liquid phase and the last term in the right side of Eq. (2) is the interphase forces. Other interphase forces including lift, virtual mass and turbulence dissipation can be ignored because they are very small in comparison to the drag force [28,29]. In this study, Schiller and Naumann's classical drag model was applied to simulate interphase forces where C_D indicates the drag coefficient of a bubble in an infinite liquid phase [30].

$$C_D = \begin{cases} \frac{24}{Re_b} (1 + 0.15 Re_b^{0.687}) Re \leq 1000 \\ 0.44 Re > 1000 \end{cases} \quad (6)$$

$$\sum_{j=1}^n \vec{R}_{ji} = \sum_{i=1}^n K_{ji} (\vec{v}_i - \vec{v}_j) \quad (7)$$

whereas K_{ji} is the exchange coefficient for bubbly or droplet phase (j) which is defined as follows

$$K_{ji} = \frac{\alpha_i \alpha_j \rho_j f}{\tau_i} \quad (8)$$

where f and τ_i are the drag force and the relaxation time, respectively. Also, Re number of the shear thinning fluid is calculated based on the effective viscosity of liquid. Eq. (9) indicates the Reynold number for a helical ribbon impeller which is obtained by Fuente et al. [31].

$$Re = \rho \frac{Nd^2}{\mu_{\text{eff}}} \quad (9)$$

3.1.1. Turbulence model

The $k - \varepsilon$ model was adopted in the proposed study to model the turbulence. This model has two equations written for a mixture of two phases.

$$\frac{\partial}{\partial t}(\rho_m k) + \nabla \cdot (\rho_m \vec{v}_m k) = \nabla \cdot \left(\frac{\mu_{t,m}}{\delta_k} \nabla k \right) + G_{k,m} - \rho_m \varepsilon \quad (10)$$

$$\frac{\partial}{\partial t}(\rho_m \varepsilon) + \nabla \cdot (\rho_m \vec{v}_m \varepsilon) = \nabla \cdot \left(\frac{\mu_{t,m}}{\delta_\varepsilon} \nabla \varepsilon \right) + C_{1\varepsilon} G_{k,m} - C_{2\varepsilon} \rho_m \varepsilon \quad (11)$$

where k is the turbulent kinetic energy, G is the generation of turbulent kinetic energy, and ε is the dissipation rate. The mixture properties can be found from the following equations:

$$\rho_m = \sum_{i=1}^n \alpha_i \rho_i \quad (12)$$

$$\vec{v}_m = \frac{\sum_{i=1}^n \alpha_i \rho_i \vec{v}_i}{\sum_{i=1}^n \alpha_i \rho_i} \quad (13)$$

$$\mu_{t,m} = \rho_m C_\mu \frac{k^2}{\varepsilon} \quad (14)$$

Further, values for these equations ($C_\mu = 0.09$, $C_{1\varepsilon} = 1.44$, and $C_{2\varepsilon} = 1.92$) were extracted from previous literature [32].

3.1.2. Population balance model (PBM)

Computational Fluid Dynamics (CFD) simulation is a powerful method for predicting the hydrodynamics of complex multiphase agitated systems, however, this method cannot show the change in bubble size. Thus, CFD-PBM coupled method was suggested by literature to calculate the bubble size change [33].

The size of bubbles can change during the process of mixing based on the change in liquid properties as most of the fluids are non-Newtonian. Therefore, it is important to use CFD-PBM method in order to have a better prediction of bubble coalescence and breakage

The integrated CFD-PBM method is derived from the Boltzmann statistical transport equation to simulate the unsteady multiphase phenomenon such as lift [34], drag [35], and mass transfer modeling. This method describes the bubble entering/ leaving defined control volume.

$$\begin{aligned} \frac{\partial}{\partial t} n(\vec{x}, V_b, t) + \frac{\partial}{\partial z} [n(\vec{x}, V_b, t) u_b(\vec{x}, V_b)] + \frac{\partial}{\partial V_b} [n(\vec{x}, V_b, t) \frac{\partial}{\partial t} V_b(\vec{x}, V_b)] \\ = S(\vec{x}, V_b, t) \end{aligned} \quad (15)$$

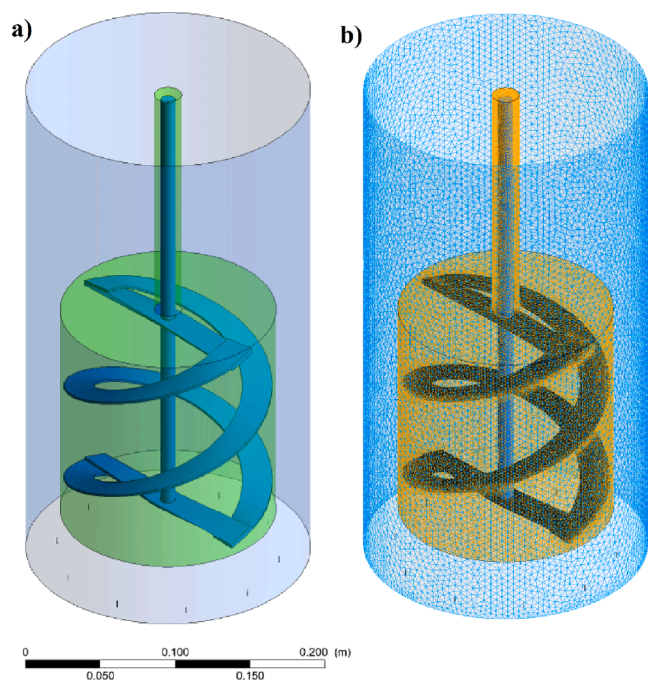


Fig. 3. Schematic view of the reactor with dual helical ribbon impeller; (a) MRF zones, (b) mesh topology.

where $n(\vec{x}, V_b, t)$ indicates bubble density distribution function at the time of t and a position of \vec{x} . V_b refers to the volume of bubbles, u_b shows the local velocity of bubbles, and $S(\vec{x}, V_b, t)$ is a source term including bubble sink or source in different situations including coalescence, breakage, phase interactions, reaction, and mass transfer. The Lue and Svendsen models suggested by ANSYS Fluent user guide has been considered in this study to model the bubble coalescence and breakup [36–38].

The discrete method was used to solve the PBM equation, discretised into five interval bubble diameters in this study. By using this method, the bubble breakage can be modelled based on the interaction between bubbles and turbulent eddies, which leads to simulate the bubble deformation. The average bubble diameter was calculated by tracking 40 bubbles obtained through the experimental phase [23]. The maximum bubble size, which was observed in image processing analysis, was 7 mm and the smallest one was 0.1 mm. More than 80% of the

bubbles had a diameter in the range of 3 to 5 mm, which can be categorized in the first and second bubble intervals.

3.2. Solution domain, mesh generation and boundary conditions

3.2.1. Mesh processing

Design modeler and ICEM 18.2 were used to construct a three-dimensional geometry of the reactor used in the experiment. The unstructured meshing method coupled with Multiple Reference Frame (MRF) approach was applied to generate five different 3-D mesh topologies as shown in Fig. 3. In MRF method, the domain was divided into two different regions; the stationary outer region, and the rotating inner part, which is rotated by the impeller. A finer mesh was applied inside the inner cylinder surrounding the impeller because the flow pattern in this region is an important parameter. Having finer mesh can enhance capturing the flow and improving the accuracy of results around the impeller region. Additionally, the outer layer is defined as non-rotating domain with coarse mesh.

The mesh independence study was carried out for five different numbers of cells by testing the average velocity of the liquid at 15 cm above the bottom of the reactor. Increasing cell numbers has changed the average velocity remarkably. However, the average velocity tends to be stable after 6×10^6 cells as is shown in Fig. 4.

3.2.2. Solver setup and boundary conditions

ANSYS Fluent R19.1 double precision solver was applied to run the simulation and to define boundary conditions. The Eulerian-Eulerian model has been applied in this study to build momentum and continuity equation for phases. The convergence rate was enhanced by solving the momentum and pressure-based continuity equations using SIMPLE method [39]. The maximum iteration number is set to 1000 for a time step of 0.001 s.

Further, the volume fraction parameters have been set in the multiphase model dialog box as explicit scheme which is time-dependent. The modified HRIC is applied here because there are sharp interfaces between both phases.

In addition, Reynolds number varied between 10 and 1000 according to previous experimental tests [23]. Reynolds number indicates the system is working in a transient regime involving both viscous and inertial forces. For this reason, the system should be modeled by either laminar or turbulent flow regimes [40].

The initial and boundary conditions in the model were considered identical to the experimental operational conditions. The nozzle holes on the top surface of the sparger were assumed as velocity inlet with the

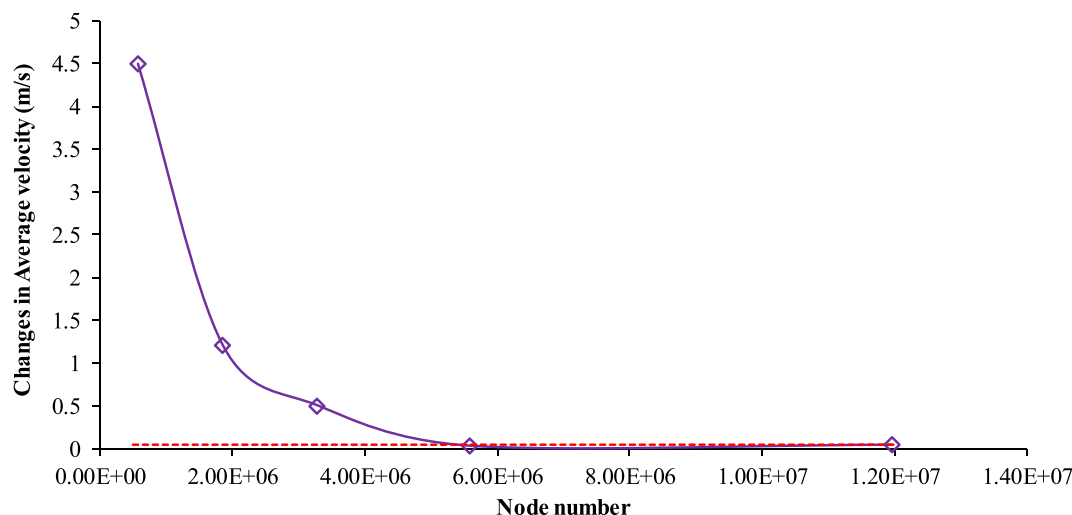


Fig. 4. The model grid sensitivity analysis.

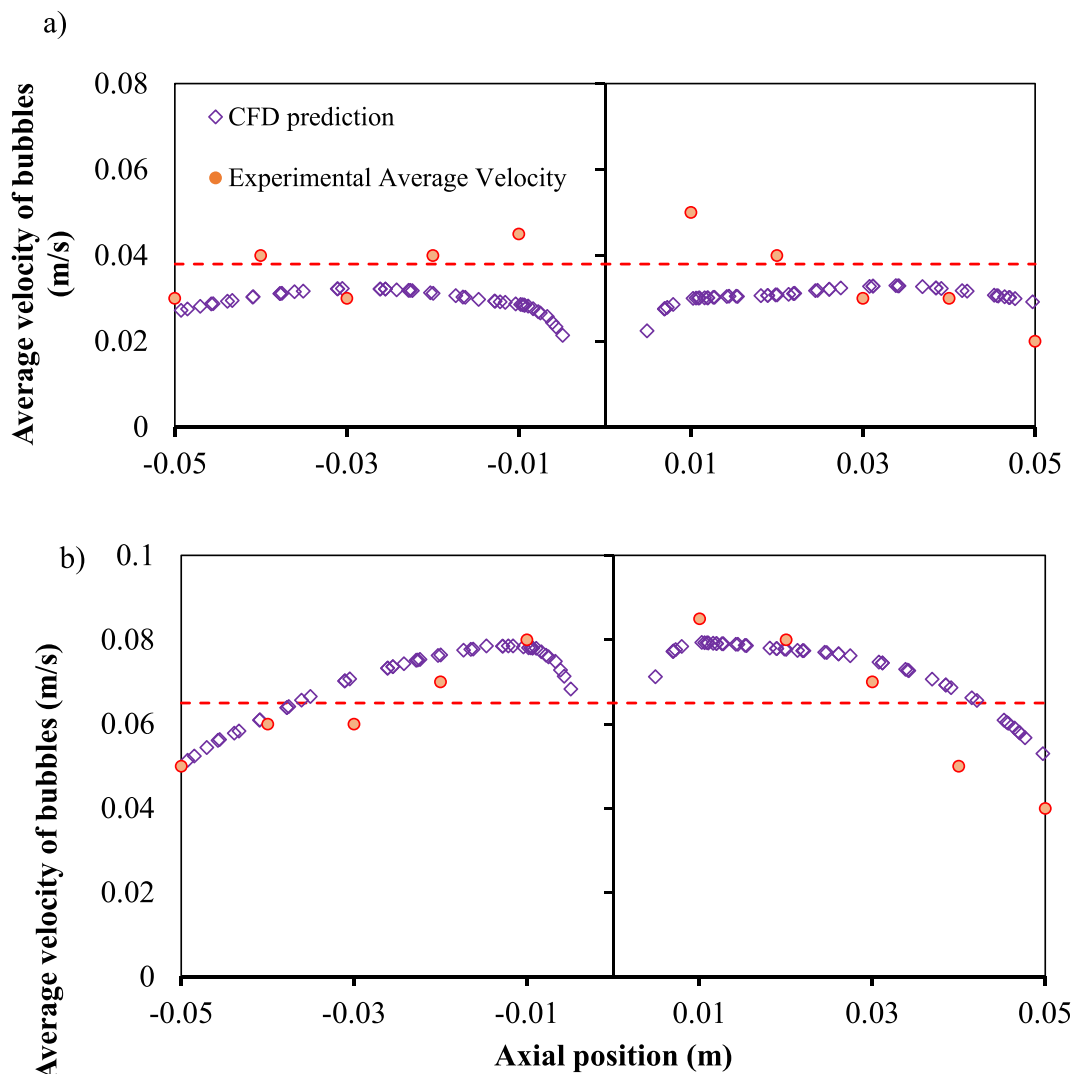


Fig. 5. Comparison of average velocities obtained from experiment and CFD simulation for the initial gas flowrates: (a) 0.5 LPM and (b) 2 LPM.

gas fraction equals 1. Further, the body of the cylinder should be treated as a standard no slipping wall. The boundary condition at the top of the cylinder which is the degassing part is considered as a pressure outlet. The whole cylinder was employed as a liquid region with a height of 0.24 m and a gas volume fraction of 0. The rotating wall situation is applied for the impeller body and its shaft. In this work, the air bubble size was considered in the range of 0.1 and 7 mm based on the experimental data gathered by the image processing method [23]. It should be mentioned that the rheological properties of the non-Newtonian fluid follow the Power-Law model based on previous studies [19].

3.2.3. Model validation

Two different methods were applied to validate the CFD results in both gas and liquid phases. First, the average rising velocity for 40 bubbles in pure water was considered to verify the gas velocity predicted by CFD simulation. Second, both the velocity magnitude and flow field of the liquid phase were captured using PIV measurement to validate the hydrodynamics of the liquid phase.

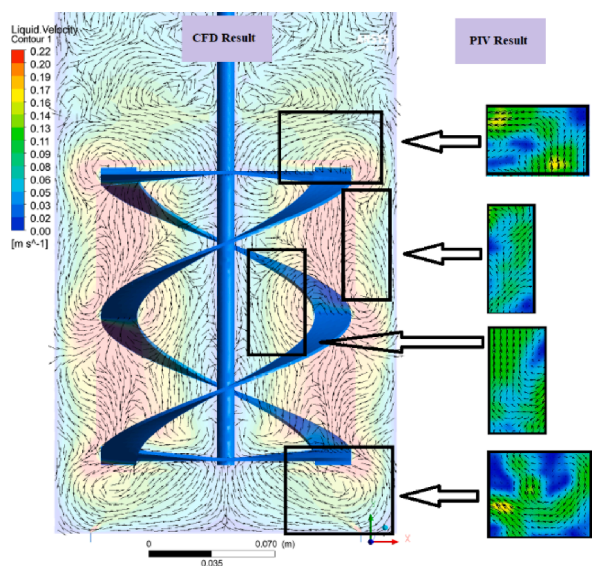
3.2.4. Gas velocity

The mean bubble velocity calculated by CFD-PBM was compared to the calculated average velocity obtained from the experiments and image processing. The validation tests were carried out in two different initial airflow rates of 0.5 and 2 LPM which are shown in Fig. 5. The

bubble motion was recorded using a high-speed camera (Samsung digital Camera 12 M P with a speed of 1.4 μm including dual-pixel autofocus) for further evaluation by image J software. The mean velocity for bubbles has been calculated for 10 sec after stabilizing the system.

3.2.5. Hydrodynamics

Capturing and distinction of the flow field using PIV is extremely challenging when a large impeller rotating in a two-phase reactor due to the interference and interaction of moving bubbles with impeller shadow. To reduce the interference of gas flow, a filtered lens and fluorescent dye were applied. Despite this, PIV still captures some parts of sparged gas and accumulated bubbles on the back of the blades which interfere with the results. Fig. 6a, b shows both the velocity vectors and magnitude captured by CFD and PIV at 75 and 150 rpm. The overall flow shows a similar pattern in different regions including the upper, middle, and bottom of the impeller which are identified by large red vectors. In addition, the velocity magnitude captured by PIV is approximately equal to the CFD prediction when the rotational speed of the impeller is 75 rpm. Although at 150 rpm, the direction of velocity vectors captured by PIV shows similar results to CFD results, the velocity magnitudes estimated by CFD is higher than the values obtained from PIV measurements.



b)

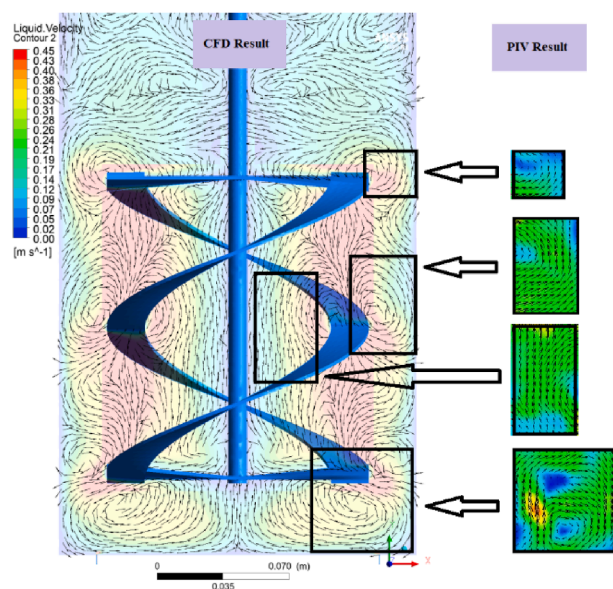


Fig. 6. Comparison of the flow field and velocity magnitude between CFD simulation (left image) and PIV measurements (right image); at (a) 75 rpm, and (b) 150 rpm.

4. Results and discussion

4.1. Effect of impeller speed on bubble size distribution and gas holdup

The size distribution of the bubbles can be evaluated by breakage and coalescence rates which is governed by the dissipation rate of kinetic energy. Fig. 7 shows the bubble size distribution in three rotational impeller speeds of 25, 75, and 150 rpm. In the lower rotational speed, it is observed that the flow is channelized in the outer edge of the blades. This can be also observed in Fig. 8 which indicates the total gas fractions for different rotational speeds of 25, 75, 150 rpm. Fig. 8 demonstrates that low impeller speed has an insignificant effect on the hydrodynamics of the gas phase. Therefore, bubbles skew, slowly move, and are possibly

stuck in gel-like structure of the fluid. It can be concluded that coalescence is the predominant phenomenon when impeller speed is too low. As a result, the interfacial area between two phases reduces which negatively influences the interphase mass and heat transfer. The CFD result indicated that the bubble size is changing between 0.25 and 0.65 mm due to the coalescence at 25 rpm. By increasing the impeller speed from 25 to 75 rpm, the bubbles scattered through the system due to the induced shear stress. Accelerated bubbles hit the wall of the vessel and blades resulting in breakage. Simultaneously, accelerated bubbles may strike together and merge to form a larger bubble through the coalescence process. Simultaneous breakage and coalescence of the bubbles resulting in a homogeneous distribution of various bubble size in the range of 0.25 to 0.65 at 75 rpm. Additionally, Fig. 8 confirms that the gas-phase is well distributed at 75 rpm leading to an increase in interfacial area between phases and gas hold up. Doubling the rotational speed of the impeller up to 150 rpm increases the rate of bubble breakage and coalescence, due to the intensity of turbulent flow. The size of the bubbles at 150 rpm varies in a wider range between 0.1 and 0.65 mm. Further Fig. 8 illustrates that bubbles are well distributed in the radial direction. Although raising the rotational speed results in better distribution of bubbles and larger interfacial area, the limiting factors should be also considered. High shear stress not only increases the operating cost, power consumption, also distracts the suitable environment for bioactivity. Therefore, it cannot be concluded that increasing the rotational speed necessarily enhances the bioreactor efficiency and requires more investigation from the microbial view point [4].

4.2. Velocity contour

A combined CFD-PBM model was applied in this study to enhance the understanding of flow visualization inside the multiphase stirred reactor as demonstrated in Fig. 9a, b, and c. To study the impact of impeller speed on the flow field, the gas flow rate is kept constant at 1.8 LPM, and the impeller rotational speed varies from 25 to 150 rpm. The color intensity of contours and streamlines indicates the magnitude of velocity in each region. According to Fig. 9, the flow field generated by the impeller mostly develops in the axial direction leading to the weak flow movement near the bottom and top of the vessel and around the shaft. Fig. 9 also indicates that an increase in the rotational speed resulting in a higher liquid velocity in the system. The results in this figure demonstrate the insufficient mixing pattern in 25 rpm, where there are some stagnant regions at the top and bottom of the tank, as well as near the shaft. The stagnant regions have been highlighted by purple rectangular box and circles. As a result, the channelling happens around the impeller outer edge at 25 rpm. It can be seen that an increase in the rotational speed of the impeller leads to reducing the stagnant regions. However, having a higher rotational speed requires more energy consumption which influences the operational and maintenance costs. The flow field contours indicate that doubling the rotational speed from 75 to 150 rpm does not have any significant contribution to the removal of stagnant regions, while the energy consumption increases remarkably. In addition, a high rotational speed of more than a certain level could destroy the microbial growing and seedling environment.

Additionally, the high performance of a dual helical ribbon rather than the other types of impellers has been confirmed previously by literature [7,41]. This study indicated that the uniformity of fluid approximately has been achieved at 75 rpm. Additionally, the stagnant regions are not observed in the whole system at 75 rpm. In this case, operating the system at a higher rotational speed does not contribute to mixing performance. Previous experimental findings also suggest that increasing the impeller speed up to an optimum certain level could enhance the performance of the mixing system [23]; While beyond that level, the power consumption only rises sharply with a limited positive contribution to the mixing performance [23].

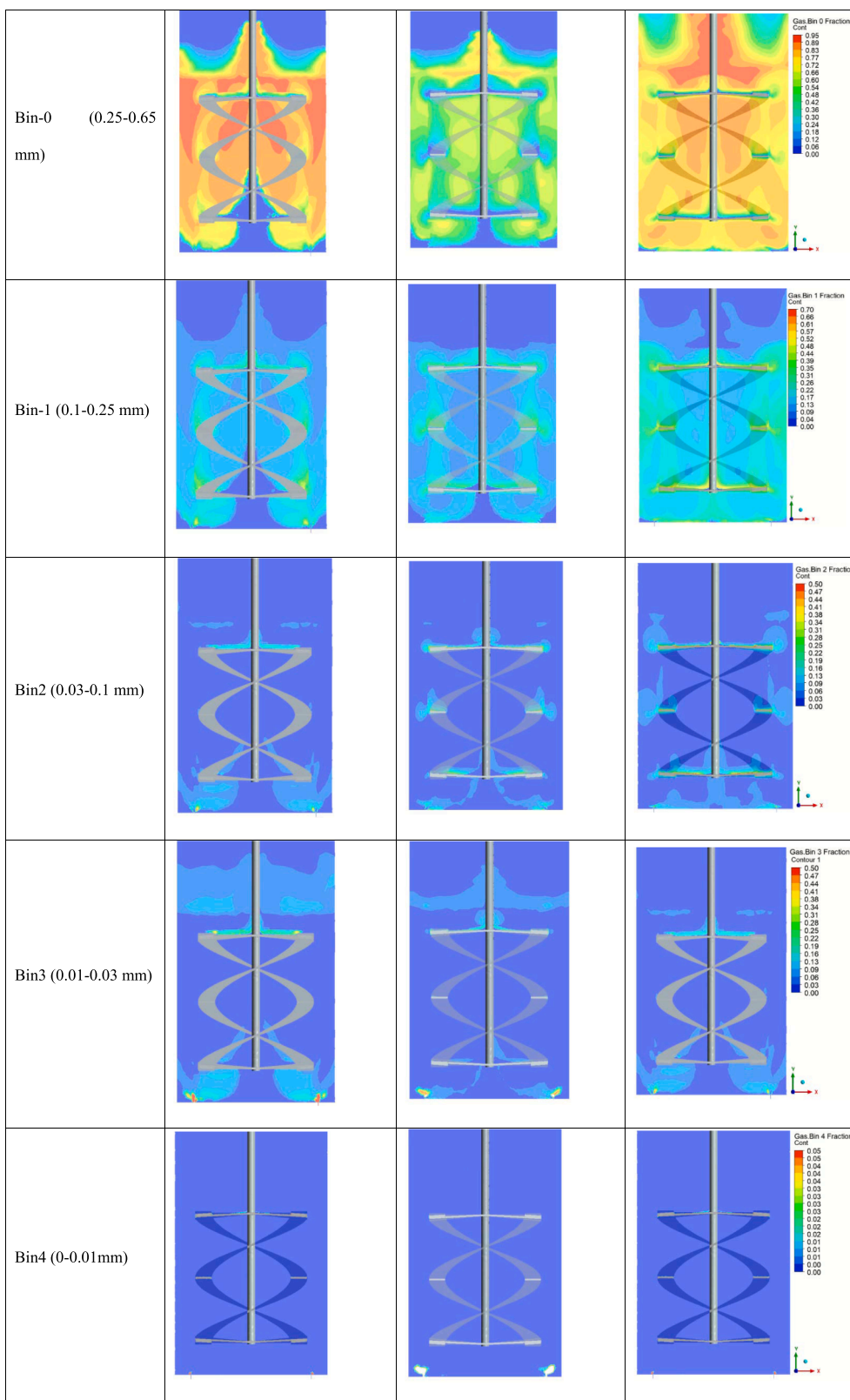


Fig. 7. Bubble size distribution at rotational speed 25 rpm, column 2; 75 rpm, column 3; and 150 rpm, column 4.

4.3. Effective viscosity contour

Fig. 10 shows the sensitivity and dependency of the effective viscosity of NaCMC as a shear-thinning fluid to the shear stress induced by the blade rotating at various speeds of 25, 75, 150 rpm. The results are

compared in two perpendicular positions of blades as shown in Fig. 10. According to the previous experiments carried out by the same authors [23], the viscosity of the diluted solution of NaCMC (0.5 %WT) varies between 0.15 and 0.3 Pa s when the shear rate is between 20 and 200 rpm [19]. The CFD prediction contours shown in Fig. 10 indicate that

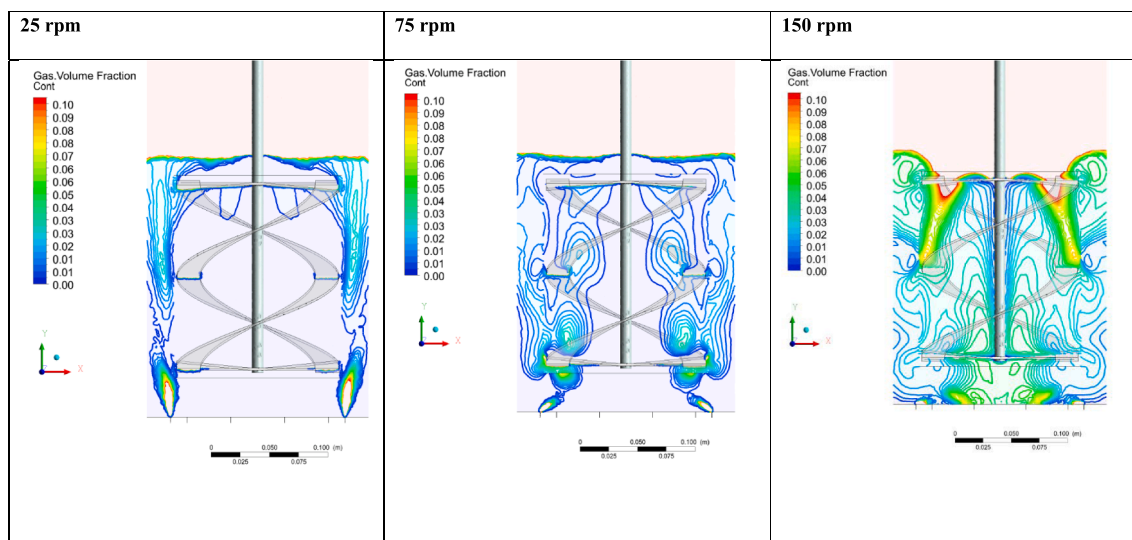


Fig. 8. Gas volume fraction profile at rotational speed 25, 75, and 150 rpm.

the rotating blade causes fluid–structure destruction leading to a decrease in the effective viscosity to 0.17 Pa s.

Fig. 10a indicates that when the rotational speed is around 25 rpm, the viscosity shows a significant drop leading to enhancement of the mixing pattern. In this case, the fluid polymer network is destroyed due to the shear stress induced by the blades and consequently, the bubble upward movement facilitates due to the lower effective viscosity of the fluid. By increasing the speed up to 75 and beyond, some high viscous regions were formed with a time delay where the blade passed quickly which are shown in Fig. 10b and 10c. Due to the high rotational speed, the contact time between the blade and fluid–structure is not enough to transfer the shear stress from the blade to the adjacent fluid layer. In other words, blades are quickly slipping over the layer of fluid, while the shear still has not completely transferred to the fluid layers leading to the development of several static vortices. Consequently, the likelihood of bubble trapping in static vortices increases leading to forming stagnant regions and incomplete mixing.

It can be concluded that increasing the rotational speed of the impeller could not always contribute positively to enhancing the mixing pattern. By gradually increasing the rotational speed, vortices have been formed in some regions which disturb the biomass activities, the interaction between phases, and heat and mass transfer. Therefore, it is suggested that the best impeller speed and optimum mixing pattern should be studied for each non-Newtonian fluid separately based on its rheological characteristics.

5. Conclusions

A combination of CFD and Population balance model was applied to evaluate the performance of a dual helical ribbon impeller on the size distribution of bubbles, hydrodynamic behavior, and viscosity of a shear-thinning fluid. The standard $k - \epsilon$ model and Eulerian-Eulerian (E-E) multiphase approach was considered to solve the governing equations. Further, a discrete method was applied to predict the bubbles' deformation. A mesh independence test was carried out to check the grid sensitivity of the model. The results of CFD simulation were verified by the PIV tests under the same operating conditions.

By increasing the rotational speed of the impeller from 25 to 150 rpm, the rate of bubble coalescence reduces, while the likelihood of bubble breakage increases. Bubble coalescence happens at a lower speed because the bubbles are skewed from the outer edge of the blades and trapped in gel-like structure of fluid leading to an increase in the chance of striking and merging. When the rotational speed increases, not only

destroying the gel structure of the fluid, but also bubbles hit the blades and walls of the cylinder resulting in bubble breakage. Therefore, by increasing the rotational speed, bubble distribution improves and enhances the interfacial area.

The CFD results showed that the gas holdup reduces when the impeller rotates with a low speed. The maximum gas hold-up occurs at 150 rpm. It seems that maximizing the interfacial area and gas hold-up positively contributes to improving the mass transfer between the liquid and gas-phases. Therefore, the influence of rotational speed on heat and mass transfer for a shear-thinning fluid needs to be investigated further for this specific type of impeller.

At lower rotational speed, poor mixing was observed in the system, which can be improved by increasing the speed of the impeller. However, after a certain level of shear stress, several parameters act as limiting factors like power consumption, operational and maintenance costs, the level of shear stress tolerating by substrate, and fluid. In other words, the working and operating conditions of a particular mixer should be specified through optimization methods based on the type and size of the impeller and vessel, rheological, chemical, and physical characteristics of the fluid, and the level of shear stress and temperature tolerated by microorganisms.

The results obtained by experiment and CFD predictions indicated that by raising the impeller speed, viscosity drops from 0.3 to 0.17 Pa s. However, an increase in the rotational speed of the impeller does not necessarily enhance the mixing pattern of a shear thinning fluid. By increasing the rotational speed beyond 75 rpm, there is not enough time to transferring the shear stress from the blade to the non-Newtonian fluid surrounding the impeller. Consequently, some static vortices form leading to poor mixing. It is suggested that the sensitivity of microorganism to the different shear stress level to be tested. Since the desire and optimum mixing pattern should be achieved based on not only the rheological characteristics of a non-Newtonian fluid (substrate) but the level of shear stress which can be tolerated by microorganism.

CRedit authorship contribution statement

Maryam Amirafabi: Conceptualization, Data curation, Formal analysis, Investigation, Writing, Methodology, Validation, Original draft. **Mehdi Khiadani:** Conceptualization, Methodology, Project administration, Supervision, Validation, Review and editing. **Hussein A. Mohammed:** Conceptualization, Software Supervision, Methodology, Supervision, Review and editing. **Arslan Arshad:** Data Curation, Visualization.

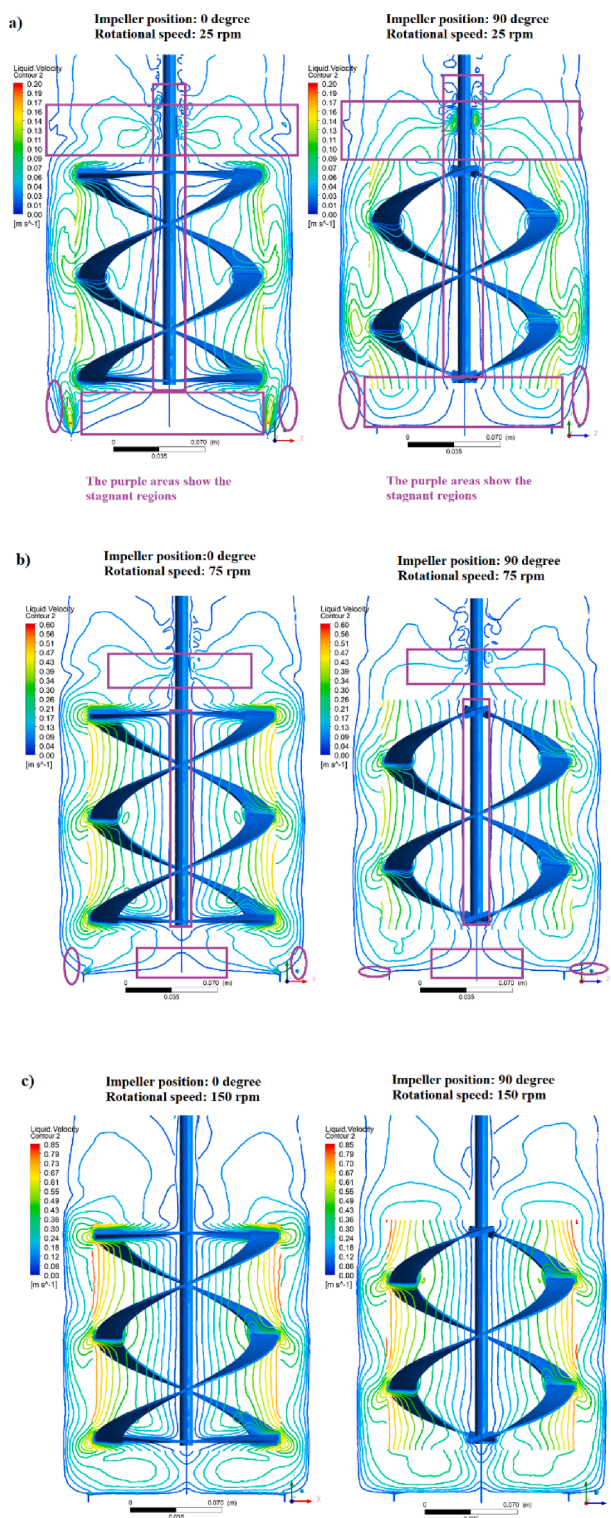


Fig. 9. Flow field and velocity magnitude at rotational speeds 25, 75, and 150 rpm at two perpendicular positions of blades.

Declaration of Competing Interest

The authors declare that they have no known competing financial interests or personal relationships that could have appeared to influence the work reported in this paper.

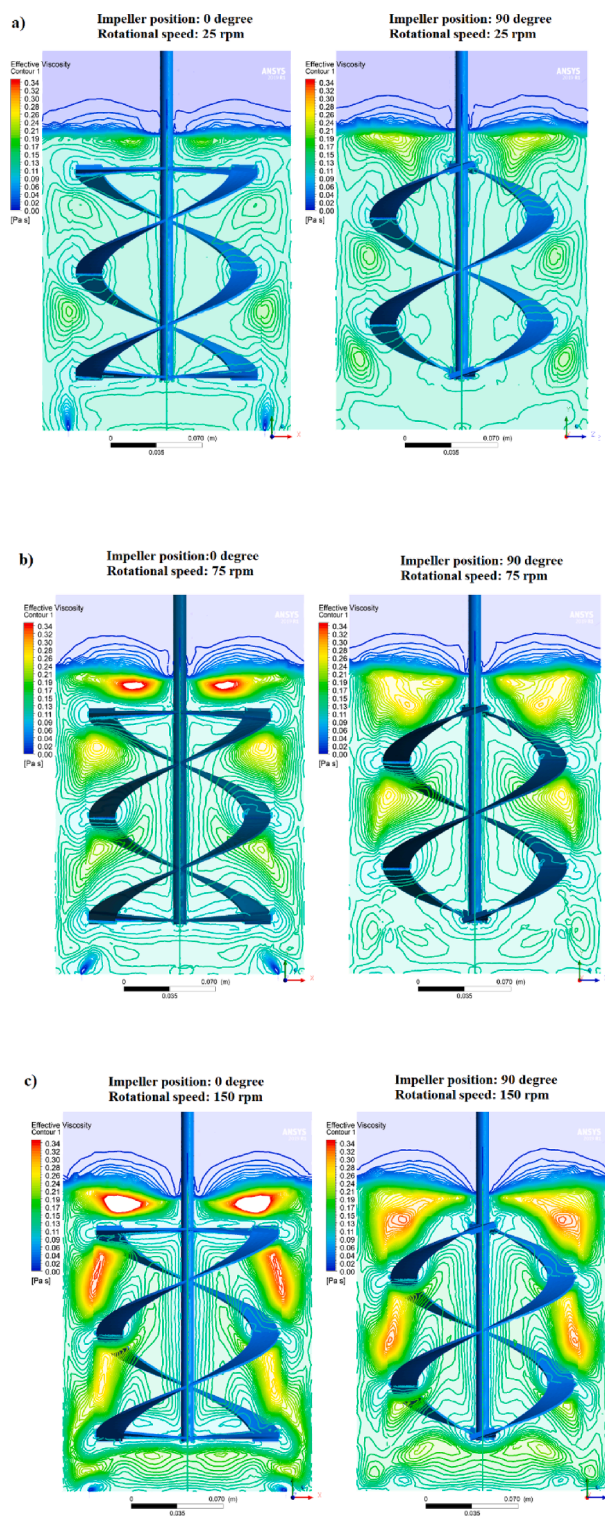


Fig. 10. Changes in effective viscosity based on rotational speeds 25, 75, and 150 rpm and two perpendicular blade positions.

References

- [1] J. Jiang, J. Wu, S. Poncin, H.Z. Li, Effect of hydrodynamic shear on biogas production and granule characteristics in a continuous stirred tank reactor, *Process Biochem.* 51 (2016) 345–351, <https://doi.org/10.1016/j.procbio.2015.12.014>.
- [2] M. Gumulya, J.B. Joshi, R.P. Utikar, G.M. Evans, V. Pareek, Bubbles in viscous liquids: Time dependent behaviour and wake characteristics, *Chem. Eng. Sci.* 144 (2016) 298–309, <https://doi.org/10.1016/j.ces.2016.01.051>.
- [3] D. Fernandes del Pozo, A. Liné, K.M. Van Geem, C. Le Men, I. Nopens, Hydrodynamic analysis of an axial impeller in a non-Newtonian fluid through

- particle image velocimetry, *AIChE J.* 66 (2020), <https://doi.org/10.1002/aic.16939>.
- [4] P. Doran, *Bioprocess Engineering Principles*, Harcourt Brace & Company, 1995.
- [5] Z. Trad, C. Vial, J.P. Fontaine, C. Larroche, Modeling of hydrodynamics and mixing in a submerged membrane bioreactor, *Chem. Eng. J.* 282 (2015) 77–90, <https://doi.org/10.1016/j.cej.2015.04.119>.
- [6] A. Eftaxias, V. Diamantis, C. Michailidis, K. Stamatelatou, A. Aivasidis, Comparison of anaerobic digesters performance treating palmitic, stearic and oleic acid: determination of the LCFA kinetic constants using ADM1, *Bioprocess Biosyst. Eng.* 43 (2020) 1329–1338, <https://doi.org/10.1007/s00449-020-02328-2>.
- [7] H. Ameur, Energy efficiency of different impellers in stirred tank reactors, *Energy* 93 (2015) 1980–1988, <https://doi.org/10.1016/j.energy.2015.10.084>.
- [8] M.R. Shahnazari, Z. Ahmadi, L.S. Masooleh, Perturbation analysis of heat transfer and a novel method for changing the third kind boundary condition into the first kind, *J. Porous Media* 20 (2017) 449–460, <https://doi.org/10.1615/jpormedia.v20.i5.60>.
- [9] L. Samandari-Masouleh, N. Mostoufi, A. Khodadadi, Y. Mortazavi, M. Maghrebi, Modeling the growth of carbon nanotubes in a floating catalyst reactor, *Ind. Eng. Chem. Res.* 51 (2012) 1143–1149, <https://doi.org/10.1021/ie201137j>.
- [10] L. Niño, M. Peñuela, G.R. Gelves, Gas-liquid hydrodynamics simulation using CFD in a helical ribbon impeller applied for non-Newtonian fluids, *Int. J. Appl. Eng. Res.* 13 (2018) 9353–9359.
- [11] S. Miryahyaei, K. Olinga, M.S. Ayub, S.S. Jayaratna, M. Othman, N. Eshtiaghi, Rheological measurements as indicators for hydrolysis rate, organic matter removal, and dewaterability of digestate in anaerobic digesters, *J. Environ. Chem. Eng.* 8 (2020), 103970, <https://doi.org/10.1016/j.jece.2020.103970>.
- [12] L. Samandari-Masouleh, N. Mostoufi, A.A. Khodadadi, Y. Mortazavi, M. Maghrebi, Kinetic modeling of carbon nanotube production and minimization of amorphous carbon overlayer deposition in floating catalyst method, *Int. J. Chem. React. Eng.* 10 (2012), <https://doi.org/10.1515/1542-6580.2972>.
- [13] Y. Bao, Y. Lu, Q. Liang, L. Li, Z. Gao, X. Huang, S. Qin, Power demand and mixing performance of coaxial mixers in a stirred tank with CMC solution, *Chinese J. Chem. Eng.* 23 (2015) 623–632, <https://doi.org/10.1016/j.cjche.2015.01.002>.
- [14] A. Lebranchu, S. Delaunay, P. Marchal, F. Blanchard, S. Pacaud, M. Fick, E. Olmos, Impact of shear stress and impeller design on the production of biogas in anaerobic digesters, *Bioresour. Technol.* 245 (2017) 1139–1147, <https://doi.org/10.1016/j.biortech.2017.07.113>.
- [15] H. Ameur, Y. Kamla, D. Sahel, Performance of helical screw impellers for mixing of viscous liquids in cylindrical reactors, *ChemistrySelect* 2 (2017) 1891–1894, <https://doi.org/10.1002/slct.201602072>.
- [16] B. Oyegbile, G. Akdogan, Hydrodynamic characterization of physicochemical process in stirred tanks and agglomeration reactors, *Lab. Unit Oper. Exp. Methods Chem. Eng.* (2018), <https://doi.org/10.5772/intechopen.77014>.
- [17] M. Basavarajappa, T. Draper, P. Toth, T.A. Ring, S. Miskovic, Numerical and experimental investigation of single phase flow characteristics in stirred tanks using Rushton turbine and flotation impeller, *Miner. Eng.* 83 (2015) 156–167, <https://doi.org/10.1016/j.mineng.2015.08.018>.
- [18] H. Ameur, A. Ghenaim, Mixing of complex fluids in a cylindrical tank by a modified anchor impeller, *ChemistrySelect* 3 (2018) 7472–7477, <https://doi.org/10.1002/slct.201801047>.
- [19] M. Amirafabi, Mehdi Khiadani, Transparent polymers to emulate the rheological properties of primary, activated, and digested sludge, *Chem Eng. Res. Des.* (2019), <https://doi.org/10.1016/j.mex.2019.03.017>.
- [20] K.M. Dhanasekharan, J. Sanyal, A. Jain, A. Haidari, A generalized approach to model oxygen transfer in bioreactors using population balances and computational fluid dynamics, *Chem. Eng. Sci.* 60 (2005) 213–218, <https://doi.org/10.1016/j.ces.2004.07.118>.
- [21] B.C.H. Venneker, J.J. Derksen, H.E.A. Van den Akker, Population balance modeling of aerated stirred vessels based on CFD, *AIChE J.* 48 (2002) 673–685, <https://doi.org/10.1002/aic.690480404>.
- [22] M.J. Hounslow, R.L. Ryall, V.R. Marshall, A discretized population balance for nucleation, growth, and aggregation, *AIChE J.* 34 (1988) 1821–1832, <https://doi.org/10.1002/aic.690341108>.
- [23] M. Amirafabi, M. Khiadani, H.A. Mohammed, Performance of a dual helical ribbon impeller in a two-phase (gas-liquid) stirred tank reactor, *Chem. Eng. Process. – Process Intensif.* 148 (2020), 107811, <https://doi.org/10.1016/j.cep.2020.107811>.
- [24] L. Wiedemann, F. Conti, T. Janus, M. Sonnleitner, W. Zörner, M. Goldbrunner, Mixing in biogas digesters and development of an artificial substrate for laboratory-scale mixing optimization, *Chem. Eng. Technol.* 40 (2017) 238–247, <https://doi.org/10.1002/ceat.201600194>.
- [25] M.S. Amirafabi, N. Mostoufi, M. Hosseinzadeh, M.R. Mehrnia, Reduction of membrane fouling by innovative method (injection of air jet), *J. Environ. Heal. Sci. Eng.* 12 (2014) 1–8, <https://doi.org/10.1186/s40201-014-0128-0>.
- [26] B.A. Ali, S. Pushpavanam, Analysis of unsteady gas – liquid flows in a rectangular tank : Comparison of Euler – Eulerian and Euler – Lagrangian simulations, *Int. J. Multiph. Flow.* 37 (2011) 268–277, <https://doi.org/10.1016/j.ijmultiphaseflow.2010.10.002>.
- [27] Y. Sato, M. Sadatomi, Momentum and heat transfer in two-phase bubble flow, *Int. J. Multiph. Flow.* 7 (1981) 167–177.
- [28] F. Scargiali, A. D’Orazio, F. Grisafi, A. Brucato, Modelling and simulation of gas - Liquid hydrodynamics in mechanically stirred tanks, *Chem. Eng. Res. Des.* 85 (2007) 637–646, <https://doi.org/10.1205/cherd06243>.
- [29] B. Liu, F. Fan, X. Chen, J. Liu, Z. Jin, The influence of impeller combination on the gas-liquid dispersion performance of a coaxial mixer in viscous fluids, *Int. J. Chem. React. Eng.* 15 (2017), <https://doi.org/10.1515/ijcre-2016-0191>.
- [30] X. Guan, X. Li, N. Yang, M. Liu, CFD simulation of gas-liquid flow in stirred tanks: effect of drag models, *Chem. Eng. J.* (2019), <https://doi.org/10.1016/j.cej.2019.04.134>.
- [31] E. Brito-De La Fuente, L. Choplin, P.A. Tanguy, Mixing with helical ribbon impellers: effect of highly shear thinning behaviour and impeller geometry, *Chem. Eng. Res. Des.* 75 (1997) 45–52, <https://doi.org/10.1205/026387697523381>.
- [32] V. V. Ranade, *Computational Flow Modeling for Chemical Reactor Engineering*, Volume 5 (Process Systems Engineering), (2001) 480. <http://www.amazon.com/Computational-Modeling-Chemical-Reactors-Engineering/dp/0125769601>.
- [33] D.L. Marchisio, R.D. Vigil, R.O. Fox, Quadrature method of moments for aggregation-breakage processes, *J. Colloid Interface Sci.* 258 (2003) 322–334, [https://doi.org/10.1016/S0021-9797\(02\)00054-1](https://doi.org/10.1016/S0021-9797(02)00054-1).
- [34] A. Tomiyama, I. Žun, H. Higaki, Y. Makino, T. Sakaguchi, A three-dimensional particle tracking method for bubbly flow simulation, *Nucl. Eng. Des.* 175 (1997) 77–86, [https://doi.org/10.1016/S0029-5493\(97\)00164-7](https://doi.org/10.1016/S0029-5493(97)00164-7).
- [35] X. Jiang, N. Yang, B. Yang, Computational fluid dynamics simulation of hydrodynamics in the riser of an external loop airlift reactor, *Particology.* 27 (2016) 95–101, <https://doi.org/10.1016/j.partic.2015.05.011>.
- [36] J.C. Baudez, P. Slatter, N. Eshtiaghi, The impact of temperature on the rheological behaviour of anaerobic digested sludge, *Chem. Eng. J.* 215–216 (2013) 182–187, <https://doi.org/10.1016/j.cej.2012.10.099>.
- [37] B.V. Machon, M. Jahoda, Liquid Homogenization in Aerated Multi-Impeller Stirred Vessel, *Technol. Med. Sci.* 23 (2012) 1–1. doi: <http://dx.doi.org/10.1201/b11330-2>.
- [38] T.D. Canonsburg, *ANSYS Fluent User’s Guide*, 15317 (2013) 724–746.
- [39] *ANSYS Fluent User’s Guide*, No Title, (n.d.).
- [40] R.P. Chhabra, J.F. Richardson, *Non-Newtonian Flow in the Process Industries* British Library Cataloguing in, Publication Data, 1999.
- [41] H. Ameur, M. Bouzit, A. Ghenaim, Hydrodynamics in a vessel stirred by simple and double helical ribbon impellers, *Cent. Eur. J. Eng.* 3 (2013) 87–98, <https://doi.org/10.2478/s13531-012-0045-x>.

Chapter 6: CFD-PBM and experimental investigation of a shear thinning fluid in a gas-liquid tank agitated by a helical ribbon impeller

the Reynold number for a helical ribbon impeller which is obtained by Fuente et al. (Brito-De La Fuente, Choplin, and Tanguy 1997).

$$Re = \rho \frac{Nd^2}{\mu_{eff}} \quad \text{Equation 6-9}$$

6.4.2 Turbulence model

The $k - \varepsilon$ model was adopted in the proposed study to model the turbulence. This model has two equations written for a mixture of two phases.

$$\frac{\partial}{\partial t} (\rho_m k) + \nabla \cdot (\rho_m \vec{v}_m k) = \nabla \cdot \left(\frac{\mu_{t,m}}{\delta_k} \nabla k \right) + G_{k,m} - \rho_m \varepsilon \quad \text{Equation 6-10}$$

$$\frac{\partial}{\partial t} (\rho_m \varepsilon) + \nabla \cdot (\rho_m \vec{v}_m \varepsilon) = \nabla \cdot \left(\frac{\mu_{t,m}}{\delta_\varepsilon} \nabla \varepsilon \right) + C_{1\varepsilon} G_{k,m} - C_{2\varepsilon} \rho_m \varepsilon \quad \text{Equation 6-11}$$

where, k is the turbulent kinetic energy, G is the generation of turbulent kinetic energy, and ε is the dissipation rate. The mixture of these properties can be found from the following equations:

$$\rho_m = \sum_{i=1}^n \alpha_i \rho_i \quad \text{Equation 6-12}$$

$$\vec{v}_m = \frac{\sum_{i=1}^n \alpha_i \rho_i \vec{v}_i}{\sum_{i=1}^n \alpha_i \rho_i} \quad \text{Equation 6-13}$$

$$\mu_{t,m} = \rho_m C_\mu \frac{k^2}{\varepsilon} \quad \text{Equation 6-14}$$

Further, values for these equations ($C_\mu = 0.09$, $C_{1\varepsilon} = 1.44$, and $C_{2\varepsilon} = 1.92$) were extracted from previous literature (Ranade 2001).

6.4.3 Population balance model (PBM)

Computational Fluid Dynamics (CFD) simulation is a powerful method for predicting the hydrodynamics of complex multiphase agitated systems; however, this method does not show

Chapter 6: CFD-PBM and experimental investigation of a shear thinning fluid in a gas-liquid tank agitated by a helical ribbon impeller

change in bubble size. Thus, the CFD-PBM coupled method has been suggested within the literature in order to calculate change in bubble size (Marchisio, Vigil, and Fox 2003).

The size of bubbles can change during the process of mixing based on changes in liquid properties as most of applied fluids are non-Newtonian. Therefore, it is important to use the CFD-PBM method in order to better predict bubble coalescence and breakage.

The integrated CFD-PBM method is derived from the Boltzmann statistical transport equation, to simulate \ unsteady multiphase phenomenon such as lift (Tomiya et al. 1997), drag (X. Jiang, Yang, and Yang 2016), and mass transfer modeling. This method describes the bubble entering/ leaving defined control volume.

$$\frac{\partial}{\partial t} n(\vec{x}, V_b, t) + \frac{\partial}{\partial z} [n(\vec{x}, V_b, t) u_b(\vec{x}, V_b)] + \frac{\partial}{\partial V_b} [n(\vec{x}, V_b, t) \frac{\partial}{\partial t} V_b(\vec{x}, V_b)] = S(\vec{x}, V_b, t) \text{ Equation}$$

6-15

where $n(\vec{x}, V_b, t)$ indicates bubble density distribution function at the time of t and a position of \vec{x} . V_b refers to the volume of bubbles, u_b shows the local velocity of bubbles, and $S(\vec{x}, V_b, t)$ is a source term including bubble sink or source in different situations including coalescence, breakage, phase interactions, reaction, and mass transfer. The Lue and Svendsen models suggested by ANSYS Fluent user Guid has been considered in this study to model the bubble coalescence and breakup (Baudez, Slatter, and Eshtiaghi 2013; B. V Machon and Jahoda 2012; Canonsburg 2013).

The discrete method was used to solve the PBM equation, discretised into five interval bubble diameters in this study. By using this method, the bubble breakage can be modelled based on the interaction between bubbles and turbulent eddies, which leads to simulate the bubble deformation. The average bubble diameter was calculated by tracking 40 bubbles obtained through the experimental phase (M. Amirafabi, Khiadani, and Mohammed 2020). The maximum bubble size, which was observed in image processing analysis, was 7 mm and the smallest one was 0.1 mm. More than 80% of the bubbles had a diameter in the range of 3 to 5

Chapter 6: CFD-PBM and experimental investigation of a shear thinning fluid in a gas-liquid tank agitated by a helical ribbon impeller

mm, which can be categorized in the first and second bubble intervals (Laakkonen, Honkanen, et al. 2005).

6.5 Solution domain, mesh generation and boundary conditions

6.5.1 Mesh Processing

Design modeler and ICEM 18.2 were used to construct three-dimensional geometry of the reactor used in the experiment. An unstructured meshing method, coupled with the Multiple Reference Frame (MRF) approach, was applied to generate five different 3-D mesh topologies as shown in Figure 6-3. In the MRF method, the domain was divided into two different regions; the stationary outer region, and the rotating inner part that is rotated by the impeller. A finer mesh was applied inside the inner cylinder surrounding the impeller as the flow pattern in this region is an important parameter. Having finer mesh can enhance flow capture and improve the accuracy of results around the impeller region. Additionally, the outer layer is defined as a non-rotating domain with coarse mesh.

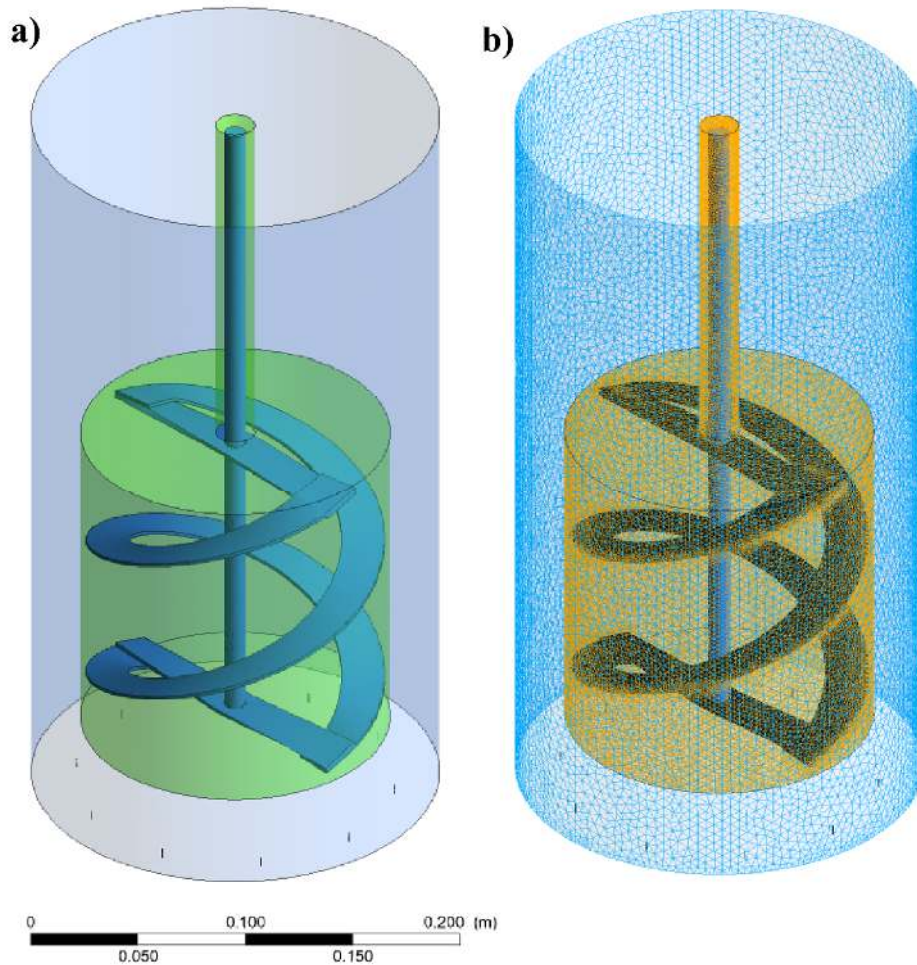


Figure 6-3 Schematic view of the reactor with dual helical ribbon impeller; a) MRF zones, b) mesh topology.

A mesh independence study was carried out for five different numbers of cells by testing the average velocity of the liquid at 15 cm above the bottom of the reactor. Increasing cell numbers changed the average velocity remarkably. However, the average velocity tended to be stable after 6×10^6 cells, as shown in Figure 6-4.

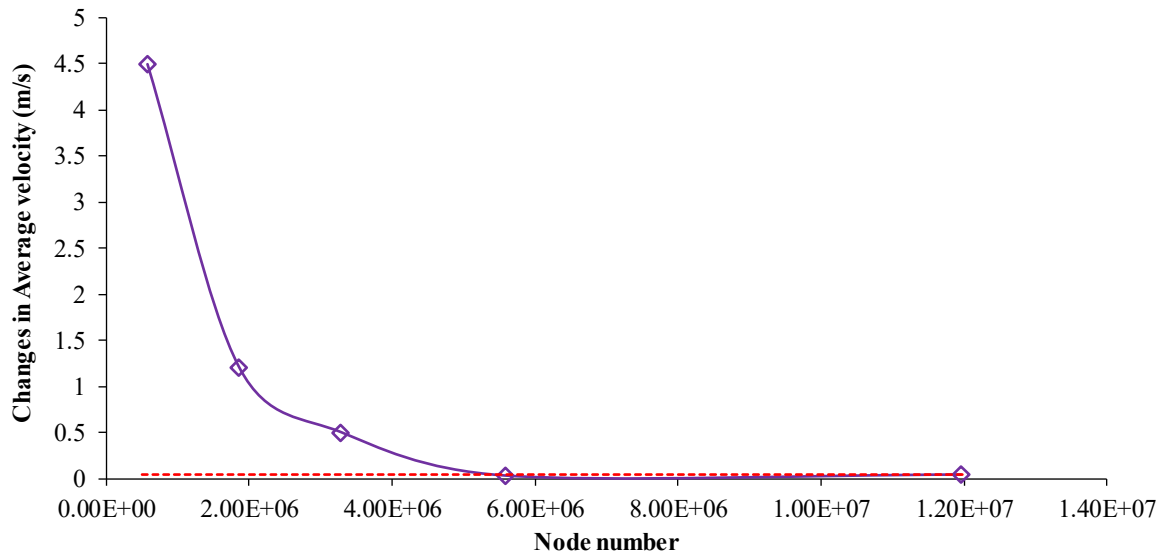


Figure 6-4 The model grid sensitivity analysis

6.5.2 Solver setup and boundary conditions

ANSYS Fluent R19.1 double precision solver was applied to run the simulation and to define boundary conditions. The Eulerian-Eulerian model has been applied in this study to build momentum and continuity equation for phases. The convergence rate was enhanced by solving the momentum and pressure-based continuity equations using SIMPLE method (ANSYS Fluent User's Guide, n.d.). The maximum iteration number is set to 1000 for a time step of 0.001 s.

Further, the volume fraction parameters has been set in multiphase model dialoge box as explicite scheme which is time-dependent. The modified HRIC are applied here because there is a sharp interfaces between both phases.

In addition, the Reynolds number varied between 10-1000 according to previous experimental tests (M. Amirafabi, Khiadani, and Mohammed 2020). Reynolds numbers indicate a system is working in a transient regime involving both viscous and inertial forces. For this reason, the system should be modeled by either laminar or turbulent flow regimes (Chhabra and Richardson 1999).

Chapter 6: CFD-PBM and experimental investigation of a shear thinning fluid in a gas-liquid tank agitated by a helical ribbon impeller

The initial and boundary conditions in the model were considered identical to the experimental operational conditions. The nozzle holes on the top surface of the sparger were assumed as velocity inlet with a gas fraction equal to 1. Further, the body of the cylinder was treated as a standard with no slipping wall. The boundary condition at the top of the cylinder, which is the degassing part, is considered as a pressure outlet. The whole cylinder was employed as a liquid region with a height of 0.24 m and a gas volume fraction of 0. The rotating wall situation was applied for the impeller body and its shaft. In this work, the air bubble size was considered in the range of 0.1 and 7 mm based on experimental data gathered through the image processing method (Laakkonen, Honkanen, et al. 2005). It should be noted here that the rheological properties of the non-Newtonian fluid follow the Power-Law model based on previous studies (M. Amirafabi and Khiadani Mehdi 2019a).

6.5.3 Model validation

Two different methods were applied to validate the CFD results in both gas and liquid phases. First, the average rising velocity for 40 bubbles in pure water was considered to in order verify gas velocity predicted by CFD simulation. Second, both the velocity magnitude and flow field of the liquid phase were captured using PIV measurement to validate the hydrodynamics of the liquid phase.

6.6 Gas velocity

The mean bubble velocity calculated by CFD-PBM was compared to the calculated average velocity obtained from the experiments and image processing (Laakkonen, Honkanen, et al. 2005). The validation tests were carried out in two different initial airflow rates of 0.5 and 2 LPM which are shown in Figure 6-5. The bubble motion was recorded using a high-speed camera (Samsung digital Camera 12 M P with speed of 1.4 μm including dual-pixel autofocus)

for further evaluation by image J software. The mean velocity for bubbles has been calculated for 10 sec after stabilizing the system.

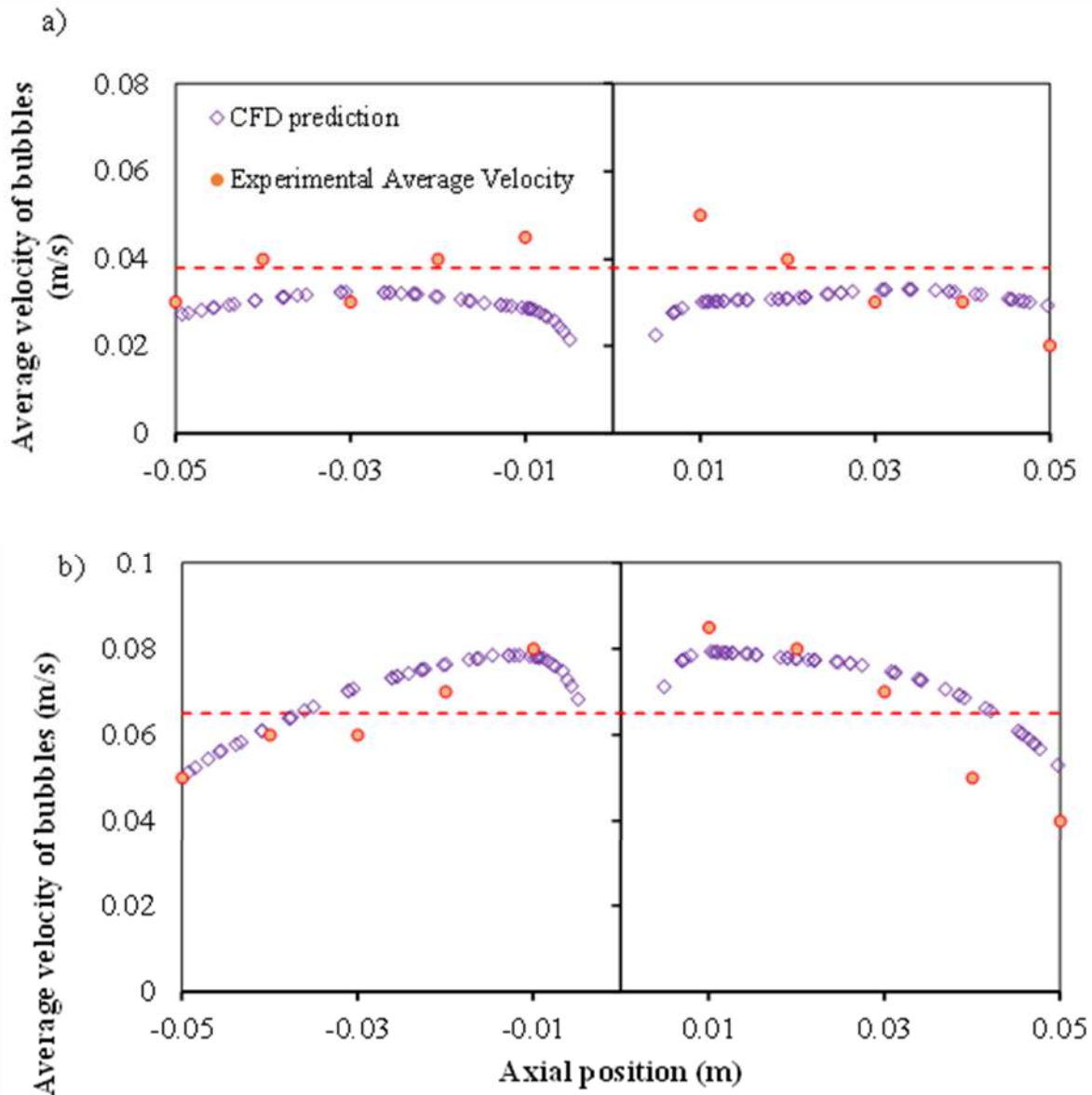


Figure 6-5 Comparison of average velocities obtained from experiment and CFD simulation for the initial gas flowrates: a) 0.5 LPM and b) 2 LPM when the impeller speed is equal to 0.

6.7 Hydrodynamics

The capture and distinction of the flow field using PIV is extremely challenging when a large impeller rotates in a two-phase reactor, due to the interference and interaction of moving bubbles with impeller shadows. To reduce the interference of gas flow, a filtered lens and fluorescent dye were applied. Despite this measure, the PIV still captured some sparged gas

Chapter 6: CFD-PBM and experimental investigation of a shear thinning fluid in a gas-liquid tank agitated by a helical ribbon impeller

and bubbles accumulated on the back of the blades, which interfered with the results. Figures 6-6 a and 6-6 b show both the velocity vectors and magnitude captured by CFD and PIV at 75 and 150 rpm, respectively.

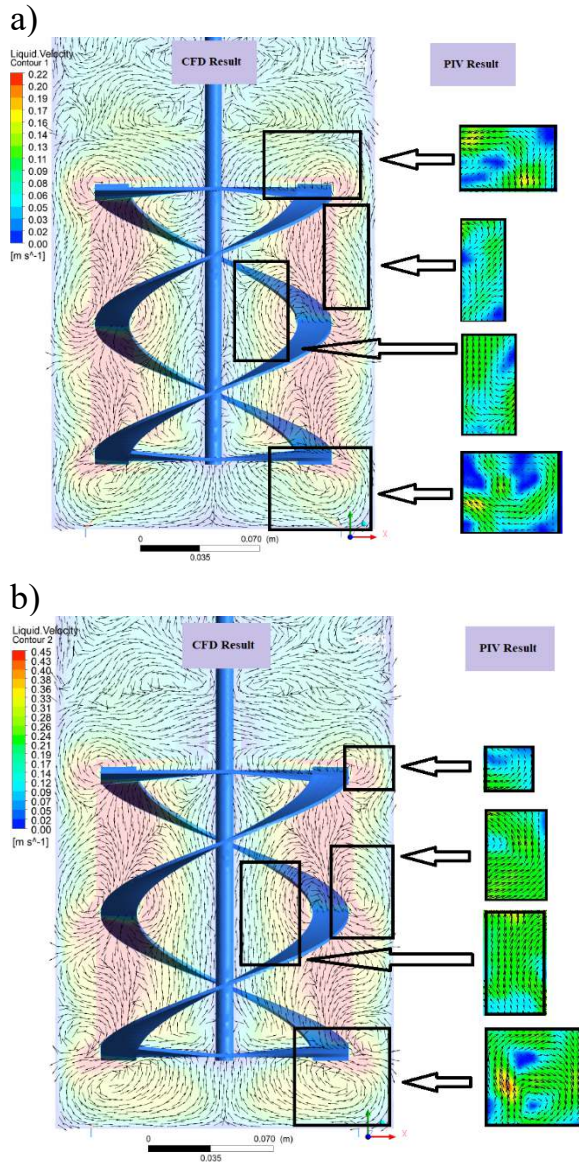


Figure 6-6 Comparison of the flow field and velocity magnitude between CFD simulation (left Image) and PIV measurements (right image); at a) 75 rpm, and b) 150 rpm

The overall flow shows a similar pattern in different regions including the upper, middle, and bottom of the impeller, which are identified by large red vectors. In addition, the velocity magnitude captured by PIV is approximately equal to CFD prediction when the rotational speed of the impeller is at 75 rpm. Whilst at 150 rpm the direction of velocity vectors captured by the

PIV show similar results to CFD results, the velocity magnitudes estimated by CFD are higher than the values obtained from PIV measurements.

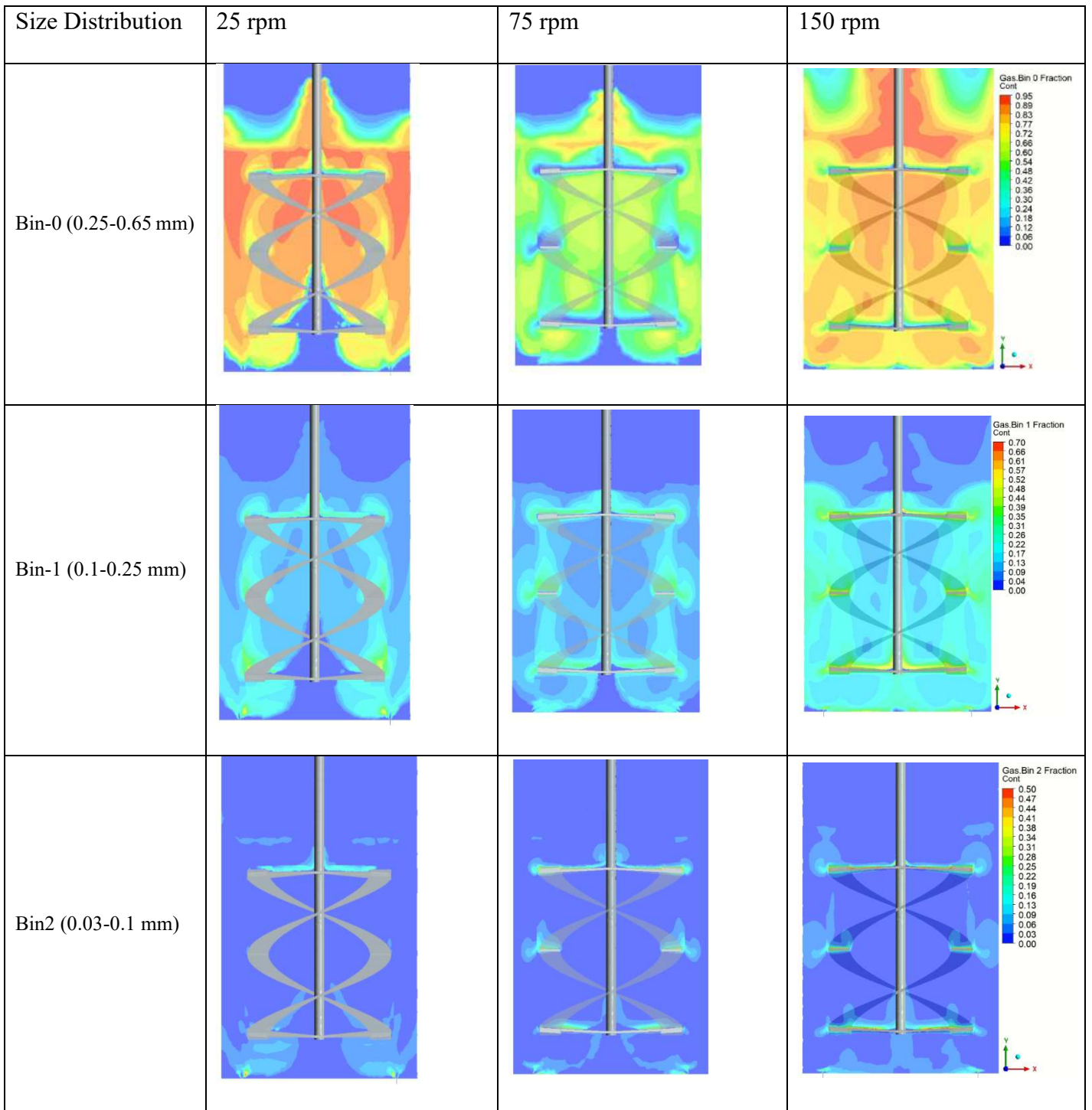
6.8 Results and discussion

6.8.1 Effect of impeller speed on bubble size distribution and gas holdup

The size distribution of bubbles can be evaluated by breakage and coalescence rates, which are governed by the dissipation rate of kinetic energy. Figure 6-7 shows bubble size distribution at three rotational impeller speeds of 25, 75, and 150 rpm.

At the lower rotational speed, it can be observed that the flow is channelled into the outer edge of the blades. This can be also observed in Figure 6-8, indicating the total gas fractions for different rotational speeds of 25, 75, and 150 rpm. Fig. 6-8 also demonstrates that low impeller speed has an insignificant effect on the hydrodynamics of the gas phase. Therefore, bubbles can skew, move more slowly, or possibly become stuck in the gel-like structure of the fluid. Accordingly, it can be concluded that coalescence is a predominant phenomenon when impeller speed is too low. As a result, the interfacial area between two phases reduces, negatively influencing interphase mass and heat transfer. CFD results indicate that the bubble size changes between 0.25 to 0.65 mm due to coalescence at 25 rpm. When increasing impeller speed from 25 to 75 rpm, bubbles scatter throughout the system due to induced shear stress. Accelerated bubbles hit the wall of the vessel and blades, resulting in breakage. Simultaneously, accelerated bubbles may strike together and merge to form a larger bubble through the coalescence process. Simultaneous breakage and coalescence of bubbles can result in homogeneous distribution of various bubble size in the range of 0.25 to 0.65 mm at 75 rpm.

Chapter 6: CFD-PBM and experimental investigation of a shear thinning fluid in a gas-liquid tank agitated by a helical ribbon impeller



Chapter 6: CFD-PBM and experimental investigation of a shear thinning fluid in a gas-liquid tank agitated by a helical ribbon impeller

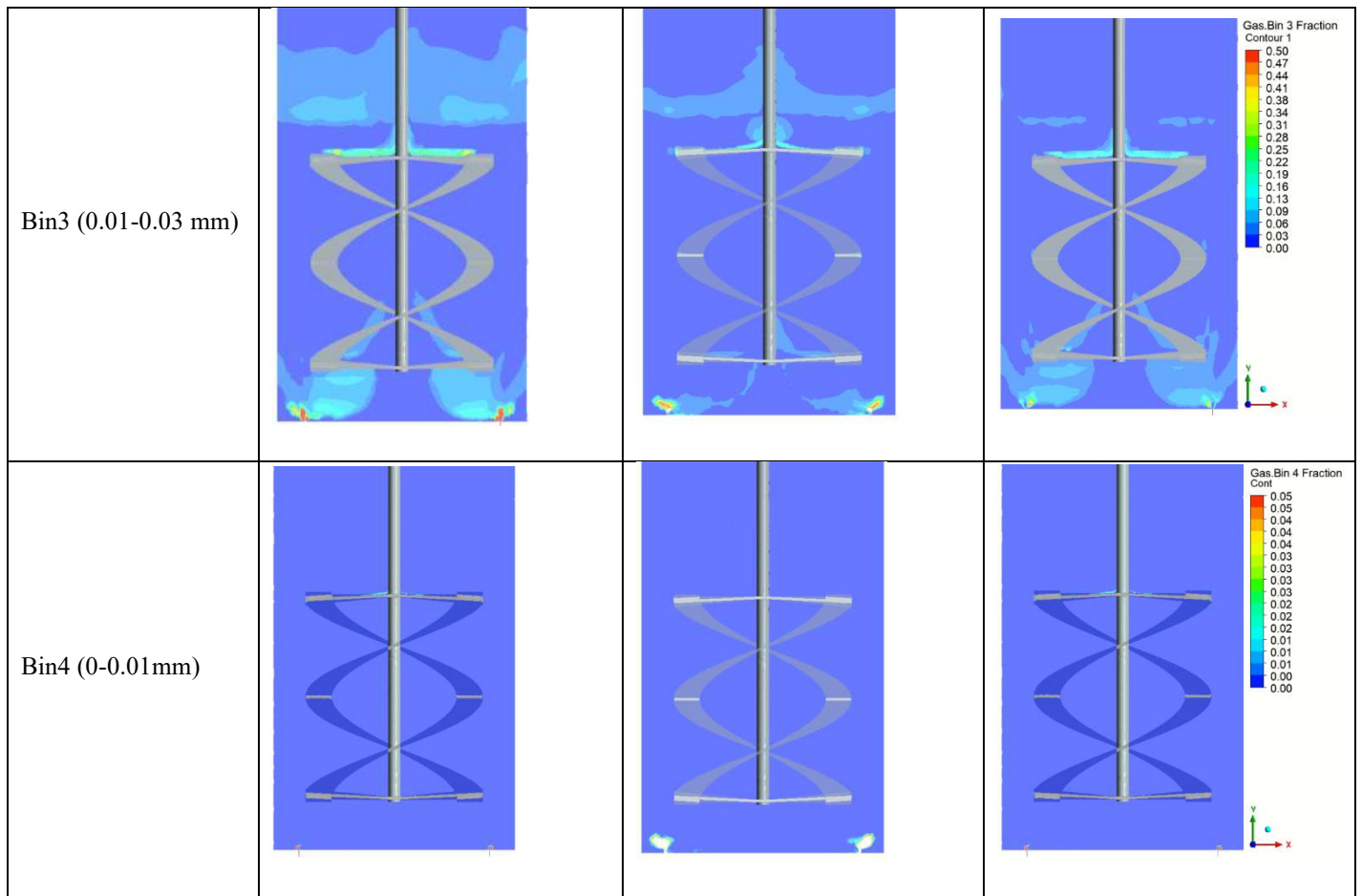


Figure 6-7 Bubble size distribution at rotational speed 25 rpm, column 2; 75 rpm, column 3; and 150 rpm, column 4.

Additionally, Fig. 6-8 confirms that the gas-phase is well distributed at 75 rpm leading to an increase in interfacial area between phases and gas hold up. Doubling the rotational speed of the impeller up to 150 rpm increases the rate of bubble breakage and coalescence, due to the intensity of turbulent flow. The size of the bubbles at 150 rpm varies in a wider range between 0.1 to 0.65 mm.

25 rpm	75 rpm	150 rpm
--------	--------	---------

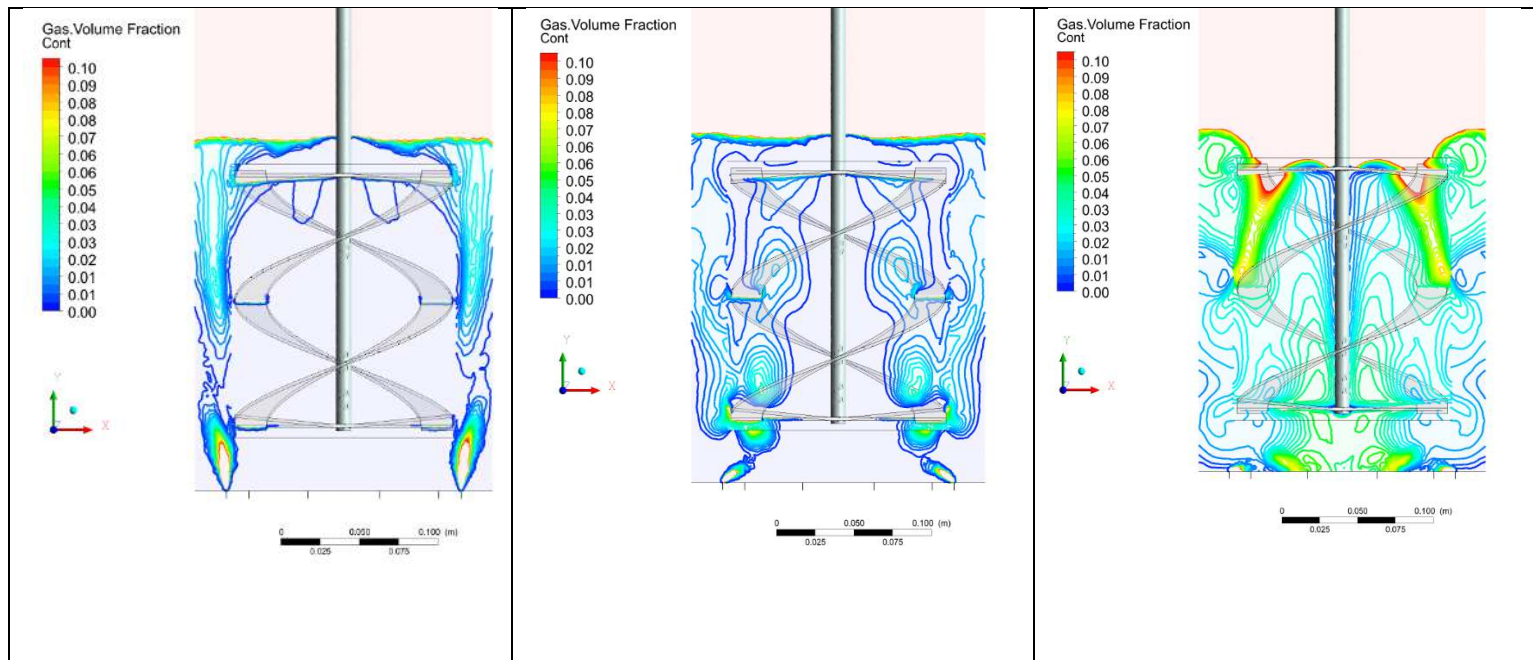


Figure 6-8 Gas volume fraction profile at rotational speed 25, 75, and 150 rpm.

Further, Fig. 6-8 illustrates that bubbles are well distributed in the radial direction. Although increasing rotational speed results in better distribution of bubbles and a larger interfacial area, where the limiting factors should be also considered. High shear stress not only increases operating costs and power consumption, but also disturbs the environment's bioactivity suitability. Therefore, it cannot be concluded that increasing the rotational speed necessarily enhances bioreactor efficiency, where more investigation is required from a microbial perspective (Doran 1995)..

6.8.2 Liquid velocity contour

A combined CFD-PBM model was applied in this study to enhance the understanding of flow visualization inside a multiphase stirred reactor, as demonstrated in Figures 6-9 a, b, and c. To study the impact of impeller speed on the flow field, the gas flow rate was kept constant at 1.8 LPM, with the impeller rotational speed varying from 25 to 150 rpm. The color intensity of contours and streamlines indicate the magnitude of velocity in each region. According to Figure 6-9, the flow field generated by the impeller mostly develops in the axial direction leading to

Chapter 6: CFD-PBM and experimental investigation of a shear thinning fluid in a gas-liquid tank agitated by a helical ribbon impeller

weak flow movement near the bottom and top of the vessel and around the shaft. The figure also indicates that an increase in rotational speed leads to a higher liquid velocity in the system. The results in this figure also indicate the mixing pattern at 25 rpm to be insufficient, where there are some stagnant regions at the top and bottom of the tank, as well as near the shaft. The stagnant regions have been highlighted by purple rectangular and circles. As a result, channelling happens around the impeller outer edge at 25 rpm. Further, it can be observed that an increase in the rotational speed of the impeller leads to a reduction of these stagnant regions. However, having a higher rotational speed requires more energy consumption, which increases operational and maintenance costs. The flow field contours indicate that doubling the rotational speed from 75 to 150 rpm does not produce any significant contribution to the removal of stagnant regions, while the energy consumption increases remarkably. In addition, a high rotational speed of more than a certain level could destroy the microbial growing and seedling environment.

Chapter 6: CFD-PBM and experimental investigation of a shear thinning fluid in a gas-liquid tank agitated by a helical ribbon impeller

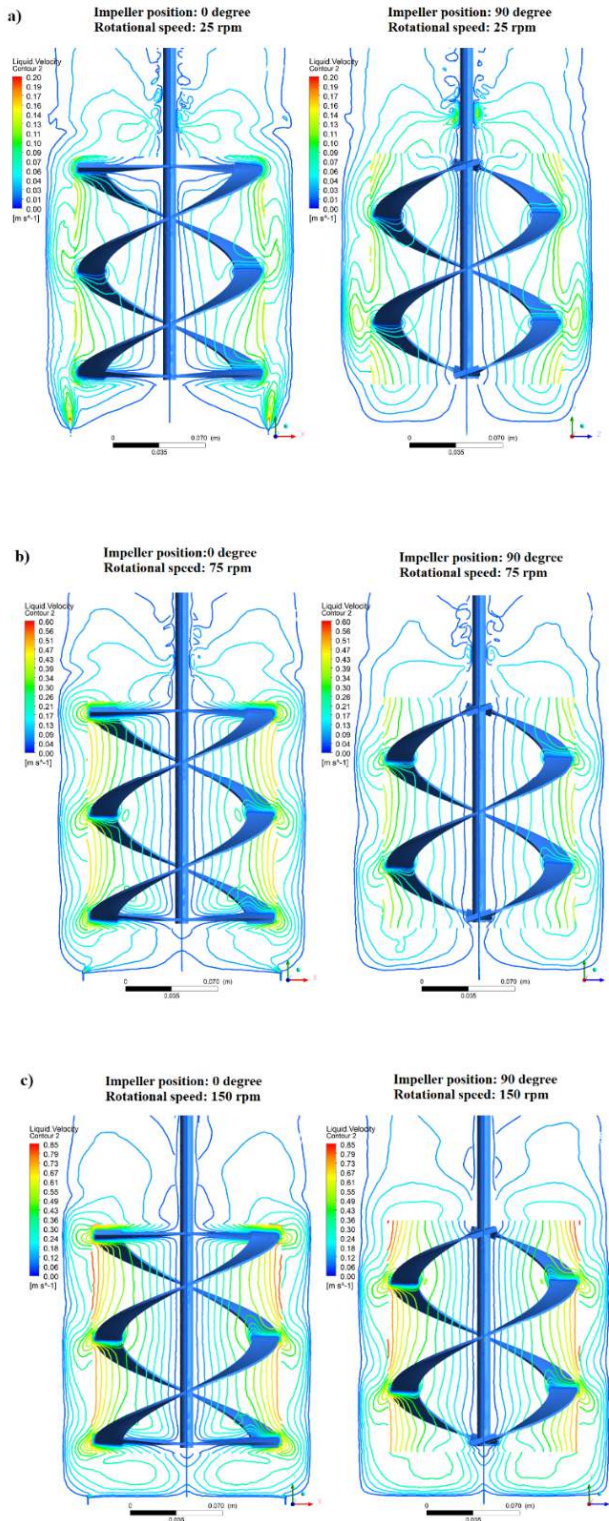


Figure 6-9 Flow field and velocity magnitude at rotational speeds 25, 75, and 150 rpm at two perpendicular positions of blades.

Additionally, the high performance of a dual helical ribbon in comparison with other types of impellers has been confirmed previously within research (Houari Ameer, Bouzit, and Ghenaim

2013; Houari Ameer 2015). This study indicates that the uniformity of fluid has been approximately achieved at 75 rpm. Additionally, stagnant regions are not observed in the whole system at 75 rpm. In this case, operating the system at a higher rotational speed does not contribute to mixing performance. Previous experimental findings also suggest that increasing the impeller speed up to a certain optimum level may enhance the performance of a mixing system (M. Amirafabi, Khiadani, and Mohammed 2020); however, beyond this level power consumption rises sharply with limited positive contribution to mixing performance (M. Amirafabi, Khiadani, and Mohammed 2020).

6.8.3 Effective viscosity contour

Figure 6-10 shows the sensitivity and dependency of the effective viscosity of NaCMC as a shear-thinning fluid to the shear stress induced by the blade rotating at various speeds of 25, 75, and 150 rpm.

Chapter 6: CFD-PBM and experimental investigation of a shear thinning fluid in a gas-liquid tank agitated by a helical ribbon impeller

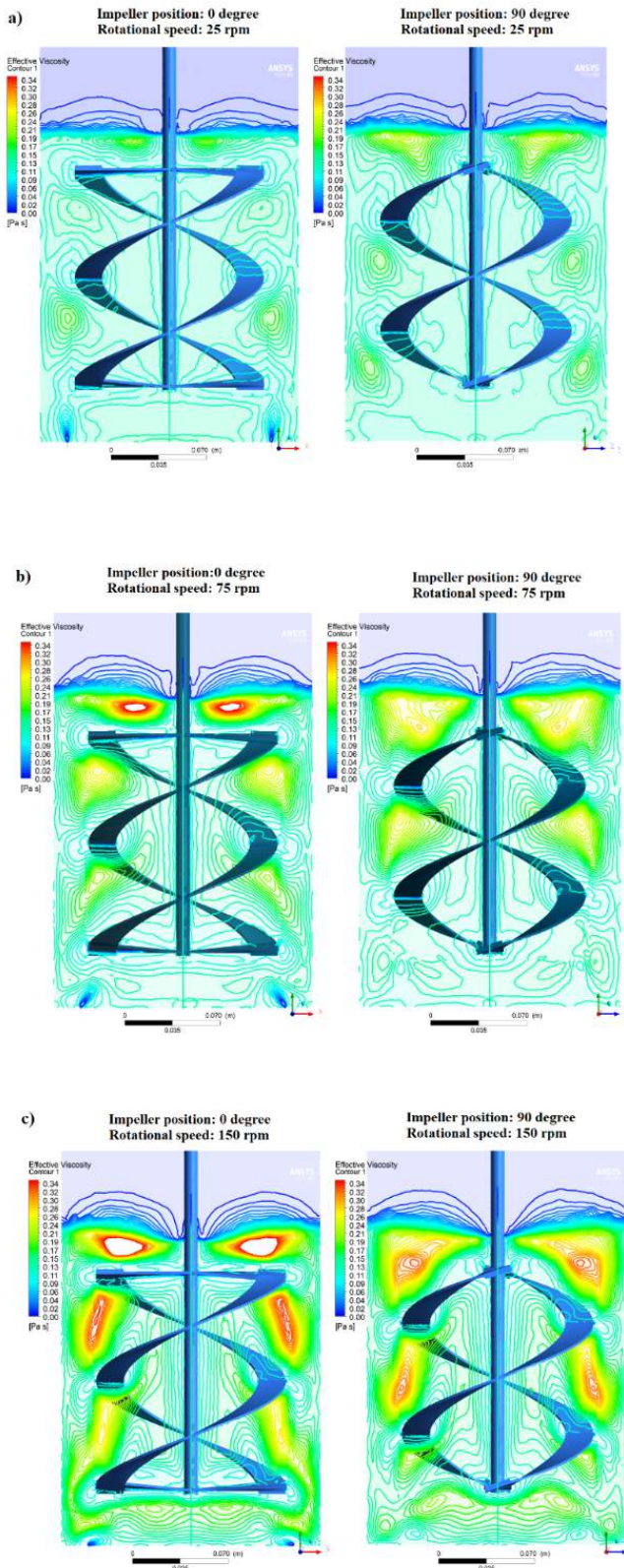


Figure 6-10 Changes in effective viscosity based at rotational speeds 25, 75, and 150 rpm and two perpendicular blade positions.

The results have been compared in two perpendicular blade positions, as shown in Fig. 6-10.

Chapter 6: CFD-PBM and experimental investigation of a shear thinning fluid in a gas-liquid tank agitated by a helical ribbon impeller

According to previous experiments carried out by the same authors (M. Amirafabi, Khiadani, and Mohammed 2020), the viscosity of the diluted solution of NaCMC (0.5 %WT) varies between 0.15 to 0.3 Pa.s when the shear rate is between 20-200 rpm (M. Amirafabi and Khiadani Mehdi 2019a). The CFD prediction contours shown in Fig. 6-10 indicate that the rotating blade causes fluid-structure destruction, leading to a decrease in effective viscosity to 0.17 Pa.s.

Figure 6-10 a indicates that when the rotational speed is around 25 rpm, the viscosity shows a significant drop that leads to an enhancement of the mixing pattern. In this case, the fluid polymer network is destroyed due to the shear stress induced by the blades. Consequently, upward movement of bubbles occur due to the lower effective viscosity of the fluid. By increasing the speed up to 75 rpm and beyond, some high viscous regions were formed with a time delay where the blade passed quickly, as shown in Figs. 6-10 b and 6-10 c. Due to this high rotational speed, the contact time between the blade and fluid-structure is not enough to transfer shear stress from the blade to the adjacent fluid layer. In other words, the blades quickly slip over the layer of fluid, while the shear still has not completely transferred to the fluid layers, leading to the developing of several static vortices. Consequently, the likelihood of bubble trapping in static vortices increases, leading to the formation of stagnant regions and incomplete mixing.

Thus, it can be concluded that increasing the rotational speed of the impeller may not always positively contribute to enhancing mixing patterns. By gradually increasing rotational speed, vortices can form in some regions, disturbing biomass activities, the interaction between phases, and heat and mass transfer. Therefore, it is suggested that the best impeller speed and optimum mixing pattern should be studied for each non-Newtonian fluid separately, based on its specific rheological characteristics.

6.9 Conclusions

A combination of CFD and the Population balance model was applied to evaluate the performance of a dual helical ribbon impeller on the size distribution of bubbles, hydrodynamic behavior, and viscosity of a shear-thinning fluid. The standard $k - \varepsilon$ model and Eulerian-Eulerian (E-E) multiphase approach was considered to solve the governing equations. Further, a discrete method was applied to predict bubble deformation. A mesh independence test was carried out to check the grid sensitivity of the model. The results of CFD simulation were verified by the PIV tests under the same operating conditions.

When increasing the rotational speed of an impeller from 25 to 150 rpm, the rate of coalescence reduces, while the likelihood of bubble breakage increases. Bubble coalescence happens at lower speed because the bubbles are skewed from the outer edge of the blades and trapped in the gel-like structure of the fluid, leading to an increase in the chance of striking and merging. When rotational speed increases, not only is the gel-like structure of the fluid destroyed, but bubbles also hit the blades and walls of the cylinder, resulting in bubble breakage. Therefore, by increasing the rotational speed, bubble distribution improves and enhances the interfacial area.

The CFD results showed that gas holdup reduces as impeller speed decreases, where maximum gas hold-up occurs at 150 rpm. Thus, it appears that maximizing the interfacial area and gas hold-up positively contributes to improving mass transfer between the liquid and gas-phases. Accordingly, the influence of rotational speed on heat and mass transfer for a shear-thinning fluid for this specific type of impeller requires further investigation

At lower rotational speed, poor mixing was observed in the system, which can be improved by increasing the speed of the impeller. However, after reaching a certain level of shear stress, several parameters act as limiting factors like power consumption, operational and maintenance costs, as well as the level of shear stress tolerated by substrate and fluid. Therefore, the working

Chapter 6: CFD-PBM and experimental investigation of a shear thinning fluid in a gas-liquid tank agitated by a helical ribbon impeller

and operating conditions of a particular mixer should be specified through optimization methods based on the type and size of the impeller and vessel, the rheological, chemical, and physical characteristics of the fluid, and the level of shear stress and temperature tolerated by microorganisms.

The results obtained by experiment and CFD predictions indicate that by increasing impeller speed, viscosity drops from 0.3 to 0.17 Pa.s. However, an increase in the rotational speed of an impeller does not necessarily enhance the mixing pattern of a shear thinning fluid. When increasing the rotational speed beyond 75 rpm, there is not enough time to transfer shear stress from the blade to the non-Newtonian fluid surrounding the impeller. Consequently, some static vortices form that lead to poor mixing. To obtain the desired and optimum mixing pattern, it is essential to specify the rheological characteristics of a non-Newtonian fluid (substrate) as well as the shear stress level which can be tolerated by microorganisms, before adjusting the operating conditions.

6.10 References

Ali, B Ashraf, and S Pushpavanam. 2011. "Analysis of Unsteady Gas – Liquid Flows in a Rectangular Tank : Comparison of Euler – Eulerian and Euler – Lagrangian Simulations." *International Journal of Multiphase Flow* 37: 268–77. <https://doi.org/10.1016/j.ijmultiphaseflow.2010.10.002>.

Ameur, Houari. 2015. "Energy Efficiency of Different Impellers in Stirred Tank Reactors." *Energy* 93: 1980–88. <https://doi.org/10.1016/j.energy.2015.10.084>.

Ameur, Houari, Mohamed Bouzit, and Abdellah Ghenaim. 2013. "Hydrodynamics in a Vessel Stirred by Simple and Double Helical Ribbon Impellers." *Central European Journal of Engineering* 3 (1): 87–98. <https://doi.org/10.2478/s13531-012-0045-x>.

Ameur, Houari, and Abdellah Ghenaim. 2018. "Mixing of Complex Fluids in a Cylindrical Tank by a Modified Anchor Impeller." *ChemistrySelect* 3 (26): 7472–77. <https://doi.org/10.1002/slct.201801047>.

Chapter 6: CFD-PBM and experimental investigation of a shear thinning fluid in a gas-liquid tank agitated by a helical ribbon impeller

Ameur, Houari, Youcef Kamla, and Djamel Sahel. 2017. "Performance of Helical Screw Impellers for Mixing of Viscous Liquids in Cylindrical Reactors." *ChemistrySelect* 2 (5): 1891–94. <https://doi.org/10.1002/slct.201602072>.

Amirafabi, Maryam, and Khiadani Mehdi. 2019. "Transparent Polymers to Emulate the Rheological Properties of Primary, Activated, and Digested Sludge Authors:" *Chemical Engineering Research and Design*. <https://doi.org/10.1016/j.mex.2019.03.017>.

Amirafabi, Maryam, Mehdi Khiadani, and Hussein A. Mohammed. 2020. "Performance of a Dual Helical Ribbon Impeller in a Two-Phase (Gas-Liquid) Stirred Tank Reactor." *Chemical Engineering and Processing - Process Intensification* 148: 107811. <https://doi.org/10.1016/j.cep.2020.107811>.

Amirafabi, Maryam Sadat, Navid Mostoufi, Mostafa Hosseinzadeh, and Mohammad Reza Mehrnia. 2014. "Reduction of Membrane Fouling by Innovative Method (Injection of Air Jet)." *Journal of Environmental Health Science and Engineering* 12 (1): 1–8. <https://doi.org/10.1186/s40201-014-0128-0>.

ANSYS Fluent User's Guide. n.d. "No Title."

Bao, Yuyun, Yu Lu, Qianqin Liang, Li Li, Zhengming Gao, Xiongbing Huang, and Song Qin. 2015. "Power Demand and Mixing Performance of Coaxial Mixers in a Stirred Tank with CMC Solution." *Chinese Journal of Chemical Engineering* 23 (4): 623–32. <https://doi.org/10.1016/j.cjche.2015.01.002>.

Basavarajappa, Manjunath, Teri Draper, Pal Toth, Terry A. Ring, and Sanja Miskovic. 2015. "Numerical and Experimental Investigation of Single-Phase Flow Characteristics in Stirred Tanks Using Rushton Turbine and Flotation Impeller." *Minerals Engineering* 83: 156–67. <https://doi.org/10.1016/j.mineng.2015.08.018>.

Baudez, J.C., Paul Slatter, and Nicky Eshtiaghi. 2013. "The Impact of Temperature on the Rheological Behaviour of Anaerobic Digested Sludge." *Chemical Engineering Journal*. <https://doi.org/10.1016/j.cej.2012.10.099>.

Brito-De La Fuente, E., L. Choplin, and P. A. Tanguy. 1997. "Mixing with Helical Ribbon Impellers: Effect of Highly Shear Thinning Behaviour and Impeller Geometry." *Chemical Engineering Research and Design* 75 (1): 45–52. <https://doi.org/10.1205/026387697523381>.

Chapter 6: CFD-PBM and experimental investigation of a shear thinning fluid in a gas-liquid tank agitated by a helical ribbon impeller

Canonsburg, Technology Drive. 2013. "ANSYS Fluent User's Guide" 15317 (November): 724–46.

Chhabra, R P, and J F Richardson. 1999. "Non-Newtonian Flow in the Process Industries British Library Cataloguing in Publication Data."

Dhanasekharan, Kumar M., Jay Sanyal, Anupam Jain, and Ahmad Haidari. 2005. "A Generalized Approach to Model Oxygen Transfer in Bioreactors Using Population Balances and Computational Fluid Dynamics." *Chemical Engineering Science* 60 (1): 213–18. <https://doi.org/10.1016/j.ces.2004.07.118>.

Doran, Pauline. 1995. *Bioprocess Engineering Principles*. Harcourt Brace & Company.

Eftaxias, Alexandros, Vasileios Diamantis, Christos Michailidis, Katerina Stamatelatou, and Alexandros Aivasidis. 2020. "Comparison of Anaerobic Digesters Performance Treating Palmitic, Stearic and Oleic Acid: Determination of the LCFA Kinetic Constants Using ADM1." *Bioprocess and Biosystems Engineering* 43 (7): 1329–38. <https://doi.org/10.1007/s00449-020-02328-2>.

Fernandes del Pozo, David, Alain Liné, Kevin M. Van Geem, Claude Le Men, and Ingmar Nopens. 2020. "Hydrodynamic Analysis of an Axial Impeller in a Non-Newtonian Fluid through Particle Image Velocimetry." *AIChE Journal* 66 (6). <https://doi.org/10.1002/aic.16939>.

Guan, Xiaoping, Xinju Li, Ning Yang, and Mingyan Liu. 2019. "CFD Simulation of Gas-Liquid Flow in Stirred Tanks: Effect of Drag Models." *Chemical Engineering Journal*, no. xxxx. <https://doi.org/10.1016/j.cej.2019.04.134>.

Gumulya, Monica, Jyeshtharaj B. Joshi, Ranjeet P. Utikar, Geoffrey M. Evans, and Vishnu Pareek. 2016. "Bubbles in Viscous Liquids: Time Dependent Behaviour and Wake Characteristics." *Chemical Engineering Science* 144 (2000): 298–309. <https://doi.org/10.1016/j.ces.2016.01.051>.

Hounslow, M. J., R. L. Ryall, and V. R. Marshall. 1988. "A Discretized Population Balance for Nucleation, Growth, and Aggregation." *AIChE Journal* 34 (11): 1821–32. <https://doi.org/10.1002/aic.690341108>.

Chapter 6: CFD-PBM and experimental investigation of a shear thinning fluid in a gas-liquid tank agitated by a helical ribbon impeller

Jiang, Jiankai, Jing Wu, Souhila Poncin, and Huai Z. Li. 2016. "Effect of Hydrodynamic Shear on Biogas Production and Granule Characteristics in a Continuous Stirred Tank Reactor." *Process Biochemistry* 51 (3): 345–51. <https://doi.org/10.1016/j.procbio.2015.12.014>.

Jiang, Xuedong, Ning Yang, and Bolun Yang. 2016. "Computational Fluid Dynamics Simulation of Hydrodynamics in the Riser of an External Loop Airlift Reactor." *Particuology* 27: 95–101. <https://doi.org/10.1016/j.partic.2015.05.011>.

Laakkonen, Marko, Markus Honkanen, Pentti Saarenrinne, and Juhani Aittamaa. 2005. "Local Bubble Size Distributions, Gas-Liquid Interfacial Areas and Gas Holdups in a Stirred Vessel with Particle Image Velocimetry." *Chemical Engineering Journal* 109 (1): 37–47. <https://doi.org/10.1016/j.cej.2005.03.002>.

Lebranchu, Aline, Stéphane Delaunay, Philippe Marchal, Fabrice Blanchard, Stéphane Pacaud, Michel Fick, and Eric Olmos. 2017. "Impact of Shear Stress and Impeller Design on the Production of Biogas in Anaerobic Digesters." *Bioresource Technology* 245: 1139–47. <https://doi.org/10.1016/j.biortech.2017.07.113>.

Liu, Baoqing, Fangyi Fan, Xiaoge Chen, Jinliang Liu, and Zhijiang Jin. 2017. "The Influence of Impeller Combination on the Gas-Liquid Dispersion Performance of a Coaxial Mixer in Viscous Fluids." *International Journal of Chemical Reactor Engineering* 15 (6). <https://doi.org/10.1515/ijcre-2016-0191>.

Machon, By V, and Milan Jahoda. 2012. "Liquid Homogenization in Aerated Multi-Impeller Stirred Vessel." *Technology and Medical Sciences* 23: 1–1. <https://doi.org/10.1201/b11330-2>.

Marchisio, Daniele L., R. Dennis Vigil, and Rodney O. Fox. 2003. "Quadrature Method of Moments for Aggregation-Breakage Processes." *Journal of Colloid and Interface Science* 258 (2): 322–34. [https://doi.org/10.1016/S0021-9797\(02\)00054-1](https://doi.org/10.1016/S0021-9797(02)00054-1).

Miryahyaei, S., K. Olinga, M. Sh. Ayub, Sh. Sh. Jayaratna, M. Othman, and N. Eshtiaghi. 2020. "Rheological Measurements as Indicators for Hydrolysis Rate, Organic Matter Removal, and Dewaterability of Digestate in Anaerobic Digesters." *Journal of Environmental Chemical Engineering* 8 (4): 103970. <https://doi.org/10.1016/j.jece.2020.103970>.

Chapter 6: CFD-PBM and experimental investigation of a shear thinning fluid in a gas-liquid tank agitated by a helical ribbon impeller

Niño, L, M Peñuela, and G R Gelves. 2018. "Gas-Liquid Hydrodynamics Simulation Using CFD in a Helical Ribbon Impeller Applied for Non-Newtonian Fluids." *International Journal of Applied Engineering Research* 13 (11): 9353–59. <http://www.ripublication.com>.

Oyegbile, Benjamin, and Guven Akdogan. 2018. "Hydrodynamic Characterization of Physicochemical Process in Stirred Tanks and Agglomeration Reactors." *Laboratory Unit Operations and Experimental Methods in Chemical Engineering*. <https://doi.org/10.5772/intechopen.77014>.

Ranade, Vivek V. 2001. "Computational Flow Modeling for Chemical Reactor Engineering, Volume 5 (Process Systems Engineering)," 480. <http://www.amazon.com/Computational-Modeling-Chemical-Reactor-Engineering/dp/0125769601>.

Samandari-Masouleh, Leila, Navid Mostoufi, A. A. Khodadadi, Y. Mortazavi, and Morteza Maghrebi. 2012a. "Kinetic Modeling of Carbon Nanotube Production and Minimization of Amorphous Carbon Overlayer Deposition in Floating Catalyst Method." *International Journal of Chemical Reactor Engineering* 10 (1). <https://doi.org/10.1515/1542-6580.2972>.

Samandari-Masouleh, Leila, Navid Mostoufi, Abbasali Khodadadi, Yadollah Mortazavi, and Morteza Maghrebi. 2012b. "Modeling the Growth of Carbon Nanotubes in a Floating Catalyst Reactor." *Industrial and Engineering Chemistry Research* 51 (3): 1143–49. <https://doi.org/10.1021/ie201137j>.

Sato, Y, and M. Sadatomi. 1981. "Momentum and Heat Transfer in Two-Phase Bubble Flow." *International Journal of Multiphase Flow* 7: 167–77.

Scargiali, F., A. D’Orazio, F. Grisafi, and A. Brucato. 2007. "Modelling and Simulation of Gas - Liquid Hydrodynamics in Mechanically Stirred Tanks." *Chemical Engineering Research and Design* 85 (5 A): 637–46. <https://doi.org/10.1205/cherd06243>.

Shahnazari, M. R., Z. Ahmadi, and L. S. Masooleh. 2017. "Perturbation Analysis of Heat Transfer and a Novel Method for Changing the Third Kind Boundary Condition into the First Kind." *Journal of Porous Media* 20 (5): 449–60. <https://doi.org/10.1615/jpormedia.v20.i5.60>.

Tomiya, A., I. Žun, H. Higaki, Y. Makino, and T. Sakaguchi. 1997. "A Three-Dimensional Particle Tracking Method for Bubbly Flow Simulation." *Nuclear Engineering and Design* 175 (1–2): 77–86. [https://doi.org/10.1016/S0029-5493\(97\)00164-7](https://doi.org/10.1016/S0029-5493(97)00164-7).

Chapter 6: CFD-PBM and experimental investigation of a shear thinning fluid in a gas-liquid tank agitated by a helical ribbon impeller

Trad, Zaineb, Christophe Vial, Jean Pierre Fontaine, and Christian Larroche. 2015. "Modeling of Hydrodynamics and Mixing in a Submerged Membrane Bioreactor." *Chemical Engineering Journal* 282: 77–90. <https://doi.org/10.1016/j.cej.2015.04.119>.

Venneker, Bart C.H., Jos J. Derksen, and Harrie E.A. Van den Akker. 2002. "Population Balance Modeling of Aerated Stirred Vessels Based on CFD." *AIChE Journal* 48 (4): 673–85. <https://doi.org/10.1002/aic.690480404>.

Wiedemann, Leonhard, Fosca Conti, Tomasz Janus, Matthias Sonnleitner, Wilfried Zörner, and Markus Goldbrunner. 2017. "Mixing in Biogas Digesters and Development of an Artificial Substrate for Laboratory-Scale Mixing Optimization." *Chemical Engineering and Technology* 40 (2): 238–47. <https://doi.org/10.1002/ceat.201600194>.

Chapter 7: General discussion and conclusions

7.1 General discussion

This project was undertaken to evaluate the hydrodynamic characteristics and flow field generated by a dual helical ribbon impeller in a multiphase reactor filled with a non-Newtonian fluid. Referring to the experimental and numerical findings from this work and the review of literature, a helical ribbon impeller has a significant contribution to homogenizing a system that contains shear-thinning fluid such as polymers and sludge. Complexity of sludge rheology, expensive analytical instrument, safety and health regulations, opaque nature of sludge and complicated hydrodynamics of mixed bubbly flow make the study of hydrodynamic characteristics unfeasible. To overcome some of these limitations, CFD simulation has been considered as a complementary method in this thesis. Due to the opaque nature of sludge, hydrodynamic visualization methods have been unsuccessful. Thus, some research sought to find an alternative working fluid which emulate rheological behaviour of sludge to investigate the hydrodynamic properties of multiphase flow and the performance of mixing. The power consumption and mixing time are two quantitative factors which can be applied to evaluate the performance of a mechanical mixer. Mixing time and power uptake can be optimized for any kind of mixers by adjusting some effective factors including rotational speed of impeller, gas flowrate, rheological characteristics of fluid. These factors have been previously studied to a limited extent for a dual helical ribbon impeller.

Chapter 7: General discussion and conclusions

This study has obtained experimental and numerical data which will help to understand the hydrodynamics of an agitated gas-liquid system and the mixing performance of a dual helical ribbon impeller. To aim this target, NaCMC as a clear simulant fluid has been used in this study to facilitate the image processing procedure and PIV tests. All key research questions have been covered successfully (i) to make a comparison between the rheological behaviour of several polymers with activated and digested sludge to find the best simulant polymer (**Chapter 4**); (ii) to adjust rotational speed of impeller, gas flow rate, viscosity, and clearance to the bottom in order to reduce time and energy required to reach the complete mixed pattern (**Chapter 5**); (iii) to analyse the hydrodynamics (flow field, velocity, bubble distribution, and viscosity) of an agitated multiphase system filled with non-Newtonian fluid (**Chapter 6**).

Chapter 7 summarises the main objectives of this research. Further, the last part of this chapter includes some suggestions for improvement and speculating on future directions.

7.1.1 Rheological study

A series of experiment have been carried out to compare the rheological characteristics of simulant polymers with primary, activated, and digested sludge. Flow curve, thixotropy, and viscoelasticity of the polymers have been measured using a rheometer. Then the collected data has been fitted to the common practical equations like Herschel-Bulkley and Power-Law that describe the relation between shear stress and viscosity of shear thinning fluids. In addition, some complimentary tests have been conducted to evaluate the pH resistance of the polymers since the hydrodynamic visualization tests have been carried out using titration method. The chemical and physical stability of solution should be checked to ensure that the flocculation and settlement can be ignored during the rheological test. Although findings suggested xanthan gum solution's rheological behavior is the closest to sludge, xanthan gum solution was semi-clear which is a hindrance to visualization study. Additionally, result indicated NaCMC is still

another popular alternative for digested sludge in terms of transparency and its similar rheological characteristics, therefore NaCMC was used in this project (**Chapter 4**).

The present study confirms previous findings and provides evidence that suggests xanthan gum and NaCMC can be applied as a stable and safe simulant of sludge with different solid contents.

Chapter 4 compared the rheological behavior of four polymers emulating the rheological characteristics of sludge which has practical applications from both industrial and scientific perspectives studying the rheological characteristics of sludge.

7.1.2 Performance of a dual helical ribbon impeller

In this research, the performance of a helical ribbon impeller in agitating a non-Newtonian fluid in a cylindrical two-phase reactor has been evaluated. The performance of impeller can be judged based on the mixing time and power consumption. Impeller rotational speed, gas flow rate, viscosity, and clearance to the bottom of the tanks have been mentioned in literature as the most influential factors which can change the power consumption and mixing time. To optimize these factors in the lab-scale tank, the RSM method has been applied. Two practical correlations have been suggested by applying ANOVA test to predict mixing time and power consumption under various operating conditions. Based on the ANOVA analysis and RSM approach, the following key parameters have a significant impact on mixing time and power consumption (**Chapter 5**), respectively.

- Impeller rotational speed
- Viscosity
- Gas flow rate

It has been indicated in Chapter 5 that the power number calculated for a dual helical ribbon impeller correlates inversely proportional to the square root of Reynolds number.

7.1.3 CFD Simulation

Due to the experimental limitations, CFD simulation can be applied as a complementary method to investigate the hydrodynamic behaviour of gas-liquid system in detailed. A 3D geometry has been designed to put into the FLUENT solver to simulate the non-identical rotating shape of impeller. After mesh sensitivity analysis, the operating conditions have been adjusted based on the optimized data obtained in Chapter 5. A combination of CFD-PBM models has been applied to develop an understanding of bubble size and distribution. Bubbles have been discretised in five size categories in this research. A classic drag model of Schiller-Naumann has been used to characterize interphase forces and gradient of pressure. PIV tests have been carried out to verify the reliability of CFD model. Velocity profile predicted by CFD complies PIV and experimental results.

The results indicated that the impeller rotational speed has had a significant effect on bubble breakage and coalescence rates. The rate of bubble breakage and coalescence can control the mass and nutrient transfer between phases which can change the performance of a multiphase reactor. Further, an increase in rotational speed of impeller causes a remarkable drop in viscosity of fluid which improves mixing pattern and reduces the volume of inactive regions **(Chapter 6)**.

7.2 Conclusions

The final section draws upon the entire thesis, tying up the various theoretical, numerical, and experimental strands. The present study makes several noteworthy contributions to enhancing the mixing performance of an anaerobic digester in industries. The experimental and numerical findings in this study provide a new understanding of hydrodynamics of an agitated gas-liquid reactor filled with a non-Newtonian fluid. Some findings of this research project were classified as follows:

- I) Analysis of stability, pH sensitivity, Zeta potential, and rheological characteristics of various polymers indicated that:
 1. Xanthan gum is a pH resistant stimulant which can replicate the rheological behavior of activated sludge.
 2. NaCMC is a clear polymer which shows the similar rheological behavior to digested sludge in terms of flow curve and viscoelasticity.
 3. Polymers mentioned in this work are stable and there is no evidence of agglomeration in solutions.
 4. Analysis data collected from rheometer demonstrated that the viscosity has an adverse effect on mixing and shearing the material.
- II) The optimum level of operating conditions has been analyzed by statistical method to achieve the maximum mixed volume, minimum mixing time and energy consumption.
 1. Rotational speed, viscosity, gas flow rate has the most influence on mixing time and power consumption, respectively.
 2. The clearance of impeller from bottom of the tank can be ignored since there is insignificant effect on the rheological properties of fluid and hydrodynamics of system.

Chapter 7: General discussion and conclusions

3. Presence of bubbles leads to a reduction in mixing time and power uptake.
 4. Reynolds and power numbers are correlated practically for helical ribbon agitator.
 5. The results show there is a threshold level for impeller rotational speed considering economic mixing in a shorter period.
 6. Power consumed by a helical ribbon impeller has a reverse proportional function with a square root of Re .
- III) The CFD-PBM simulation of an agitated gas-liquid mixed reactor filled with a non-Newtonian fluid to analyse the velocity field, viscosity gradient, bubble size and distribution, and flow pattern.
1. A comparative study indicates that the simulation predictions comply with PIV results.
 2. CFD modelling successfully predict hydrodynamic characteristics of both liquid and gas phases.
 3. By increasing the rotational speed of impeller, the rate of bubble breakage has been increased. The distribution of bubbles also improved by increasing the rotational speed.
 4. There is a threshold level in impeller rotational speed which beyond that the mixing time reduces insignificantly, while power consumption increases.
 5. A helical ribbon impeller shows a significant contribution to make a multiphase system homogenous where the liquid phase is shear thinning.
 6. The viscosity drops remarkably when the rotational speed of impeller increases.

7.3 Future recommendation

The findings of this study have a number of important implications for future investigation. Several questions remain unanswered at present work suggested as future areas of research.

- I) Sludge always contains some floccules and solids which are ignored in most numerical studies. It is recommended to model sludge as a three-phase fluid to understand the influence of the presence of particles on viscosity, bubble deformation, volume of dead zone, and mixing patten.
- II) More detailed study is required to measure the biogas production in an anerobic digester to evaluate the mixing performance of a dual helical ribbon impeller to make the system homogenous.
- III) It is recommended to optimize the operating conditions for an agitated multiphase reactor equipped with other types of impellers to compare them from an economical point of view.
- IV) There is still a gap in the optimum number of blades in a helical ribbon impeller to enhance the biogas production.
- V) The impact of rotational speed of a dual helical ribbon in transferring mass and heat between phases and the speed of reactions taking place in system (hydrolysis, acidogenesis, acetogenic, and methanogenesis) need to be studied.
- VI) CFD-PBM method can be used to examine the effect of different drag models on bubble breakage and coalescence.
- VII) There are still many gaps in literature on how shear stress influences real sludge viscosity with different percentage of solid particles.
- VIII) In this study, power-law non-Newtonian fluid was used to represent rheological property. It is recommended that this study repeats for a thixotropic fluid following Herkel-Bulkley equation to compare the results.

Chapter 7: General discussion and conclusions

- IX) CFD-PBM method can be used to study the mixing time through injection function and compare to experimental data.
- X) This study compared the rheological behavior of polymers to municipal sludge. It would be suggested that the similar study extended to other types of sludge including poultry and animal farm.